Identification and Characterisation of Host Factors Essential for Human Cytomegalovirus Infection

A thesis submitted in candidature for the degree of
Doctor of Philosophy (PhD)

Pragati Sabberwal Amratia

March 2022

Division of Infection and Immunity
School of Medicine
Cardiff University

Acknowledgements

First and foremost, I would like to thank my supervisor, Prof Ian Humphreys, for his unwavering support, encouragement, and optimism over the last four years. Thank you for guiding me professionally and personally - your mentorship always helped me bounce back in the face of adversity. I would also like to thank my amazing co-supervisors, Prof Richard Stanton, and Dr Ceri Fielding, for their incredible support and expertise. A special thanks to Prof Gavin Wilkinson for his helpful insights during the early stages of my PhD.

I would like to extend my gratitude to Prof Kosuke Yusa (Kyoto University, Japan) for his CRISPR expertise; Shelley Rundle for her help in PCR purification; Dr Angela Marchbank (Genome Research Hub, Cardiff University) who performed high-throughput next-generation sequencing of CRISPR screen; and Dr Robert Andrews for his help with sequencing data analysis. I am also grateful to Systems Immunity Research Institute at Cardiff University for funding this project.

A massive thanks to the HCMV and Adenovirus Research Group, especially Morgan Marsden, Dr Mathew Clement (God of FACS), Dr Jessica Forbester and Dr Sandra Dimonte for a steady flow of insightful discussions and technical expertise. I am also deeply grateful to Dr Silvia Gimeno for helping me settle into the lab; Lucy Chapman for all things ROS; Marta Williams & Dr Ellie Pring for our impromptu brainstorming sessions and Dr Farah Latif & Dr Mark Ponsford for their great company. I would also like to thank Anzelika Rubina, Dawn Roberts, Dr Evelina Statkute, Lauren Jones, Dr Lauren Kerr and Nia Hughes for their incredible friendship and for making challenging times a whole lot easier. A huge thanks to everyone in UG10 as well for some great office banter over the years, especially Dr James Davies for never-ending chats about the Marvel and DC Universe.

I would also like to thank Dr Stefan Milutinovic for letting me vent off my frustrations over countless coffee/lunch breaks and for all those mojitos after work. Bots, Bran, Jo and Jj, thank you for your amazing friendship and for keeping me sane during the lockdown.

I dedicate this thesis to you, Mumma and Papa. No words can express how grateful I am to both of you, so thank you for everything. I also owe a great debt of gratitude to my Dadi, Dadu and Nani for their unconditional love and support. Unnu, a special thanks to you for always having time for me. You are the greatest sister ever. Finally, Kish, thank you for being the most incredible person. I couldn't have done this without you. Thank you for believing in me and for making me believe in myself.

Summary

Human cytomegalovirus (HCMV) is a widespread β-herpesvirus that establishes lifelong infection in hosts. Although the infection is typically asymptomatic in healthy individuals, it causes significant morbidity and mortality in the immunocompromised and individuals with an immunologically immature immune system. There are no licensed vaccines available against HCMV and current therapeutic approaches that target key viral proteins are highly toxic with antiviral drug resistance emerging rapidly in HCMV. Thus, targeting host genes and pathways that are essential for viral infection offers an alternative antiviral strategy. I show that HCMV requires host oxidative immune responses for efficient viral replication. Accumulation of reactive oxygen species (ROS) drives intracellular oxidative stress responses. Using a panel of ROS scavengers, I identified that peroxynitrite, a potent oxidant and nitrating agent, enhanced viral replication in both *in vitro* and *in vivo* models of CMV. Inhibition of peroxynitrite prior to or at the onset of HCMV infection alleviates viral replication in both cell-free and cell-to-cell infection systems, indicating that peroxynitrite may impact virus entry and/or the initiation of replication. Additionally, I conducted a genome-wide assessment of host factors and identified six novel genes (*NF2, KIRREL, MED23, LATS2,* C16orf72 and *KIF5B*) as essential for HCMV infection required for HCMV replication. Three of these unique hits are known to be involved in Hippo signalling. Preliminary experiments demonstrated that inhibition of the Hippo pathway dramatically reduced the production of infectious progeny. However, additional functional assays are required to elucidate the underlying molecular mechanisms by which these factors support HCMV replication. Nonetheless, this thesis identifies several potential pro-viral host factors that could possibly be targeted by pharmacologic treatments to combat HCMV.

Table of Contents

List of Tables

List of Figures

List of Abbreviations

1400W	1400W dihydrochloride
3-3'-DT	3-3'-dityrosine
3-NT	3-nitrotyrosine
5-HT	5-hydroxytryptamine
5-HT	5-Hydroxytryptamine hydrochloride (Serotonin hydrochloride)
AAV	Adeno-associated virus
Ab	Antibody
ADP	Adenosine diphosphate
Ag	Antigen
APC	Allophycocyanin
APCs	Antigen presenting cells
ARPE-19	Adult Retinal Pigment Epithelial cell line-19
ATP	Adenosine triphosphate
β2M	β-2 microglobulin
BAC	Bacterial Artificial Chromosome
BH4	Tetrahydrobiopterin
bp	Base pairs
Cas9	Clustered regularly interspaced short palindromic repeats associated protein
CMV	Cytomegalovirus
CNS	Central Nervous System
CPE	Cytopathic Effect
CRISPR	Clustered regularly interspaced short palindromic repeats
crRNA	CRISPR RNA
D10	DMEM media + 10% FCS
DC	Dentritic cells
DMEM	Dulbecco's Modified Eagle Medium
DMSO	Dimethyl sulfoxide
DNA	Deoxyribonucleic acid
DOPA	Dihydroxyphenylalanine
dpi	Days post infection
DSB	Double-stranded break
dTHP1	Differentiated THP1 cells
EBV	Epstein–Barr virus
EGFR	Epidermal growth factor receptor
EM	Electron microscope
eNOS	Endothelial nitric oxide synthase
ER	Endoplasmic reticulumn
ERK	Extracellular signal-regulated kinase
eROS	Essential for reactive oxygen species
EXT1	Exostosin Gylcotransferase 1
FAK	Focal adhesion kinase

FCS	Fetal calf serum
FDR	False discovery ratio
FeTMPyP	5,10,15,20-Tetrakis(N-methyl-4'-pyridyl) porphinato Iron (III) Chloride
FeTPPS	5,10,15,20-Tetrakis(4-sulfonatophenyl)porphyrinato Iron (III) Chloride
FITC	Fluorescein isothiocyanate
gB	Glycoprotein B
GFP	Green fluorescent protein
gH	Glycoprotein H
gL	Glycoprotein L
GLCE	Glucuronic Acid Epimerase
gM	Glycoprotein M
gN	Glycoprotein N
gO	Glycoprotein O
GoF	Gain-of-function
GPCR	G-protein coupled receptor
gRNA	Guide RNAs
H_2O_2	Hydrogen peroxide
HCMV	Human cytomegalovirus
HDR	homology-directed repair
HFFF	Human Foetal Foreskin Fibroblasts
HFFF-TERT	Human telomerase reverse transcriptase (hTERT) immortalised HFFF
HFFF-TET	HFFF-TERTs expressing tetracycline repressor (TETR)
HIV	Human immunodeficiency virus
HLA	Human leukocyte antigen
hpi	Hour post-infection
HS6ST1	Heparan-sulfate 6-O-sulfotransferase 1
HSV-1/2	Herpes simplex virus-1/2
i.p.	Intra-peritoneally
IE, E, L	Immediate-Early, Early, Late
IFN	Interferon
Ig	Immunoglobulin
IL	Interleukin
iNOS	Inducible nitric oxide synthase
iTERT	Infected HFFF-TERTs
IκB	Nuclear factor of kappa light polypeptide gene enhancer in B-cells inhibitor
JAK	Janus kinases
JNK	c-Jun N-terminal kinase
Kb	Kilobase
Kbp	Kilobase pairs
KIF5B	Kinesin Family Member 5B
KIRREL	Kirre-like Nephrin Family Adhesion Molecule
KO	Knockout

KSHV	Kaposi's sarcoma-associated herpesvirus
LATS2	Large Tumor Suppressor Kinase 2
L-NMMA	NG-Monomethyl-L-arginine
L-NMMA	NG-Monomethyl-L-arginine
LoF	Loss-of-gene function
MAGeCK	Model-based analysis of genome-wide CRISPR knockout
MAPK	Mitogen-activated protein kinase
MCMV	Murine cytomegalovirus
MED23	Mediator of RNA Polymerase II Transcription Subunit 23
MHC	Major histocompatibility complex
MIEP	Major immediate early promoter
MLE	Maximum Likelihood Estimation
MOI	Multiplicity of infection
mRNA	Messenger RNA
mut	Mutated
NAC	*N*-Acetyl-L-cysteine
NAD+	Nicotinamide adenine dinucleotide
NADPH	Nicotinamide adenine dinucleotide phosphate
NEC	Nuclear egress complex
NF2	Merlin
NF-κB	Nuclear factor kappa-light-chain-enhancer of activated B cells
NHEJ	Non-homologous end joining
NK	Natural killer
NO	Nitric oxide
NO_2	Nitrogen dioxide
NOS	Nitric oxide synthases
NOX	NADPH oxidases
Nrf2	Nuclear factor-erythroid 2-related factor 2
NRG2	Neuregulin-2
Nrp2	Neuropilin-2
$ONOO^-$	Peroxynitrite
ONOOH	Peroxynitrous acid
OR14I1	Olfactory Receptor Family 14 Subfamily I Member 1
ORF	Open reading frames
OriLyt	Origin of lytic replication
PAM	Protospacer-adjacent motif
PARP-1	Polymerase-1
PB	Pacific Blue
PBN	N-tert-butyl-α-Phenylnitrone
PBS	Phosphate Buffer Saline
PCPA	4-Chloro-DL-Phenylalanine methyl ester hydrochloride
PCPA	4-Chloro-DL-Phenylalanine methyl ester hydrochloride
PCR	Polymerase chain reaction
PDGFR	Platelet-derived growth factor receptor
PDGFRA	PDGFRα

PE/Cy7	Phycoerythin-Cyanine 7
PFA	Paraformaldehyde
PFU	Plaque forming units
PI3K	Phosphatidyl inositol-3-kinase
PKC	Protein Kinase C
PMA	Phorbol 12-myristate 13-acetate
pp	Phosphoprotein
PRR	Pattern recognition receptors
PTAR1	Protein prenyltransferase alpha subunit repeat containing 1
PTEN	Phosphatase and Tensin Homolog
RNA	Ribonucleic acid
RNS	Reactive nitrogen species
ROS	Reactive oxygen species
rpm	Revolutions per minute
RRA	Robust rank aggregation
RT	Room temperature
RTK	Receptor tyrosine kinase
SAV1	Salvador family WW domain-containing protein 1
sgRNA	Single guide RNA
SLC39A9	Solute Carrier Family 39 (Zinc Transporter) Member 9
SOD	Superoxide dismutases
STK	Serine-threonine kinases
TALEN	Transcription activator-like effector nucleases
TAPR1	Telomere Attrition and p53 Response 1
TAZ	Transcriptional coactivator with PDZ-binding motif
TetR	Tetracycline repressor
TGFβRIII	Transforming growth factor-beta receptor type 3
TLR	Toll-like receptor
TNF	Tumour necrosis factor
TNF-α	Tumour necrosis factor-alpha
TPH	Tryptophan hydroxylase
tracrRNA	Trans-activating CRISPR RNA
TR_L	Terminal Repeat Long
TR_S	Terminal Repeat Short
U_L	Unique long
Us	Unique short
uTERT	Uninfected HFFF-TERTs
vAC	Virus assembly compartment
VC	Vehicle control
VZV	Varicella-zoster virus
WT	Wild-type
XO	Xanthine oxidases
YAP	Yes-associated protein
ZFN	Zinc finger

1 General Introduction

1.1 Human cytomegalovirus (HCMV)

1.1.1 Herpesviridae Family

Human cytomegalovirus (HCMV), also known as Human Herpesvirus-5 (HHV-5), is one of the nine herpesviruses known to infect humans. It is a member of the *Herpesviridae* family of DNA viruses that can establish life-long infection in hosts[1,2]. Characteristically, herpesviruses establish latency, that is the ability of a pathogenic virus to persist in a non-infectious state and lie dormant within a cell, with periodic reactivation and shedding of virus, following primary infection[3,4]. The *Herpesviridae* family is divided into alpha (α)-, beta (β)- or gamma (γ)-herpesvirus, depending on the genetic organisation, host cell tropism and replication strategies[1,2,5]. Alpha-herpesviruses predominantly infect epithelial cells and establish latency in sensory nerve ganglia[1,4]. Members of the α-herpesviruses family known to infect humans include herpes simplex virus (HSV)-1, HSV-2, and varicella-zoster virus (VZV) [1,3]. They are known to cause cold sores, genital herpes, and chickenpox/shingles, respectively[1,4]. There are four human β-herpesviruses: HCMV, HHV-6A, HHV-6B and HHV-7[1,3,6]. Unlike α-herpesviruses, β-herpesviruses replicate and establish latency in several different cell types[1,4,7]. Finally, Kaposi's sarcoma-associated herpesvirus (KSHV) and Epstein-Barr virus (EBV) are γ-human herpesviruses that primarily establishes latency in lymphoid cells, causing infectious mononucleosis upon lytic infection[1,4].

Human herpesviruses have a spherical virion composed of four layers: the core, capsid, tegument, and envelope[1,5,8]. They have a relatively large genome ranging from 125 kbp (VZV) to 235-240 kbp (HCMV) [1,8]. The inner core contains the viral genome packaged as a linear double-stranded DNA molecule surrounded by the capsid[1,8]. The tegument is an amorphous matrix between the capsid and envelope that contains most of the viral proteins[1,8]. The phospholipid envelope surrounding the tegument is derived from the host membrane of the infected cell and contains

viral glycoprotein spikes that play a vital role in cell attachment and subsequent virus entry[1,8]. Herpesvirus genome replication, viral gene transcription and capsid assembly occur in the nucleus of the infected host cell[6]. These processes are regulated by a set of genes that is highly conserved among each subfamily of human herpesviruses[1,8]. During the lytic cycle, all herpesviruses exhibit a sequentially coordinated expression of viral genes (Figure 1.2)[6,9]. In contrast, although the viral genome is retained in the nucleus during latency, the expression of viral genes is highly restricted with no production of viral progeny[4]. The latent virus can be reactivated following environmental triggers, leading to the generation of viral progeny[4].

1.1.2 Human cytomegalovirus genome and virion structure

HCMV is the largest (~235 kb) human herpesvirus, encoding approximately 165 genes and non-coding RNAs, the majority of which undergo extensive post-transcriptional modifications such as splicing[10,11]. HCMV genome is composed of a unique long (U_L) and a unique short (U_S) region[10,11]. Each domain is flanked by inverted repeats at terminal ends (TR_L/TR_S) and at the internal U_L/U_S intersection (IR_L/IR_S), resulting in TR_L-U_L-IR_L-IR_S-U_S-TR_S genome organisation (Figure 1.1A) [10,11]. Terminal repeat sequences contain signals that regulate genome packaging and cleavage[10,11]. Homologous recombination events can occur between the inverted repeat sequences during replication, producing four possible genomic isomers by changing the orientation of unique domains (Figure 1.1B) [10,11].

A significant portion of the HCMV genome is composed of various multigene families, including US6, US12, US22, RL11, UL14, UL18, UL25 and UL120[12–15]. Each family consist of multiple genes with functions ranging from cell tropism, entry, viral replication, and virion assembly[12–15]. The majority of the protein-coding genes are devoted to the modulation of host immune responses[12–15]. Table 1 provides a summary of HCMV gene families.

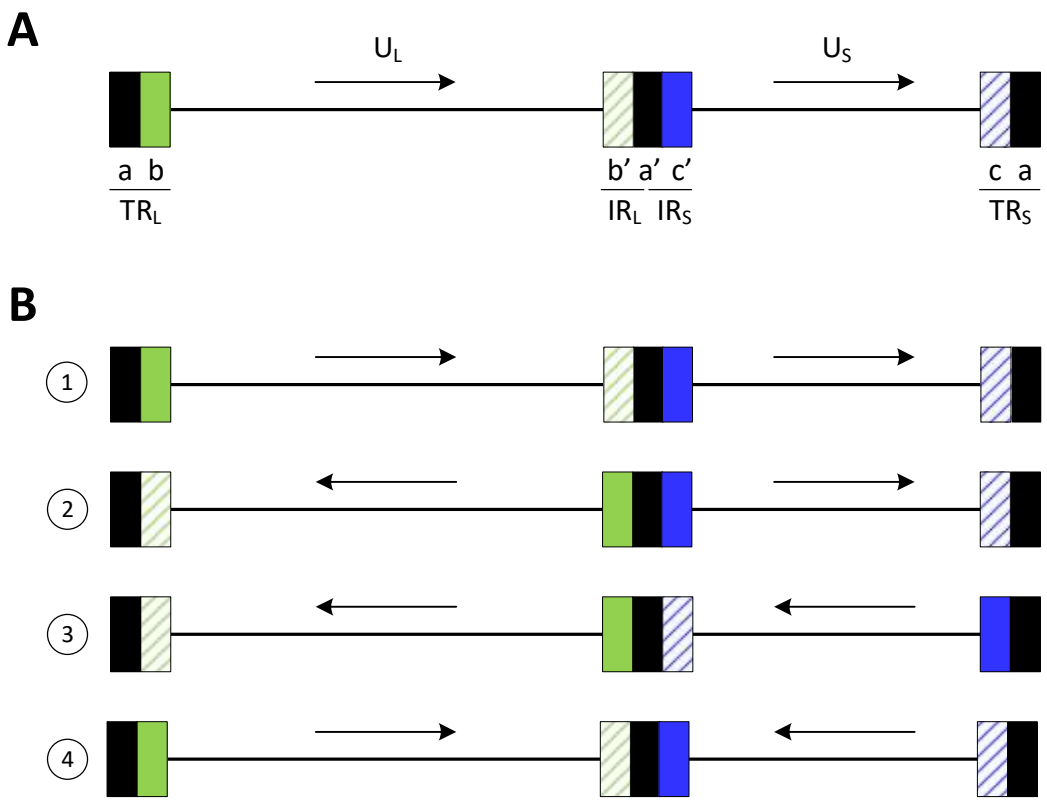

Figure 1.1: HCMV genome structure and alternative isomeric forms.

(A) The HCMV genome contains a unique long (U_L) and a unique short (U_S) region, flanked by inverted repats at terminal ends (TR_L/TR_S) and at the internal U_L/U_S junction (IR_L/IR_S), resulting in TR_L-U_L-IR_L-IR_S-U_S-TR_S genome organisation. Sequence a/a' (solid **black**) is shared by both long and short ends; sequence b/b' (solid/striped **green**) correspond specifically to terminal/internal long and sequence c/c' (solid/striped **blue**) denote terminal/internal short. **(B)** Four HCMV genome isomers (1-4) are possible due to homologous recombination between inverted pairs (corresponding solid and striped coloured boxes). Arrows mark the direction of inversion from isomer 1.

Table 1: HCMV gene families [adapted from 16]

Gene Family	Known members	Main features and/or function(s)
RL11	RL5, RL6, RL11-13, UL1 and UL4-11	The majority are membrane glycoproteins.
US1	US1, US31 and US32	Not fully characterised.
US2	US2 and US3	Membrane glycoproteins involved in immune evasion
US6	US6 – US11	Membrane glycoproteins involved in immune evasion
US12	US12 – US21	The majority are transmembrane proteins.
US22	US22-US24, US26, UL23, UL24, UL26, UL28, UL29, UL36, UL43, IRS1 and TRS1	Tegument proteins that are important for modulating cellular response.
UL14	UL14 and UL141	Immunoglobulin domain-containing membrane glycoproteins. UL141 is vital to evade NK cell activity.
UL18	UL18 and UL142	MHC-I associated membrane glycoproteins that play an important role in immune evasion
UL25	UL25 and UL35	Tegument proteins
UL120	UL120 and UL121	Membrane glycoproteins
UL146	UL146 and UL147	Chemokines
DURP	UL31, UL72, UL82 – UL84	The majority are tegument proteins that have multiple roles in modulating cellular response
GPCR	US27, US28, UL33 and UL72	Chemokine receptors

The HCMV virion comprises a double-stranded DNA enclosed inside an icosahedral nucleocapsid, which is shielded by a "proteinaceous matrix" known as the tegument[17]. HCMV virions are enveloped in a lipid bilayer that contains several host and viral glycoproteins[17]. Mature HCMV virions can be between 200-300 nanometres (nm) [17]. The tegument layer contains most of the viral proteins[17]. HCMV tegument proteins regulate several processes during the viral life cycle, including nuclear entry, virion assembly and modulation of host immune responses[12–15,17]. The most abundant tegument protein is the phosphoprotein 65 (pp65); a product of the UL83 (deleted unique long as already abbreviated earlier) gene[17]. Other major tegument proteins include the UL32-encoded capsid-interacting pp150, UL82-encoded virion-transactivating pp71, the UL99-encoded pp28 and the largest tegument protein, pUL48[17]. The viral tegument also consists of several cellular proteins[18]. The roles of these cellular tegument proteins have not been identified or characterised[18]. Additionally, virions also contain viral and cellular RNAs that are considered important for maintaining the structural stability of the virion[18].

The phospholipid envelope surrounding the tegument layer contains many viral glycoproteins that play a vital role in cell attachment and subsequent virus entry[17]. These include glycoprotein B (gB), gH, gL, gM, gN and gO encoded by HCMV genes UL155, UL75, UL115, UL100, UL73 and UL74, respectively[17,19]. These glycoproteins are essential for virus entry into host cells, cell-to-cell virus transmission and virion maturation[20,21]. For example, the gH-gL-gO trimeric complex facilitates the entry of cell-free HCMV into fibroblasts[20–22]. Interestingly, a gO-null mutant has been shown to produce virions that contain higher levels of pentameric glycoprotein[23]. The gH-gL-UL128-pUL130-UL131 pentameric complex is dispensable for HCMV entry into fibroblasts[24–26]. In contrast, the pentamer is essential for the entry and cell-to-cell dissemination of HCMV in non-fibroblast cells[24–27].

1.1.3 Tropism

HCMV is a specialist human pathogen that can establish infection in almost any organ. Histopathologic assessment of biopsy tissue has shown that HCMV can infect a wide spectrum of cell types *in vivo*, including various connective tissue cells, organ-specific parenchyma cells, hematopoietic cells, and cells of the myeloid lineage[28]. Fibroblasts, epithelial, endothelial, smooth muscle and terminally differentiated myeloid cells are prime sites for lytic HCMV replication[29–31].

Efficient HCMV replication in epithelial cells plays an important role in inter-host viral transmission, particularly through infection of the epithelial lining of mucosal surfaces[31]. HCMV can replicate in almost every organ system, most likely due to its ability to infect cell types that are ubiquitously distributed throughout the host. HCMV primarily spreads by direct cell-to-cell transmission within the host[31,32]. Infection of endothelial cells facilitates systemic dissemination of HCMV as these cells line the inner surfaces of all blood vessels[32]. Virus particles are transported throughout the body by circulating leukocytes[26,28].

Monocytes are essential for the hematogenous dissemination of HCMV into organs[33,34]. Although bone-marrow derived $CD34^+$ hematopoietic progenitor cells (HPCs) and $CD14^+$ monocytes are susceptible to HCMV entry, they do not support productive replication[7]. Instead, HCMV establishes latency in these cell types[7]. Latent HCMV can occasionally reactivate when naïve cells infiltrate into solid tissues and differentiate into macrophages or dendritic cells (DCs) [34,35]. Immunosuppression, cytokine signalling and/or oxidative stress responses regulate cellular differentiation[36].

The broad HCMV cell tropism highlights the complex relationship between HCMV and its host. HCMV can adapt to conditions that alter the cellular microenvironment. An insufficient immune response allows HCMV replication in permissive cells to exceed the threshold for clinical manifestations[17,36]. Specialised parenchyma cells, such as hepatocytes in the liver, smooth muscle cells in the

gastrointestinal tract, neuronal cells in the brain and lung alveolar cells, are highly permissive for HCMV lytic replication, contributing to multiple organ-specific pathologies associated with HCMV[31,37].

Due to restricted host specificity, it is challenging to develop animal models that completely recapitulate HCMV infection. However, several *in vitro* cell models have been developed to closely mimic HCMV entry, replication, spread and latency. Susceptible primary and immortalised cell lines available include fibroblasts (skin and lung), human umbilical vein endothelial cells (HUVECs), retina epithelial cells (RPE, ARPE-19), hepatocytes and terminally differentiated monocyte-like cells[38–41]. These cell lines can support productive infection and allow quantification of virus replication *in vitro*. $CD14^+$ monocytes and $CD34^+$ HPCs derived from peripheral or umbilical cord blood, respectively, are often used as models for HCMV latency *in vitro*[33,42,43]. Naturally immortalised monocyte-like cell lines (isolated from individuals with acute monocytic leukaemia) are also routinely used to study HCMV latency[40,44]. More recently, induced pluripotent stem cells (iPSCs) have been developed into a tool for modelling HCMV latency and reactivation[45]. In contrast to primary cells, iPSCs are easier to isolate and have the unique ability to differentiate into multiple different types of cells, including myeloid cells[45]. *In vitro*, cell cultures can be supplemented with cytokines to selectively facilitate the transition of naïve monocytes into macrophages or DCs[44,45]. For example, it has been shown that exposure to interferon-gamma (IFN-γ) and interleukin-4 (IL-4) drives the differentiation of monocytes towards macrophages[46,47].

Fibroblasts and HUVECs are extensively used in culture as models for HCMV replication[48]. They are susceptible to persistent HCMV, allowing isolation and serial propagation of clinical HCMV isolates[39,49]. During initial passages, clinical isolates of HCMV are pre-dominantly cell-associated, resulting in only a small percentage of cultured cells being infected[29,50–55]. However, as HCMV undergoes extensive *in vitro* passaging, it adapts to cell culture and rapidly generates viral progeny, releasing high titres of cell-free virus[29,50–55]. Therefore, the cell type used

to propagate clinical isolates can affect the tropism of the resulting virus[29,50–55]. For example, long-term propagation in endothelial cells selects for strains with relatively broader cell tropism compared to viral isolates grown in fibroblasts[29,50–55].

Fibroblasts are the most used cells *in vitro* for the long-term propagation of all HCMV strains[29,50–55]. Extensive passaging in fibroblasts has led the virus to gradually accumulate mutations during adaptation to cell culture[50–5529,50–55]. These mutations are commonly acquired in the RL13, UL128 and U_Lb' regions, thereby selecting strains with enhanced infectivity for fibroblasts[50–55].

1.1.4 HCMV pathogenesis

HCMV has a prevalence of 50-90% within the human population, depending on geographical location, socio-economic status, and age[56,57]. HCMV can spread through direct contact with infected bodily secretions, including blood, breast milk, saliva, semen, and urine[58]. Viral transmission can also occur during clinical procedures such as organ transplantation and blood transfusion[58]. Additionally, transplacental transmission of HCMV has also been observed during pregnancy[59].

Primary infection in immunocompetent individuals is generally asymptomatic[56]. It is well-controlled by the host immune response, leading to the clearance of infected cells that are actively producing the virus (Section 1.1.8) [56]. However, infected cells that are no longer producing viral progeny remain within the host in a state of latency[56,57]. Under certain conditions, the latent virus can reactivate and produce infectious virions[56,57]. Although reactivation of latent HCMV is not associated with severe disease in immunocompetent individuals, it can cause severe pathologies in the immunocompromised (e.g., patients with with acquired immunodeficiency syndrome (AIDS) following human immunodeficiency virus (HIV) infection) and the immunosuppressed (e.g., transplant recipients) [56,57].

HCMV is the most common congenital infection, affecting approximately 0.6% of births in developed countries, with a higher rate in developing countries[60]. The risk

of transmission and severe disease in the developing foetus is higher if the mother has an asymptomatic infection during pregnancy or childbirth[59–61]. Congenital HCMV can cause a wide range of physical and mental disabilities, including hearing loss, visual impairment, and intellectual disability[56,61].

HCMV is also considered to be a highly opportunistic pathogen in immunocompromised and immunosuppressed individuals, most likely due to a dampened adaptive immune response[56,57]. For example, HCMV is one of the most common opportunistic pathogens in individuals with AIDS/HIV [56,57]. HCMV reactivation has been associated with hepatitis, retinitis, sepsis, and pneumonia[56,57]. However, CMV disease is less of a clinical problem following highly active antiretroviral treatment (HAART), which uses a combination of three or more antivirals that block different stages of infection[62,63]. For example, in AIDS patients, CMV-associated disease has been shown to decrease by ~80% following customised HAART[62]. Despite this, some patients develop end-organ disease due to low CD4+ T lymphocytes and HCMV reactivation after treatment is discontinued[62].

HCMV infection is very common after transplantation, most likely due to the reactivation of latent infection and subsequent active viral replication[57,64,65]. The risk of CMV disease in transplant recipients is dependent on the serostatus of the donor/recipient, the type of transplant and prophylactic care[57,64,65]. Overall, 60% of solid-organ transplant (SOT) patients develop symptomatic HCMV infection[66]. In SOT patients, the combination of HCMV-positive donor (D+) and HCMV-negative recipient (R-) poses the greatest threat of CMV disease, with complications frequently occurring between 30 to 90 days post-transplantation[64,67]. In contrast, in hematopoietic stem cell transplantation (HSCT), active infection typically occurs within 30 days post-transplantation, especially with graft versus host disease (GvHD)[67]. In HSCT, the highest incidence of HCMV-associated complications occurs when seropositive recipients receive grafts from a seronegative donor (R+/D-), likely due to the absence of pre-existing HCMV-specific memory T lymphocytes[57,64,65]. Here, uncontrolled active viral replication coupled with the effects of

immunosuppressive treatment can lead to life-threatening disease, primarily from CMV pneumonia and gastrointestinal disease, which are associated with high mortality (>70%)[57,64]. Although less common, CMV-associated retinitis, encephalitis and hepatitis can also occur in HSCT patients with productive HCMV infection[64].

Although the use of prophylaxis and pre-emptive therapy has reduced the incidence of HCMV-related complications (~10%) in the first-year post-transplant, they have been shown to delay the production of HCMV-specific T-cells, increasing the rates of HCMV reactivation and disease when antivirals have been discontinued[64].

1.1.5 Genetic variation in laboratory adapted HCMV strains

HCMV strains display genetic diversity in multiple regions of the genome but have been found to be approximately 80% similar at the nucleotide level[10,68]. The genotypic and phenotypic differences between laboratory HCMV strains is well-documented in the literature. Compared to naturally derived wild-type (WT) HCMV, laboratory strains have been extensively passaged *in vitro*[10,69]. Consequently, they display altered cell and tissue tropism[10,69]. The most widely used laboratory strains are AD169, Merlin, TB40/E and Towne[10].

AD169 and Towne were originally isolated to develop into attenuated vaccine candidates by passaging more than 100 times in fibroblasts[10,70]. Since then, they have been extensively used for *in vitro* studies[10,69,70]. High-throughput sequence analysis revealed that AD169 and Towne have acquired multiple mutations compared to the initial HCMV clinical isolate they were derived from[10,69,70]. AD165 was missing around 20 genes due to a 15kbp deletion in its U_L*b*' region (UL133-UL151) [10,69,70]. It had acquired many gene duplications (RL 1-RL14) and multiple additional alterations within the UL128 gene locus[10,69,70]. AD169 also had substitutions in UL36 and UL111A genes[10,69,70]. This gene encodes a protein that would normally suppress apoptosis[10,69,70]. Similarly, Towne was missing around 15

genes due to a 13 kbp deletion in the $U_L b'$[10,69–71]. Towne also had 8 duplicated genes and a 346 bp deletion in UL40[10,69–71]. This gene encodes a protein that is essential to evade natural killer (NK) cell responses[10,69,70]. Both AD169 and Towne had mutations in US1, US9, RL13, UL1, UL40 and UL130[10,69,70].

TB40/E was originally derived from a mixed mutant population of HCMV variants from the throat of a bone marrow transplant patient[10,72]. TB40/E propagates well *in vitro* and shows a broad cell tropism[10,72]. Unlike AD169 and Towne, TB40/E can propagate efficiently in fibroblasts and non-fibroblast cells, even after extensive passaging in fibroblasts (> 40 times) after isolation[10,72]. Sequencing revealed that TB40/E did not have large deletions in the $U_L b'$. Instead, it had multiple genes mutations, including a frameshift in UL141[10,72]. Cloning the viral genome into a bacterial artificial chromosome (BAC) allowed isolation of a highly 'endotheliotropic' variant of TB40/E (TB40-BAC4) [10,53,72,73]. TB40-BAC4 had an intact trimeric (gH/gL/gO) and pentameric complex (gH/gL/UL128/UL130/UL13A) [10,53,72,73]. Consequently, TB40-BAC can efficiently infect a range of cell types, including epithelial, endothelial, and myeloid cells, making it an attractive variant to use for *in vitro* HCMV studies[10,53,72,73].

The Merlin strain was isolated from a urine sample of a congenitally infected neonate after 3 passages in fibroblasts[10,53,73,74]. The Merlin genome was sequenced after the third passage and is widely accepted as the reference genome for HCMV[53,74]. The complete Merlin genome has been cloned into a BAC[73,74]. Sequencing revealed mutations in the UL128 locus (UL128L) and RL13 gene in the Merlin-BAC[52,53,73,74]. These mutations were sequentially repaired to match the sequence of the original HCMV clinical isolate[52,53,73,74]. However, it was found that restoring mutations in both genes dramatically impaired the ability of the virus to replicate *in vitro*[52,53,73,74]. The issue was addressed by placing RL13 and UL128L under conditional expression[27,52,53,73,74]. This restored propagation of Merlin in cell culture while retaining clinically important phenotypic characteristics of the WT virus[27,52,53,73,74].

1.1.6 HCMV life cycle

All herpesviruses have two phases of infection: lytic and latent[75,76]. During the lytic phase, new infectious virions are generated[75,76]. The key regulatory mechanisms at each distinct stage in the replication cycle of HCMV are common to all herpesviruses (Figure 1.2). The HCMV replication cycle is regulated by a tightly controlled and well-balanced gene expression cascade system[75–78]. Mechanisms that mediate HCMV entry are not fully understood but seem to depend on several factors, including pH and cell type[21,75,76].

Cell-free HCMV initiates a series of events following the attachment of viral glycoproteins to cell-surface receptors[21,75,76]. For example, the gM/gN dimer tethers HCMV to cell membranes by interacting with heparan sulphate proteoglycans (HSPGs) [21,75,76,79,80]. Viral gB and gH/gL are essential for HCMV entry into multiple different types of cells[21,75,76,81]. HCMV gB mediates membrane fusion, possibly by forming low-affinity interactions with HSPGs[21,75,76,79,80]. The HCMV gH/gL dimer can also interact with gB to promote membrane fusion[21,75,76,81]. Viral gB can also interact with other transmembrane proteins on the cell surface. For example, TB40/E gB has been shown to interact with epidermal growth factor receptor (EGFR) to promote virus internalisation in monocytes[21,75,76,82,83]. Additionally, gB-null mutants were unable to enter target cells, *in vitro*[23]. Treatment with a chemical fusogen restores entry gB-null mutants[23].

The gH/gL/gO trimeric complex is essential for HCMV entry into fibroblasts[21,84–86]. It binds to platelet-derived growth factor receptor alpha (PDGFRα) and facilitates pH-independent viral fusion at the host cell membrane[22,75,76,87,88]. The HCMV trimer can also interact with other membrane-bound proteins, such as transforming growth factor-beta receptor type 3 (TGFβRIII) and neuregulin-2 (NRG2), to mediate entry into fibroblasts[76]. In contrast, HCMV pentameric complex (gH/gL/UL128/UL130/UL131) is necessary for entry into epithelial, endothelial, and

myeloid cells[21,53,75]. It binds to neuropilin-2 (Nrp2) to mediate viral entry by low pH-dependent endocytosis in epithelial and endothelial cells[21,28,89]. The pentamer has also been shown to bind to CD147 (transmembrane glycoprotein) [21,76,90], CD46 (membrane co-factor) [76,91] and Olfactory Receptor Family 14 Subfamily I Member 1 (OR14I1) [28,92] to facilitate HCMV entry into epithelial cells.

Following entry, capsid and tegument proteins are released into the cytoplasm. Capsids translocate to the nucleus and deliver the viral genome, initiating transcription of viral genes[18,76]. Tegument proteins bound to the viral capsid play an important role in transporting the virus to the nucleus[18,76]. It is believed that tegument proteins, pUL147 and pUL48, interact with host microtubule machinery to assist nuclear translocation[18,76]. Simultaneously, some tegument proteins localise to different subcellular locations to inhibit intracellular immune response. For instance, the most abundant tegument (UL83 encoded pp65) is rapidly transported to the nucleus from where it modulates host immune responses by downregulating the expression of major histocompatibility complex class II (MHC-II), reducing host protein synthesis and impairing IFN-mediated signalling[18,76,93]. Many other HCMV-encoded proteins also regulate cellular signalling and metabolism.

During productive infection, expression of HCMV-encoded viral genes can be divided into immediate-early (IE), early (E) and late (L) phases[75–77,94]. Viral pp71 induces activation of IE genes upon entry into the nucleus[75,76]. The first set of transcribed genes encodes transcriptional activators of other HCMV genes[75–77]. These usually appear within an hour post-infection (hpi) and peak between 4-8 hpi[75–77]. Viral major immediate early promoter (MIEP) drives lytic replication[75,76,95]. The UL22-encoded IE2 protein bound to MIEP is predominantly responsible for activating transcription of other HCMV genes[75–77]. Transcription of early genes by host polymerase II encodes proteins that facilitate HCMV replication[75–77]. HCMV amplifies its genome by rolling-circle replication (RCR) [96]. The RCR mechanism repeatedly copies the viral genome multiple times and strings

the units together to produce one long continuous strand of DNA known as a concatemer[97].

Viral DNA amplification occurs after the expression of early genes and before late gene expression[75–77,94]. The origin of lytic replication (oriLyt) is located in the U_L domain[75,98,99]. It is the only genomic region at which viral DNA synthesis is initiated by the ppUL84-IE2 complex[75,98,99]. *In vitro*, this usually occurs within 24 hpi[75–77]. Several genes are involved in viral replication, including six 'core replication components' common among all herpesviruses[75]. The 'core' set of viral genes interact to form the DNA-polymerase (UL44/UL54) and the helicase-primase (UL57/UL102/UL105/UL170) complexes[75,100–103].

Late HCMV genes are exclusively expressed after viral DNA replication and primarily encode structural proteins required for virion assembly[6,75,76]. Once the genome is replicated, viral DNA is packaged into capsids and subsequently released from the nucleus[6,75,76,104]. The whole process involves interactions between multiple genes and proteins. In brief, capsid assembly is initiated and regulated by pUL180[6,75,76,104]. HCMV terminase complex (pUL51/pUL52/pUL56/pUL77/pUL89/pUL93) binds and cleaves the concatemeric DNA into individual units for packaging[6,75,76,104]. After assembly, pUL150 and pUL153 interacts with viral kinase (pUL197) to form the nuclear egress complex (NEC) [6,75,76,104]. The NEC exports the newly assembled viral capsids from the nucleus to the cytoplasm via a process called nuclear egress[6,75,76,104]. This nuclear export mechanism is a two-step process that involves temporary envelopment of capsid at the inner nuclear membrane, followed by de-envelopment as it buds out into the cytoplasm at the outer nuclear membrane[75,76,105,106]. Additional tegument proteins (such as pp150, pp65 and pp28) bind to the 'naked' viral capsid and direct it to the virus assembly compartment (vAC) [107–109]. HCMV microRNAs reorganise Golgi bodies and endosomal membranes within the cell to form the vAC[75,76,110]. Viral envelope and tegument proteins tend to accumulate here during the late stages of infection[75,76,110]. HCMV pUL48, pUL94 and pUL103 also help with vAC

formation[75,76,110,111]. At the vAC, tegument-coated virus capsids bud into the lumen of intracellular organelles and acquire a host-derived envelope enriched with HCMV-encoded proteins[75,76,111]. The final envelopment occurs as the viral capsid buds out of the Golgi into trans-Golgi vesicles, producing a mature virion[18,75,76]. Vesicles transport mature virions to the cell membrane where they are released via direct membrane fusion or the exocytic pathway[18,75,76]. Peak release of infectious viral progeny can take up to 72hpi in fibroblasts and does not occur until 120 hpi in the RPE-1 cell line, *in vitro*[77,112]. Alternatively, virions can interact with receptors on an adjacent cell, facilitating the cell-to-cell transfer of HCMV. Previous studies have shown that the HCMV pentamer is important for cell-to-cell virus dissemination[27].

HCMV genes have also been categorised based on time and pattern of gene expression during lytic replication[77,112]. In brief, five distinct temporal classes were identified (Tp 1-5) [77]. Functional contributions can be deduced from changes in the protein profile changes over time[77]. For example, UL23-encoded IE1 is a Tp1 protein, which peaks between 6-24 hpi[77]. In contrast, late acting pUL94 exhibited a Tp5 profile, appearing between 24-72 hpi and peaking at 96 hpi[77]. Furthermore, mapping the changes in expression of both viral and host proteins during infection has provided unique insights into virus-host interactions[77,112–114].

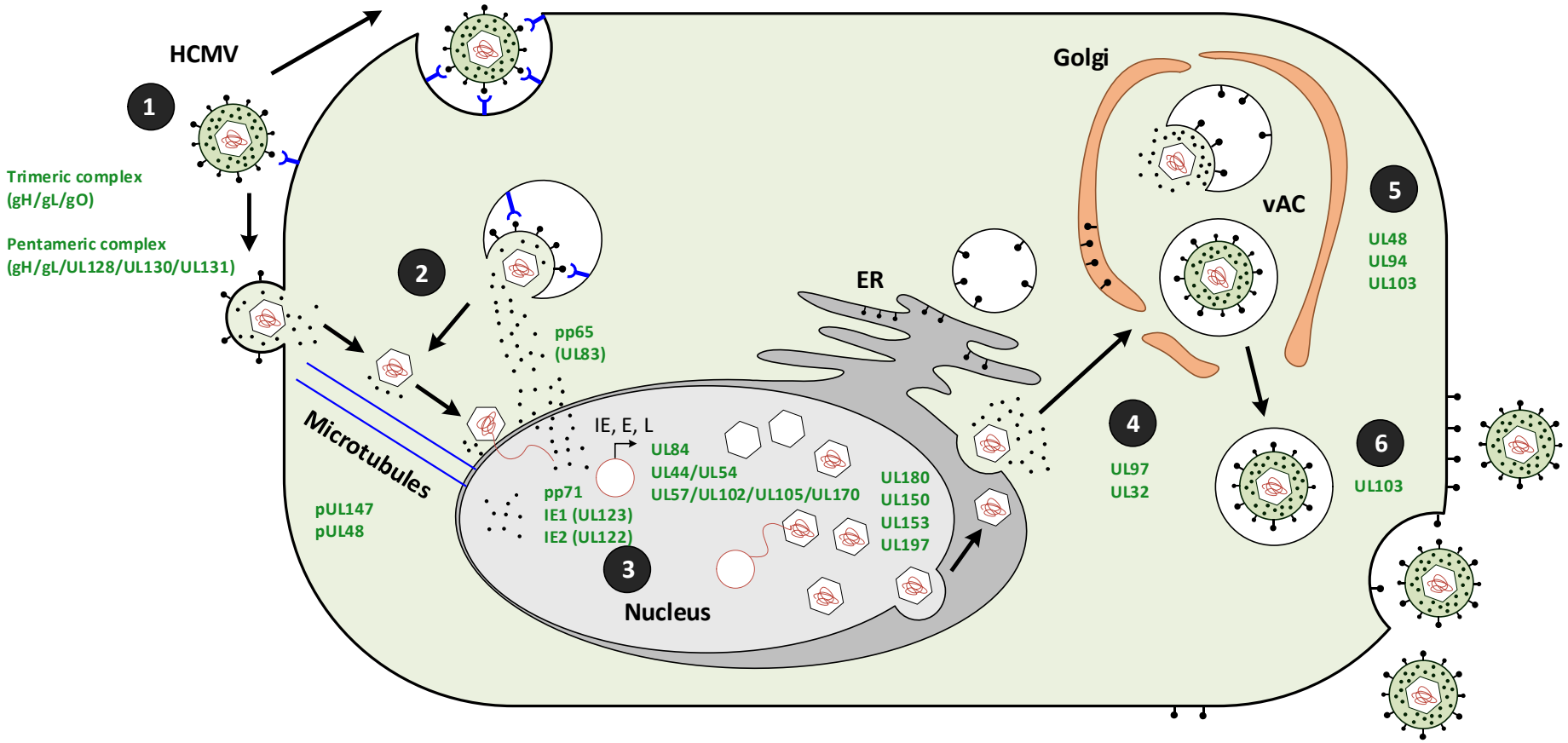

Figure 1.2: HCMV lytic cycle

(1) HCMV glycoproteins interacts with cell surface receptors to mediate entry by direct fusion or receptor-mediated endocytosis. **(2)** Uncoating of virions releases capsid and tegument proteins into the cytoplasm. Capsid is directed to the nucleus by microtubule while viral proteins modulate host immune responses. **(3)** Capsid releases viral genome into the nucleus and sequential viral gene expression (IE→E→L) is initiated by tegument proteins. This facilitates DNA replication. Late gene expression initiates capsid assembly, packaging, and nuclear egress. (**4)** The naked capsid is directed by tegument proteins to virion assembly complex (vAC) in the cytoplasm. **(5)** The tegument-bound capsid acquires host-derived envelope enriched HCMV-encoded proteins. **(6)** The mature virion is transported to the plasma membrane where it is released by exocytosis. Some HCMV genes/proteins involved at different stages are highlighted in green. Figure is a modified version from [92] reproduced with permission from [92].

1.1.7 HCMV latency and reactivation

Following primary infection, HCMV can establish latency in different end organs, where it lies dormant for most of its life cycle. HCMV latency requires an intricate interplay between mechanisms that: (1) maintain viral genome in an infected cell, (2) restrict viral gene expression and (3) avoid detection by host immune responses[36,115].

$CD34^+$ HPCs are understood to be long-term stores for latent HCMV[7,115]. Although these cells can differentiate into several different types of blood cells, HCMV is only passed down the myeloid lineage[36]. HCMV genomes have not been detected in cells of the lymphoid lineage, including B and T-lymphocytes[36]. HCMV can also establish latency in $CD14^+$ monocytes, however, these cells are relatively short-lived so are most likely important for systemic dissemination of the virus[33,36]. Latently infected monocytes can travel via the bloodstream to virtually any organ[33,36].

Several viral genes interact with host factors to drive transcriptional silencing during latency[36,115]. For example, viral G-protein coupled receptor (pUS28) inhibits several pro-inflammatory signalling cascades, including mitogen-activated protein kinase (MAPK) and nuclear factor kappa-light-chain-enhancer of activated B cells (NF- κ B) pathways[75,76,115,116]. pUS28 is also involved in the suppression of MIEP[36,75,76,117]. It recruits components to remodel the chromatin structure around the promoter[36,75,76,117]. For example, cellular heterochromatin protein-1 (HP-1) and histone deacetylases (HDACs) help form a repressive chromatin structure around MIEP through methylation and deacetylation of associated histones[118]. This makes MIEP inaccessible to regulatory factors, including transcription factors[118].

During latent infection, UL115 encodes a viral homolog of human IL-10 (vIL-10) [76,119,120]. There are two isoforms of vIL-10: cmvIL10 and LAcmvIL10[76,119,120]. The LAcmvIL10 isoform is upregulated in latent infection and inhibits cellular antiviral

defences, including synthesis and secretion of inflammatory cytokines[76,119,120]. Interestingly, vIL-10 regulates the production and secretion of cellular IL-10[76,119,120]. These findings suggest a crucial role of vIL-10 in the spread and persistence of latent HCMV [76,119,120].

Reactivation of latent HCMV is linked to cellular differentiation and activation of signalling pathways that facilitate the re-expression of viral genes[36,116]. For example, it is believed that the binding of host transcriptional activators, such as the facilitating chromatin transcription (FACT) complex, to MIEP remodels the surrounding chromatin structure, making MIEP more accessible to host RNA polymerase II[121]. Additionally, treatment of latently infected monocytes with HDAC inhibitors restores viral replication, *in vitro*[122]. Interestingly, it has been shown that activation of MIEP alone is not sufficient to drive lytic replication[36,116,117]. *In vitro* studies in THP-1 have shown that despite MIEP activation, infectious virions were not produced[117,123]. Recently, it has been suggested that HCMV reactivation may not be MIEP-dependent[36,115]. Instead, HCMV might use alternative promoters within the MIE gene locus to drive reactivation from latency, with MIEP remaining silent during replication[36,115].

1.1.8 Immune response to HCMV infection

HCMV induces a robust immune response within the host, involving both innate and adaptive immunity. During acute infection, HCMV can activate cellular pattern recognition receptors (PRR) located at the cell surface or distributed within membranes of intracellular compartments[76,124,125]. For example, viral gB and gH have been shown to trigger toll-like receptor 2 (TLR2), TLR3 and/or TLR9[76,124,125]. TLR activation, in turn, triggers several pro-inflammatory pathways, leading to the production of type I IFN and other inflammatory cytokines, including tumour necrosis factor-alpha (TNF-α) and IL-6[76,124,125]. For example, TLR2 can activate NF-κB and interferon regulatory factor 3 (IFR3) [76,124,125]. These transcription factors promote the transcription of antiviral genes such as α and β interferons[76,124,125].

Upon infection, HCMV also induces the production of reactive oxygen species (ROS)[126–128]. The build-up of ROS activates multiple pro-inflammatory signalling cascades, leading to oxidative stress[126–128]. Prolonged oxidative stress can induce apoptotic pathways to mediate viral clearance[126–128]. These signalling pathways can be also triggered following the detection of viral DNA (vDNA) from intracellular PRRs such as cyclic guanosine monophosphate–adenosine monophosphate (cGAMP) and cGAMP synthase (cGAS) [76,129]. cGAS recognises vDNA and rapidly induces cGAMP synthesis, which in turn activates simulator of interferon (STING) pathways, leading to production of inferno via activation of IRF3[76,130,131]. *In vitro*, inhibition of STING has been shown to enhance HCMV replication in HUVECs[130].

Accumulation of ROS, interferons, and other inflammatory cytokines recruit antigen-presenting cells (APCs), including phagocytes (macrophages and DCs) and natural killer (NK) cells to sites of infection[76,124,125]. NK cells are essential for controlling HCMV infection[76,132,133]. NK cells can interact with multiple different cell types via inhibitory and activation receptors[76,132,133]. This most likely contributes to their role in the immunosurveillance of infected cells[76,132,133]. Inhibitory NK cell receptors prevent NK cell activation if it recognises 'self' major histocompatibility complex class I (MHC-I) [76,132,133]. However, if activated NK cells do not receive an inhibitory signal, NK cells promote killing of target cells via perforin-mediated-cytotoxicity or death receptor-induced apoptosis[76,132,133]. For example, HCMV-induced production of TNF-α has been shown to increase the presentation of death receptors (a subset of TNF receptors that contain a death domain) on the surface of an infected cell[76,132,133]. NK cells express TNF receptor-related ligands that bind to these specific death receptors[76,132,133]. Furthermore, it has been shown that HCMV downregulates the expression of MHC-I during infection[76,132–134]. Consequently, if NK cells interact with death receptors in absence of MHC-I, they can initiate downstream apoptotic pathways[76,132–134]. NK cells are also involved in antibody-dependent cellular cytotoxicity (ADCC), a defence mechanism that facilitates effector cells to kill target cells coated with antigen-

specific antibodies[76,135,136]. Individuals with abnormal NK function are highly susceptible to infection from herpesviruses, particularly HCMV [135].

The contribution of intrinsic innate immunity in the control of HCMV is less understood. The intrinsic antiviral response involves host proteins that can directly interact with viral proteins to inhibit viral replication and assembly[76,125,137]. These cellular proteins are known as restriction factors (RF) and include a 100-kDa speckled protein (Sp100), the human death domain-associated protein 6 (hDaxx), promyelocytic leukaemia protein (PML) and IFN stimulating genes (ISG) such as IFN-γ inducible protein 16 (IF16) [125,137,138].

Specialised APCs, such as DC and macrophages, are vital for innate immune response. These APCs capture and present digested viral antigens to lymphocytes, leading to the production of cytokines[124,125,139]. APCs constitutively express MHC-II molecules and antigens to CD4+ T cells. Despite being targets of HCMV infection, macrophages and dendritic cells manage to regulate host immune response against HCMV[124,125,139]. For example, HCMV-infected macrophages have been shown to sustain inflammation and secrete pro-inflammatory cytokines, including IFN-γ, TNF-α and IL-6 during HCMV infection[124,125,139]. This process is mediated by respiratory burst (rapid production and secretion of ROS) during phagocytosis[124,125,140,141]. They have also been shown to retain their ability to present HCMV-derived antigens (mainly endogenous IE1) and stimulate the proliferation of CMV-specific T cells, especially during the early stages of the lytic cycle (~24 hpi) [134,142]. In fact, even at later stages (72 hpi), the ability of infected macrophages to stimulate T-cells was not completely abolished, *in vitro*[134,142]. Intriguingly, in the same study, HCMV infection in DCs severely compromised their ability to present antigens and induce T-cell proliferation[134,142]. The reasons for these differences are not fully understood.

DC are essential for activating T and B lymphocytes[35,143]. DCs are categorised by function, location, and expression of cell surface markers. There are four main subtypes of DCs: conventional (cDCs), monocyte-derived (moDCs), plasmacytoid

(pDCs) and Langerhan cells (LCs) [35,143,144]. All DCs, except LCs, are believed to be derived from $CD34^+$ hematopoietic stem cells ($CD34^+$ HSC) [35,143,144]. Immature DCs can be found in most tissues[35,143,144]. Activation of PRR and/or disruption to cellular microenvironment initiate DC maturation[35,124,125]. Mature DCs migrate to secondary lymphoid tissues and interact with naïve T lymphocytes by binding to intracellular adhesion molecule 3 (ICAM3)[143,145]. HCMV encodes many proteins that inhibit the differentiation of monocytes[35,143,146]. In fact, cmvIL-10 inhibits the maturation of immature DC, reducing their ability to direct immune responses[35,143,146]. Furthermore, HCMV uses DC-specific ICAM-grabbing non-integrin (DC-SIGN) to infect some subsets of DC[35,143,146]. Interestingly, NK cells can interact very closely with HCMV-infected macrophages and DC to either kill them or amplify their immune response[12,138]. Uninfected DCs can engulf highly apoptotic infected cells and cross-present HCMV-derived antigens to circulating T-lymphocytes[12,138]. Interactions between APCs and T-cells links the innate and adaptive immune systems[12,138].

Adaptive immunity is vital for the long-term regulation of HCMV[76,124,147]. HCMV induces a strong T-cell response, primarily contributed to by HCMV-specific $CD8^+$ T cells[124,147–149]. In infected individuals, around 10% of both $CD4^+$ and $CD8^+$ memory T-cell compartments in peripheral blood and tissues are HCMV-specific, recognising >20 different HCMV open reading frames (ORF) [147,148,150]. Overall, previous studies have identified >150 HCMV ORFs that are immunogenic for $CD4^+$, $CD8^+$ or both types of T lymphocytes[147,148,151,152]. HCMV-specific $CD8^+$ T cells gradually expand and are maintained at high frequencies for the life of the host [147–149,152]. This process of 'memory inflation' is antigen-driven and most likely occurs due to repeated episodes of HCMV reactivation throughout life[147,151,152]. Consequently, the HCMV-specific $CD8^+$ T cell population can get quite large, even reaching up to 30% of total $CD8^+$ T cells [147,148,151,152]. Although most of these inflationary $CD8^+$ T cells are short-lived effector memory cells, a small percentage develop into central memory cells[147,148,151,152]. These cells are long-lived and retain the ability to rapidly proliferate into effector cells upon re-exposure to the initial antigen[147,148,151,152].

More recently, an 'inflation-like' $CD8^+$ T cell population has been identified[151]. This intermediate population redefine the term memory inflation as they are unconventional memory T cells that accumulate at varying frequencies and drive T cell response upon antigen re-encounter without showing signs of T-cell exhaustion[151]. Although individual epitope-specific $CD4^+$ T cells don't generally accumulate at such high frequencies, HCMV-specific $CD4^+$ T cells seem to be particularly effective in preventing HCMV-associated pathologies in solid-organ transplant recipients[149,153].

Humoral virus-specific immune responses have also been shown to be important in the long-term control of HCMV [154–157]. Antibodies that target HCMV envelope glycoproteins (gB, gH/gL and gM/gN), tegument proteins (pp65 and pp150) and the transcriptional activator IE1 have been identified to be particularly important in restricting virus spread[154–157]. In fact, pre-existing HCMV-specific maternal antibodies can reduce the risk of congenital HCMV transmission[158]. Antibodies can neutralise viruses by blocking interactions between viral proteins and cellular host receptors or through the induction of ADCC[159]. HCMV elicits a robust ADCC response, predominantly through HCMV-specific immunoglobulin G (IgG) antibodies[154,160,161]. Vlahava et al. have shown that viral antigens derived from US28, RL11, UL5, UL16 and UL141 can independently induce ADCC *in vitro*[136]. They also demonstrate that UL16 and UL141 specific monoclonal antibodies isolated from seropositive individuals can efficiently activate NK cell-mediated ADCC against HCMV, offering a potential antiviral strategy for the treatment of HCMV infections[136].

1.1.9 Immune evasion by HCMV

HCMV has evolved multiple strategies to modulate host immune responses. In fact, most of its protein-coding genes are dedicated to the evasion of host antiviral defences[12,76,138,162,163]. HCMV encodes multiple inhibitors to antagonise signalling pathways that continuously produce IFN[12,76,138,162,163]. For example, US7 and US8

destabilise TLRs and target them for lysosomal degradation[76,164]. A virus with mutations in the US7-US16 region could not inhibit TLR signalling[164]. Viral proteins encoded by UL31, UL42 and UL83 can bind to cGAS to prevent cGAMP synthesis[76,163,165]. Similarly, UL82 tegument protein can directly inhibit the activation of STING[76,163,165]. Moreover, HCMV mediates upregulation of nuclear factor-erythroid 2-related factor 2 (Nrf2), which is a transcription factor that regulates the expression of cellular antioxidant proteins[166]. Consequently, it protects the infected cell from oxidate damage triggered by the generation of ROS. Furthermore, HCMV- infected macrophages exhibited diminished respiratory burst in response to stimuli, *in vitro*[167].

HCMV encodes several genes to downregulate cell surface expression of MHC I (e.g., US2, US3, US6 and US11) and MHC-II (e.g., IE1 and IE2) [76,134,168]. The US10 glycoprotein is also involved in the attenuation of IFN-γ and interferes with antigen presentation by MHC-I[76,169]. NK cells selectively kill target cells that do not express MHC molecules on the cell surface[76,133,135]. However, HCMV encodes a viral homolog of human beta-2-microglobulin (β2M) [162]. The human β2M protein is a component of the MHC-I molecule. Consequently, the viral homolog (US18) mimics 'self-MHC-I' expression to evade NK cell-mediated killing[162].

HCMV-infected cells have been shown to be highly resistant to attack by NK cells, *in vitro*, most likely because HCMV dedicates a significant number of genes to attenuate NK cell activity[135,170,171]. Viral US9 can inhibit the stimulation of NK cells by mediating IFN-β production[76,135,170,171]. Additionally, it has been shown that pUL148 increases degranulation in activated NK cells[76,135,170,171]. HCMV also downregulates membrane expression of activating NK cell ligands in infected cells. Natural Killer Group 2, member D (NKG2D) is an activating receptor that is ubiquitously expressed on the surface of NK cells[170,172–174]. NKG2D binds to different ligands, inducing MHC-I related protein A (MICA), MICB and UL16 binding proteins (ULBPs) [170,172–174]. HCMV genes US9, US18, US20, UL142 and UL148A encode proteins that downregulate MICA[76,170,172–174]. Protein UL142 can also

downregulate ULBPs[135,170–172,175]. Similarly, UL16 has been shown to reduce the expression of MICB and ULBP1/2, blocking the activation signal to the NK cell[135,170–172,175]. Proteins encoded by these HCMV genes either sequester NK ligands in cis-Golgi or target them for lysosomal degradation [135,170,171]. Most NK cells also express the activating receptor CD226, which binds to CD155[170,176]. UL141 gene product inhibits CD155 expression on the surface of infected cells[170,176]. Another NK evasion mechanism employed by HCMV is the upregulation of NK ligands that bind to inhibitory receptors located on the surface of NK cells[171]. For instance, the UL40 protein increases the cell surface expression of human leukocyte antigen E (HLA-E), an inhibitory ligand that binds to the NKG2A/B receptor and prevents the activation of NK cells[170,177]. Additionally, HCMV viral FcRs (gp34 and gp68) antagonise antibody-depended cell-mediated immune responses by preventing Fc-FcR engagement between bound IgG and NK cells[161].

HCMV also encodes several genes to evade T-cell mediated immunity[12,76,162,178]. For example, HCMV impairs the expression of CD58, a key cell adhesion molecule that generates a costimulatory signal following its interaction with CD2 on the surface of effector cells[135,170]. The UL148 protein targets CD58 for intracellular retention, preventing recognition of infected cells by CD8+ cytotoxic T lymphocytes and (CTLs) and NK cells[76,135,170]. Additionally, US2, US3, US6 and US11 encode proteins that inhibit MHC-I antigen presentation by blocking peptide loading and/or targeting the peptide-loading complex for proteasomal degradation[76,134,178]. Likewise, cmvIL-10 also downregulates MHC molecules on infected APCs and impedes APC-induced production of pro-inflammatory cytokines that facilitate T-cell activation[76,120]. Moreover, HCMV miR-US4-1 inhibits cellular proteins that process and present viral peptides to CD8+ T cells[76,179].

1.1.10 Anti-HCMV Treatments and Vaccine Development

There are no approved vaccines currently available to prevent or treat HCMV infection[180]. Fortunately, highly effective antivirals have been developed against

HCMV infection. Antiviral treatments include ganciclovir, maribavir, fosarnet and cidofovir[76,181–183]. Ganciclovir is the most favoured drug for treating active HCMV infection in a clinical setting[76,183–185]. Once administered, it selectively accumulates in HCMV-infected cells where viral UL97 encoded protein kinase phosphorylates ganciclovir[76,186–188]. Phosphorylated ganciclovir inhibits viral replication by incorporating itself into the viral DNA polymerase complex[76,186–188]. Meanwhile, maribavir inhibits viral UL97, interfering with virion assembly and egress[76,183,189,190]. Currently, its efficacy is being tested in Phase III clinical trials[76,183,189,190]. Foscarnet can directly bind to viral DNA polymerase to inhibit replication[76,184,186,191,192]. Whereas, Cidofovir prevents viral DNA elongation, and is particularly effective in treating HCMV-related retinitis[76,192,193]. Although these antivirals are highly effective for viral clearance, they can be highly toxic[188,192,193]. For example, ganciclovir treatment can cause neutropenia[76,194]. Whereas renal toxicity has been associated with foscarnet and cidofovir[76,195].

Letermovir has recently emerged as a 'break-through' anti-HCMV drug[76,185,189,193,196]. Letermovir targets pUL56 in the viral terminase complex and inhibits the virion packaging, assembly, and maturation[76,185,189,193,196]. It exhibited great efficacy in a Phase III clinical trial[76,183,185,186]. Treatment significantly reduced the risk of HCMV reactivation and/or re-infection, with minimal side effects[76,183,185,186]. Letermovir is now permitted for use in seropositive hematopoietic stem cell transplant (HSTC) recipients[76,186,197]. Recently, the emergence of major mutations in UL56 has been associated with letermovir resistance[76,186,198,199]. Mutations in UL56 did not provide the virus with additional protection against other antivirals, including ganciclovir or foscarnet[191,195]. However, there is an increase in the incidence of antiviral resistant HCMV, including the emergence of ganciclovir resistance[76,186,198,199].

Reactivation of latent HCMV is quite common after HSCT[57,64]. Current antivirals only target lytic infection and do not clear latent HCMV reservoirs[76,182,183]. Furthermore, the antivirals only provide short term protection due to drug toxicity

and the emergence of antiviral resistance[76,182,186,192,196,199]. Pilot studies have shown that adoptive CMV-specific T-cell therapy can be effective at restoring protective HCMV-specific T-cell immunity in immunosuppressed individuals[200–202]. Administration of donor HCMV-specific T-cells into matched stem cell transplant recipients resulted in rapid resolution of viremia and reduced incidence of transplant rejection[200–202].

Over the years, there have been many vaccine candidates, ranging from the live-attenuated vaccine (e.g. AD165, Towne) to virus subunit vaccines (e.g. gB) [180]. Vaccines against HCMV have largely been unsuccessful due to low efficacy[180]. The most successful candidate vaccine is the gB subunit vaccine that exhibited 50% protection in solid-organ transplant recipients[180]. *In silico* computational modelling has revealed that a multi-epitope vaccine design could be effective against HCMV[203]. This approach has previously been used to design a multi-epitope peptide to treat brucellosis[203]. The candidate has shown success in mice models by producing high levels of IgG antibodies[203]. Currently, there is a messenger RNA (mRNA) based HCMV vaccine in Phase III clinical trials (mRNA-1647, Moderna, Inc.) [204]. This candidate mRNA vaccine consists of six different mRNA species coding for HCMV gB and individual compents of the pentameric complex [204]. The mRNA vaccines have been shown to be highly effective against severe acute respiratory syndrome coronavirus 2 (SARS-CoV-2) during the coronavirus disease-2019 (COVID-19) pandemic[205,206]. Despite these advances, more prevention and treatment options are needed. Intriguingly, the occurrence of HCMV disease was significantly reduced in transplant recipients given inhibitors of mammalian target of rapamycin (mTOR), which is essential for replication in myeloid cells, particularly in late phase of viral cycle[207,208]. This presents the concept that interfering with host pathways can inhibit HCMV replication *in vivo*.

1.2 Reactive oxygen species, redox signalling, and oxidative stress

1.2.1 Free radicals

Cellular metabolism can generate free radicals within a cell[209–212]. Free radicals are atoms or molecules that contain at least one unpaired electron in their outermost shell[209–212]. The presence of unpaired electrons makes these molecules unstable, highly reactive, and very short lived[209–212]. Free radicals can interact with other molecules to accept or donate electrons through reduction-oxidation (redox) reactions[209–212].

Redox is a chemical reaction that involves the transfer of electrons and oxygen between two molecules[209–212]. Reduction involves loss of oxygen atoms and gain of electrons[209–212]. In contrast, oxidation occurs when a molecule gains oxygen and losses one or more electrons[209–212]. Consequently, a reduced molecule is an oxidant (accepts electron) and an oxidised molecule is a reductant (donates electrons) [209–212]. Both reduction and oxidation occur simultaneously[209–212].

Many different types of free radicals are generated by intracellular processes. Examples of free radicles generated in biological systems include superoxide ($O_2^{\bullet -}$), hydroxyls ($HO^{\bullet}$), peroxyl radicals ($ROO^{\bullet}$) and nitric oxide ($NO^{\bullet}$)[209–212]. Two free radicals often combine to form a more stable reactive molecule (non-radical molecules) [209–212]. Electron transfer reactions that lead to the production of different types of ROS are summarised in Figure 1.3. For example, hydrogen peroxide (H_2O_2) and peroxynitrite ($ONOO^-$) are formed when a superoxide molecule reacts with superoxide or nitric oxide, respectively[209–212]. Collectively, these molecules are known as reactive oxygen species (ROS) [209–212]. Nitric oxide and peroxynitrite are often referred to as reactive nitrogen species (RNS) as well[209–212]. Nonetheless, ROS/RNS are essential in response to physiological and pathological stimuli.

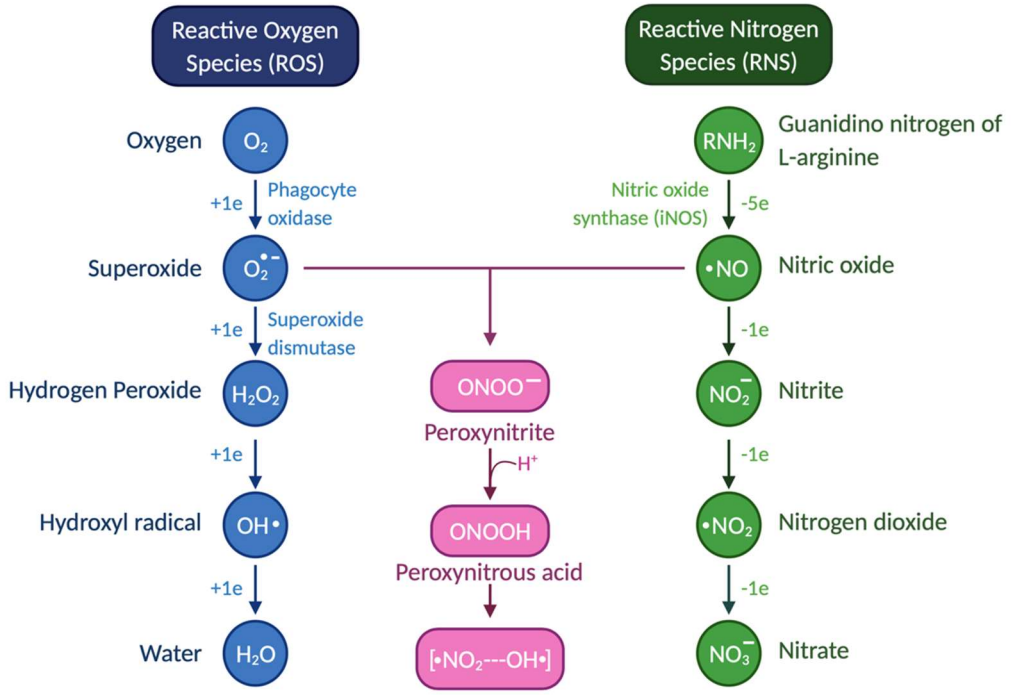

Figure 1.3: Generation of ROS/RNS through transfer of electros.

1.2.2 Reactive oxygen species (ROS)

ROS are readily produced by-products of aerobic metabolism[209–212]. ROS are oxygen-containing reactive molecules that can directly interact with multiple biomolecules (e.g., DNA, proteins, and lipids) to modulate a range of cellular functions, depending on the type, location, level, and timing of ROS production[209–212]. ROS can be divided into three types, depending on their reactivity[209–212]. Type 1 ROS are the first to be generated[209–212]. They include superoxide, hydrogen peroxide and nitric oxide[209–212]. They have relatively low reactivity and regulate physiological functions at nanomolar concentrations[209–212]. At high levels, Type 1 ROS are rapidly converted to the other two types of ROS. Type 2 ROS (e.g., peroxynitrite and hydroxyl radicals) are highly reactive and are important regulators of oxidative stress[209–212]. Whereas Type 3 ROS (e.g., nitrite, peroxyl and carbonate radicals) are considered strong inducers of oxidative stress as they mostly promote actions initiated by Type 2 ROS [209–212]. It has been demonstrated that all types of ROS can influence various signalling pathways, which in turn can impact the level of intracellular ROS[209–212]. These interactions can be complex and determine the fate of the cell in response to stimuli.

Intracellular ROS regulates a range of cellular functions including cell survival, homeostasis, immunity, and cell death[211,213–215]. ROS do not only function as signalling molecules to control multiple physiological functions at a cellular level but can also contribute to multiple pathological conditions[212,213,216,217]. Consequently, cells deploy multiple cellular antioxidant defence (AOD) mechanisms that are essential to modulate and maintain ROS at physiological levels[212,213,216–218]. The dualistic role of ROS with their constructive and destructive characteristics highlights the complexity of redox signalling.

1.2.3 Sources of ROS/RNS

There are many exogenous and endogenous sources of ROS/RNS in cellular systems. Exogenous triggers include radiation, environmental pollutants, cigarette smoking, heavy metals, drug compounds, industrial solvents, pesticides, specific foods, and nutrients[214,216]. Endogenous sources of ROS include cellular organelles, such as mitochondria, endoplasmic reticulum (ER) and peroxisomes[214,216]. There are several enzymes that are also involved in intracellular production of ROS. Superoxide is usually the first type of ROS to be generated as it necessary for production of other types of ROS. Examples of ROS generating enzymes include nicotinamide adenine dinucleotide phosphate (NADPH) oxidases (NOX), xanthine oxidases (XO), nitric oxide synthases (NOS) and superoxide dismutases (SOD) [214,216]. The complex interplay between multiple ROS generators regulates redox signalling and the outcome of oxidative stress[219–223].

The main interactions that have been observed are as follows:

i. NOX-derived ROS mediated upregulation of mitochondrial ROS (mtROS).
ii. mtROS mediated stimulation of NOS
iii. Mitochondrial/NOX-derived regulation of NOS and XO.

1.2.3.1 Mitochondrial electron transport chain

Mitochondrial electron transport chain (ETC) and NOX are major sources of ROS *in vivo*[214,216,219,224,225]. Most intracellular ROS is thought to come from the mitochondria[214,216,219,224,225]. The ETC is a series of electron transporters located throughout the inner mitochondrial membrane[214,216,219,224,225]. It is composed of four protein complexes (complex I-IV) and mobile associated electron carriers[214,216,219,224,225]. Superoxide is generated from electrons that 'leak' out of the ETC during the synthesis of adenosine triphosphate (ATP) [214,216,219,224,225]. Escaped electrons react with oxygen to generate superoxide radicals[214,216,219,224,225]. There are two main sites for superoxide generation in the ETC: complex I (NADH dehydrogenase) and complex III (coenzyme Q-cytochrome c reductase)

[214,216,219,224,225]. Mitochondrial SOD (mtSOD) rapidly converts superoxide to hydrogen peroxide[214,216,219,224,225]. Furthermore, iron-sulphur (Fe-S) clusters located in the ETC are hotspots of redox reactions[214,216,219,224,225]. They attract superoxide and nitric oxide, which rapidly react and generate peroxynitrite[216,220].

1.2.3.2 The NOX Family

The NOX family are also important generators of ROS. There are 7 isoforms of NOX in humans: NOX1-5, Duox1 and Duox2[216,219,226–229]. NOX is a transmembrane enzyme located in the plasma membrane (all isoforms) and in membranes of various organelles, including the nucleus (NOX4 and 5), ER (NOX2, NOX4 and NOX5) and mitochondrial membrane (NOX4) [216,219,226–229]. NOX were first discovered in membranes of phagocytes but can also be found in endothelial cells, vSMC, stem cells and fibroblasts[216,219,226–229]. In general, the NOX enzyme is composed of two membrane-bound subunits (p22phox and gp91phox), three cytosolic subunits (p40phox, p47phox and p67phox) and an associated GTPase (Rac) [216,219,226–229]. These subunits form a complex that is necessary for NOX activation[216,219,226–229]. Additionally, *in vivo* mice models have revealed that the essential for ROS (Eros) protein is also important for NOX activity[230]. Eros is a highly conserved transmembrane protein between mice and humans, which is required for the expression of NOX membrane-bound subunits[230]. Impaired superoxide generation was observed in cells from Eros deficient mice, *in vitro*[230]. Eros deficient mice were highly susceptible to infections, most likely due to a diminished respiratory burst by phagocytes[230]. Intrigingly, In humans, EROS mutations have been shown to be a direct cause of cause chronic granulomatous disease; a hereditary immune disorder in which immune cells are unable to generate ROS, leading to chronic inflammation and increased risk of opportunistic infections[231–233]. In fact, several different mutations in phagocyte NOX2 have been linked to chronic granulomatous disease[231,232]. Additionally, mutations in different subunits of NOX have also been linked to other auto-immune disorders, including systemic lupus erythematosus (p67 phox/gp91phox), inflammatory bowel disease (p40phox/gp91phox) and arthritis (p47phox)[231]. It is widely accepted that diminished or complete loss of ROS

production is largely due to mutations in genes encoding NOX isoforms, reducing their functional capacity[231,232]. However, not all loss-of-function mutations are damaging. For example, it has been shown that gp91phox knockout mice are protected from influenza infections[234]. Most NOX produce superoxide by mediating the transfer of an electron from NADPH to oxygen[216,219,226–229]. In contrast, NOX4, Duox1 and Duox2 can directly generate hydrogen peroxide[216,219,226–229].

1.2.3.3 The NOS family

Nitric oxide is generated by the NOS family. There are three isoforms of NOS: neuronal (nNOS), endothelial (eNOS) and inducible (iNOS) [211,220,235,236]. Although the names suggest NOS isoforms are tissue-specific, that is not the case[211,220,235,236]. For example, nNOS is not exclusively expressed in neurons in the brain[211,220,235,236]. It has also been detected in the spine, pancreatic islets, vSMCs and in the epithelial lining of various organs[211,220,235,236]. eNOS is expressed in multiple cell types as well, including endothelial cells, platelets, cardiac myocytes, and renal epithelial cells[211,220,235,236]. Whereas iNOS can be induced by specific stimuli in almost every type of cell[211,220,235,236]. The NOS family catalyses the oxidation of L-arginine to produce L-citrulline and nitric oxide[211,220,235,236]. Interestingly, under specific conditions, NOS can also facilitate the production of superoxide[217,235,237]. This is largely dependent on the levels of the NOS cofactor tetrahydrobiopterin (BH4) [217,235,237]. For example, with high levels of BH4, NOS is 'coupled' with it so efficiently catalyses the production of nitric oxide from oxidation of L-arginine[217,235,237]. However, when BH4 levels are low, NOS is uncoupled and produces superoxide along with nitric oxide[217,235,237]. This, in turn, facilitates peroxynitrite generation, which rapidly oxidises BH4 to maintain the uncoupling of NOS[217,235,237].

1.2.4 Antioxidant defence mechanisms

Aerobic organisms have evolved a robust antioxidant system to regulate the redox environment[220,238,239]. Antioxidant defences (AOD) include superoxide dismutase (SOD) which play an important role in the decomposition of superoxide[220,238,239].

In humans, three SOD isoforms have been identified (SOD 1-3) [220,238,239]. SOD1 is expressed in all types of cells and tissues[220,238,239]. It predominantly catalyses the dismutation of superoxide in the cytosol or mitochondrial ETC[220,238,239]. SOD2 is also widely expressed and is particularly active in the mitochondrial matrix to protect against ROS-mediated apoptosis[220,238,239]. Whereas SOD3 is selectively expressed in lungs, kidneys, and blood vessels[220,238,239]. It is the only form of SOD that be secreted into the extracellular matrix and can remove superoxide in the extracellular space. [220,238,239]. Removal of superoxide prevents the activation of many ROS pathways. In contrast, thiol peroxidases are particularly efficient at degrading peroxynitrite[220,238,239]. Similarly, catalases (CAT) are important in protecting cells from hydrogen peroxide-mediated damage[220,238,239]. They catalyse the decomposition of hydrogen peroxide into water and oxygen[220,238,239]. These enzymes are mainly found in peroxisomes and are enriched in erythrocytes and different types of liver cells[220,238,239]. CAT only breaks down hydrogen peroxide if the level exceeds the physiological threshold[220,238,239]. In contrast, glutathione peroxidases (GPx) can sense even the slightest increase of hydrogen peroxide and trigger its removal[220,238,239]. They are also involved in the decomposition of free radicals [220,238,239].

1.2.5 Molecular Targets of ROS

ROS can interact with a wide range of biomolecules, including but not limited to nucleic acids, amino acids, proteins, and lipids[215,216,219,240]. ROS can directly bind to DNA, causing oxidation of deoxyribose or single-stranded breaks[215,216,219,240]. Purine nucleotides are particularly vulnerable to ROS-mediated oxidation and subsequent adduct formation[215,216,219,240]. Occasionally, ROS-mediated cellular damage may be irreversible, resulting in cell death by apoptosis or necrosis[215,216,219,240]. Similarly, ROS can also interact with lipids, resulting in peroxidation and the formation of oxidation-induced lipid adducts[215,216,219,240]. Such lipid modifications can lead to degradation of lipid membranes, increasing membrane permeability and altering membrane fluidity[215,216,219,240]. Lipid peroxidation can initiate apoptosis (NF-κB, MAPK, and PKC) and autophagy (mTOR),

leading to cell death[215,216,219,240]. ROS also modify redox-sensitive groups (such as cysteine, methionine, tyrosine residues) in proteins, altering structure and function[215,216,219,240]. For example, ROS enhances the expression and phosphorylation of numerous transcription factors, facilitating transcriptional upregulation of genes under their control[215,216,219,240].

1.2.6 Cellular functions of ROS

1.2.6.1 The role of ROS in innate Immunity

Innate immunity is a non-specific defence mechanism that provides the first line of defence against all invading pathogens, including different types of bacteria and viruses[241,242]. The cells involved in the innate immune response recognise invading pathogens with TLRs and induce the production of proinflammatory cytokines and chemokines[241,242]. These, in turn, initiate complex inflammatory signalling cascades through the activation of inflammatory cells and stimulation of ROS-forming enzymes[216,217,219,242–244]. Certain cells involved in the innate immune response may phagocytose foreign substances and activate the adaptive immune system by presenting segments of the digested pathogen on their cell surface[241,242,244]. During phagocytosis of pathogen or infected cells, professional phagocytes increase oxygen consumption due to an increase in cellular metabolism[140,141,227,241,242,245]. This triggers respiratory burst, a process in which phagocytes rapidly release high levels of ROS due to catalytic reduction of molecular oxygen to superoxide and other oxygen-containing derivatives[140,141,227,242,246]. This action is predominantly driven by the enhanced activity of membrane-bound NOX[226,227,242,246]. Studies have shown that NOX2 expression is upregulated in membranes of vesicles that contain engulfed particles[226,227,242,246]. These vesicles are known as phagosomes and are vital for the degradation of unwanted biological materials[226,227,242,246]. Other intracellular ROS-producing enzymes, such as NOS, are equally important in producing a robust immune response against pathogens[214,216,219,242]. The rapid release of increasingly high quantities of ROS inside the phagosome shortly after phagocytosis prevents biological material to escape into the cytoplasm [214,216,219,242]. Furthermore, TLR signalling can also trigger

other sources of ROS, including mitochondrial ETC [214,216,219,242]. For instance, endosomal ROS production is increased in response to many viruses, mainly due to ligation of TLR7[247]. Mice deficient in TLR7 demonstrated a diminished antiviral response due to the complete absence of virus-induced generation of endosomal ROS[247].

ROS also modulates other aspects of innate immunity, including type 1 IFN signalling and antigen presentation[247]. For example, ROS regulates the production of type I IFNs[247]. These pleiotropic cytokines possess antiviral and immunomodulatory functions[247]. Consequently, dysregulation of type 1 IFN signalling can lead to autoimmunity and ineffective antiviral response[247]. For instance, loss of the p47phox NOX subunit has been linked to increased expression of type 1 IFN genes in models of autoimmune diseases, including arthritis and chronic granulomatous disease[231,247]. Furthermore, macrophages deficient in the gp91phox NOX subunit have been shown to enhance IFN signalling[247]. Overall, these studies suggest that ROS-mediated inhibition of type I IFN might be essential to prevent autoimmunity[247]. However, it is important to note that type I IFNs are crucial for antiviral immunity. For example, in absence of SOD2, RNA virus-driven IFN production and release of proinflammatory cytokines are severely impaired, leading to enhanced viral replication[247]. This highlights the crucial role of antioxidant systems in modulating ROS-mediated suppression of type I IFN signalling; to ensure ROS production is maintained at levels that efficiently prevent autoimmunity without compromising antiviral immune responses[247].

ROS can also influence antigen presentation by innate immune cells, ultimately affecting adaptive immune responses as well[247]. In fact, dendritic cells that are deficient in NOX2 demonstrate enhanced protein degradation and impaired cross-presentation[247]. Intriguingly, it has been demonstrated that ROS can control autophagy; an important cellular process for the recycling of proteins and degradation of damaged components[247,248]. ROS can activate several enzymes that activate autophagy and generate a negative feedback loop, inhibiting the

production of ROS, especially when levels exceed the physiological threshold[247–249]. Excessive ROS production leads to the accumulation of ROS-induced damage, which can have detrimental effects on health.

Several non-phagocytic cells can also initiate the production of ROS in response to invading pathogens, including epithelial that line organs such as the gastrointestinal tract, lung alveoli and kidney tubules[246]. Additionally, studies have shown that ROS can also function as regulators of signal transduction[216,219]. Overall, ROS have important physiological significance due to their (1) direct biocidal effects on invading pathogens and (2) role as second messengers of intracellular signalling pathways[216,219].

1.2.6.2 The direct role of ROS in elimination of pathogens

ROS can eliminate pathogens by direct oxidative-induced damage[242,246,250]. Superoxide cannot diffuse across membranes and thus may not be sufficient to efficiently kill microbes[242,246,250]. However, superoxide undergoes spontaneous or enzymatic dismutation upon infection, resulting in the production of hydrogen peroxide[216,219]. Furthermore, superoxide rapidly reacts with nitric oxide to generate peroxynitrite[216,219]. Unlike superoxide, these molecules can easily diffuse through membranes, causing excessive damage to genomes, proteins, and lipid structures in pathogens[217,246,251,252]. The microbicidal effect of hydrogen peroxide mainly stems from its ability to oxidise iron to form highly reactive hydroxyl radicals[217,246,251,252]. These molecules are extremely small and can freely diffuse through the outer membranes of viruses and bacteria[217,246,251,252]. For example, hydroxyl radicals can induce the peroxidation of lipids and/or proteins in viral envelopes and capsids, inhibiting virus-host interactions[217,246,251,252]. Similarly, peroxynitrite can alter protein structure and function following its interaction with cysteine residues[217,246,251,252]. ROS can also interact with both purine and pyrimidine bases, causing modifications that can lead to single or double-stranded breaks in DNA[217,246,251,252]. For example, hydroxyl radicals can disrupt disulphide

bonds in DNA[217,246,251,252]. Likewise, peroxynitrite-mediated oxidation or nitration of guanine nucleobases leads to DNA fragmentation and endonuclease cleavage, respectively[217,246,251,252]. Type 2 and 3 ROS can also enter the extracellular matrix where mediate pathogen degradation and trigger the activation of immune responses in neighbouring cells[217,246,251,252].

1.2.6.3 The role of ROS in transcriptional regulation

The primary regulatory mechanism controlling cell signal transduction is reversible protein phosphorylation, which involves a tightly coordinated balance between the activity of multiple kinases and phosphatases[215,216,219]. ROS can readily interact with components of intracellular signalling cascades, shifting this delicate balance.

It is well established that activation of cell surface receptors (PDGFR and EGFR) triggers ROS generation [215,219,220]. ROS can act upstream or downstream of these receptors to facilitate receptor-mediated signalling[215,219,220]. For example, ROS readily activates mitogen-activated protein kinase (MAPK) and other downstream targets of PDGFRα signalling[215,219,220]. These are involved in modulating cellular responses to mitogens, osmotic stress, and proinflammatory cytokine[215,219,220]. At the same time, ROS can act upstream and continuously activate PDGFRα [253]. Prolonged PFGFRα activation has been shown to increase the production of mtROS and enhance suppression of autophagy through activation of mTOR[253].

Similarly, activation of TNFR can also induce ROS production, which activates NF-kB and mediates its translocation to the nucleus[215,216,219,220]. NF-kB regulates expression on several pro-inflammtory genes, including those that encode inflammatory cytokines such as IL-6 and TNF-α [215,216,219,220]. NF-kB is also important in regulating genes required for cell survival and activation of innate immunity[215,216,219,220]. ROS also activates other transcription factors, such as activator protein 1 (AP-1) and hypoxia-inducible factor 1α (HIF-1α), that regulate

several genes involved in proliferation, differentiation, cellular adaptation, and apoptosis[215,216,219,220].

Apart from activating transcription factors that drive pro-inflammatory gene expression, elevated levels of ROS also activate Nrf2 by dissociating it from its cytosolic inhibitor, kelch-like ECH-associated protein-1 (Keap1) [215,216,219,220]. Phosphorylated Nrf2 can translocate to the nucleus and initiate transcription of anti-inflammatory genes, including those that encode antioxidants that can attenuate the harmful effects of ROS[215,216,219,220]. Therefore, Nrf2 activation helps maintain a physiological microenvironment by reducing oxidative stress and systemic inflammation[215,216,219,220].

1.2.6.4 The role of ROS in regulating the physiological and pathological response to stimuli

The cellular redox environment is constantly changing. At homeostasis, intracellular mechanisms maintain a balance between generation and elimination of ROS[213,214]. Here, brief pulses of Type 1 ROS are enough to ensure cell survival, metabolism, proliferation, and differentiation (Figure 1.4) [216,217]. Intracellular pathways can suppress or increase ROS production as the need of the cell changes. For example, activation of cell surface receptors upon pathogen recognition triggers ROS production and subsequent activation of multiple signalling cascades[215,216,219]. Accumulation of ROS eventually leads to oxidative stress, which is necessary for the physiological response to stimuli[216,238]. Consequently, Nrf2 is activated by increased ROS to upregulate the expression of antioxidant genes, thereby regulating oxidative stress-mediated physiology[215,216,219]. At this stage, antioxidant defence systems can often reduce, reverse, or repair oxidative damage to maintain an environment that encourages physiological signalling (Figure 1.4) [216]. However, prolonged oxidative stress can cause detrimental damage to DNA and other macromolecules, ultimately leading to the activation of pathways that trigger cell death (Figure 1.4) [216,254].

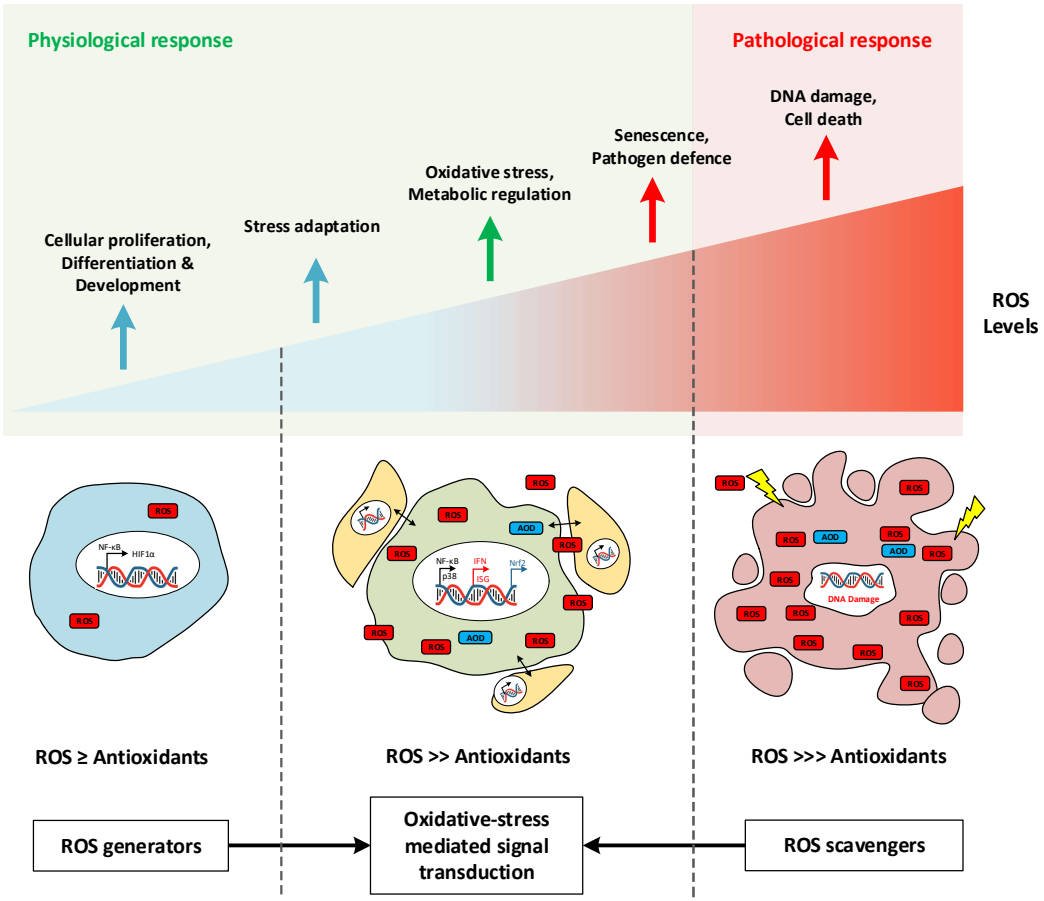

Figure 1.4: Role of ROS in cellular physiology and pathology.

At homeostasis, ROS production and elimination are well balanced, creating a cytostatic environment. A brief increase in ROS mediates proliferation and differentiation (Left panel, blue cell). As ROS levels continue to increase, cells trigger mechanisms to ensure they can adapt to changes in the redox environment. Accumulation of ROS triggers oxidative stress (middle panel, green cell). Transient oxidative stress is required for conducive physiological signalling (e.g., in response to invading pathogen). Oxidative stress activates multiple signalling cascades required for Intra – and intercellular signalling in response to stimuli (e.g., cell survival via MAPK, NF-KB etc). Nrf2 is also activated by increased ROS to trigger the expression of antioxidant genes, thereby regulating oxidative stress-mediated physiology. Antioxidant defence (AOD) systems work to reduce, reverse, or repair oxidative damage, maintaining a redox-adapted environment. However, when ROS production exceeds the capacity of AODs, cellular damage will be irreversible, leading to oxidative stress-mediated programmed cell death (Right panel, red cell). Figure generated with reference to [213] and [245].

1.2.7 The pro-viral effects of ROS

It is well established that many viruses increase oxidative stress[128,255]. While the exact role of ROS in some viral infections remains unclear, certain viruses use intracellular ROS to enhance replication and/or pathogenesis[128,255]. For example, ROS has been shown to enhance HIV, HSV-1, influenza and KSHV entry and replication[128,255]. Intriguingly, these pathogens have also evolved multiple ways to combat ROS-mediated host immune response through modulation of Nrf2-mediated antioxidative signalling[255]. The three most common mechanisms exploited by different viruses to regulate intracellular ROS include (1) deregulation of mitochondria, (2) upregulation of NOX and (3) modulation of the Nrf2 pathway[255].

Different viruses increase the production of mtROS by targeting different ROS-forming components within the mitochondria. For example, HSV-1 and HSV-2 decrease the membrane potential of mitochondria causing electrons to leak from the ETC into the cytoplasm; where they rapidly reduce oxygen molecules to form superoxide[255]. Similarly, adenovirus, rhinovirus and human papillomavirus have been reported to destabilise the mitochondrial membrane[255]. Furthermore, viruses such as rubella, rabies, HIV and hepatitis C have the ability to increase the enzymatic activity of mitochondrial complexes in the ETC[255]. Additionally, HIV encoded accessory protein, viral protein R, has been shown to increase membrane permeability by binding to inner channel of the mitochondrial permeability transition pore[255]. Although the exact mechanisms are unknown, SARS-CoV-2, Zika and Influenzas viruses are also known to deregulate mitochondria[255].

The majority of viruses also influence the enzymatic activity of NOX. They can activate NOX enzymes and/or upregulate the expression of NOX isoforms at their subcellular locations[255]. The activation of NOX isoforms increases the production of superoxide. For example, EBV and vaccinia virus increase the NOX2-derived ROS in endosomes[255]. In fact, EBV encoded EBNA-1 protein has been shown to activate transcription of NOX2[255]. In contrast, coxsackievirus B3 upregulates the expression

of NOX4[255]. Similarly, hepatitis C triggers superoxide formation by activating NOX1 and NOX4 through its NS5A viral protein[255]. Intriguingly, Influenza A can induce activation of several NOX enzymes, including enhanced NOX2 activity in macrophages following activation of TLR7[255]. Relatedly, several HIV encoded proteins also modulate the activation of different NOX enzymes[255]. For example, HIV envelope protein, gp120, induces ROS through activation of NOX2 and NOX4, whereas, HIV Nef protein directly interacts with compoenents of NOX1-3, activating superoxide formation[255]. Dengue virus and rhinovirus have been shown to increase NOX-derived ROS but the specific NOX enzyme it influences remains unknown[255].

Finally, most viruses have evolved mechanisms to modulate the Nrf2-induced antioxidant signalling. H5N1 and H7N9 strains of Influenza A virus reduce activation of Nrf2, delaying activation of anti-inflammatory responses[255]. In contrast, HCMV upregulates the expression of Nrf2, using Nrf2-mediated signalling to evade host immune response by increasing the ability of host cells to cope with virus-induced oxidative stress[166,255]. Intriguingly, some viruses can both activate or inhibit the nuclear translocation of Nrf2[255]. For instance, the dengue virus activates Nrf2 during the initial stages of viral replication but targets Nrf2 for proteasomal degradation at later stages of infection[255]. Other viruses, including HSV, EBV, HIV and Zika have also been shown to modulate Nrf2-mediated antioxidant responses during infection[255].

Overall, these studies show that intracellular ROS production could be a potential target for developing novel antiviral treatments, where using pharmacologic inducers of Nrf2 and/or selective inhibitors of NOX and mtROS inhibits viral replication[255].

1.3 CRISPR-Cas9: a powerful gene-editing tool

1.3.1 Adaptive immunity in prokaryotes

Clustered-regularly interspaced short palindromic repeats (CRISPR) and their associated proteins (Cas) form the adaptive immune system in most bacteria and archaea[256]. Upon encountering mobile genetic elements, many bacteria and archaea employ CRISPR-associated nucleases (Cas) to create double-stranded breaks (DSB) in viral DNA[256]. The genomic region targeted by the CRISPR-defence system is located upstream of a protospacer-adjacent motif (PAM) [256]. PAM is a short DNA sequence that is crucial for target site recognition by Cas proteins[256]. Cleavage of viral DNA results in two main outcomes: viral clearance and anti-viral memory[256]. Consequently, if the prokaryotic cell were to re-encounter the same virus, the CRISPR-Cas defence system can rapidly recognise, target, and inactivate the threat. The CRISPR-Cas defence system can be categorised into three main types, depending on the expression of Cas genes. All types and subtypes of CRISPR-Cas systems contain Cas1 and Cas2 proteins[256]. However, type I is specifically associated with Cas3, type II with Cas9 and type III with Cas10[256].

1.3.2 The CRISPR-Cas9 Defence System

The CRISPR-Cas9-mediated adaptive immune response can be divided into two phases: acquisition and defence (Figure 1.5) [256,257]. In the acquisition phase, bacteria are immunised against invading viruses. Upon bacteriophage infection, Cas1-Cas2 cleave viral DNA and integrate the fragments (known as spacers) into the bacterial genome at CRISPR loci, generating phage-specific CRISPR arrays that provide a memory of primary infection[256,257]. Bacteria and archaea can have single or numerous CRISPR arrays in their genomes[256,257]. Following re-exposure to the same bacteriophage (phase 2), CRISPR arrays are rapidly transcribed into trans-activating CRISPR RNA (tracrRNA) and precursor CRISPR RNA (pre-crRNA), containing Cas protein binding sites and complementary target sequences, respectively[256,257]. This pre-crRNA is processed into mature crRNA that forms a

complex with tracrRNA, generating multiple virus-specific guide RNAs (gRNA) [256,257]. Cas9 is directed by gRNA to complementary sites within the infiltrating viral DNA[256,257]. CRISPR-Cas9-mediated cleavage occurs following the binding of crRNA to the target DNA[256,257]. The stages of the CRISPR-Cas9 system are described in Figure 1.5.

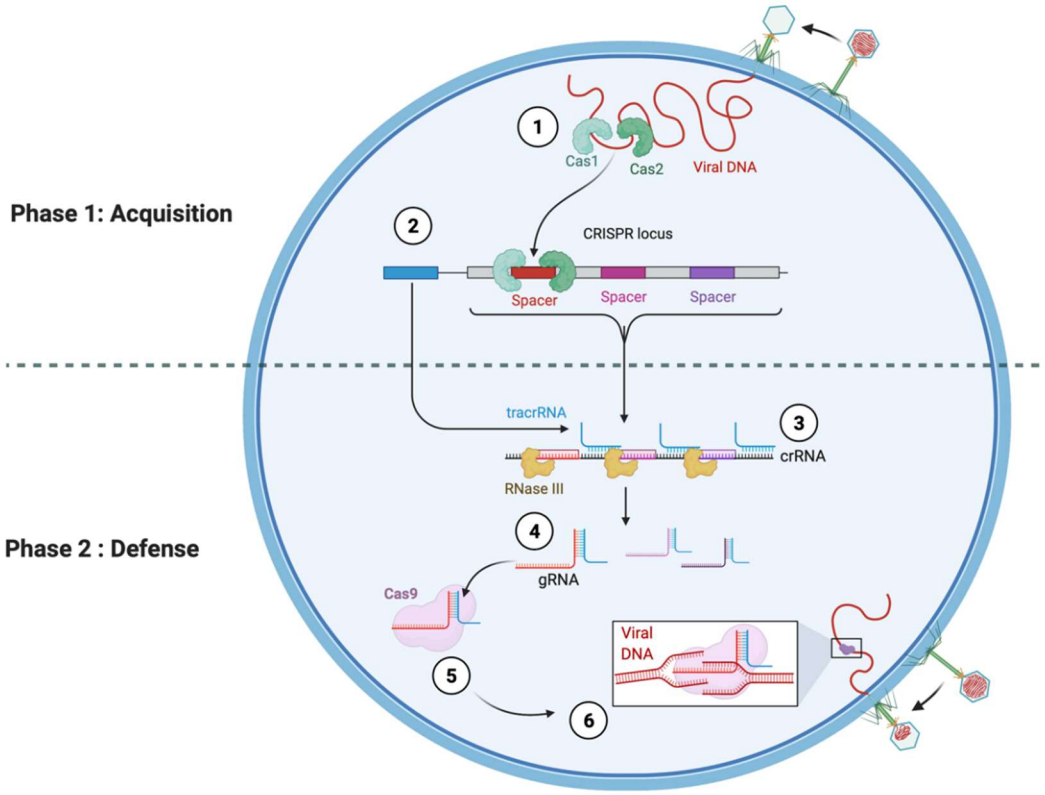

Figure 1.5: CRISPR-Cas9-mediated adaptative immunity in bacteria.

Upon initial exposure (1) Cas1-Cas2 complex process and cleave viral DNA.(2) Fragments of viral DNA are incorporated as spacers within the CRISPR locus of the bacterial genome to provide memory of initial encounter. (3) Following re-infection, memory is retrieved during transcription of tracrRNA and pre-crRNA. (4) Pre-crRNA are processed into crRNA that bind to tracrRNA and produce gRNA. (5) gRNAs bind to Cas9-gRNA and direct it to complementary sites in the viral DNA. (6) Cas9-mediated cleavage degrades viral genome. Adapted from "CRISPR-Cas9 Adaptive Immune System of *Streptococcus pyogenes* Against Bacteriophages'', by BioRender.com (2022). Retrieved from https://app.biorender.com/biorender-templates

1.3.3 CRISPR-Cas9 as a tool for gene editing.

Recent advances in genome engineering technologies have led to cost-effective gene-editing tools, allowing genetic material to be modified with great precision and ease. The Nobel-prize winning CRISPR-Cas9-based system is largely accepted as the most efficient tool for genome modification due to the simplicity with which it can introduce loss-of-function mutations in target cells[258–260]. Other genome-editing tools, such as zinc-finger nucleases (ZFN) and transcription activator-like effector nucleases (TALEN) requires one to engineer and synthesize specific proteins to recognise target sites through DNA-protein interactions[261,262]. The design and assembly of ZFNs and TALENs can be a long, complicated, and expensive process[261,262]. Furthermore, even though ZFNs and TALENs recognise target DNA sequences at high specificity, the genome editing efficiency remains low[261,262]. In contrast, CRISPR does not require one to synthesise specific proteins to edit the target sequence. Instead, it uses guide RNAs (gRNA) to direct a DNA endonuclease, such as CRISPR-associated protein 9 (Cas9), to a specific genomic location to introduce mutations to be introduced in the target cell[261,262].

1.3.4 CRISPR-Cas9-mediated gene editing

Cas9 derived from *Streptococcus pyogenes* is the most widely used endonuclease for genetic editing[259,260]. However, many Cas9 orthologs exist in other bacterial and archaeal species[259,260]. These Cas9 alternatives may have additional characteristics more suitable for certain applications[259,260]. For example, Cas9 from *Staphylococcus aureus* is significantly smaller than the Cas9 from *Streptococcus pyogenes,* allowing it to be efficiently packaged into smaller expression systems such as adeno-associated virus (AAV) vectors[259,260]. Furthermore, several Cas9 variants have been engineered to cater for specific genome editing needs such as increasing the target range, or editing efficiency[259,260].

The genomic region targeted by the CRISPR-Cas9 system is located upstream of a protospacer-adjacent motif (PAM) [259,260]. PAM is a short DNA sequence, about 2-6

nucleotides in length, and is crucial for target site recognition by the Cas9-gRNA complex[259,260]. The PAM sequence recognised by Cas9 from *Streptococcus pyogenes* is NGG[259,260]. Alternative CRISPR-Cas endonucleases recognise different PAM sequences[259,260] . Once the target site has been identified, the gRNA base pairs to the target DNA sequence that is adjacent to PAM[259,260]. Complementary base-pairing of the gRNA to target DNA promotes R-loop formation within the gRNA, enabling endonuclease activation and subsequent double-strand scission upstream of the PAM[259,260].

Cleavage of DNA by Cas9 activates cellular DNA repair mechanisms to maintain genome stability within a cell[259,260]. There are two main pathways that can be activated to repair DSB in mammalian cells: the non-homologous end joining (NHEJ) pathway or the homology-directed repair (HDR) pathway (Figure 1.6) [259,260]. The NHEJ pathway is activated when a repair template is not present[259,260]. This system is error-prone and allows random mutagenesis to occur during the NHEJ repair[259,260]. For example, NHEJ can result in frameshift mutations due to random insertions or deletions (indels) at the DSB repair site (Figure 1.6) [259,260]. Alternatively, it can cause substitutions when repairing the DSB, resulting in loss-of-gene function (LoF) (Figure 1.6) [259,260]. In contrast, the HDR pathway uses a repair template, containing a DNA sequence identical to the one at the repair site prior to DSB, to repair the DSB (Figure 1.6) [259,260]. The presence of homologous donor DNA makes HDR error-free[259,260]. Consequently, this system can be harnessed to introduce site-specific gene modifications by delivery of a donor template designed to promote homologous recombination at the targeted repair site (Figure 1.6) [259,260]. For example, gain-of-function (GoF) mutations can be made by DNA templates that allow precise knock-ins, replacements or corrections (Figure 1.6) [259,260]. Similarly, precise LoF mutations can be introduced with a donor template containing precise point mutations[259,260].

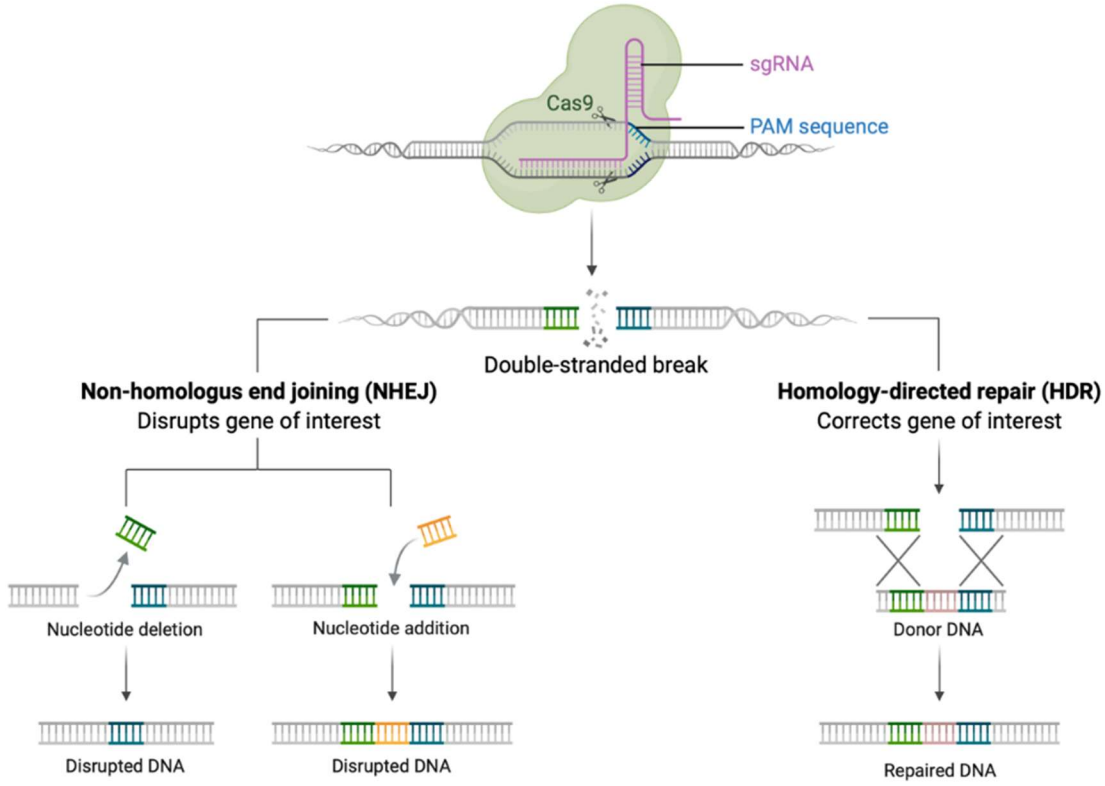

Figure 1.6: CRISPR-Cas9 as a tool for gene editing.

Cas9 is directed by a synthetic gRNA to induce DSB at a chosen site within target gene locus. DNA repair by the error prone NHEJ method randomly introduces indels to disrupt gene function. Alternatively, HDR can facilitate precise genome editing using a replacement DNA template with complementary ends. Adapted from "CRISPR/Cas9 Gene Editing", by BioRender.com (2022). Retrieved from https://app.biorender.com/biorender-templates

1.3.5 Applications of CRISPR-Cas9 system

The CRISPR-Cas9 system was originally used to knock out target genes in various cell lines and model organisms, however, modifications to Cas enzymes have expanded the applications of this technology[257,259,263]. For example, Cas9 can be modified such that it retains the ability to bind to DNA but can no longer cleave the target. This inactive Cas9 variant can then be fused with transcriptional repressors or activators, enabling CRISPR-mediated gene repression or activation, respectively[257,259,263]. Similarly, gene expression can be altered without inducing double-strand scission by fusing an epigenetic modifier to a mutated Cas protein[257,259,263]. This has revolutionary implications for gene therapy where genetic material can be introduced to cells to compensate for mutated and/or missing genes or generate functional proteins to prevent and/or treat a range of genetic diseases and disorders. For example, CRISPR-Cas9 technology has been shown to restore the function *dystrophin* in both *in vitro* and *in vivo* models of Duchenne muscular dystrophy; a fatal neuromuscular disease[264,265]. In contrast, delivery of gRNAs targeting multiple genes simultaneously provides a simple framework for large-scale mutagenesis studies[266,267]. The application of this strategy to genome-wide CRISPR-based screens has enabled the identification of novel genes involved in regulating phenotypes, including genes essential for drug resistance, viral infections, tumour growth and metastasis[268–270]. For example, CRISPR-mediated loss-of-function genetic screens have helped identify and characterise host genes that are essential for Influenza A, HIV, West-Nile, Dengue and Zika viruses[271–274].

1.4 Aims and Hypothesis

It is well-established that HCMV relies on multiple host factors to establish infection. Despite this, surprisingly few HCMV-host interactions have been fully characterised, especially those involved in viral replication, assembly, and egress[275]. Current anti-HCMV therapies are focused on targeting viral genes and proteins[(183)]. This approach against HCMV can be effective but the scope is limited due to the emergence of antiviral resistance among HCMV strains[(199)]. Efforts made to understand the role of host genes, proteins and intracellular biochemical networks could provide important insights for developing novel antiviral strategies.

I hypothesise that targeting host genes and pathways that are essential for HCMV could help inhibit viral replication.

This thesis aims to:

1. Characterise the contribution of ROS generation in HCMV replication.
2. Conduct a genome-wide assessment to identify host factors required for productive HCMV infection.
3. Validate novel candidate host genes implicated in promoting HCMV replication.

2 Materials and Methods

2.1 Buffers, media, and solutions

Unless stated otherwise, all chemicals used were purchased from Merck or Fisher Scientific and all tissue culture reagents were from Gibco™ Life Technologies. Fetal calf serum (FCS) was heat inactivated prior to use. UltraPure distilled water (dH_2O) was used for preparation of buffers, media, and solutions. Table 2 provides details of buffers, media and solutions used.

Table 2: Details of buffers, media and solutions used

Reagent	Description
2% Avicel RC-591 solution	2 % (w/v) Avicel RC-591 (FMC Biopolymer) in dH_2O.
2$\boldsymbol{X}$ DMEM	50% (v/v) dH_20, 20% (v/v) 10X MEM, 20% (v/v) FCS, 1000 U/L penicillin, 1000 µg/L streptomycin, 4 mM L-glutamine and 0.45% (w/v) sodium bicarbonate.
2xYT medium	16 g/L tryptone, 10 g/L yeast extract (Oxoid) and 5 g/L sodium chloride in dH_2O.
4 % Paraformaldehyde (PFA)	4 % (w/v) paraformaldehyde in PBS.
Agar + ampicillin plates	5 g/L sodium chloride, 5 g/L yeast extract (Oxoid), 10 g/L tryptone, 20 g/L agar (Oxoid) and 50 mg/mL ampicillin in ddH_2O. Approximately 20 mL per 100 mm petri dish to set. Store at 4°C.
Ampicillin solution	50 mg/mL ampicillin sodium salt in 50% (v/v) absolute ethanol: dH_2O. Sterilized by passing through 0.22 µm filter.

D10	DMEM supplemented with 4.5 g/L L-glucose, 10% (v/v) FCS, 250 U/mL penicillin/streptomycin, 0.26 mg/mL L-Glutamine and 97 mg/mL sodium pyruvate.
D10 conditioned media	D10 media was conditioned by incubation with sub-confluent wild-type HFFF-TERT/ HFFF-TETs for 3 days. After, the collected media was centrifuged (1500 rpm, 5 min) to remove debris and the supernatant was filtered using a 0.22µm filter before use.
FACS Buffer	2% (v/v) FCS and 0.05% (w/v) sodium azide in PBS.
Freezing media	90% (v/v) FCS and 10% (v/v) DMSO.
Luria-Bertani (LB) broth	20 g/L of LB low salt broth (Melford) in dH_2O.
R10	RPMI 1640 supplemented with 10% (v/v) FCS, 250 U/mL penicillin/streptomycin, 2 mM L-glutamine, and 97 mg/ml sodium pyruvate.
Transfection mix	3% (v/v) Genejuice Transfection Reagent (Millipore) in R0 media (i.e., RPMI 1640 without FCS, antibiotics, or L-glutamine). The mix was incubated for 5 minutes at room temperature (RT) prior to use.

2.2 Tissue Culture

2.2.1 Cell lines

Human cell lines used are described in Table 3. All cell lines were regularly tested for Mycoplasma infection. Cas9-expressing target cells were generated as described in Section 2.7.1.2.

2.2.2 Maintenance of master stocks of each cell line

Approximately 1×10^6 cells/mL were suspended in freezing media (Section 2.1) and stored in Cryo.S 1 mL cryovials (Grenier Bio-One). The cells were first cooled to -80°C, at the rate -1°C per minute, before being transferred to vapor-phase liquid nitrogen (below -180°C).

2.2.3 Resuscitation of frozen cell lines

Cryovials were transferred to a 37°C water bath until most of the cells were thawed (approximately 1-2 minutes). Once completely thawed, the cells were gently pipetted into a falcon tube containing 10 mL of pre-warmed growth media. The cells were then centrifuged (at 1,500 rpm, for 5 min, at room temperature (RT) to remove any cryopreservation solution. The supernatant was discarded, and the cell pellet resuspended in 5 mL of complete growth media. The cell suspension was then transferred into a T25 tissue culture flask (Thermo Fisher) until confluent. After, the cells were maintained as described in Section 2.2.4 below.

2.2.4 Maintenance of cell lines in culture

Cell culture was carried out in a sterile Class II biological safety cabinet using aseptic techniques. All cells were incubated at 37°C and 5.0% carbon dioxide (CO_2). Cells were cultured in an appropriate cell culture medium (Table 2) pre-warmed to 37°C in a water bath, unless specified otherwise. Media was replaced every 3-4 days. All adherent cell lines were grown as monolayers in flat-bottomed cell culture flasks and/or plates. Suspension cell lines were initially propagated in tissue culture flasks and then differentiated as described in Section 2.2.5 before being used for

experiments. Mono-Mac-6 cells are semi-adherent and were cultured in 'Cell Bind' flasks and/or plates (Corning).

Once the cells were 80-90% confluent, they were passaged, usually every 3-4 days. All adherent cell lines were first washed with phosphate buffered saline (PBS), after which, they were incubated with 1×Trypsin-EDTA (for 2-4 minutes at 37°C) in order stimulate cell detachment. Once the cells detached from the flask surface, complete media was added to inactive trypsin-EDTA. The cells were then transferred to a falcon tube and centrifuged (at 1500 rpm, for 5 min, at RT). Supernatant was discarded, and the pellet was resuspended in an appropriate volume of complete media. The cells were seeded in cell-culture flasks and/or plates at the desired ratio. Suspension cells were passaged when they began to clump, at a ratio of 1:10, usually every 4-5 days.

2.2.5 Differentiation of monocytic cell lines

To differentiate monocytic cell lines (Table 3) into macrophages, cells were cultured in regular growth medium supplemented with 100 ng/mL phorbol 12-myristate 13-acetate (PMA). After 48h, by which time differentiated cells should have adhered to the culture dishes, PMA-containing media was replaced with regular growth medium. Degree of differentiation was also assessed by flow cytometry (Section 2.5) through expression of macrophage specific markers (CD14 and CD11b). HCMV infections were carried out the following day, after overnight incubation in PMA-free media.

Table 3: Details of cell lines used

Cell Type	Cell Line	Description	Media
Fibroblast	Primary HFFF*	Human Foetal Foreskin Fibroblasts	D10
	HFFF-TERT*	Human telomerase reverse transcriptase (hTERT) immortalised HFFF	
	HFFF-TET*	HFFF-TERTs expressing tetracycline repressor (TET_R)	
Epithelial	ARPE19*	An immortalised human retinal epithelial cell	D10
Kidney	293T*	Immortalised human embryonic kidney cells transformed with large T-antigen	D10
Monocytic	THP-1**	Human monocytic cell line derived from a patient with acute monocytic leukaemia	R10
	Mono-Mac-6**	Human monocytic cell line derived from peripheral blood of a patient with monoblastic leukaemia	
	U937**	Pro-monocytic human leukaemia cell line derived from patient with histocytic lymphoma	
Astrocytic	U373 MG (Uppsala)*	Human glioblastoma astrocytoma cell line	D10

2.3 HCMV generation

2.3.1 Virus stocks

All HCMV strains were provided by Prof Richard Stanton (Cardiff University) and are described in in Table 4. To monitor HCMV infection *in vitro*, all HCMV strains were previously engineered to express green fluorescent protein one day post infection (dpi), allowing infection state to be monitored through flow cytometry (Section 2.5).

Table 4: HCMV strains

HCMV-GFP strain	Cell type used for virus production	Description	pAL number
Merlin-UL128^{wt} *	HFFF-TET	Pentamer is restored after one round of replication in HFFF-TERT.	2344
Merlin-UL128^{mut} **	HFFF-TERT	Pentamer-deficient	2414
TB40/E	HFFF-TERT	Trimer and Pentamer	2413

wt = wildtype (repaired)
mut = mutated
* Merlin variant where the *UL128* locus, that acquired mutation during passage in fibroblasts prior to BAC cloning, has been repaired to wildtype.
** Merlin variant that contains a single point mutation in the *UL128* locus.

2.3.2 Growing HCMV

Confluent cell factories of HFFF-TETs or HFFF-TERTs were infected with virus at multiplicity of infection (MOI) of 0.01. MOI was calculated using the following formula:

$$volume\ of\ virus\ (mL) = \frac{MOI \times number\ of\ cells}{virus\ titer\ \left(\frac{PFU}{mL}\right)}$$

Once greater than 90% of the cells showed cytopathic effect (CPE), supernatants were harvested and replaced with fresh medium. This process was repeated every two days, until all cells were dead (usually around 8 days, giving 4 harvests per virus

preparation). The supernatants were transferred to 250 mL high-speed centrifuge pots and centrifuged (at 14000 rpm, for 2 hours, at 26°C) using JLA-16.250 rotor. The supernatant was discarded, and the virus pellet was resuspended in 1 mL of regular growth medium per centrifuge pot. The prep was then pooled, passed through a needle 4-5 times and transferred to a universal container. Aliquots were made and stored at -80°C until required. The viral titer was determined by plaque assay as described in Section 2.3.3.

2.3.3 Titrating HCMV

Primary HFFFs were used for titrating all HCMV strains. Titrations were performed in six-well plates containing 2.25×10^5 cells/well. After 24h, serially diluted virus was added in duplicates an incubated on a rocking platform (for 2h, at 37°C). The inoculum was then removed and replaced with 50:50 mix of 2% Avicel (Section 2.1) and $2X$ DMEM (Section 2.1). Cells were cultured under this semi-solid overlay for two weeks. After, the overlay was removed, and the cells were washed with PBS. Plaques were counted and the virus titer was calculated as plaque forming units per mL (PFU/mL) using the following formula:

$$\frac{PFU}{mL} = \frac{Average\ number\ of\ infected\ cells\ per\ field \times number\ of\ fields\ per\ well}{dilution\ factor \times volume\ of\ virus\ (mL)}$$

2.4 HCMV Infection Assays

2.4.1 Cell-free infection assay

A schematic diagram of cell free infection is shown in Figure 2.1A. Approximately 1 $\times 10^6$ HFFFF-TERT or HFFF-TETs were seeded in T25 tissue culture flask in serum free DMEM media. The following day, cells were infected with HCMV at required MOI and incubated on a rocking platform (20-25 rpm, for 2 h, at 37°C). After, the inoculum was removed and replaced with fresh D10 before returning the flask back into the incubator to allow HCMV to spread through the monolayer as per experimental protocol. For spinoculation, cells were seeded into plates and wrapped with parafilm before centrifugation (2,800 rpm for 2 hours at 26°C).

2.4.2 Co-culture infection assay

A schematic of co-culture infection setup is shown in Figure 2.1B. Approximately 5 $\times 10^5$ HFFF-TERTs were seeded in T25 tissue culture flask and infected at MOI 5 and incubated on a rocking platform (20-25 rpm, for 2h, at 37°C). Seventy–two hours post infection (hpi), infected HFFF-TERTs (iTERTs) were stained with CellTrace™ Far Red DDAO-SE dye (1µM), for 15 min at 37**°**C, before setting up the co-culture. DDAO staining helps distinguish HFFF-TERTs (DDAO+) from target cells (DDAO-). DDAO stained iTERTs were trypsinised and counted before overlaying an appropriate amount on top of target cells that were set up a day before (24-well plate, containing 1 $\times$ 10^5 target cells/well). DDAO stained uninfected HFFF-TERTs (uTERTs) were used as control.

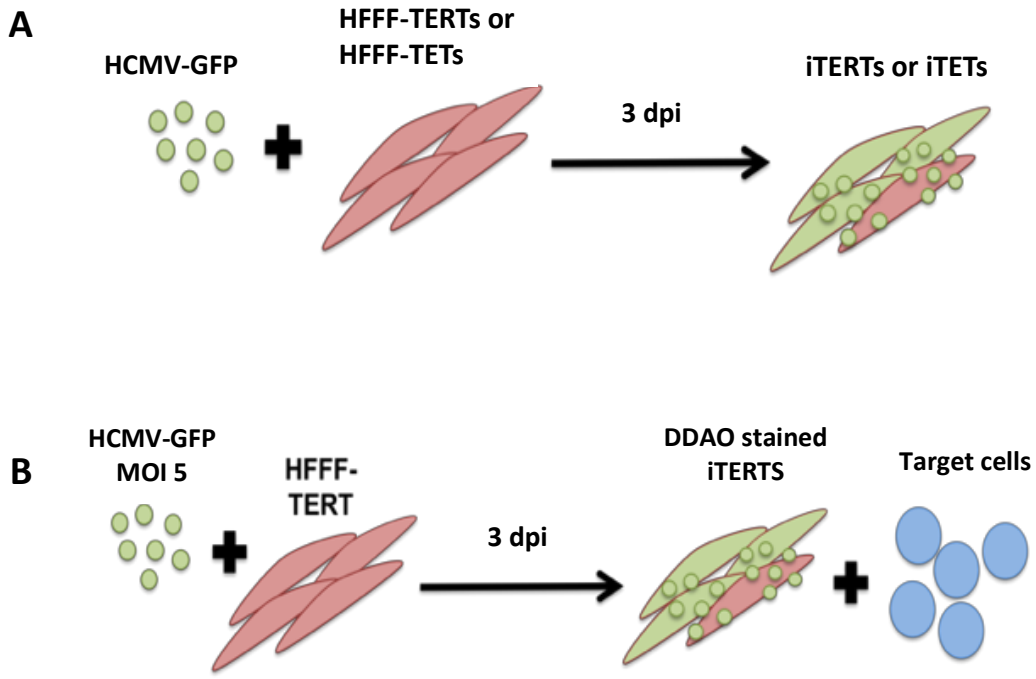

Figure 2.1: Diagrammatic representation of HCMV infection assays.

(A) Cell-free HCMV infection assay setup for fibroblast cell lines; where HFFF-TERT/TET cells are infected with GFP-tagged HCMV (on rocker for 2h at 37°C) at different MOIs. **(B)** HCMV infection assay for non-HFFF cell lines; where HFFF-TERTs were first infected at MOI 5 as shown in **(A)**. After 3 days, target cells were co-cultured with infected HFFF-TERTs (iTERTs); allowing cell-to-cell HCMV transmission. HCMV infection was monitored in both assays through percentage of GFP-positive cells after relevant days post infection (dpi) using flow cytometry.

2.5 Flow cytometry

2.5.1 Cell surface staining to assess HCMV infection in target cells

Cells were harvested at required timepoints as described in Section 2.2.4. The pellet was resuspended in 200µL PBS and transferred to a 'V-bottom' 96-well plate (Fisher). The cells were washed twice with PBS (centrifugation at 2000 rpm, for 2 min, at RT) prior to any staining. FACS staining was done in the dark, at room temperature. Zombie Aqua Fixable Viability Kit (Biolegend) was first used to stain for dead cells; where cells were incubated with Zombie Aqua Fixable (diluted 1:500 in PBS) for 5 minutes. The cells were then stained with various antibodies diluted in FACS buffer to allow detection of cell surface proteins (Table 5). Samples were incubated with 25µL of the diluted antibody, for 20 minutes and fixed with 4% paraformaldehyde prior to flow cytometric analysis. Antibody-capture beads (BD Pharmingen) were used to carry out electronic compensation. FITC anti-human CD14 and APC anti-human TNF-α antibodies were used to compensate for GFP expression and Cell Trace™ Far Red DDAO-SE dye, respectively. Data was acquired using Attune NxT Flow Cytometer (Thermo Fischer), unless stated otherwise, and analyzed using FlowJo software (TreeStar).

Table 5: Antibodies used for fluorescence compensation in flow cytometry

Antibody Conjugate	Antibody	Clone	Company	Dilution
CD11b-PE/Cy7	CD11b	M1/70	BD Pharmingen	1 µg per 10^6 cells in 100 µL volume
CD14-V500	CD14	MϕP9	BD Biosciences	
CD14-FITC	CD14	M5/E2	BioLegend	
HLA-A.B,C-PB	HLA-A.B,C	W6/32	BioLegend	
TNF- α-APC	TNF- α	MAb11	BioLegend	

Note: PE/Cy7 = Phycoerythin-Cyanine 7; FITC = Fluorescein isothiocyanate; PB = Pacific blue; APC = Allophycocyanin

2.6 Inhibition of reactive oxygen/nitrogen species (ROS/RNS)

2.6.1 Treatment with inhibitors of reactive oxygen/nitrogen species

Cells were seeded in either a 24-well plate or a 25 cm^2 tissue culture (T25) flask (Thermo Fisher Scientific) one day prior to treatment with inhibitors. Unless stated otherwise, cells were pre-treated with ROS/RNS inhibitors at different timepoints prior to HCMV infection at concentrations stated in Table 6. Sterile distilled water or DMSO were used as vehicle control. Infections were set up as described in Section 2.4.1. Cells were maintained in media counting inhibitors/controls throughout the assay. The experiments were performed in triplicate and repeated four times in cells from four different batches.

2.6.2 Measurement of intracellular level of peroxynitrite

The concentration of intracellular peroxynitrite was measured using cell-based peroxynitrite assay kit (ab233470, Abcam). Samples were prepared as recommended by manufacturer's protocol. Cells were scraped and resuspended in serum-free media at a density of 1×10^6 cells/ mL. The cells were transferred into a Nunc™ F96 MicroWell™ white polystyrene, flat-bottom microplate (Thermo Fisher Scientific) and co-incubated with Peroxynitrite Sensor Green (1 µL/0.4 mL of cells). The fluorescent signal was monitored after addition of HCMV (Merlin or TB40/E at MOI = 10 or 20) at Ex/Em = 490/530 nm, every 10-15s for three hours, by a fluorescence microplate reader (CLARIOstar®, BMG Labtech, Germany). The experiments were performed in duplicate and repeated four times in cells from four different batches.

Table 6: Inhibitors of reactive oxygen/nitrogen species

Inhibitor	Acronym	Solubility	Concentration		Pre-treatment duration (h)	Company
			in vitro	in vivo		
1400W Dihydrochloride	1400W	DMSO	500 µM	-	24	Cayman Chemicals
5-Hydroxytryptamine hydrochloride (Serotonin hydrochloride)	5-HT	Water	500 µM	-	24	Sigma-Aldrich
5,10,15,20-Tetrakis(N-methyl-4'-pyridyl)porphinato Iron (III) Chloride	FeTMPyP	Water	25 µM	-	0.5	Cayman Chemicals
5,10,15,20-Tetrakis(4-sulfonatophenyl)porphyrinato Iron (III) Chloride	FeTPPS	Water	25 µM	20 mg/kg	0.5	Cayman Chemicals
NG-Monomethyl-L-arginine	L-NMMA	Water	10-500 µM	-	24	Tocris (Bio-Techne)
N-Acetyl-L-cysteine	NAC	Water	10 mM	-	2	Sigma-Aldrich
4-Chloro-DL-Phenylalanine methyl ester hydrochloride	PCPA	Water	-	200 mg/kg	2	R & D Systems
N-tert-butyl-α-Phenylnitrone	PBN	DMSO	16 mM	-	2	Sigma-Aldrich

2.6.3 Delayed Treatment Assay

Cells were seeded in 24-well plates in serum-free media and incubated for 24 h in cell culture incubator. FeTPPS (25 µM) was added to media at different timepoints before and after HCMV infection (-0.5h, 0h, 2h, 6h, 12h, 24h and 48h). HCMV was added to media as indicated in Sections 2.4.1 at 0h time point. After 72h, all samples were stained and fixed as described in Section 2.5.1. To determine if FeTPPS inhibited HCMV entry and replication, percentage of infected cells was determined by flow cytometry. The experiments were performed in triplicate and repeated two-three times in cells from four different batches

2.6.4 Extraction of viral DNA from cultured cells

Viral DNA (vDNA) was isolated using DNeasy Blood & Tissue kit (QIAGEN), following the protocol provided by the manufacturer. In brief, cells were harvested (Section 2.2.4) and resuspended in 200 µL of PBS. Next, 20 µL of Proteinase K and 200 µL of lysis buffer AL (without ethanol) were added to the cell suspension. Samples were vortexed to obtain a homogenous solution and incubated for 10 min at 56° C for lysis. Then, 200 µL of ethanol (96-100%) was added and the samples were thoroughly vortexed once again. The mixture was pipetted into the DNeasy Mini Spin-Column and centrifuged (8,000 rpm, 1 min, RT). The flow-through was discarded and the column was washed with 500 µL of Buffer AW2 (14,000 rpm, 3 min, RT). The DNeasy membrane was dried by centrifugation (14,000 rpm, 3 min, RT) prior to DNA elution.

2.6.5 Quantitative Polymerase Chain Reaction (qPCR)

DNA concentration (ng/µL) was measured using NG1000 NanoDrop spectrometer (Thermo Fisher Scientific). DNA was diluted in Ambion® diethylpyrocarbonate (DEPC)-treated water (Thermo Fisher) such that the total amount of sample DNA was 100 ng per reaction. Each qPCR reaction contained 100 ng DNA, 500 nM of each primer, 1× iTaq™ Universal SYBR® Green Supermix (Bio-Rad) and adjusted to a total reaction volume of 20 µL. The samples were prepared in triplicates and analysed

using Quant Studio™3 Real-Time PCR System (Applied Biosystems). The thermocycling conditions are described in Table 7. Viral gene expression was quantified using primers gB-Forward (CTGCGTGATATGAACGTGAAGG) and gB-Reverse (ACTGCACGTACGAGCTGTTGG). The primers were designed to amplify HCMV gB (UL55) gene. Expression of glyceraldehyde-3-phosphate dehydrogenase (GAPDH), a common 'housekeeping' gene, served as an internal control. GAPDH was amplified using the following primers: GAPDH-Forward (CCTCTGACTTCAACAGCGACAC) and GAPDH-Reverse (TGTCATACCAGGAAATGAGCTTGA). Serial dilutions of plasmids containing both genes, and DNA extracted from HFFF-TERT cells, were used to generate a standard curve. All reagents, including plasmids and primers, were provided by Dr Lauren Kerr, Cardiff University.

Table 7: Thermal cycling conditions for qPCR using Quant Studio 3 System

Stage	Step	Temperature (°C)	Time	Cycles
Hold	Reverse Transcription	50	2 min	1
	Initial denaturation	95	10 min	1
Cycling	Denaturation	95	15 s	40
	Annealing/Extension	60	1 min	
Continuous melting	Melting curve	95	15 s	1
		60	1 min	1
		60-95	0.5°C/s	1

2.6.6 HCMV pp65 antigen assay to detect HCMV replication in samples pre-treated with/without FeTPPS

HFFF-TERTs were seeded in ibidi µ-Plate 96-well black plates at a concentration of 1 × 10^4 cells/well. The outer-ring of wells were avoided to ensure that the black skirted edge did not hinder the microscope lens from taking clear images. Cells were pre-treated with FeTPPS or vehicle control 0.5h prior to HCMV infection. Samples were kept in FeTPPS or vehicle control throughout the assay. After 24h, media was removed, and cells were washed in PBS. Cells were fixed in 4% PFA (15min incubation, in dark, at RT), washed in PBS once again and resuspended in 0.5% NP-40 solution to permeabilise membranes (15 min incubation, in dark, at RT). Cells were incubated with primary antibody (Table 8) for 30 min, at 37°C, on a rocking platform. After two washes, cells were incubated with the secondary antibody and nuclear stain (Table 8) for 30 min, at 37°C, on a rocking platform. Samples were washed twice and covered in Dabco® mounting solution (Sigma-Aldrich) prior to imaging.

Table 8: Antibodies and stains used in immunofluorescence assays

Antibody/Stain	Company	Concentration
CMV pp65 monoclonal primary antibody	Virusys (CA003)	1 :100
Alexa Fluor-488 (AF488) anti mouse (goat) secondary antibody	Invitrogen (A-11017)	1 :500
DAPI (4',6-diamidino-2-phenylindole) nuclear stain	Sigma-Aldrich	1: 30,000

2.6.7 Detection of pp65 HCMV antigen by Immunofluorescence

The Zeiss microscope (Axio Observer Z1) was used for fluorescence imaging. The Zeiss Apotome allowed optical sectioning of samples without scattered light. A magnification of ×40 or ×100 with oil (Immersol 518F, Zeiss) was used, unless specified otherwise. The blue and green fluorescence imaging channels were used to detect nuclear dye DAPI (461nm wavelength) and AF488-labelling (488nm wavelength), respectively. Zen2 Pro software (Zeiss) was used to adjust exposure such that the background levels in FeTPPS-treated samples were minimal compared to the control. Images were captured independently for every channel and then merged to create a multi-channel image (Dr Lauren Kerr, Cardiff University).

2.6.8 In vivo experiments

2.6.8.1 Mice

All *in vivo* studies were conducted by Prof Ian Humphreys, Dr Mathew Clement and/or Morgan Marsden under UK Home Office approved Project License (PPL No. P7867DADD) and in accordance with Home Office regulations. C57BL/6 mice were purchased from Charles River (UK) and housed in pathogen-free scantainer cabinets at the Home Office designated animal research facility located at Heath Park Campus, Cardiff University.

2.6.8.2 Mice Immunization

Mice were injected intra-peritoneally (i.p.) with MCMV (2×10^5 PFU) at day 0. MCMV was a gift from Morgan Marsden (Cardiff University, UK). They were also treated with FeTPPS or PBS at days 0 and 2. Percentage change in body weight was measured over four days. On day 4, mice were sacrificed, and organs were harvested to quantify viral load in different tissues.

For experiments with PCPA, mice were administered PCPA or PBS i.p. 30 min prior to MCMV. They were also treated with PCPA or PBS on days 0 and 1. Percentage change in body weight was measured over two days. On day 2, mice were sacrificed, and organs were harvested for quantification of viral load in different tissues.

2.6.8.3 Plaque assays

Viral load in mouse organs (spleens and livers) were quantified using plaque assays (kindly performed by Lucy Chapman, Cardiff University). In brief, NIH-3T3 cells were seeded into Corning® CellBIND® 24-well flat bottom plates (Corning, Birmingham, UK), at a concentration of 1×10^5 cell per well. Tubes were weighed before and after harvest to estimate the weight of each organ. Mouse organs were homogenized in RPMI. The homogenized suspension was serially diluted and 200 µL of each dilution was added to confluent monolayer of NIH-3T3 cells, in duplicates. MCMV was titred by centrifugation ($1000 \times g$, for 30 min, at 4°C). The suspension

was removed and replaced with pre-warmed semi-viscous CMC overlay media. Cells were incubated for six days (37°C, 5% CO_2). The CMC overlay was removed, and the plates were fixed and stained for four hours with 10% formaldehyde (in PBS) and 0.5% crystal violet, respectively, at room temperature. Plates were gently rinsed under running water and left to air-dry overnight. The following day, plaques were counted, and virus load was quantified, as PFU/g of tissue, using the following equation:

$$\frac{PFU}{g} = \frac{average\ number\ of\ plaques\ \times\ dilution\ \times\ 5}{organ\ weight}$$

Note: multiplying by 5 accounted for adding only 200 µL of diluted homogenised suspension per well (i.e., a fifth of 1 mL).

2.6.9 Statistical Analysis

Unless otherwise stated, statistical analyses were not performed when the sample size was too small (n <7). Although normality tests offered by PRISM9 to make inferences about data distribution could not be performed due to the small sample size, the Mann-Whitney test was used to compare two unpaired groups (if n ≥ 7). It was stated that "for a sample size <7, the Mann-Whitney test would always result in a p-value that is greater than 0.05, regardless of how much the two groups differed" (GraphPad PRISM9 Statistics Guide). In contrast, to compare three or more unmatched groups, the Kruskal-Wallis non-parametric test was used. In both tests, if the p-value <0.05 it was concluded that the populations are distinct and statistically significant.

2.7 Genome-wide CRISPR knockout screening

2.7.1 Generation and validation of Cas9-expressing target cells

2.7.1.1 Lentivirus production

Approximately 1.1×10^6 293T cells were seeded, in 2 mL D10, per required number of wells of a 6-well plate. The cells were transfected the following day. Transfection complex mix per well was prepared as follows: 1. 337 µg lentiviral vector (pKLV2-EF1a-BsdCas9-W or pHAGE-GFP) was mixed with packaging plasmids (1.337 µg pVSVG, 1.337 µg pRSV-REV and 1.337 µg pMDL) and incubated with 150 µL transfection mix (Table 2) in a sterile universal tube for 30 minutes at room temperature; allowing transfection complexes to form. Lentiviral vectors used were a gift from Kosuke Yusa (Wellcome Trust Sanger Institute, UK). After, 150 µL of the transfection complex mix was added to 293T cells. The supernatant, now containing lentivirus, was harvested from transfected 293T cells 72 hours post transfection. The viral supernatant was centrifuged (3000rpm for 15 minutes at room temperature) to pellet debris and filtered using 0.45 µm low adsorption polyethersulfone filters (Sartorius).

2.7.1.2 Generation of Cas9-expressing cell lines

ARPE19, HFFF-TERT and HFFF-TETs were transduced with lentivirus expressing Cas9 and blasticidin-S deaminase (produced as described in Section 2.7.1.1 using pKLV2-EF1a-BsdCas9-W lentiviral vector). Transduction was carried out in T25 tissue culture flask as follows: 1×10^6 target cells and 2 mL of filtered lentiviral supernatant was mixed with 4 mL of D10 supplemented with 6 µg/mL polybrene. Blasticidin-S selection was initiated 4 days after transduction at minimum concentration required to kill non-Cas9 expressing cells, that is, 5µg/mL for Cas9 expressing fibroblasts and 25µg/mL for ARPE19-Cas9 cells. THP1Cas9 cells were provided by Dr Jessica Forbester (The Wellcome Trust Sanger Institute) and were cultured in media supplemented with 25µg/mL blasticidin-S.

2.7.1.3 Isolation and expansion of monoclonal cell populations

Individual Cas9-expressing clones were isolated from a polyclonal pool of Cas9-expressing cells by limiting dilution. First, 1×10^4 Cas9-expressing cells were resuspended in 1mL of 50:50 conditioned: D10 media (Table 2). This cell suspension was used to make 10 mL of cell solution at a cell density of 5 cells/mL in 50:50 conditioned: D10 media. After, 200 µL of 5 cells/mL cell suspension into a flat-bottomed 96-well plate (Fisher), thereby seeding at a density of 0.5 cells/well. The cells were left undisturbed in the incubator for two weeks. Wells were then scanned for single-cell colonies. Any wells with multiple colonies were discarded. Once confluent, cells were harvested as described in Section 2.2.4 and seeded into larger tissue culture plates and flasks. When individual monoclonal cell lines were sufficiently expanded, Cas9 activity was evaluated (Section 2.7.1.4). The clone that showed low basal GFP-expression and high GFP-expression following HCMV infection was used for genome-wide CRISPR screening (i.e., TERTCas9_clone13).

2.7.1.4 Validation of CRISPR-Cas9-mediated genetic editing

Neon® Transfection System (Thermo Fischer) was used to deliver β2M-specific single guide RNA (sgRNA) construct (5'-GGCCGAGATGTCTCGCTCCG-3') into Cas9-expressing target cells. GFP-sgRNA was used as a control for electroporation efficiency. The electroporation parameters were set as per manufacturer's protocol (Table 9). After a week, loss of MHC-I expression, due to β2M knockout, was measured by flow cytometry (Section 2.5). Non-Cas9-expressing were used as an additional control.

Table 9: Electroporation parameters for Neon™ Transfection System

Pulse Voltage (V)	Pulse Width (ms)	Number of Pulses	Cell Density (cells/mL)	Neon™ Tip -Type
1400	20	2	1×10^7	10 µL
1700	20	1	1×10^7	10 µL

2.7.2 Pooled genome-wide CRISPR-Cas9 mediated knockout screening

2.7.2.1 The Brunello CRISPR knockout pooled library

The 'human Brunello genome-wide CRISPR knockout lentiviral pooled library' consists of 76,441 sgRNAs, with an average of 4 sgRNAs targeting each gene, and 1000 non-targeting control sgRNAs[276]. The genome-wide positive selection (survival) screen was carried out in Cas9-expressing HFFF-TERTs. The Brunello library, pre-packaged in the lentiGuide-Puro vector, was a gift from David Root and John Doench, Broad Institute of MIT and Harvard, USA (Addgene Cat. No. 73178-LV). An aliquot of purified plasmid DNA (pDNA) pool (which generated the batch of lentivirus for my project) was also provided by Addgene to use as reference when performing post-CRISPR screen analysis.

2.7.2.2 Optimization of lentivirus infection conditions for pooled screening

The clone with the highest Cas9-cutting efficiency (TERTCas9_clone13) was seeded into multiple T25 flasks at a concentration of 1×10^6 cells per flask. Cells were infected with GFP-LV (Section 2.7.1.2) at MOIs ranging between 0.3 – 5. After one week, the percentage of cells that were GFP-positive was assessed by fluorescence microscopy (Zeiss) and quantified by flow cytometry. The additional 'testing aliquot' of lentivirus provided by Addgene was used validate optimal infection condition (unpublished observations from our laboratory). MOI of 1 corresponded to 30% lentiviral infection efficiency was used to perform screening-scale infections.

2.7.2.3 Genome-wide CRISPR knockout screening

Approximately 130 million TERTCas9 (clone 13) cells were transduced with the Brunello lentiviral library, with pre-determined MOI, to achieve $\geq$ 500-fold representation of each sgRNA post puromycin selection. After 24h, non-transduced cells were removed with puromycin (1 μg/mL). One week later, genomic DNA (gDNA) was extracted from two-thirds of mutant cell population to use as baseline control. The remaining puromycin-resistant cells were propagated in culture. After

approximately two weeks, puromycin-resistant cells were pooled, resuspended in serum-free media, and seeded into multiple T175 flasks at a concentration of 6×10^6 cells per flask. The following day, 150 million puromycin-resistant cells (~25 × T175 flasks) were infected with HCMV Merlin-UL128^{mut} at an MOI of 0.5 (as described in Section 2.4.1). Six weeks later, cells were seeded into fresh flasks and re-infected with HCMV. After six additional weeks, gDNA was extracted from surviving cells. An uninfected 'mock' population was propagated alongside as an additional control.

2.8 Illumina Sequencing

2.8.1 Extraction of gDNA from cell pellets

Genomic DNA was isolated from puromycin-resistant cells using Blood & Cell Culture DNA Maxi Kit (Cat. No. 13362, QIAGEN), according to manufacturer's protocol. In brief, cells were harvested (Section 2.2.4) and resuspended to a concentration of 1×10^7 cells/mL in ice-cold PBS. The samples were lysed with lysis buffer C1 (10 min, on ice) and digested with proteinase K solution (60 min, at 50°C). The cell suspension was vortexed vigorously for 10s and transferred to an equilibrated QIAGEN Genomic-tip, letting it enter the resin by gravity flow. Bound DNA was washed twice by allowing wash buffer to flow through the QIAGEN Genomic-tip. DNA was eluted with buffer pre-warmed to 50°C and precipitated by centrifugation (5000 $\times$ g , 15 min, at 4°C) with addition of room-temperature isopropanol. DNA pellet was washed with ice-cold 70% ethanol (centrifuged at 5000 $\times$ g , 15 min, at 4°C) and air-dried. The pellet was resuspended in TE buffer and dissolved overnight on a rocking platform.

2.8.2 PCR amplification of sgRNA cassette and Illumina adapter ligation

KAPA HiFi HotStart ReadyMix PCR Kit (Cat. No. KK2602, Roche, Switzerland) was used to amplify sgRNA-containing fragments, append Illumina adapters and barcode individual samples for multiplex sequencing. For each sample, multiple 50µL PCR reactions were set-up in parallel, containing components listed in Table 10. The sequences of PCR primers (that include P5/P7 flow-cell attachment sequences) are shown in Table 11. Fragments were amplified using the cycling parameters described in Table 12.

Table 10: Components required for each 50 µL PCR reaction

Component	Volume per 50 µL reaction	Final concentration
2× KAPA HiFi HotStart ReadyMix*	25 µL	1×
10 µM Forward Primer	1.5 µL	0.3 µM
10 µM Reverse Primer	1.5 µL	0.3 µM
Template DNA	as requred	10 µg
PCR-grade water	up to 25 µL	-

* Contains 2.5 mM $MgCl_2$, 0.3 mM or each dNTP and 0.5 U of 1 U of KAPA HiFi Hot Start DNA Polymerase.

Table 11: PCR primers used for sgRNA amplification for Illumina sequencing

Sample	Primer	Label	Sequence (5' – 3') *
Universal**	P5/Forward	SEF01	AATGATACGGCGACCACCGAGATCTACACTCTTTCCCTACACGACGCTCTTCC GATCTTCTTGTGGAAAGGACGAAACACCG
pDNA	P7/Reverse	SER01	CAAGCAGAAGACGGCATACGAGATAACGTGATGTGACTGGAGTTCAGACGT GTGCTCTTCCGATCTTCTACTATTCTTTCCCCTGCACTGT
Baseline		SER02	CAAGCAGAAGACGGCATACGAGATAAACATCGGTGACTGGAGTTCAGACGT GTGCTCTTCCGATCTTCTACTATTCTTTCCCCTGCACTGT
Control		SER03	CAAGCAGAAGACGGCATACGAGATATGCCTAAGTGACTGGAGTTCAGACGT GTGCTCTTCCGATCTTCTACTATTCTTTCCCCTGCACTGT
HCMV		SER04	CAAGCAGAAGACGGCATACGAGATAGTGGTCAGTGACTGGAGTTCAGACGT GTGCTCTTCCGATCTTCTACTATTCTTTCCCCTGCACTGT

*Sequences were provided by Addgene (as per reference paper insert ref).
**Common to all samples.
Key: Complimentary P5/P7 flow-cell attachment sequence; unique index sequence/sample identifier ; Illumina sequencing primer; Lentiviral vector binding primer sequence.

Table 12: PCR cycling parameters to prepare samples for Illumina sequencing

Step	Temperature (°C)	Time	Cycles
Initial Denaturation	98	30s	1
Denaturation	98	10 s	35
Annealing	66	15 s	
Extension	72	20 s	
Final Extension	72	5 min	1
Hold	4	∞	-

2.8.3 PCR clean-up prior to Illumina Sequencing

Agencourt AMPure XP PCR Purification Kit (Beckman Coulter, 63880) was used to purify PCR products, following protocol provided by the manufacturer. For each sample, all PCR products were pooled together into, gently mixed and redistributed as 100 µL aliquots in 96-well round bottom plate (Thermo Fisher). Then, 100 µL of magnetic beads (resuspended in AMPure XP reagent) was added to each sample and pipetted thoroughly until homogenous mixture was formed. The mixture was incubated for five minutes, at room-temperature. The reactions were then placed onto a magnet (DynaMag-96 side, Thermo Fisher) for two minutes, allowing beads to separate. The cleared solution was carefully aspirated and discarded. The separated product was washed thrice by incubating samples in 70% ethanol for thirty seconds, at room temperature. The ethanol was carefully aspirated and discarded. The plate was removed from the magnet and air-dried for three minutes. The purified PCR product was eluted with supplied TE buffer (50 µL / well). The plate was placed back onto the magnet for five minutes. For each sample, the eluted product was collected/pooled into an Eppendorf tube and stored at -20°C till required for next-generation sequencing (NGS).

2.8.4 Illumina sequencing

Illumina sequencing was performed by Dr Angela Marchbank (Genome Hub, Cardiff University, UK) using NextSeq 500 System (Illumina, USA). Samples were sequenced to a depth of 20 million reads per sample (50 bp single-end reads), as previously described [277]. Low heterogeneity across samples was addressed by using standard Illumina sequencing primers with addition of 25% PhiX. NGS data was exported/stored in FASTQ file format; which were used as inputs for tools that perform downstream data analysis.

2.9 Model-based analysis of genome-wide CRISPR knockout (MAGeCK)

Post-CRISPR screen data analysis was performed using Model-based Analysis of Genome-wide CRISPR Knockout (MAGeCK) bioinformatics pipeline[278]. MAGeCK is an open-source computational tool that allows identification of essential sgRNAs, genes and pathways from CRISPR knockout screens. For this study, the term 'essential' refers to positively selected hits, that is, mutations that render cells resistant to multiple rounds of HCMV infection. The accompanying MAGeCKFlute package was used for additional downstream analysis, including biological function and pathway enrichment analysis[(279)]. Workflow for post-CRISPR screen analysis is summarised in Figure 2.2.

MAGeCK/MAGeCKFlute was run as previously described. Original run commands (available from respective web-based source code repositories) were adapted to perform bioinformatic analysis of data files generated in my project. Briefly, packages were installed via the anaconda bioconda channel and run in RStudio integrated development environment (IDE). Raw FASTQ data files were used as inputs for MAGeCK. The associated Brunello library file (downloaded from MAGeCK SourceForge) was also provided so MAGeCK recognises the sgRNA sequences and their corresponding gene targets. The trimming length (required to remove adapter sequences located upstream of sgRNA sequence) was automatically detected by MAGeCK using the provided library file. The '*--mageck count*' and '*--mageck test*' subcommands were run in the terminal to generate the read count table and sgRNA/gene summaries, respectively.

The read count table was processed using MAGeCKFlute pipeline to assess quality of sequencing data, including sequence composition, read depth and sgRNA distribution. The mock-infected control dataset was excluded from downstream analysis as it failed to pass MAGeCKFlute quality check. Consequently, the Maximum Likelihood Estimation (MLE) method could not be used to identify hits as

MAGeCK MLE can only be used to analyse data from CRISPR screens that have a minimum of three conditions (e.g. day 0, mock-treated and treated). Instead, the integrated Robust Rank Aggregation (RRA) method was used to compare uninfected baseline and HCMV-infected datasets.

MAGeCK RRA returned a ranked list of essential genes, with corresponding false discovery rate (FDR) estimates. The genes were ranked using normalised sgRNA distribution and the statistical significance of sgRNA abundance changes between the two experimental conditions (calculated by integrated RRA algorithm).

The ranked gene list generated by MAGeCK RRA was then used to identify enriched pathways, with Geno Ontology (GO) and Kyoto Encyclopedia of Genes and Genomes (KEGG) databases, using the FLuteRRA function.

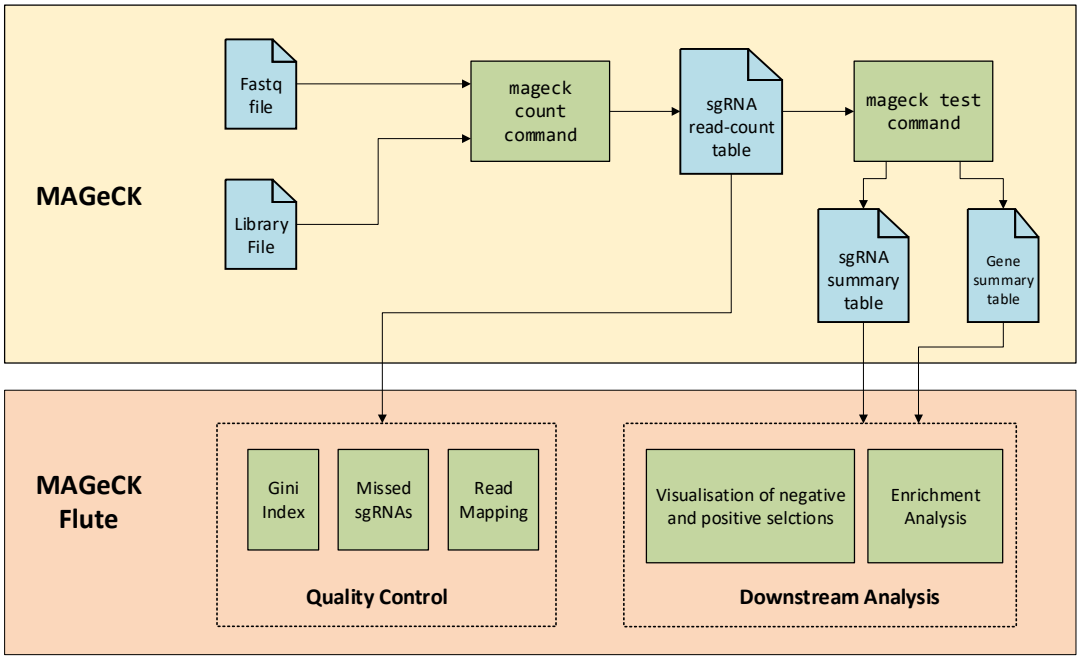

Figure 2.2: CRISPR screen data analysis workflow

2.10 Validation of CRISPR-screen hits

Out of the possible 11 hits identified (FDR <1%), six targets were selected for screen validation. Except for *PDGFRA*, five anti-HCMV candidates were chosen based on novelty; genes that were not previously known to be involved in HCMV replication. Several databases, including OMIM, KEGG, STRING and ProteomeXchange Consortium, were used to determine gene novelty. *PDGFRA* was selected as a control. Knockout (KO) cell lines were generated to elucidate the strength of each hit independently.

Pre-designed synthetic sgRNA (Thermo Fisher) (Table 13) were used to generate individual KO cells, as previously described (Section 2.7.1.4). Polyclonal KO cells were seeded into T25 flasks at a concentration of 1×10^6 cells per flask. Cells were infected with multiple rounds of HCMV Merlin-UL128^{wt} or Merlin-UL128^{mut} at MOI 5 (Section 2.4.1). Protection against HCMV infection was determined via electron microscopy and flow cytometry (% GFP+ cells)

Table 13: Synthetic sgRNAs used to generate individual KO cell lines

Gene Target	TrueGuide™ Synthetic sgRNA sequence (5'-3')
KIF5B	AACACCCGATCAAATGCATA
KIRREL	GGATGGCTTCGTTCATGCTT
LATS2	CCATCCAAGTCTTCGGTTCA
MED23	CCGAACCAGTTTAAATGTTA
NF2	AACCCAAGACGTTCACCGTG
PDGFRA	CTTCCAAGACCGTCACAAAA

3 Investigating the role of peroxynitrite during CMV infection

3.1 Introduction

3.1.1 Peroxynitrite: Properties and Generation

Free radicals are usually highly reactive as they are comprised of at least one unpaired electron in the outer shell[280]. Oxygen molecules (O_2) are very stable, however, oxygen-containing radicals, such as superoxide ($O_2^{\bullet}$-) and hydroxyl ($^{\bullet}OH$) radicals, can be highly unstable[280]. These reactive oxygen species (ROS) act as important signalling molecules in biological systems, regulating homeostasis and mediating 'normal' physiological processes[280]. They may also contribute to cellular damage and disease pathogenesis in chronic conditions[280]. Nitrogen-centred free radicals, such as nitric oxide ($NO^{\bullet}$), are also highly reactive chemical molecules[280]. They can generate reactive nitrogen species (RNS) by chemically reacting with other free oxygen-containing radicals[280]. For example, the reaction of nitric oxide with superoxide generates peroxynitrite ($ONOO^-$), a very potent oxidising and nitrating agent[280].

A wide variety of stimuli, including toxins, ultraviolet light, stress, inflammation and invading bacteria or viruses, can induce peroxynitrite generation[280]. Peroxynitrite is a transient reactive molecule generated by the rapid reaction of superoxide and nitric oxide radicals[280]. It is widely accepted that the sites of peroxynitrite production are spatially located close to sources of superoxide[280]. This is because superoxide is shorter-lived, relatively unstable and is not as diffusible across bio-membranes as nitric oxide[280]. Primary intracellular sources of superoxide include the mitochondria, XO, NOX and processes such as catechol oxidation, where ROS is generated as a by-product[280].

In physiological conditions, it is estimated that the concentration of intracellular peroxynitrite is maintained in the nanomolar range(270). There are many

endogenous antioxidant defence mechanisms that prevent the accumulation of reactive species(270). Superoxide dismutase (SOD) is the most efficient at eliminating the accumulation of superoxide anions [280]. There are different forms of SODs located in the cytoplasm (SOD1), mitochondria (SOD2) or extracellular matrix (SOD3) that rapidly convert superoxide to water[280]. However, when redox homeostasis is disrupted, such as during an immune response to a virus, nitric oxide reacts faster with superoxide than its decomposition by SOD[280]. The estimated rate at which peroxynitrite is generated can get as high as 50-100 µM per minute in certain physiological conditions[281]. Although short-lived (<10ms), sudden exposure to high concentrations of peroxynitrite can be physiologically significant and result in an array of biological effects[217,280,281].

Peroxynitrite is highly diffusible across cellular membranes and thus peroxynitrite generation in one cell can trigger a response in neighbouring cells[281]. At low concentrations, peroxynitrite acts as a nitric oxide donor or carrier and can have beneficial effects [217,280,281]. The production of oxidants, such as superoxide and nitric oxide, are essential for the elimination of invading microorganisms by macrophages and neutrophils[217,280,281]. However, continuous production of peroxynitrite in a vicious cycle can lead to peroxynitrite-induced cellular damage[282]. Therefore, at higher concentrations, effects of peroxynitrite shift from physiological to pathological, causing irreversible oxidation/nitration of biological molecules[282]. Consequently, elevated levels of superoxide and nitric oxide, coupled with the rapid generation of peroxynitrite is often referred to as the 'devil's triangle' (Figure 3.1) [282].

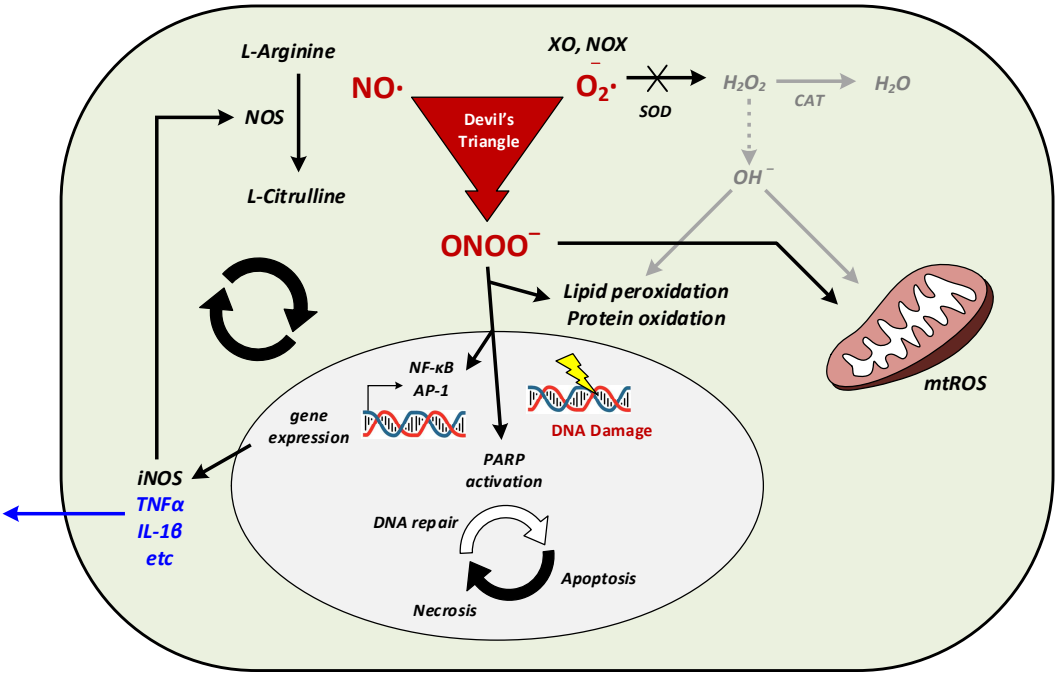

Figure 3.1: Formation and effects of peroxynitrite within a cell

Peroxynitrite (ONOO-) formation rapidly occurs following simultaneous production of superoxide and nitric oxide at close proximity. Nitric oxide ($NO^{\bullet}$) out competes SOD for superoxide ($O_2^{\bullet}$-) to generate peroxynitrite, which can be beneficial or harmful depending on the concentration it is maintained at. Low levels of peroxynitrite can activate multiple signalling pathways leading to production of proinflammatory cytokines such as TNF. These in turn can activate other ROS-forming enzymes, promoting generation of ROS. Peroxynitrite can directly interact with DNA to induce single or double stranded breaks, which are often reversible through activation of DNA repair pathways. However, continuous production of peroxynitrite in a vicious cycle can lead to irreversible cellular damage, triggering cell death. The figure is a modified version from [272].

3.1.2 Biological functions of peroxynitrite

Peroxynitrite is involved in a variety of biological functions, either as a consequence of direct interactions with other molecules or via peroxynitrite-derived molecules[280,281]. The stability, reactivity, and ability of peroxynitrite to cross membranes is pH-dependent[280,281]. At neutral pH, the majority of peroxynitrite is anionic[280,281]. The anionic form of peroxynitrite is stable in alkaline conditions[280,281]. In contrast, at acidic pHs, such as inside phagocytic vacuoles, peroxynitrite is mainly protonated and exists as peroxynitrous acid (ONOOH)[280,281]. Both anionic and protonated forms of peroxynitrite participate in nitro-oxidative reactions by one- or two-electron reactions[280,281]. The anionic form of peroxynitrite is presumably responsible for direct reactions however, just like its protonated form (peroxynitrous acid), it can also decompose into nitrogen dioxide ($NO_2^{\bullet}$) and hydroxyl ($OH^{\bullet}$) radicals, initiating secondary nitro-oxidative reactions[280,281]. Although modifications by peroxynitrite-derived free radicals are considered fundamentally important, they are typically low-yield processes[280,281].

The biological effects of peroxynitrite can be highly dependent on its concentration and availability of other ROS/RNS in the local microenvironment. Intriguingly, peroxynitrite can generate positive feedback loops to promote the production of intracellular radicals through oxidation of co-factors or inhibition of enzymes involved in antioxidant systems such as SOD[217,281]. For example, peroxynitrite can cause uncoupling of eNOS through oxidisation of eNOS cofactor BH4[237,281]. Uncoupled eNOS further promotes events that favour peroxynitrite production and help maintain a peroxynitrite-rich environment[237,281]. This process has been known to contribute to oxidative stress facilitated dysfunction of endothelial vasculature in various inflammatory diseases[217,280].

Peroxynitrite and peroxynitrite-derived molecules can affect a wide-range of biomolecules, including but not limited to lipids, thiols (-SH containing molecules), nucleic acids and proteins[217,280,281]. Peroxynitrite can readily nitrate, dimerize or

hydroxylate tyrosine to form 3-nitrotyrosine (3-NT), 3-3'-dityrosine (3-3'-DT) or 3,4'dihydroxyphenylalanine (DOPA), respectively[217,280,281]. Peroxynitrite-mediated tyrosine nitration has been widely observed in many different cells *in vitro,* affecting protein structure, enzymatic activity, and intracellular signal transduction[283]. The relevance of tyrosine nitration *in vivo* is yet to be fully established as the yield of 3-NT generation during nitro-oxidative stress is relatively small as compared to that seen *in vitro*[283]. Nonetheless, tyrosine nitration has been detected in >50 human diseases[217]. Although the presence of nitrated tyrosine does not imply a direct pathogenic role, it does indicate that peroxynitrite and other RNS are upregulated in disease conditions[217,280,281].

Peroxynitrite also interacts with lipids, resulting in peroxidation and the formation of oxidation-induced nitrated lipid adducts[217,280,281]. Peroxidation of lipids can further mediate the oxidation of tyrosine residues in proteins and nitration of bio-membranes and lipoproteins[217,280,281]. Production of hydroxyl and nitrogen dioxide radicals can be functionally relevant to lipid peroxidation processes as well[217,280,281]. Peroxynitrite-induced lipid modifications can lead to degradation of lipid membranes, increasing membrane permeability and altering membrane fluidity[217,280,281].

Peroxynitrite can covalently bind to thiols to form thiyl radicals (by one-electron oxidation) or sulfenic acid (by two-electron oxidation) [217,280,281]. Oxidised thiols can further activate radical-dependent chain reactions[217,280,281]. Thiyl radicals have been established as key intermediates in several biochemical redox reactions, including electron transfer and degradation of hydrocarbons[217,280,281]. Thiyl radicals can react with oxygen molecules to form peroxyl radicals, which are important in hydrocarbon degradation[217,280,281]. Peroxynitrite can also react with thiols to generate S-nitrosothiols[217,280,281]. S-nitrosylation is a key post-translation modification that has been shown to regulate the conformation and function of many structural, metabolic, and regulatory proteins involved in signal transduction within a cell[217,280,281]. Peroxynitrite can readily oxidise thiol groups of platelet

membrane proteins and increase the concentration of intracellular calcium, triggering platelet activation *in vitro*[217,280,281]. Peroxynitrite can also interact with the proteasome, affecting the turnover of proteins and proteolysis[280]. It can directly modulate proteasomal activity as well as alter the susceptibility of proteasomal substrates to proteolysis[280]. Similarly, sulfenic acid is essential in the redox control of peroxiredoxins. Peroxiredoxins are important regulators in redox signalling[280]. They modulate intracellular hydrogen peroxide (H_2O_2) concentration, maintaining low levels at homeostasis and high levels during intracellular signalling[280].

Peroxynitrite or peroxynitrite-derived molecules can also bind to DNA, causing oxidation of deoxyribose or single-stranded breaks[214,270,27]. Purine nucleotides are particularly vulnerable to peroxynitrite-mediated oxidation and subsequent adduct formation[214,270,27]. Occasionally, peroxynitrite-mediated cellular damage may be irreversible, resulting in cell death by apoptosis or necrosis[214,270,27]. Severe genomic damage by peroxynitrite can lead to the overactivation of DNA repair enzyme, poly(ADP ribose) polymerase-1 (PARP-1), leading to depletion of nicotinamide adenine dinucleotide (NAD+) and the energy molecule adenosine triphosphate (ATP) [214,270,27]. Overactivation of DNA repair processes can exhaust cells of energy (ATP), leading to necrosis[214,270,27]. This PARP-mediated 'suicide' of cells is associated with the pathogenesis of several diseases[214,270,27].

3.1.3 Effects of peroxynitrite on cell signalling

The primary regulatory mechanism controlling cell signal transduction is reversible protein phosphorylation, which involves a tightly coordinated balance between the activity of multiple kinases and phosphatases[217,281,283]. Peroxynitrite and peroxynitrite-derived molecules can readily interact with components of intracellular signalling cascades, shifting the delicate balance[217,281,283].

Most extracellular signals are detected by cell membranes receptors, which predominantly belong to the G-protein coupled receptor (GPCR) or receptor tyrosine kinase (RTKs) family[217,283,284]. GPCRs interact with guanine nucleotide-binding proteins (G-proteins) to activate several downstream effectors such as cyclic nucleotides, calcium, or inositol trisphosphate[217,283,284]. These secondary messengers further modulate protein phosphorylation within cells. In contrast, RTKs are transmembrane glycoproteins, which include receptors that detect insulin and growth factor receptors[217,283,284]. Specific ligands interact with RTKs to upregulate binding sites for protein phosphotyrosine domains[217,283,284]. Docking of phosphotyrosine binding domains to RTKs recruits and activates downstream effectors, including mitogen-activated protein kinase (MAPK) cascades and phosphoinositide 3'-kinase (PI3K) pathways[217,283,284]. These signalling pathways modulate cellular processes such as proliferation, differentiation, survival, and intra- and extracellular stress responses[217,283,284].

Protein kinases selectively modify other proteins through phosphorylation, which is a process that involves the transfer of phosphates to tyrosine, serine, or threonine residues[217,283,284]. Peroxynitrite can post-translationally modify redox-sensitive groups (such as cysteine, methionine, tyrosine residues) in proteins, altering structure and function[217,283,284]. For instance, peroxynitrite-mediated tyrosine nitration can affect the phosphorylation of tyrosine kinases[217,283,284]. There are three main types of tyrosine kinases: Janus kinases (JAKs) involved in cytokine-dependent signalling; focal adhesion kinase (FAKs), which modulate adhesion-dependent signals, and src kinases, triggered by GPCR signalling[217,283,284]. Peroxynitrite can inhibit or activate phosphotyrosine-dependent signalling. It is not fully understood why peroxynitrite exerts paradoxical effects on the same signalling pathway, but peroxynitrite concentration, cell type and the redox microenvironment all seem to influence peroxynitrite reactivity[217,283,284]. For example, at higher concentrations, peroxynitrite rapidly nitrates tyrosine residues in kinases, inhibiting phosphotyrosine signalling[217,283,284]. Nitrated tyrosine kinases are unable to phosphorylate tyrosine residues in other proteins[217,283,284. In

contrast, at lower concentrations, peroxynitrite can activate phosphotyrosine-dependent signalling pathways through permanent inactivation of tyrosine phosphatases, or via upregulation of RTKs, particularly growth factor receptors[217,283,284]. RTK activation, in turn, triggers downstream signalling pathways, including MAPK cascades and PI3K pathways[217,283,284].

Peroxynitrite has also been shown to interact with serine-threonine kinases (STKs) as well[217,283,284]. Protein kinase B (PKB), also known as Akt, is crucial for integrating growth-factor dependant signalling events[217,283,284]. PKB activation is equally important in promoting mechanisms that limit apoptosis during oxidative stress[217,283,284]. PKB activation critically depends on phosphorylated phosphoinositides, which are generated via PI3K signalling[217,283,284]. Peroxynitrite triggers PKB activation through modulation of PI3K signalling[217,283,284]. Peroxynitrite also activates platelet-derived growth factor receptors α/β (PDGFR α/β) that are located on the surface of many different cells[217,283,284]. Peroxynitrite-mediated activation of PDGFR α/β can subsequently trigger PI3K/PKB phosphorylation, activating transcription factors and other downstream effectors in *vitro*[217,283,284]. Paradoxically, peroxynitrite has also been shown to inhibit PI3K signalling and subsequent PKB activation in several cells *in vitro*[217,283,284].

Exposure of cells to peroxynitrite has also been shown to activate three major MAPK signalling cascades: the extracellular signal-regulated kinase 1 and 2 (ERK1/2), c-Jun N-terminal kinase (JNK) and p38 MAPK pathways[217,283,284]. MAPKs are another subset of STKs that affect protein function by modifying serine and threonine residues in proteins[217,283,284]. They are involved in modulating cellular responses to mitogens, osmotic stress, and pro-inflammatory cytokines[217,283,284]. Peroxynitrite-mediated activation of the ERK pathway transduces extracellular signals to the nucleus where genes involved in cell growth, division and/or differentiation can be activated[217,283,284]. The role of peroxynitrite on ERK pathways is cell type-specific [217,283,284]. Peroxynitrite is also very efficient in activating p38 MAPK[217,283,284]. Even at a very low concentration (<10μM),

peroxynitrite rapidly induces phosphorylation of p38 MAPK in a variety of cells, including cardiomyocytes, endothelial cells, bronchial epithelial cells, smooth muscle cells, hepatocytes, and neural cells[217]. One of the functions of peroxynitrite-mediated p38 MAPK activation is induction of apoptosis[217,283,284]. It has been reported that peroxynitrite activates p38 MAPK in response to upstream activation of ERK by zinc ions in primary neurons, enhancing apoptosis-dependent cell death in the brain[217]. In fact, excessive peroxynitrite production in neurons has been associated with the development of many neurological disorders[217].

Peroxynitrite also impacts the NF-κB signalling pathway[217,285]. NF-κB is a critical transcription factor that activates inflammatory and anti-apoptotic genes in response to diverse stimuli[217,285]. Low levels of peroxynitrite (10-200 μM) have been shown to activate NF-κB, possibly through nitration of its inhibitor IκB-α[217,285]. In contrast, at 200 μM, peroxynitrite inhibited nuclear translocation of NF-κB *in vitro*[217,285]. The fact that peroxynitrite downregulates the expression of pro-inflammatory mediators such as NF-κB suggests that peroxynitrite creates a feedback loop, forming a counterregulatory system that prevents oxidative stress-mediated pathological conditions[217,285]. Overall, peroxynitrite has been shown to exert dual effects on many signalling pathways. The conditions that determine the type of impact peroxynitrite will have on a particular signalling pathway remain unclear.

In summary, peroxynitrite has a concentration-dependent effect on cellular signalling, exerting dual effects at different concentrations[217]. The biphasic nature of peroxynitrite-specific signalling explains the conflicting results reported in the literature, where several peroxynitrite-mediated effects have been shown to be both cytotoxic and cytoprotective[217]. Figure 3.2 summarizes major signalling pathways affected by peroxynitrite *in vitro*. The lack of confirmation of peroxynitrite-mediated modulation of signal transduction *in vivo* poses a challenge to fully understanding the effects of peroxynitrite reactivity on critical cell signalling pathways in health and disease. Nonetheless, novel and stable pharmacological

drugs aimed at neutralising intracellular peroxynitrite in a dose-dependent manner could be a great therapeutic tool to combat peroxynitrite-induced inflammation and subsequent pathogenesis[281].

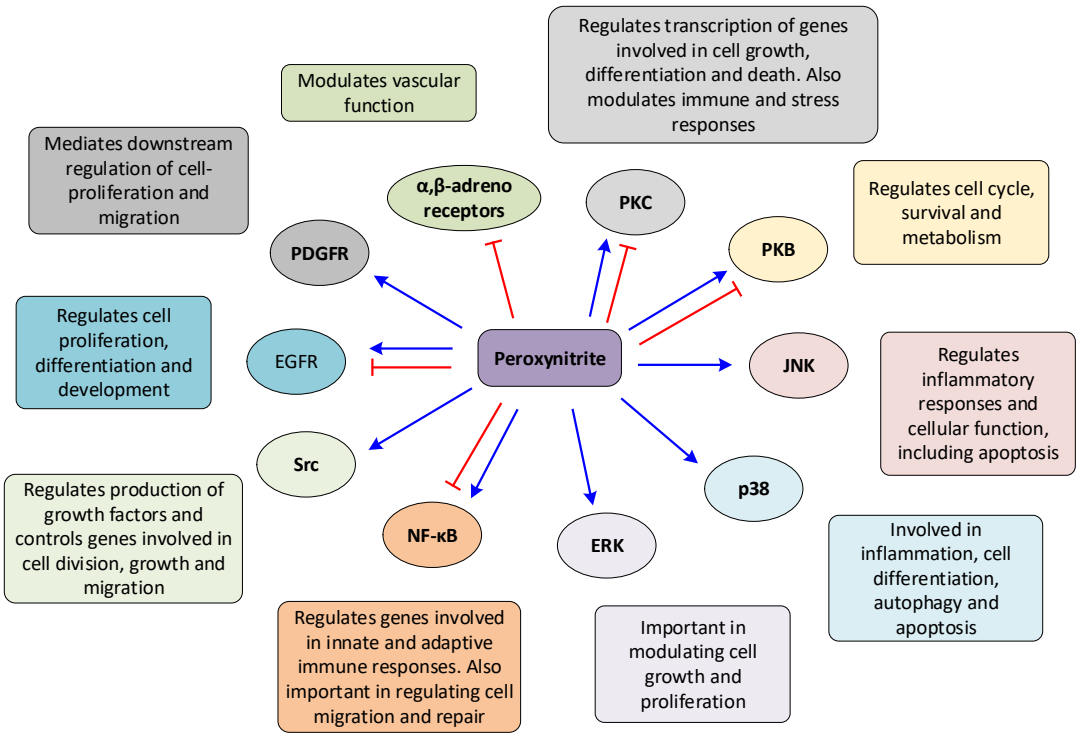

Figure 3.2: Peroxynitrite-mediated modulation of cellular signalling pathways

Peroxynitrite can activate (blue arrow) and/or inhibit (red) signalling pathways based on cell type, concentration, and redox microenvironment. Figure is a modified version of image in [254].

3.1.4 Pathological effects of Peroxynitrite.

The effects of peroxynitrite in biological systems can be paradoxical. During homeostasis, endogenous antioxidant defence systems keep peroxynitrite production low, minimising oxidative damage[211]. However, even a modest increase in simultaneous production of superoxide and nitric oxide can induce peroxynitrite generation[211]. In fact, it has been reported that a 10-fold increase in superoxide and nitric oxide formation subsequently results in a 100-fold increase in the generation of peroxynitrite[217]. Consequently, pathological conditions can dramatically increase the production of peroxynitrite[217]. In fact, superoxide and nitric oxide generation can be increased by 1000-fold in activated macrophages, inevitably increasing peroxynitrite formation by 1,000,000-fold[217].

In the presence of persistent causative stimuli (such as exposure to high levels of UV, hyperglycaemia, chemical toxins, and pathogens), iNOS is quickly activated, leading to rapid production of peroxynitrite[217,280,281]. The effects of peroxynitrite will be deleterious if it is spontaneously generated, maintained at high levels or if it triggers a robust nitro-oxidative response[217,280,281]. Interestingly, even moderate fluctuations in peroxynitrite production over long periods of time can lead to considerable levels of oxidative damage[217,280,281]. Accumulation of peroxynitrite will induce overt inflammation and oxidative stress, leading to cell damage, dysfunction of intracellular process, disruption to signalling pathways and, ultimately, apoptosis or necrosis[217,280,281].

Oxidative stress is inevitable in many chronic diseases and occurs due to redox imbalance; where the production of reactive species overwhelms the ability of intracellular antioxidant mechanisms to decompose these reactive molecules[211]. Accumulation of reactive molecules can activate many signalling pathways, exacerbating the pathological state[211]. For example, peroxynitrite can cause uncoupling of eNOS through oxidisation of eNOS cofactor BH4[217,280,281]. Uncoupled eNOS further promotes events that favour peroxynitrite production and help

maintain a peroxynitrite rich environment[217,280,281]. This process has been known to contribute to oxidative stress-facilitated dysfunction of endothelial vasculature in various inflammatory diseases[217,280].

In chronic conditions, the cellular stress environment becomes more "nitro-oxidative" rather than purely oxidative[282]. The cytotoxic potential of peroxynitrite can be explained by its ability to trigger both oxidative and nitrosative biochemical reactions within a cell[217,280,281]. Being a potent oxidising and nitrating agent allows peroxynitrite to alter the structure and function of multiple proteins, disrupt metabolic pathways, degrade lipids through peroxidation and irreversibly damage nucleic acids, triggering cellular pathways of DNA repair via activation of PARP (Figure 3.1)[217,280,281]. If peroxynitrite-induced damage exceeds the capacity of repair mechanisms within the cell, apoptotic or necrotic cell death pathways are activated (Figure 3.1)[217,280,281].

3.1.5 Practical aspects of working with peroxynitrite

The volatile nature of peroxynitrite makes it challenging to monitor peroxynitrite-mediated effects *in vitro* and *in vivo*. It is very important to consider the pH of tissue culture media when working with peroxynitrite[217,280,281]. Peroxynitrite is relatively stable in basic solutions, however, decomposition of peroxynitrite is very rapid (within minutes) at neutral pH and instantaneous (<10 ms) in acidic conditions[217,280,281]. Therefore, it may be important to increase the pH of media (usually between 6.8-7.2) using sodium hydroxide prior to working with peroxynitrite[217,280,281]. Additionally, peroxynitrite may interact with some of the constituents of tissue culture media. The type, quality and number of supplements added to basic culture media can affect the nature of the biological response produced by peroxynitrite. Thus, it may be necessary to optimise experiments in serum-free media. The short-lived nature of peroxynitrite makes it difficult to effectively monitor peroxynitrite production in living cells[281,286–288]. Superoxide and nitric oxide concentrations can indirectly indicate the degree of peroxynitrite production; however, this approach may not be accurate as these are themselves rapidly turned over[281,286–288]. Alternatively, the contribution of peroxynitrite in cellular processes is often confirmed through inhibition of superoxide and/or nitric oxide production because the absence of superoxide/nitric oxide will abrogate peroxynitrite generation, attenuating any peroxynitrite-mediated biological effects[281,286–288]. Other methods involve using probes that directly react with peroxynitrite or its secondary radicals[281,286–288]. There are many commercially available kits that use a fluorescent probe designed to 'specifically' bind to intercellular peroxynitrite, thus generating a fluorescent signal for quantification[281,286–288]. Another approach is to measure 3-NT, which is a stable product formed from the reaction of downstream products derived from peroxynitrite and tyrosine residues[281,286–288]. Although many methods are available to quantify peroxynitrite, the probes may not be highly specific or particularly sensitive[281,288]. For example, many types of ROS may be involved in modulating the same biological processes, making it particularly challenging to

conclude whether the observed biological effect is explicitly due to the action of peroxynitrite[288]. Therefore, peroxynitrite-specific scavengers are regularly used to examine the biological effect of peroxynitrite[281]. Similarly, scavengers of other reactive molecules (such as H_2O_2) generated downstream of superoxide or nitric oxide, through independent branches of ROS/RNS signalling (Figure 3.3), should not alter the peroxynitrite-specific effect. Hence, it is often recommended to use a panel of specific and non-specific peroxynitrite scavengers to validate results[281,288].

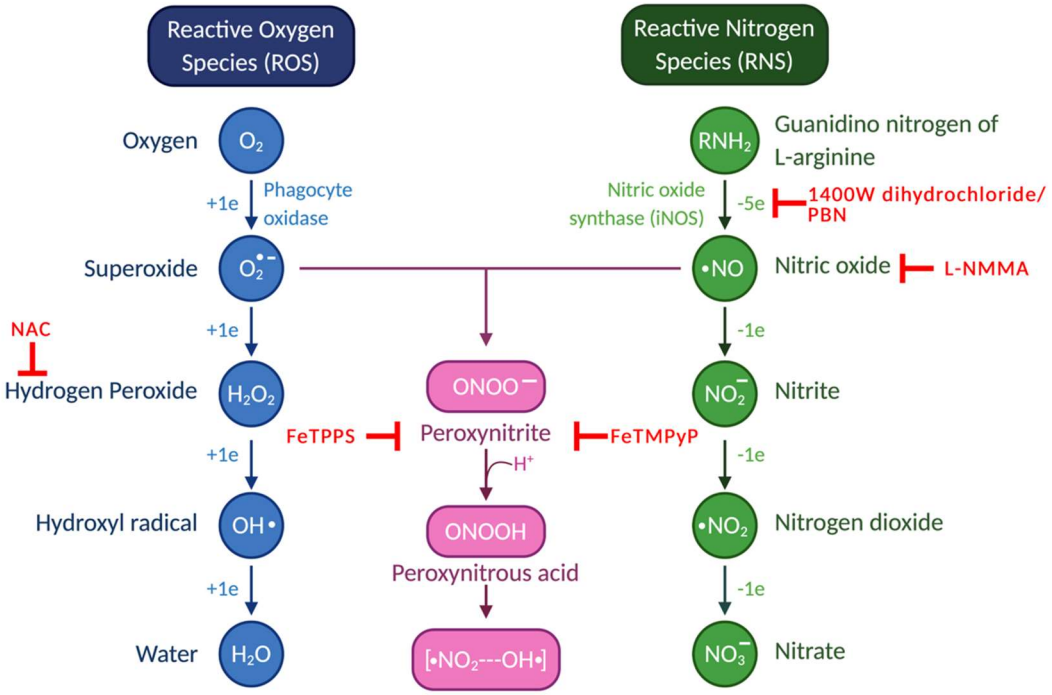

Figure 3.3: Targets of inhibitors that can directly or indirectly confirm peroxynitrite-specific signalling by targeting molecules upstream of peroxynitrite.

Inhibitors of ROS-producing enzymes or scavengers of specific ROS are shown in red. Details of each inhibitor is provided in Table 6.

3.1.6 Aims

The intracellular redox micro-environment within a cell has an important role in regulating many host-virus interactions[128,255]. The susceptibility of host cells to viruses, including Human Immunodeficiency Virus (HIV), coxsackievirus, influenza viruses and herpes simplex virus-1 (HSV-1), is affected by redox signalling pathways and oxidative stress[128,255]. It has also been demonstrated that ROS are involved in many viral-associated immunopathogeneses[289–292].

Cells produce high levels of reactive species in response to HCMV infection[291,293,294], especially immune cells. A significant amount of superoxide production has been observed in cells following infection with HCMV *in vitro*[291,293,294]). Additionally, immune cells infiltrate and release nitric oxide at localised sites of HCMV infection to inhibit HCMV replication, thereby creating an ideal environment for peroxynitrite production[291,293,294]. Intriguingly, peroxynitrite has been shown to both inhibit (coxsackievirus) and promote (HIV) viral entry and replication[295,296]. Consequently, I hypothesised that peroxynitrite is involved in regulating the HCMV replication cycle.

The aims of this chapter are as follows:

1. Characterize the role of peroxynitrite during cell-free HCMV infection.
2. Identify when during the HCMV lytic cycle peroxynitrite impacts HCMV replication.
3. Determine whether inhibition of peroxynitrite influences CMV replication *in vivo*.

3.2 Results

3.2.1 Peroxynitrite is required for lytic HCMV replication

3.2.1.1 HCMV rapidly induces the production of peroxynitrite

HCMV infection has been associated with the production of ROS, especially within minutes of viral entry into target cells[291]. Furthermore, levels of ROS have been shown to increase with persistent HCMV replication[291]. Accordingly, I first sought to investigate whether peroxynitrite was generated upon HCMV infection.

Several cells of the myeloid lineage (such as monocytes, macrophages, and dendritic cells) are thought to be important cellular host targets for HCMV *in vivo* (Section 1.1.3). Although monocytes are not permissive for lytic HCMV replication, they are reservoirs for latent HCMV, which can be reactivated upon the terminal differentiation of monocytes[33]. Consequently, the THP-1 monocytic cell line, which could be stimulated into macrophage-like cells, served as a useful *in vitro* model for HCMV replication[40]. Additionally, infection with HCMV strains containing an enhanced green fluorescent protein (GFP) linked to IE gene UL36 ORF with a P2A self-cleaving peptide (UL36-P2A-GFP), led to high-level GFP expression by 24 hpi, allowing the infection state to be monitored by flow cytometry or fluorescence microscopy[66]. TB40-BAC4 HCMV strain tagged with GFP (TB40/E-GFP) was used to infect differentiated THP-1 cells. As explained in Sections 1.1.3 and 1.1.5, TB40/E contains both trimeric (gH/gL/gO) and pentameric (gH/gL/UL128/UL130/UL13A) complexes, enabling cell-free infection of epithelial, endothelial, and myeloid cells despite extensive passaging in fibroblasts.

To detect peroxynitrite generation, THP-1 cells were first stimulated with PMA to differentiate into macrophage-like cells and thus permit lytic HCMV replication[40]. Prior to infection with TB40/E-GFP, differentiated THP-1 cells were incubated with a fluorescent probe designed to specifically bind to intracellular peroxynitrite and produce a bright-green, fluorescent product that can be detected using a

fluorescent microplate reader (Ex/Em = 490/530 nm; Section 2.6.2). This cell-based assay enabled the detection of peroxynitrite generation in HCMV infected cells in real-time. Although GFP-expressing HCMV was used for all infections, GFP is not expressed until 24 hpi and, thus, is unlikely to interfere with the signal emitted by the peroxynitrite probe (Ex/Em = 490/530 nm).

HCMV rapidly induced the production of peroxynitrite upon infection of PMA-differentiated THP-1 cells (Figure 3.4). As compared to uninfected control, intracellular peroxynitrite levels increased within the first few seconds of HCMV infection (Figure 3.4). This suggested that HCMV binding to host cell membrane receptors might be sufficient to trigger simultaneous production of superoxide and nitric oxide, leading to the generation of peroxynitrite. The estimated basal rate of peroxynitrite generation in cells is between 0.1 to 0.5 μM per second[217,283]. Many studies have shown that the production of peroxynitrite occurs despite the presence of antioxidant enzymes such as SOD[217,283]. In fact, nitric oxide is the only known molecule that readily outcompetes SOD for superoxide[217,283]. This highlights that the reaction of nitric oxide with superoxide, which occurs at a rate of 6.7×10^9 moles per litre per second (mol/L/s), is so fast that it kinetically outcompetes enzyme-catalysed decomposition of superoxide[217,283]. Therefore, peroxynitrite formation occurs very soon after the initial production of both superoxide and nitric oxide occurs within close proximity to each other.

As mentioned in Section 3.1.1, peroxynitrite has a very short half-life, making it challenging to detect and monitor its effects in biological systems[288]. Accordingly, different approaches are required to confirm peroxynitrite formation in response to HCMV. To ensure that the fluorescent peak detected in my assay represented the generation of peroxynitrite, differentiated THP-1 cells were treated with a potent peroxynitrite scavenger (FeTPPS) prior to HCMV infection. FeTPPS strongly inhibited HCMV-induced peroxynitrite generation from the onset of infection, generating a signal below the baseline throughout the assay (Figure 3.4). A similar phenotype was also observed when the cells were pre-treated with a different

peroxynitrite scavenger (FeTMPyP) prior to HCMV infection (Figure 3.4). Furthermore, incubation of cells with NAC, a selective hydrogen peroxide inhibitor[294], did not affect HCMV-induced peroxynitrite production (Figure 3.4), further validating that FeTPPS and FeTMPyP specifically inhibited peroxynitrite production.

Macrophages are phagocytic cells that are known to produce ROS in response to pathogens (Section 1.2.6.1). Therefore, to ensure that the observed production of peroxynitrite was virus-induced and not cell-type specific, peroxynitrite generation was also monitored in HCMV-infected fibroblasts. HCMV infection triggered peroxynitrite production in fibroblasts within seconds of infection. Following infection with TB40/E, levels of intracellular peroxynitrite in fibroblasts as comparable to the peak generated in differentiated THP-1 cells (Figure 3.4). Additionally, Merlin HCMV strain also induced peroxynitrite generation in fibroblasts compared to uninfected control). The peak generated by Merlin was very similar to that produced following infection with TB40/E (Figure 3.4), suggesting peroxynitrite generation is not HCMV strain specific. Furthermore, both TB40/E and Merlin were unable to trigger peroxynitrite generation in fibroblasts pre-treated with peroxynitrite scavenger (Figure 3.5). Unexpectedly, peroxynitrite concentration increased after 150 min in FeTPPS treated fibroblasts. This increase could be explained if the amount of FeTPPS available was not sufficient at scavenging peroxynitrite. Biological repeat is required to determine if the observed trend is true. It was not possible to monitor peroxynitrite production after 200 min with this experimental setup as the Peroxynitrite Sensor Green reagent depleted over time.

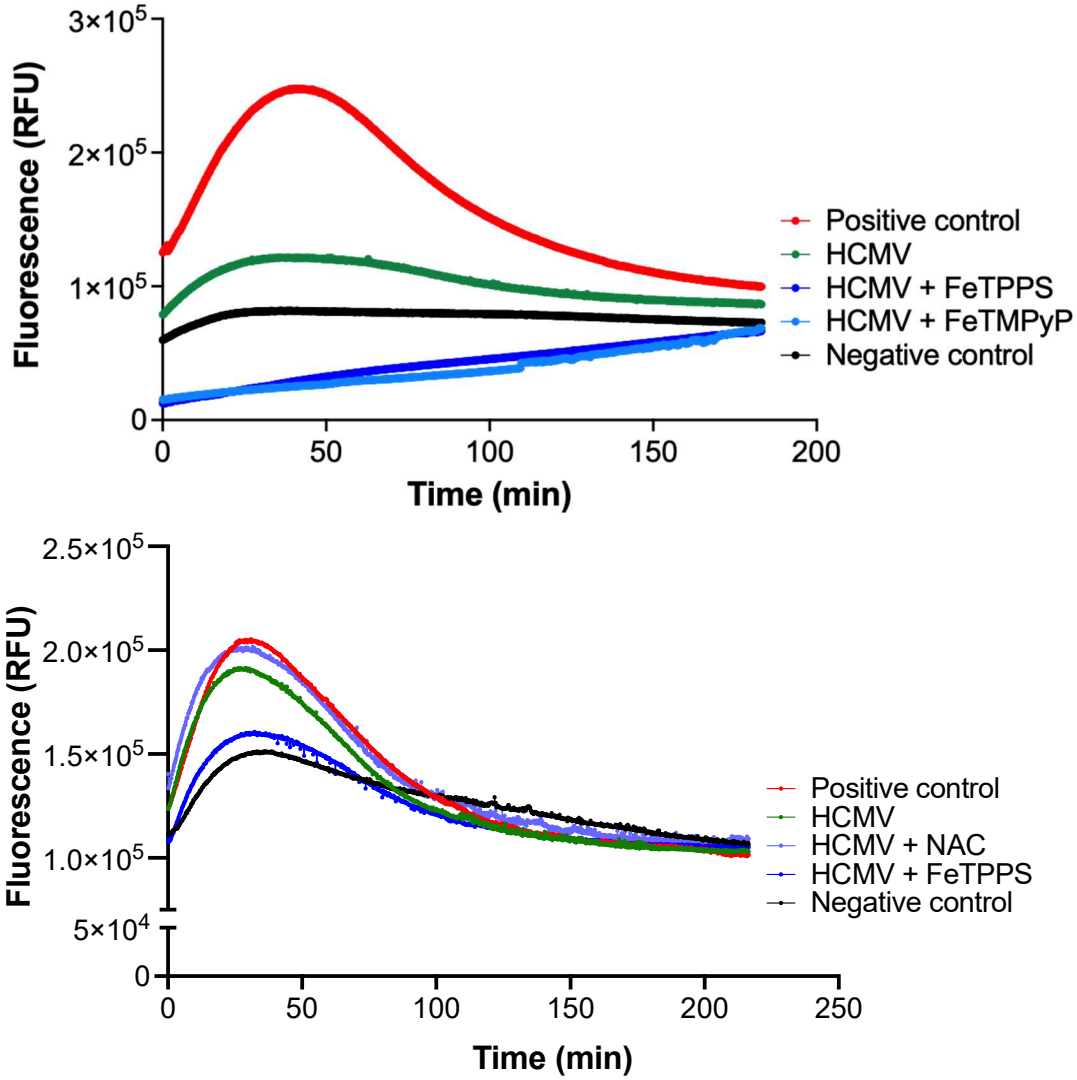

Figure 3.4: TB40/E rapidly induces production of peroxynitrite upon infection in macrophage-like cells.

Differentiated THP-1 cells, treated with or without FeTPPS (25 μM), FeTMPyP (25 μM) and NAC (10mM), were incubated with a fluorescent probe that binds to intracellular peroxynitrite. After addition of TB40/E (MOI 5), fluorescence intensity was measured (Ex/Em = 490/530 nm) every 20s for 180 (top) or >200 min (bottom). Uninfected cells that were stimulated with or without FCS were used as positive and negative controls, respectively. Average fluorescence was plotted (n = 2). The data represents trends observed in four independent experiments.

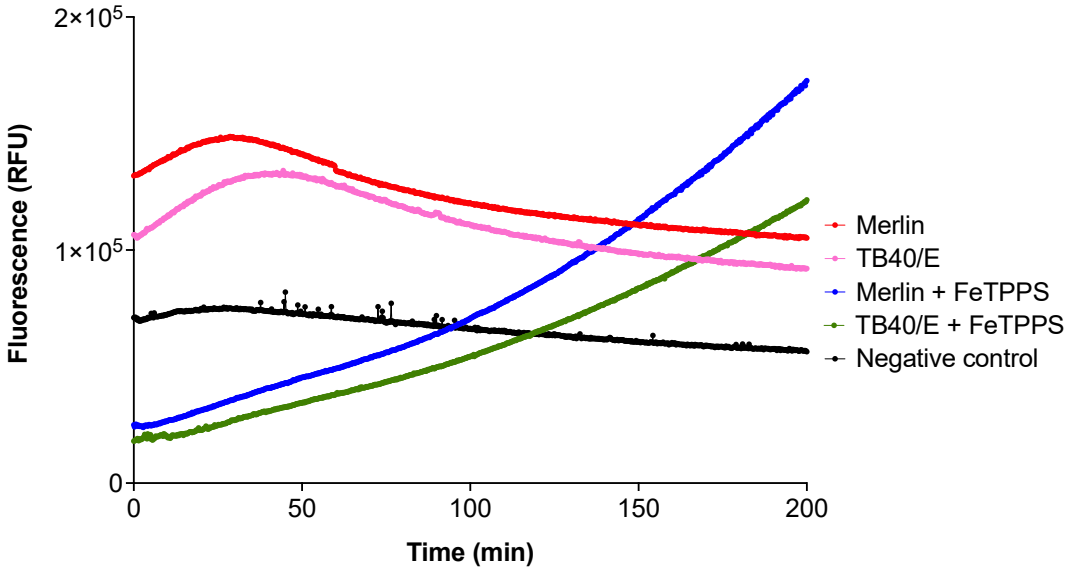

Figure 3.5: TB40/E and Merlin increase production of peroxynitrite in fibroblasts within minutes of infection.

HFFF-TERTs were incubated with a fluorescent probe that specifically binds to peroxynitrite. The fluorescence intensity was measured every 20s for 200 min, following addition of HCMV. Cells were treated with or without FeTPPS prior to infection with TB40/E or Merlin (MOI 5). Uninfected fibroblasts were used as negative control. Graph represents data of a single experiment plotted as average fluorescence (n = 2).

3.2.1.2 Inhibition of peroxynitrite reduces cell-free HCMV infection in monocyte-derived macrophages

To understand the contribution of peroxynitrite generation during HCMV infection, PMA-derived THP-1 macrophages were infected with TB40/E-GFP in the presence or absence of FeTPPS. The use of GFP-expressing HCMV (UL36-P2A-GFP), which led to high levels of GFP expression at 24 hpi, allowed detection of infected (GFP+) versus uninfected (GFP-) cells by flow cytometry[66]. Since new virions are not synthesised until 72 hpi (Section 1.1.6), the experimental setup permitted GFP expression to be used as a marker for HCMV entry and replication at 24 and 72 hpi, respectively.

FeTPPS potently inhibited HCMV replication in THP-1-derived macrophages, leading to an approximately 80% decrease in infected (GFP+) cells at 72 hpi (Figure 3.6 A). In fact, a near-complete inhibition of HCMV replication was achieved with FeTPPS (25μM), as compared to vehicle control-treated cells (Figure 3.6A-B), indicating the importance of peroxynitrite in HCMV replication. To ensure that the observed phenotype was due to depletion of peroxynitrite, differentiated THP1 cells were pre-treated with different concentrations of peroxynitrite scavenger prior to cell-free HCMV infection. A significant dose-dependent anti-HCMV activity was achieved in THP-1-derived macrophages following treatment with an alternative peroxynitrite scavenger, FeTMPyP (Figure 3.6C). At a concentration of 10 μM, FeTMPyP was able to reduce productive HCMV replication in differentiated THP-1 cells by ~50% (Figure 3.6 C). Additionally, pre-treatment of cells with FeTMPyP was able to maintain inhibition of viral replication as measured 72 hpi. Although no visual signs of toxicity were observed at lower doses of FeTMPyP (10-50 μM), a high level of cell death was observed with doses higher than 100μM.

To further validate the contribution of peroxynitrite generation in the lytic replication HCMV, differentiated THP-1 cells were incubated with different inhibitors of NOS to prevent the synthesis of nitric oxide. Surprisingly, NOS

inhibitors, 1400W dihydrochloride (50 μM) and L-NMMA (250 μM) did not reduce HCMV replication in differentiated THP-1 cells (Figure 3.6 B). Although this suggests that peroxynitrite may not be essential for HCMV replication, based on the assumption that NOS is critical for peroxynitrite production, the high percentage of infected cells after NOS inhibition is more likely a consequence of using NOS inhibitors at a concentration that was insufficient to inhibit nitric oxide production[297]. Furthermore, 1400W dihydrochloride is a slow-acting time-dependent inhibitor of NOS and may require pre-treatment for a longer time (>5 h) to be effective[298]. Overall, these results highlight the importance of pharmacokinetic and toxicokinetic studies to evaluate the effect of anti-viral test compounds. Nonetheless, the anti-viral effects of FeTPPS and FeTMPyP indicate that pre-emptive treatment with a peroxynitrite scavenger could potentially reduce the incidence of productive HCMV replication in certain clinical settings.

3.2.1.3 Inhibition of peroxynitrite reduces the cell-to-cell spread of HCMV from fibroblasts into monocyte-derived macrophages

HCMV transmission may occur via free virus particles (cell-free) or by direct cell-to-cell contact[21]. Previous studies have shown that clinical HCMV isolates can efficiently spread through the monolayer even though they are unable to generate high titres of the cell-free virus, indicating HCMV may prefer to spread by cell-to-cell contact *in vivo*[21]. Accordingly, I decided to use GFP-expressing 'wildtype' (WT), or UL128-repaired Merlin strain (Merlin-UL128^{WT}GFP), to investigate whether peroxynitrite is required for the cell-to-cell spread of HCMV *in vitro*.

As described in Section 1.1.5 and 2.3.2, Merlin-UL128^{WT} is grown in fibroblasts expressing tetracycline repressor (tetR) protein[27,52]. This keeps UL128 under the control of tetR, preventing it to acquire mutations when the virus is propagated *in vitro*[27,52]. Subsequent infection in fibroblasts lacking tetR (HFFF-TERT or HFFF) restores the pentamer in virions after a complete lytic cycle[27,52]. These conditions do not yield high quantities of cell-free virus, however, the virions produced can

spread efficiently by direct cell-to-cell contact[27,52]. Consequently, efficient infection of differentiated THP-1 cells with WT Merlin was achieved by co-culture, using HFFF-TERT infected with Merlin-UL128^{WT}GFP.

Prior to co-culture, HFFF-TERTs were infected with GFP-expressing Merlin. Furthermore, Merlin-infected HFFF-TERTs were pre-stained with CellTrace Far Red dye, allowing them to be distinguished from unstained THP-1-derived macrophages. At 72 hpi, infected HFFF-TERTs were incubated with differentiated THP-1 cells in the presence of a potent peroxynitrite scavenger. After an additional 72h, the proportion of differentiated THP-1 cells infected was determined by flow cytometry. As seen in Figure 3.6 D, FeTPPS treatment significantly reduced contact-dependent HCMV infection in monocyte-derived macrophages. The proportion of THP1-derived macrophages infected with Merlin was significantly lower in FeTPPS-treated cells (<5% GFP+) compared to untreated controls (~20% GFP+) (Figure 3.6 D). This indicated that peroxynitrite is essential for both cell-free and cell-to-cell HCMV infection. Furthermore, these results suggest that the effect of peroxynitrite on HCMV replication in myeloid cells was not virus strain-specific.

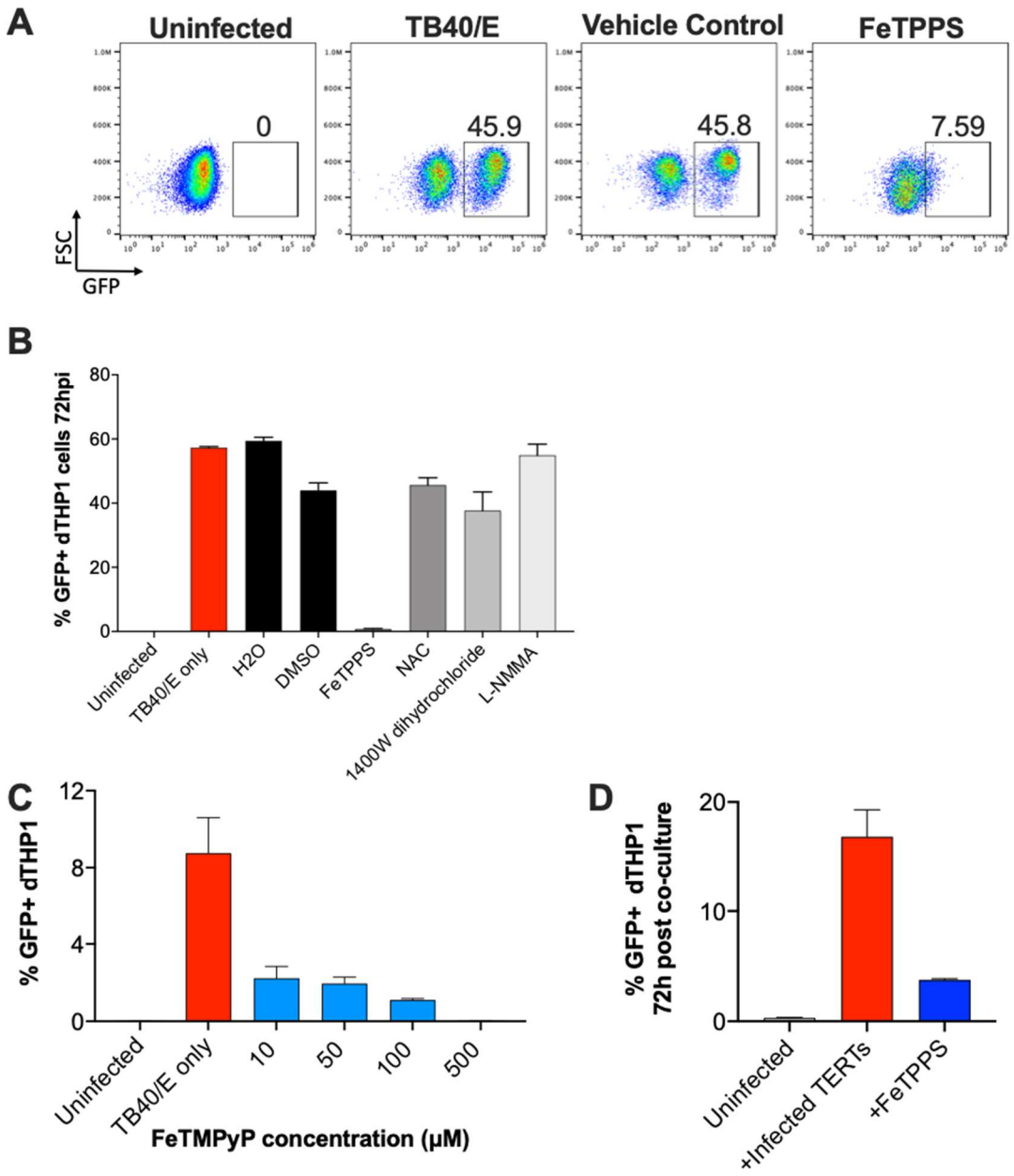

Figure 3.6: Peroxynitrite is essential for lytic HCMV replication in monocyte-derived macrophages

(A) Representative FACS plots showing the proportion of HCMV-infected differentiated THP-1 cells (GFP +) in presence or absence of FeTPPS (25 μM). H_2O was used as vehicle control. Differentiated THP-1 (dTHP1) cells were infected with TB40/E-GFP at MOI 20. **(B)** dTHP-1 were treated with FeTPPS (25 μM), NAC (10 mM), 1400W dihydrochloride (50 μM) or L-NMMA (250 μM) prior to infection with TB40/E -GFP (MOI 25). H_2O or DMSO were used as vehicle controls. **(C)** Differentiated THP-1s were treated with FeTMPyP (10-500 μM) and infected with TB40/E-GFP at MOI 5. **(D)** FeTPPS treated (25 μM) differentiated THP-1 cells were co-cultured with HFFF-TERTs infected with Merlin-UL128^{WT}GFP (1:3 ratio). For **A-D,** the percentage of GFP-positive dTHP1 cells was measured at 72 hpi by flow cytometry. Data plotted as mean ± SEM from three replicates. The results are representative of one (**C**), two (**D**) or four (**A-B**) independent experiments.

3.2.1.4 Decomposition of peroxynitrite reduces cell-free HCMV infection in primary dendritic cells (DC).

To determine whether peroxynitrite-mediated regulation of HCMV replication in myeloid cells was also evident during infection of primary cells, human blood-derived DCs (provided by Dr Lauren Kerr, Cardiff University) were infected with TB40/E-GFP in presence of FeTPPS (25 μM) or FeTMPyP (25 μM) (Figure 3.7 A-B). Although primary cells have a limited lifespan and division potential in culture, they retain most all molecular and functional properties *ex vivo* and thus are more physiologically relevant models for studying viral infections. Treatment with both peroxynitrite scavengers inhibited HCMV replication in primary DCs (Figure 3.7 A-B).

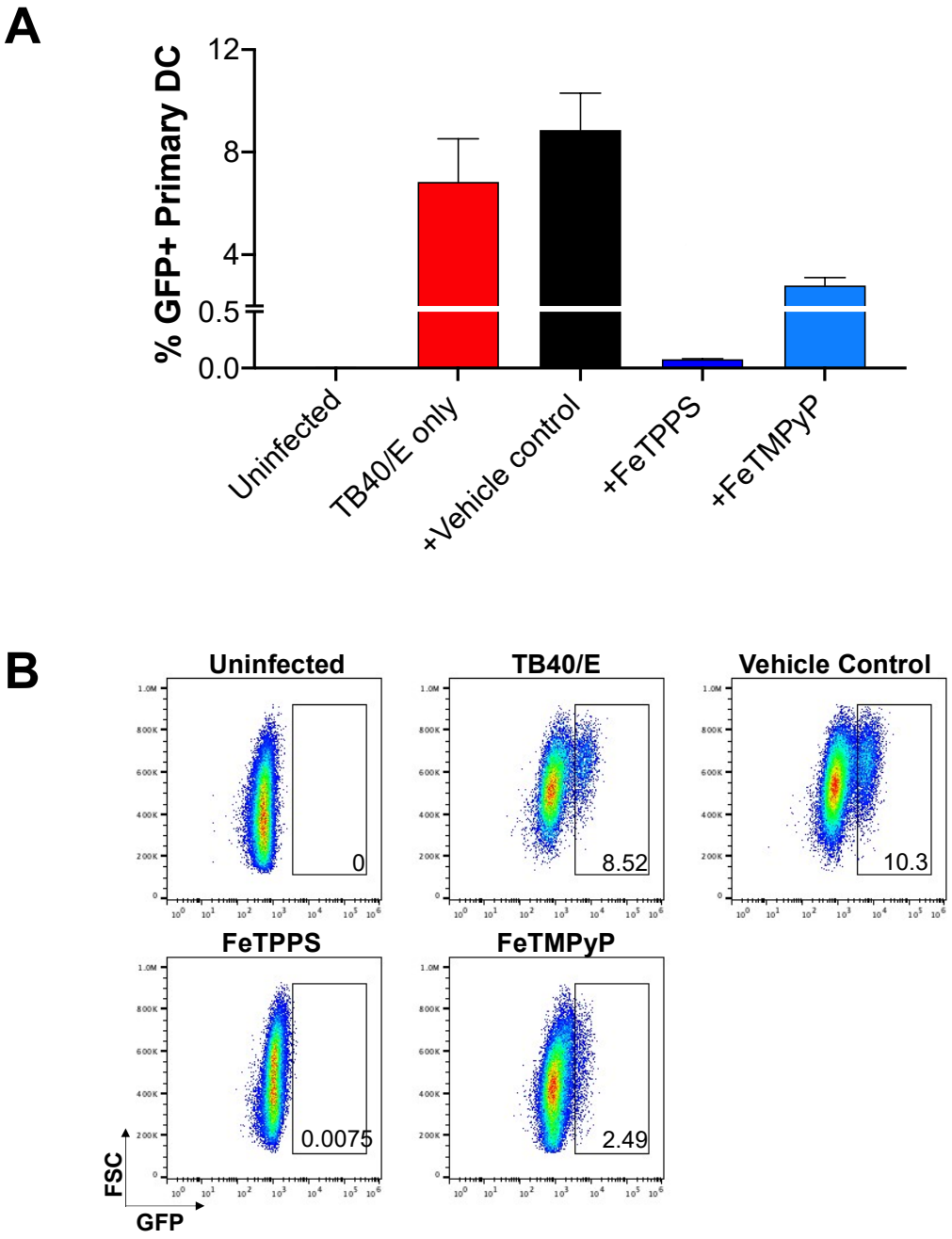

Figure 3.7: Peroxynitrite is essential for HCMV infection in primary DC.

(A) Primary CD11b+ cells (that include DC) were pre-treated with FeTPPS (25 μM) or FeTMPyP (25 μM) prior to infection with TB40/E-GFP (MOI 25). The percentage of cells expressing GFP was determined by flow cytometry at 72hpi. Data plotted as mean ± SEM (n=2) **(B)** Representative FACS plots showing percentage of HCMV infected human blood-derived CD11b+ cells (GFP+) following treatment with FeTPPS/FeTMPyP compared to that of controls. H_2O was used as vehicle control. The findings are representative of two independent experiments.

3.2.1.5 Peroxynitrite is required for cell-free HCMV infection of an immortalised human fibroblast cell line.

HCMV can enter and efficiently replicate in a range of different host cells. The extremely broad target cell range contributes to the pathogenesis of chronic HCMV infection, facilitating both intra-and inter-host spread. To determine if peroxynitrite is also required for lytic HCMV infection in non-myeloid cells, HFFF-TERTs were infected with two different GFP-expressing HCMV strains (TB40/E-GFP and Merlin-UL128^{WT}GFP) in the presence of peroxynitrite scavengers. At a concentration of 25μM, pre-treatment with FeTPPS and FeTMPyP potently inhibited cell-free HCMV infection of HFFF-TERT (Figure 3.8 and Figure 3.9). The antiviral effect of FeTPPS was concentration-dependent (Figure 3.8 A) and persisted even at 72 hpi (Figure 3.8 B), indicating peroxynitrite might be involved in the production of new virions. As compared to untreated samples (~60% GFP+), decomposition of peroxynitrite inhibited replication of both TB40/E (<15% GFP+) and Merlin (0.063% GFP+) in fibroblasts at 72 hpi (Figure 3.8 B-C). In fact, HFFF-TERT cells pre-treated with FeTPPS could not be infected with Merlin and displayed a phenotype similar to that of uninfected controls (Figure 3.8 C and Figure 3.9). At 24hpi, no obvious HCMV-induced CPE (rounding or cell detachment) was visible in FeTPPS-treated cells (Figure 3.9 C), suggesting peroxynitrite is required for the initiation of the HCMV lytic cycle.

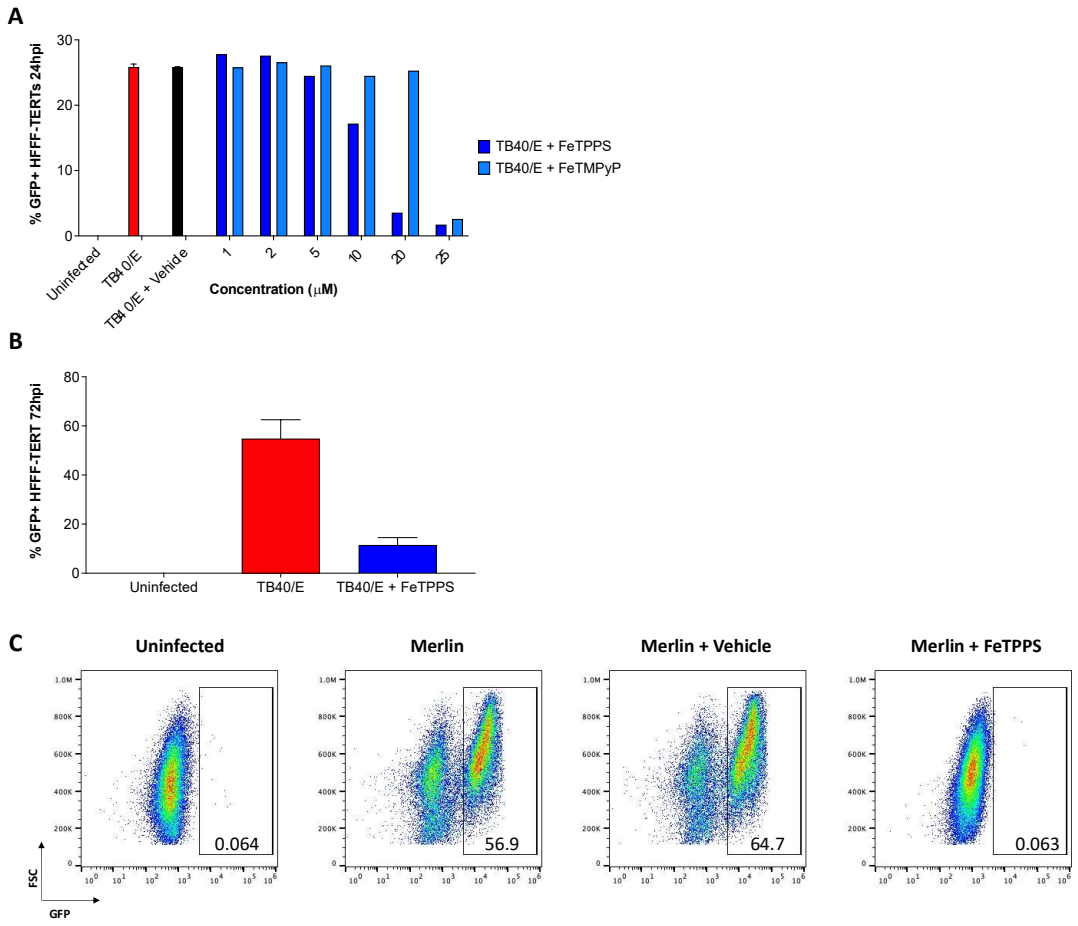

Figure 3.8: Peroxynitrite is essential for viral replication in fibroblasts, following cell-free infection with TB40/E and Merlin HCMV strains.

A) HFFF-TERTs were pre-treated with FeTPPS/FeTMPyP (1-25 μM) and infected with TB40/E-GFP (MOI 5) for 24h prior to flow cytometry analysis. **(B)** HFFF-TERTs were pre-treated with FeTPPS (25 μM) or vehicle (H_2O) and infected with TB40/E-GFP (MOI 5) for 72 hours prior to FACS. **(C)** Representative FACS plots Merlin-infected HFFF-TERT at 72 hpi. Fibroblasts were pre-treated with FeTPPS (25μM) or Vehicle (H_2O) prior infection with Merlin-UL128^{WT}GFP. At 72 hpi, proportion of infected HFFF-TERT cells (GFP+) were determined by flow cytometry. Data is presented as mean ± SEM (n =3) in A-B. The results are representative of one (**A**), two (**B**) or three (**C**) independent experiments.

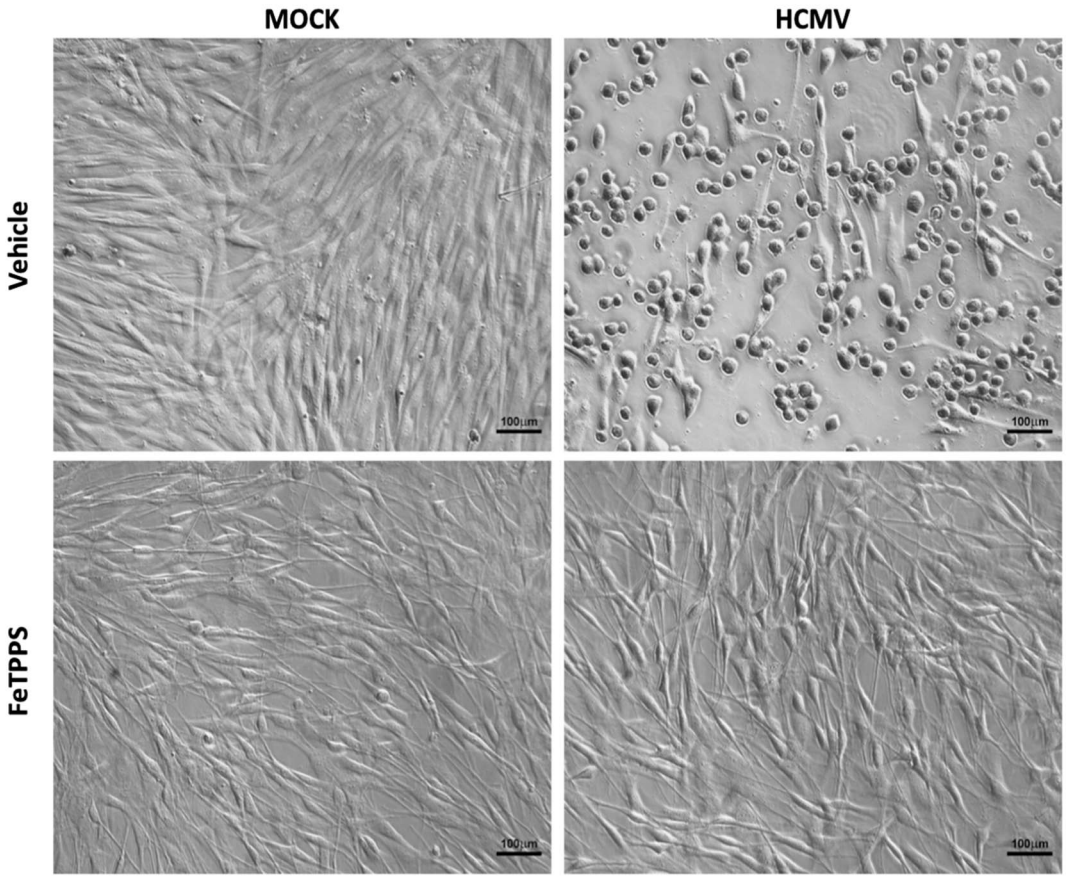

Figure 3.9: FeTPPS protects fibroblasts from HCMV-induced CPE, without compromising cellular morphology.

Representative transmission electron microscopy images of confluent cultures of fibroblasts that were pre-treated with FeTPPS (25µM) or Vehicle (H_2O control) prior to infection with Merlin-UL128^{WT} (MOI 5). Cell cultures were fixed 24hpi. Scale bar: 100 µm.

3.2.2 Peroxynitrite is essential during the initial stages of lytic HCMV infection

To help understand how peroxynitrite supports HCMV replication, I first sought to investigate when in the virus replication cycle peroxynitrite was required. TB40/E-GFP and Merlin-UL128^{WT}GFP were used to directly infect PMA-differentiated THP-1 cells and HFFF-TERTs, respectively. FeTPPS was added at 6-hourly intervals following cell-free HCMV infection. Cells that were pre-treated with FeTPPS prior to infection were also included in the study. At 72hpi, the proportion of GFP-positive cells was determined by flow cytometry (Figure 3.10). The results revealed a time-dependent anti-HCMV activity of FeTPPS treatment in monocyte-derived macrophages (Figure 3.10 A) and fibroblasts (Figure 3.10 B). The maximal anti-viral effect of FeTPPS on HCMV replication occurred within the first 12hr in both cell types (Figure 3.10). The most profound effect on HCMV replication (<0.5 % GFP+) was achieved with inhibition of peroxynitrite prior to or at the onset of HCMV inoculation (Figure 3.10), implying that peroxynitrite could be essential for facilitating cell entry and/or initiating viral replication.

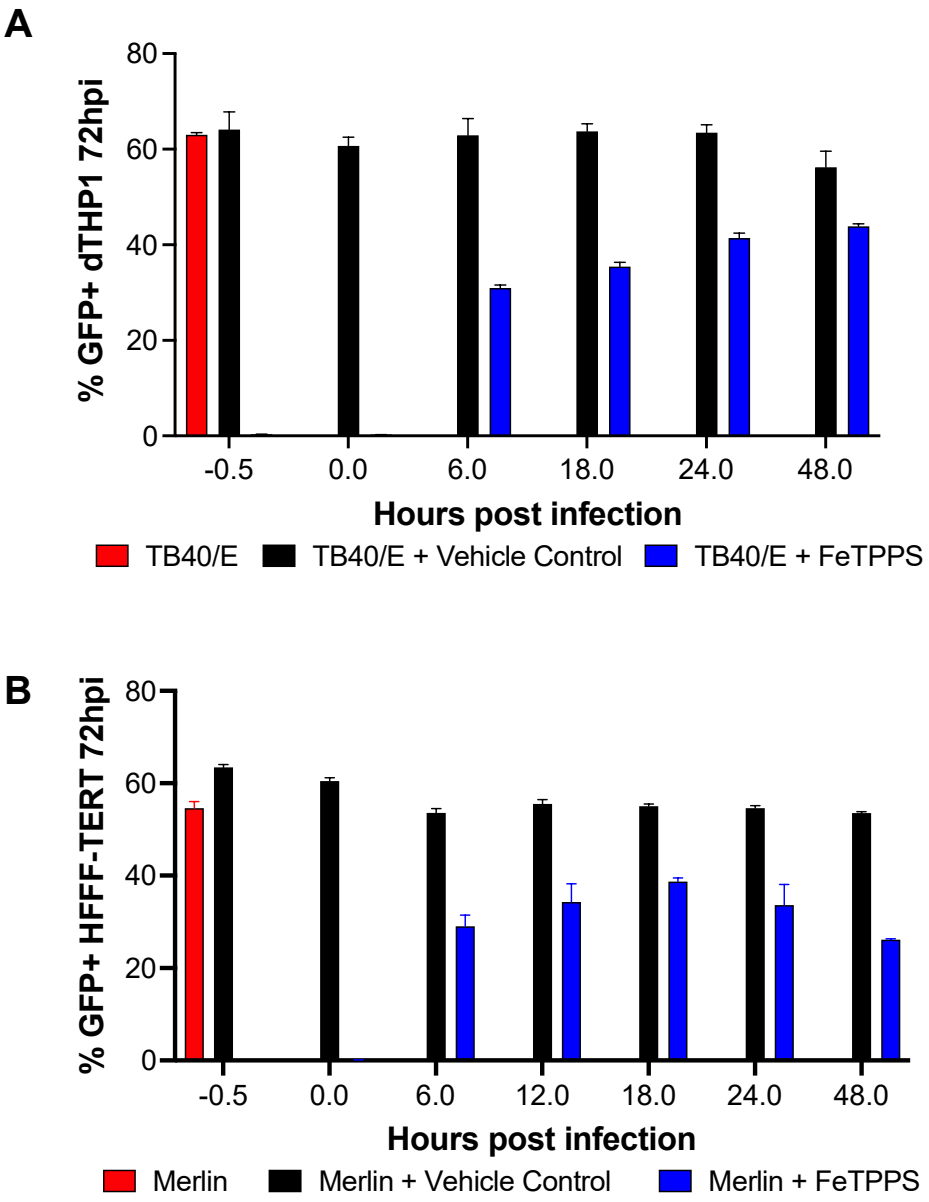

Figure 3.10: Peroxynitrite is essential at early times of cell-free HCMV infection of monocyte-derived macrophages and fibroblasts.

(A) Differentiated THP-1 cells were infected with TB40/E-GFP (MOI 25) and treated with FeTPPS (25 μM) at different timepoints (6-24 hourly intervals for 48hpi). **(B)** HFFF-TERTs were infected with Merlin-UL128^{WT}GFP (MOI 5) and treated with FeTPPS (25 μM) at different timepoints (6-24 hourly intervals for 48hpi). For **A**, samples in which FeTPPS was added 12 hpi were lost during preparation for flow cytometric analysis. For both **A** and **B**, all samples were processed together at 72 hpi and the proportion of infected (GFP+) was measured by flow cytometry. Data plotted as mean ± SEM (n=3). The results are representative of three independent experiments.

3.2.3 Peroxynitrite is essential for HCMV entry into fibroblasts following cell-free infection.

My data demonstrated that peroxynitrite was rapidly induced upon HCMV infection and early inhibition of peroxynitrite dramatically reduced HCMV infectivity. Thus, I hypothesised that peroxynitrite was required for HCMV cell entry. To assess this, I measured viral genome copy numbers at 24hpi in cell cultures treated with FeTPPS prior to cell-free infection with Merlin-UL128^{WT}. Strikingly, inhibition of peroxynitrite completely blocked cell-free entry, as indicated by the absence of Merlin genomes in the whole cell or nuclei following FeTPPS treatment (Figure 3.11 A). Furthermore, to validate that peroxynitrite is important for viral entry, I also labelled for CMV pp65 and DAPI at 24 hpi. As mentioned in Section 1.1.6, CMV pp65 is a major tegument protein that translocates to the nucleus soon after virus entry. Consequently, the expression of CMV pp65 in the nucleus within 24 hpi can be used as an indicator of viral entry into cells. As seen in Figure 3.12, FeTPPS prevented nuclear translocation of CMV pp65 following cell-free infection, suggesting a role for endogenous peroxynitrite in promoting HCMV entry, nuclear import, and/or the initiation of viral replication.

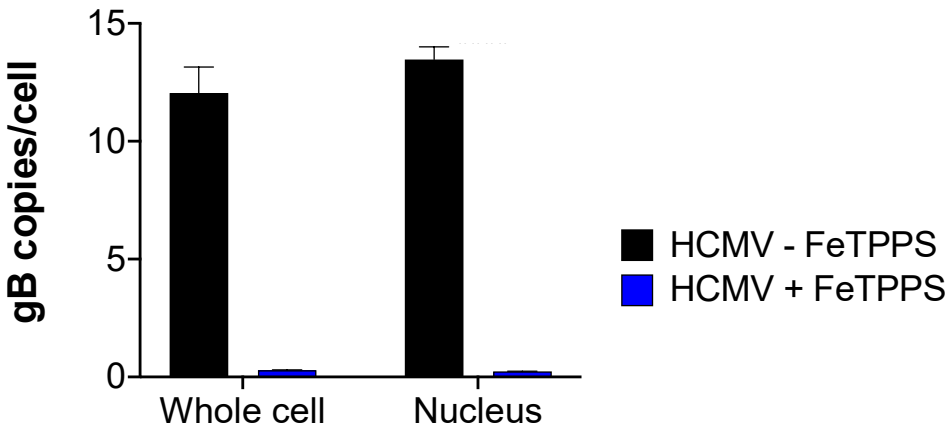

Figure 3.11: Peroxynitrite is required for entry of cell-free HCMV into fibroblasts

HCMV genomes in HFFF-TERTs following cell-free infection with Merlin (MOI 5) in presence or absence of FeTPPS (25μM). Data from a single experiment plotted as mean ± SEM (n=3).

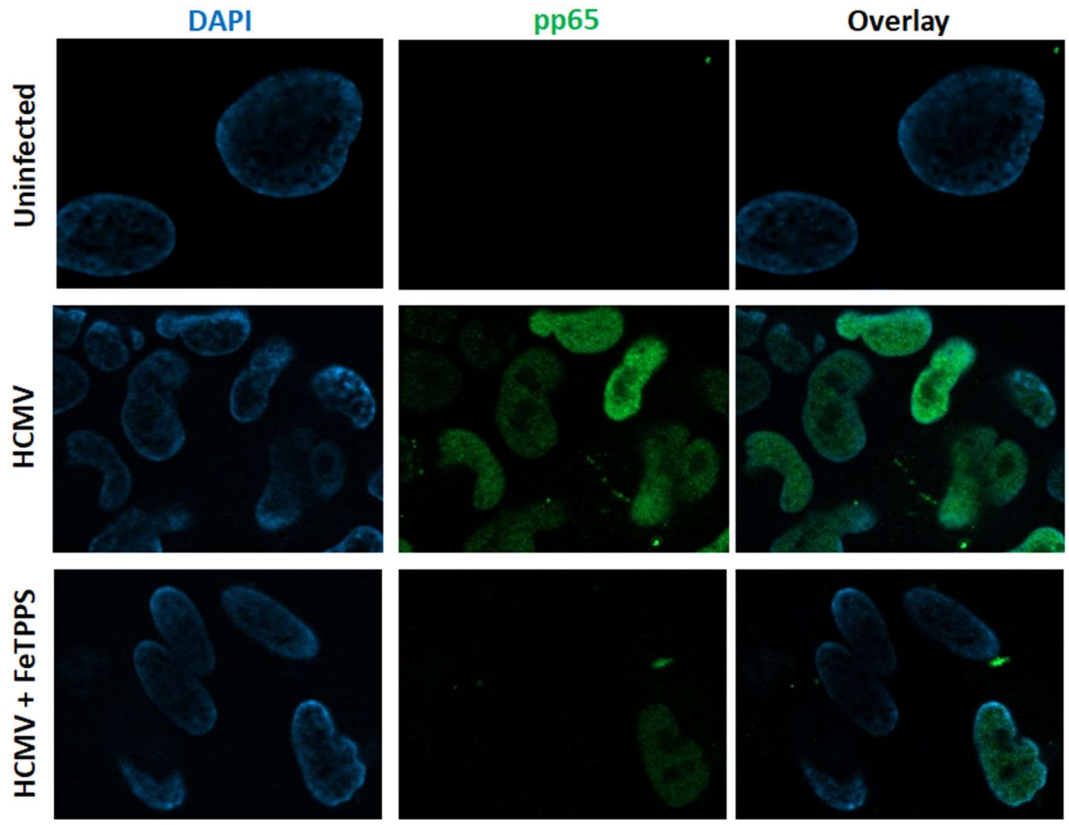

Figure 3.12: Peroxynitrite inhibition reduces pp65 expression in HCMV-infected fibroblasts following cell-free infection

Fluorescent microscopy images of confluent cultures of fibroblasts that were pre-treated with FeTPPS (25µM) or Vehicle (H_2O control) prior to cell free infection with Merlin-UL128^{WT} (MOI 5). Cells were stained for nuclei (DAPI, blue) and CMV-pp65 (CA003, green) 24hpi. All images were taken under ×40 magnification using a Axio Observer Z1 Zeiss microscope and are representative of two independent experiments.

3.2.4 Peroxynitrite is required for MCMV replication *in vitro* and *in vivo*

To investigate whether peroxynitrite could be targeted *in vivo*, I sought to use the murine cytomegalovirus (MCMV) model of infection. I first used a range of ROS and peroxynitrite scavengers to assess the effect on MCMV replication *in vitro* (Figure 3.13). Preliminary assays identified that FeTPPS and FeTMPyP potently inhibited MCMV replication in murine fibroblasts at MOIs of 0.01 and 0.1, leading to a ~2 log decrease in viral load detected in culture supernatant after 4 days (Figure 3.13). It was highly likely this decrease in MCMV infection was specifically attributed to the action of peroxynitrite as treatment with NAC (10 mM), a selective hydroxyl radical scavenger, did not impair MCMV infection *in vitro* (Figure 3.13). These findings were consistent with the antiviral effect of peroxynitrite scavengers on HCMV replication in different types of human cell lines *in vitro*. Additionally, cells treated with N-tert-butyl-α-phenylnitrone (PBN), a widely used free radical spin trap, also exhibited an anti-MCMV effect, leading to a ~2 log decrease in viral load (Figure 3.13). This was expected as lack of free radicals, particularly nitrogen-centred reactive molecules, would diminish peroxynitrite generation and subsequent effect. Surprisingly, inhibition of nitric oxide generation with L-NMMA (250 μM) did not affect MCMV load (Figure 3.13). In theory, this indicated that the inhibitory effect against MCMV was unlikely due to peroxynitrite, as nitric oxide is vital for peroxynitrite generation. However, as mentioned in Section 3.2.1.2, it could be that L-NMMA treatment needed to be optimised for this assay as the duration of pre-treatment and concentration alters the efficiency of L-NMMA. For example, it has been reported that the effect of L-NMMA is concentration-dependent which continues to release nitric oxide at low doses[297].

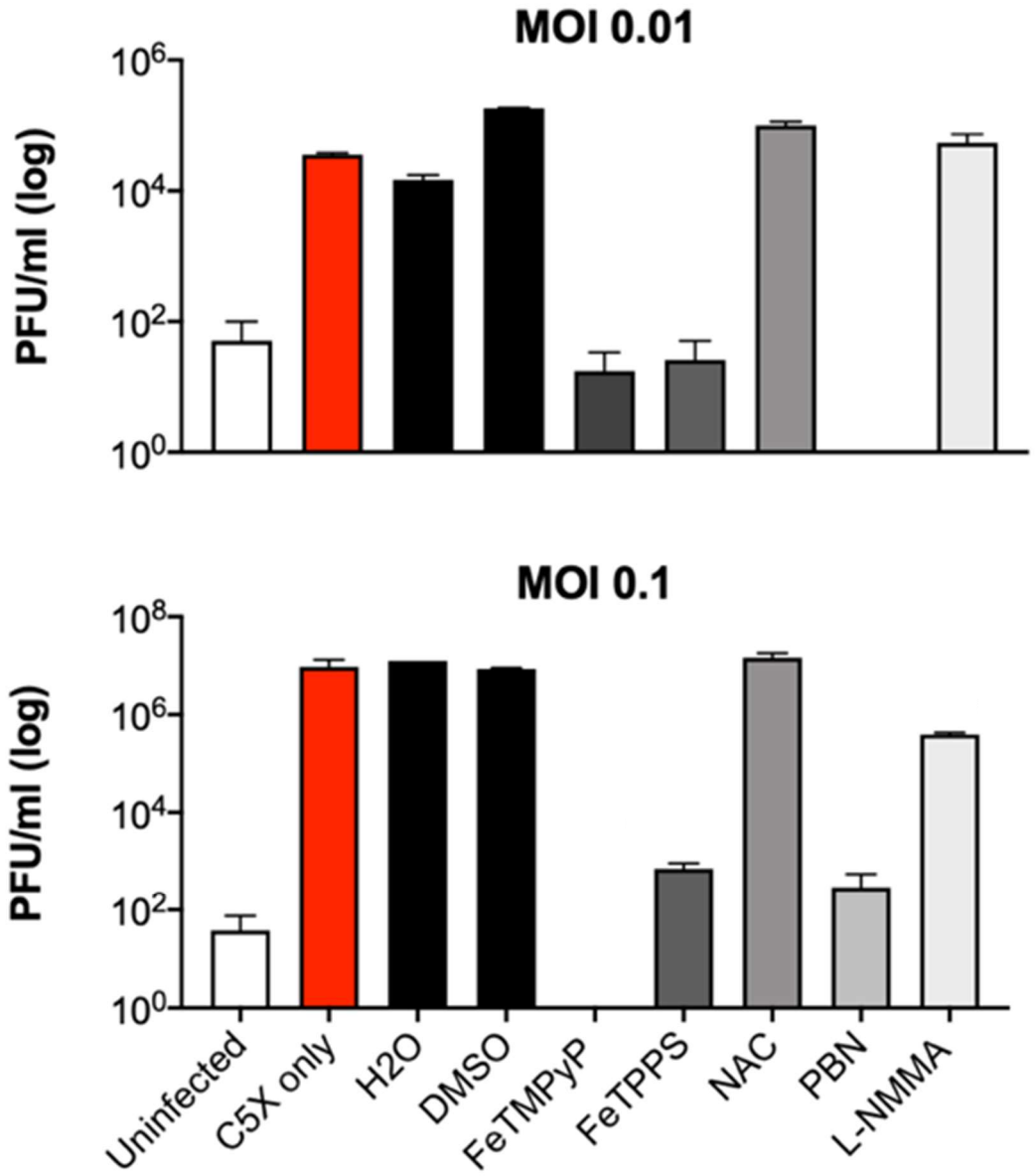

Figure 3.13: Inhibition of peroxynitrite dramatically reduces MCMV replication *in vitro.*

Murine fibroblasts (NIH-3T3 cells) were infected with MCMV (MOI of 0.01 or 0.1) and treated with a panel of inhibitors (FeTMPyP (100 μM); FeTPPS (100 μM); NAC (10 mM) ; PBN (16 mM) or L-NMMA (250 μM)). Infected cells treated with either H_2O or DMSO were used as vehicle controls. Supernatant was collected at day 4 after infection and MCMV concentration (PFU/mL) was quantified using a plaque assay. Data plotted as average of PFU/mL from 2-3 replicates. Data representative of effect observed in two independent experiments performed by Lucy Chapman.

Since peroxynitrite inhibition significantly reduced MCMV replication *in vitro*, MCMV-infected mice were treated with FeTPPS to determine if inhibition of peroxynitrite was also protective against MCMV infection *in vivo* (Figure 3.14). The experimental design is shown in Figure 3.14 A. Mice were weighed daily as a measure of virus-induced disease. The control-treated group rapidly and progressively lost weight following MCMV infection (Figure 3.14 B). In contrast, FeTPPS-treated mice did not lose weight (Figure 3.14 B). In fact, FeTPPS-treated mice maintained their pre-challenged weight throughout. On day 4, mice were sacrificed, and viral load in spleens and livers were measured. Treatment with FeTPPS significantly reduced viral load in both spleens and liver of MCMV infected mice compared to the PBS-treated control group (Figure 3.14 C). Remarkably, FeTPPS treatment eliminated detectable MCMV replication in spleens and livers of some infected mice. Collectively these data strongly indicate that peroxynitrite plays a crucial role in the establishment of CMV infection *in vivo* (Figure 3.14 C).

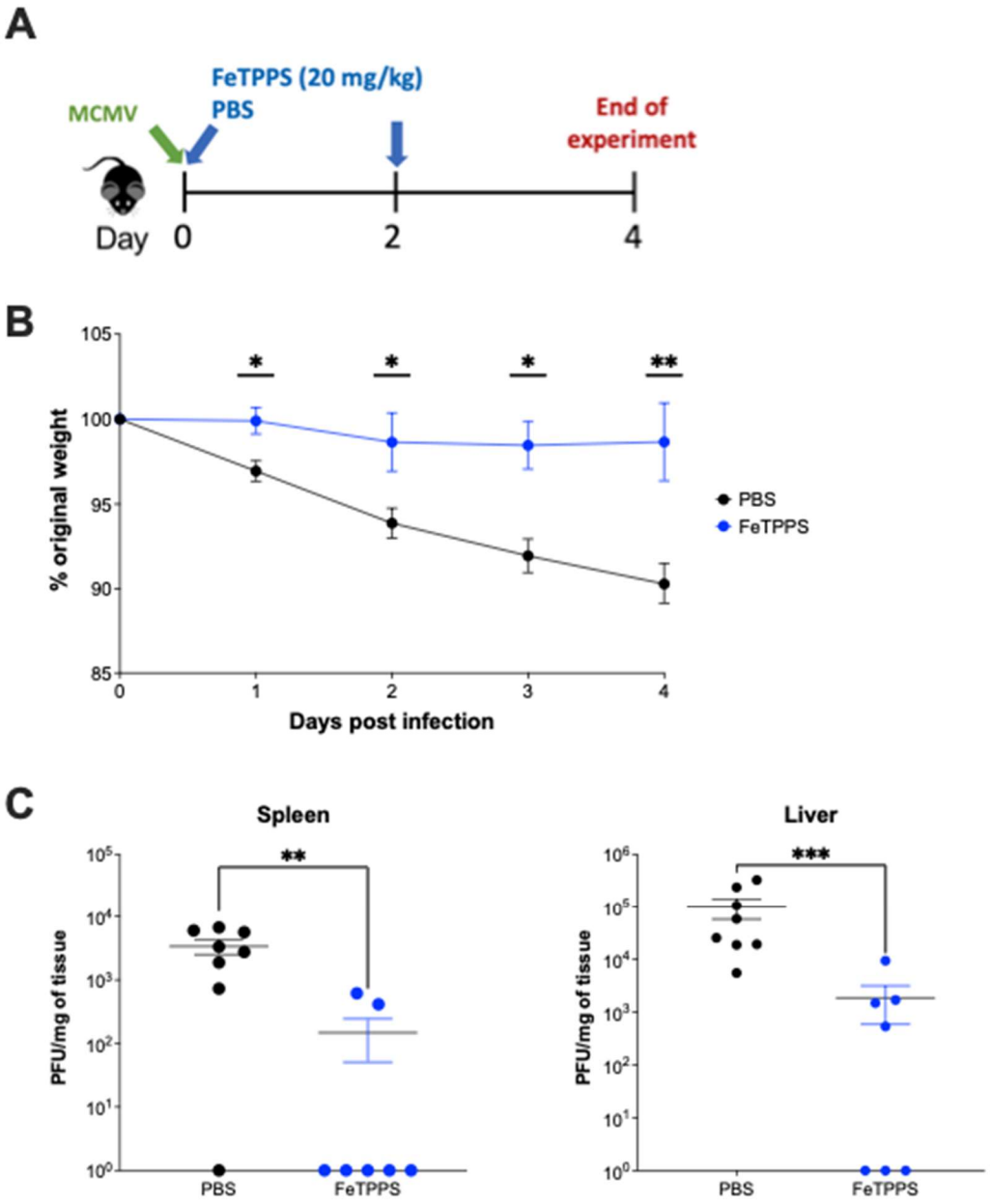

Figure 3.14: Peroxynitrite is required for MCMV replication *in vivo.*

(A) Schematic diagram of experimental procedure. C57BL/6 mice were infected with MCMV (3 x 10^4 PFU, i.p.) at day 0. They were also treated with FeTPPS (n=3) or PBS (n=4) at days 0 and 2. **(B)** Percentage change in body weights over 4 days. **(C)** Viral load in spleen and liver samples of FeTPPS treated and PBS control mice after MCMV infection. Plaque assay was used to calculate viral load (PFU/g of tissue). Graphs represent data pooled from two independent experiments (performed by Prof Ian Humphreys and Dr Mathew Clement); plotted as median ± SEM (n=7/8) with individual mice represented as **black** (PBS) or **blue** (FeTPPS) circles. Mann-Whitney test was performed to determine statistical significance (*p<0.05; **p<0.005; ***p<0.001).

3.2.5 5-hydroxytryptamine (5-HT) exhibited early anti-viral activity against HCMV

Commercially available peroxynitrite scavengers can have dose-dependent toxicity and may not be suitable for clinical use. I wanted to investigate whether naturally occurring peroxynitrite antagonists could have an impact on HCMV replication. Interestingly, the neurotransmitter and naturally occurring peroxynitrite antagonist 5-hydroxytryptamine (5-HT) [299], commonly known as serotonin, inhibited MCMV and HCMV replication *in vitro* (Figure 3.15). 5-HT potently inhibited MCMV replication in fibroblasts at MOI of 0.01 and 0.1, leading to a ~2 log reduction of virus production in the supernatant after 4 days (Figure 3.15 A). Furthermore, preliminary data showed that 5-HT treatment also inhibited HCMV replication in different cell types following cell-free infection and cell-to-cell spread of HCMV (Figure 3.15 B-C). The anti-viral effect of serotonin was not cell-type-specific as treatment impaired cell-free infection in monocyte-derived macrophages and human fibroblasts (Figure 3.15 B). As compared to FeTPPS, the inhibitory effect of 5-HT was not as potent. Preliminary experiments with 5-HT led to a < 0.5-fold reduction in HCMV replication as compared to FeTPPS treatment which led to >2-fold reduction in HCMV replication in both differentiated macrophages and fibroblasts (Figure 3.6 and Figure 3.8 versus Figure 3.15). More sophisticated functional assays are required to elucidate the mechanisms by which 5-HT inhibits HCMV-induced peroxynitrite signaling and to confirm the peroxynitrite-specific effects of serotonin inhibition of HCMV replication.

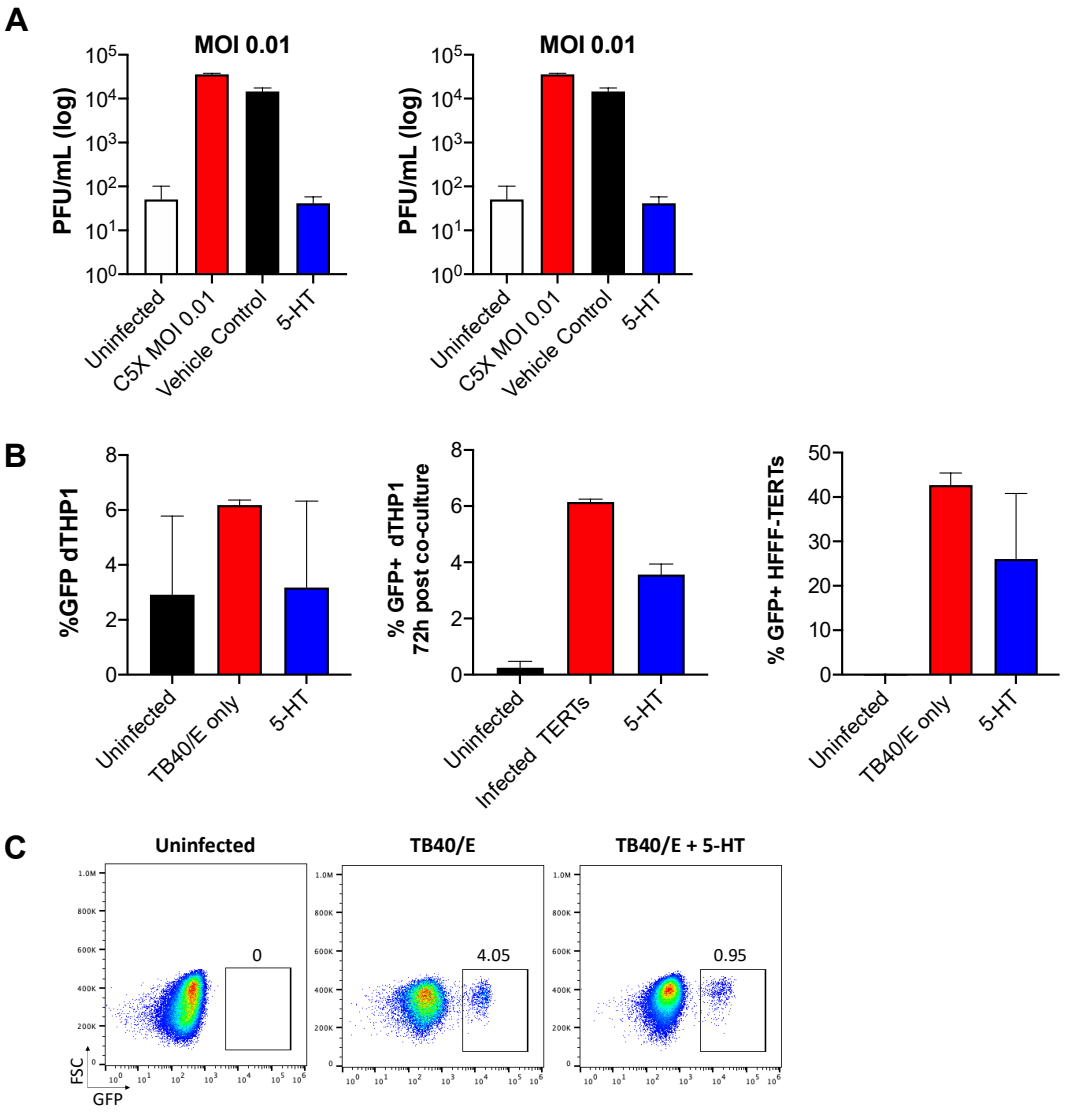

Figure 3.15: Exogenous serotonin treatment exhibited anti-CMV activity *in vitro*

(A) Murine fibroblasts (NIH-3T3 cells) were infected with MCMV (MOI 0.01 or 0.1) and treated with a 5-HT (500 μM). Infected cells treated H_2O used as vehicle controls. Supernatant was collected at day 4 after infection and MCMV concentration (PFU/mL) was quantified using a plaque assay. (Lucy Chapman). Data plotted as mean PFU/mL ± SEM of 2-3 replicates of a single experiment. **(B)** Differentiated THP-1 infected with TB40/E-GFP (MOI 5) ± 5-HT (right); Differentiated THP-1 ± 5-HT co-cultured with HFFF-TERTs (1:3 ratio) infected with Merlin-UL128^{WT}GFP (MOI 5) (middle); and HFFF-TERTs infected with TB40/E-GFP (MOI 5) ± 5-HT (left). 5-HT was added at concentration of 500 μM prior to cell-free infection or co-culture. At 72 hpi, the proportions of infected cells (GFP+) were determined by flow cytometry. Data presented as mean ± SEM of two replicates from a single experiment. **(C)** Representative FACS plots showing THP1-derived macrophages infected with TB40/E-GFP in presence or absence of 5-HT at 72hpi.

Since 5-HT is naturally produced in cellular systems to mediate certain signalling cascades, endogenous 5-HT may contribute to the control of CMV pathogenesis *in vivo*. There are two main sources of intracellular 5-HT: the brain and gut, which are responsible for producing 5% and 95% of total 5-HT, respectively[300]. Tryptophan hydroxylase (TPH) is an essential enzyme for the biosynthesis of serotonin[300]. Neuronal 5-HT is produced by TPH-2, which is almost exclusively expressed in the brain, whereas TPH-1 is highly expressed in the gut and is responsible for the majority of the 5-HT released into the periphery *in vivo*[300]. Neuronal and gut-derived 5-HT does not cross the blood-brain barrier[300]. Consequently, peripheral 5-HT modulates metabolic process independently of neuronal 5-HT and *vice versa*[300].

To determine the contribution of endogenous gut-derived 5-HT in CMV infection *in vivo*, mice infected with MCMV were administered 4-Chloro-DL-phenylalanine (PCPA), a highly selective TPH1 inhibitor[301], 30 minutes prior to MCMV (Figure 3.16 A). Pharmacokinetic and toxicokinetic studies of PCPA in mice have previously shown that peak absorption, distribution and PCPA effect was achieved at 30 minutes post-administration[302]. Mice were weighed daily to measure virus-induced weight loss. No significant body weight changes were observed between PCPA-treated and untreated MCMV infected mice (Figure 3.16 B). Both infected groups of mice showed approximately 5% weight loss 48 hpi. Additionally, there were no significant differences in the viral load in both spleens and livers between PCPA-treated and untreated MCMV infected mice (Figure 3.16 C). indicating that absence of endogenous gut-derived serotonin did not affect MCMV infection *in vivo*. Consequently, the anti-HCMV activity of exogenous 5-HT seems to be independent of the role of endogenous 5-HT produced *in vivo.*

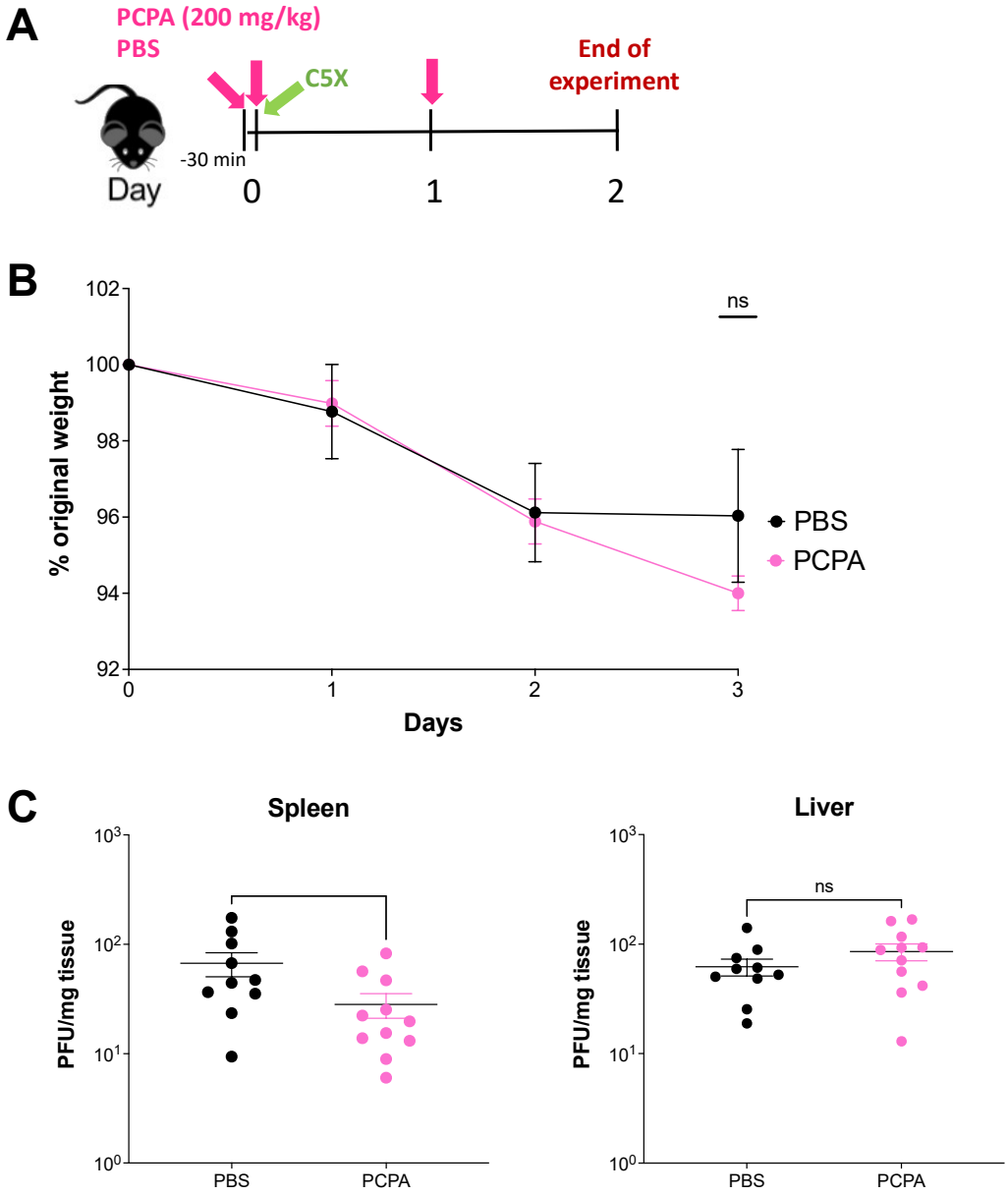

Figure 3.16: MCMV infection following PCPA treatment

(A) Schematic diagram of experimental procedure performed by Ian Humphreys. C57BL/6 mice were pre-treated with PCPA (200 mg/kg, i.p.) or PBS control 30min prior MCMV infection (MCMV; 3 x 10^4 PFU, i.p.) at day 0. They were treated again with PCPA/PBS on days 0 and 1. The experiment was carried out for 2 days. **(B)** Percentage change in body weights of infected mice treated with PCPA compared to weight loss seen in PBS treated mice. **(C)** Viral load in spleen and liver samples of PCPA/PBS treated mice after MCMV infection. Plaque assay was used to calculate viral load (PFU/mg of tissue). Graphs represent data pooled from two independent experiment (performed by Prof Ian Humphreys) plotted as median ± SEM (n=6) with individual mice represented as **black** (PBS) or **pink** (PCPA) circles. Statistical significance relative to control was determined by Mann-Whitney test (*p<0.05; ns = not significant).

3.3 Discussion

This chapter identifies a novel role of endogenous peroxynitrite, a potent oxidant and nitrating agent, in CMV infection. HCMV rapidly induced peroxynitrite generation within seconds upon cell-free infection. Treatment with peroxynitrite scavengers dramatically reduced viral replication in both *in vitro* and *in vivo* models of HCMV. Peroxynitrite inhibition prior to or at onset HCMV infection completely blocked viral replication in a range of susceptible cell types, including monocyte-derived macrophages, DC and fibroblasts. In fibroblasts, peroxynitrite appeared to be essential for cell-free HCMV entry. Although infection of THP-1-derived macrophages by co-culture revealed that peroxynitrite was also important for cell-to-cell spread of HCMV, additional studies are required to elucidate how peroxynitrite facilitates cell-to-cell viral dissemination. Measuring the concentration of intracellular peroxynitrite at different time points post HCMV infection (e.g., between 0 to 72 hpi), could provide important insights into when in the virus replication cycle peroxynitrite is required. Live-cell fluorescence microscopy could be used to measure the fluorescence signal after the 'Peroxynitrite Sensor Green' reagent is added to HCMV-infected cells at different time points post-infection. Altogether findings of this chapter indicate a role for peroxynitrite in promoting virus entry and/or facilitating the initiation of viral replication.

The mechanism by which peroxynitrite mediates viral entry are currently unclear. The impact on HCMV replication may involve peroxynitrite-induced chemical modifications in cellular receptors, proteases, kinases, and/or molecular motors involved in viral entry, uncoating, nuclear import, replication, and egress. PDGFRα is essential for entry and cell-to-cell spread HCMV in fibroblasts, with *in vitro* studies showing that HCMV virions containing only the trimeric complex cannot enter PDGFRα knockout (KO) cells[22]. Interestingly, pentamer-containing HCMV could still enter PDGFRαKO cells, although with reduced infectivity[22]. It is thought that HCMV strains that contain both trimeric and pentameric complexes use alternative

routes for viral entry and cell-to-cell spread[22]. Previous *in vitro* studies have shown that peroxynitrite-induced phosphorylation of tyrosine residues activates PDGFRα and multiple other types of receptor tyrosine kinases[217]. Here, I have shown that treatment with peroxynitrite scavengers prior to HCMV infection reduced entry and completely blocked viral replication following cell-free infection with pentamer-containing HCMV. These effects are likely due to the inhibition of peroxynitrite-mediated chemical modifications in host cell receptors involved in viral entry. It will be interesting to examine if exogenous peroxynitrite is sufficient to activate PDGFRα. In theory, peroxynitrite could rescue entry of "trimer-only" HCMV in cells treated with kinase inhibitors that block PDGFRα function.

My findings are consistent with reports that show upregulation of ROS is required for HCMV replication. Previous studies showed that treatment with ROS scavengers had a deleterious effect on viral gene expression. Many viruses activate phagocytic cells to stimulate the production of ROS and activation of pro-inflammatory proteins, including transcription factors such as NF-κB that have been associated with increased viral replication [303]. Peroxynitrite has been shown to have dual effects on NF-κB[217,285]. At certain concentrations, peroxynitrite can activate NF-κB by releasing it from its inhibitor IκB[217,285]. This allows NF-κB to translocate to the nucleus, facilitating activation of cellular and viral DNA replication[217,285]. Peroxynitrite can activate NF-κB, which has multiple binding sites within the MIEP of HCMV [304,305]. The HCMV MIEP drives the expression of viral IE proteins (IE1 and IE2) that are essential for the initiation of viral replication[304,305]. The most profound effect on HCMV replication was achieved with inhibition of peroxynitrite prior to or at the onset of HCMV inoculation, implying that peroxynitrite could be essential for initiating viral replication. The levels of IE1 and IE2 in FeTPPS-treated cells could be monitored to confirm initiation of viral gene transcription is dependent on peroxynitrite. Additional studies will be required to determine whether peroxynitrite facilitates HCMV replication through activation of NF-κB. For example, nuclear levels of NF-κB during HCMV infection could be measured in the presence of FeTPPS. Furthermore, it will be interesting to examine the effect of exogenous

peroxynitrite on the NF-κB signalling pathway in cells incubated with functional inhibitors NF-κB.

Interestingly, elevated levels of hydrogen peroxide facilitate upregulation of HCMV genes and protein, particularly pp72 and pp65[306]. Hydrogen peroxide-mediated activation of p38 MAPK has been shown to enhance HCMV replication by promoting MIEP activity and facilitating transcription of IE genes[306]. Peroxynitrite can also activate MAPK in certain cellular conditions (Section 3.1.3). Monitoring levels of p38 MAPK in presence of FeTPPS could help determine if initiation of HCMV replication is due to peroxynitrite-mediated activation of p38 MAPK. Intriguingly, it has also been shown that ROS-mediated activation of MAPK pathways promotes KSHV reaction from latency[307]. Several HCMV genes interact with host factors to drive transcriptional silencing during latency[76]. For example, viral G-protein coupled receptor (pUS28) inhibits several pro-inflammatory signalling cascades, including mitogen-activated protein kinase (MAPK) and NF-κB signalling pathways[(76)]. It will be interesting to see if exogenous peroxynitrite could induce reactivation of latent HCMV, especially if peroxynitrite facilitates viral replication by activating p38 MAPK or NF-κB. Furthermore, the effect of peroxynitrite scavengers on reactivation could have important implications in clinical settings that increase the incidence of HCMV reactivation.

Intriguingly, HCMV employs strategies to remove superoxide and nitric oxide, based on previous studies that show increased expression SOD and PTEN upon HCMV infection, inhibiting availability of superoxide and nitric oxide, respectively[308]. SOD catalyses the decomposition of superoxide, whereas PTEN inhibits eNOS activity and subsequent generation of nitric oxide[308]. Similar to other viruses, HCMV may support the upregulation of antioxidant enzymes to maintain physiological signalling and prevent oxidative-stress induced pathology. Indeed, excessive ROS levels have been shown to contribute to CMV-induced pathology *in vivo*. For example, MCMV infection promotes ROS production in the cochlea, leading to loss of hearing due to increased oxidative damage in hair cells of the inner ear[309,310].

Treatment with antioxidants ameliorates hearing loss in MCMV-infected mice[310]. This highlights the crucial role of ROS in CMV pathogenesis and the potential of antioxidant treatment regimens to prevent CMV-associated hearing loss in patients.

It will be interesting to understand the effect of blocking all superoxide and/or nitric oxide production using *in vitro* models of CMV. In theory, blocking either superoxide or nitric oxide should stop peroxynitrite generation and reduce HCMV replication. However, nitric oxide has also been shown to have an inhibitory effect on herpesvirus replication, although the mechanisms through which this occurs remain unclear[311]. For example, HSV-1, HSV-2 and EBV replication was inhibited by exposure to exogenous nitric oxide[311–313]. Furthermore, studies have shown intracellular nitric oxide promotes EBV latency by suppressing the EBV IE gene[312]. Nitric oxide has also been shown to inhibit HCMV infection *in vivo*[314]. A recent case study described overt HCMV-induced pathology following primary CMV infection in a previously healthy male with NOS2 deficiency[315]. Furthermore, NOS2-deficient mice have higher viral loads and are more susceptible to severe CMV disease[316]. Despite this, nitric oxide is also associated with immunopathogenesis during herpesvirus infection[317]. Altogether, these studies highlight the pleiotropic effects of nitric oxide and indicate a complex interplay between viral genes, host factors and ROS in the regulation of viral replication. Therefore, one of the main challenges in developing antiviral therapies targeting intracellular ROS is to selectively interfere with signalling pathways that promote viral replication without compromising innate immune responses that mediate virus clearance[]. Consequently, in the context of targeting peroxynitrite based on the findings of this chapter, it will be important to identify the source of superoxide during HCMV infection. Novel pharmacological agents that can safely and selectively target HCMV-induced peroxynitrite could potentially reduce the incidence of productive HCMV replication in certain clinical settings. Therefore, a combination of functional studies is also required to elucidate the underlying mechanisms by which peroxynitrite mediates HCMV replication.

4 Identification of host factors required for productive HCMV infection using high-throughput CRISPR-Cas9 based screening

4.1 Introduction

4.1.1 Genome-wide screening using pooled CRISPR libraries to identify essential genes for viral infection

CRISPR-Cas9 is a powerful gene-editing tool[259]. It allows genetic material to be modified with great precision and ease[259]. The CRISPR-Cas9-based system is largely accepted as the most cost-effective and efficient tool for genetic editing due to the simplicity with which it can introduce mutations in target cells[259]. It uses a guide RNA (gRNA) to direct DNA nucleases to a specific genomic location to introduce mutations in target cells[259]. The CRISPR-Cas9 system was first described as a defence mechanism used by bacteria, and certain species of archaea, against bacteriophages and other invading genetic elements[259]. It works by introducing DSBs at specific sites of foreign DNA[259]. The CRISPR-Cas9 system was initially adapted to generate knockout cell lines and model organisms[259]. However, this customisable gene-editing tool now has several applications, ranging from biological research to disease treatment[259,263]. Section 1.3 provides an overview of the CRISPR-Cas9 System.

Recent advances in functional genomic screening provide a high-throughput approach to identify genes of interest that contribute to a specific phenotype/disease. In the context of the CRISPR-Cas9 system, multiple gRNAs targeting multiple genes provides a framework for genome-wide mutagenesis studies. Pooled genome-wide CRISPR lentiviral libraries consist of thousands of lentivirus vectors, where each vector contains an individual sgRNA targeting a different gene[270]. Cas9-expressing target cells are infected with the pooled lentiviral CRISPR library to create a mutant target cell population in which each cell contains a unique disrupted gene[270]. A selection pressure is then applied, and the

surviving cells are isolated and sequenced as they most likely harbour mutations that render them resistant to the selection pressure[270]. This system can be used to identify genes that make target cells sensitive to a selection agent, such as a virus, which is applied during CRISPR screening. For example, genome-wide CRISPR-based screens have successfully been used to find host factors that facilitate productive viral infection. Such loss-of-function genetic screens have helped identify and characterise host genes that are essential for HIV, West Nile, Dengue, Influenza A, Zika and, more recently, SARS-CoV-2 infection[271–274,318]. Genome-wide CRISPR-Cas9 mediated knockout screen also identified PDGFRα as a host factor essential for pentamer-deficient or "trimer-only" HCMV replication in fibroblasts[22]. Most of these screens used cell survival post-viral infection to identify host dependency factors (HDFs), which are host gene-encoded cellular proteins that facilitate or enhance viral infection.

Antiviral therapies are traditionally focused on targeting viral genes and gene products. This approach against viral infections can be effective but can also suffer from the emergence of antiviral resistance mutations in the virus. Viruses are "obligate intracellular parasites" that lack the necessary machinery required to successfully reproduce without a host[275]. They have evolved mechanisms to evade host immune defences to exploit and manipulate host cellular machinery to successfully replicate[76]. Consequently, targeting host genes and cellular pathways that are essential for productive viral infection may offer an alternative approach to developing novel antiviral drugs[275].

4.1.2 Key considerations when designing a genome-wide CRISPR - based screen

Genome-wide knockout screening using pooled CRISPR libraries is a multi-step process. Prior to its execution, it is important to first optimize and validate a range of technical and practical aspects of the screen[268]. One of the most important initial considerations is to decide on the most suitable CRISPR-Cas9 system to investigate genes regulating the desired phenotype[268,270]. There are several pre-designed gRNA libraries that are commercially available. Some CRISPR libraries can be ordered such that they are pre-packaged into lentivirus[266,268]. CRISPR libraries can come as one-plasmid or two-plasmid systems[266,268]. One-plasmid system delivers gRNA and Cas9 in the same vector, whereas two-plasmid system requires co-infection with a separate Cas9-expressing plasmid or the use of Cas9-expressing cells[266,268]. The two-plasmid system has a slight advantage over the one-vector system as it allows the generation of an initial starting population, in which every cell contains Cas9 inserted at an identical site[266,268]. This reduces inherent cellular heterogeneity that may influence the cutting efficiency of Cas9 on a cell-to-cell basis[266,268]. Inconsistent Cas9 cutting efficiencies can lead to variable gene deletion and skewed results, as certain sgRNAs might be enriched or depleted due to varied Cas9- activity across cells[268]. Consequently, it is often recommended to generate a monoclonal Cas9-expressing cell line[268]. Overall, it may take longer to conduct a screen using the two-plasmid system as it requires multiple selection steps; first to select for Cas9-expression and then for successful mutagenesis[268].

There are many factors that need to be considered prior to a CRISPR-Cas9 screen, starting with what cell line to choose for a CRISPR-Cas9 based screening. It is often recommended to perform the screen in multiple cell types to avoid cell-type-specific characteristics, particularly lentiviral transduction efficiency and/or susceptibility to the selection agent being used[268]. It is important to choose a cell line that has high transduction efficiency[266,268]. Target cells are usually transduced with lentiviral CRISPR libraries at a low MOI to ensure each cell only receives a single gRNA, resulting in a single gene knockout per cell[268,319]. The volume of the lentiviral

library required for mutagenesis depends on the lentiviral titre and transduction efficiency of the chosen cell line[268]. Additionally, to achieve good gRNA representation within the mutant target cell population, it is advised to infect around 500 times more cells than the number gRNAs in the library[268,319]. Consequently, cell lines that are easy to propagate *in vitro* will be more appropriate for conducting a genome-wide CRISPR screen[268,319].

Following mutagenesis of the target cell population using the selected CRISPR knockout library, selection pressure is often applied to identify essential genes[268]. The selection can either be positive or negative[268]. Positive selection CRISPR screens help identify genes that are essential for making cells sensitive to the selection agent (e.g., virus) as gene knockout leads to cell survival (sgRNA maintained following selection) [268]. Positive screens tend to be very robust as they rely on a highly stringent selection criterion, that is, the selection pressure must be strong enough to ensure the majority of the cells die[268]. In contrast, most cells survive in a negative selection CRISPR screen, allowing the identification of genes that are essential for regulating subtle phenotypes[268]. For example, negative selection screens are often used to identify genes that are essential for making cells resistant to certain conditions (e.g., following treatment with anti-viral drugs or antibiotics) [268]. Negative selection screens can be more challenging as it can be difficult to identify significant changes in gRNA representation when the majority of the cells survive under selection pressure[268]. Therefore, it requires comparing gRNA representation in cells that undergo selection to that of a control population (selection not applied) [268].

4.1.3 Aims

HCMV heavily relies on host machinery to replicate[275]. Consequently, HDFs that are essential for HCMV replication are attractive targets for the development of anti-viral therapies[320]. Therapeutics that target host factors effectively avoid the emergence of resistance compared to treatments that target viral factors[199]. Positive genome-wide CRISPR knockout screening provides an excellent way to rapidly scan the entire genome to identify pro-viral host factors[268]. I hypothesise that novel host pathways that support HCMV replication may be identified by a genome-wide CRISPR screen. The aims of this chapter are as follows:

1. Establish a cell system for identifying host genes essential for HCMV infection using high-throughput CRISPR-Ca9 based screening.
2. Perform genome-wide CRISPR-Cas9 screen to identify host genes required for HCMV infection.
3. Validate contribution of novel candidate host factors in HCMV infection.

4.2 Results

4.2.1 Engineering physiologically relevant cell lines for genome-wide CRISPR screen

4.2.1.1 Stable Cas9-expression could be achieved in a range of target cells

As described in Section 1.1.3, HCMV can infect and efficiently replicate in a range of different host cells. The extremely broad target cell range contributes to the pathogenesis of chronic HCMV infection, facilitating both intra-and inter-host spread. For example, epithelial cells, endothelial cells, smooth muscle cells, fibroblasts, macrophages, and dendritic cells are all prime targets for HCMV replication. Therefore, I first engineered a range of target cells to express Cas9, making them suitable for pooled genome-wide CRISPR knockout screening. A representative cell line of myeloid (THP1), epithelial (ARPE-19) and fibroblasts (HFFF-TERT or HFFF-TET) were transduced with lentivirus expressing Cas9 and blasticidin-S deaminase (Section 2.7.1.2). Consequently, stable Cas9 expression could be maintained in culture under blasticidin selection.

There were no visible differences in the morphology of target cells and their Cas9-derivatives (data not shown), indicating that intracellular expression of Cas9 did not alter general cell morphology. Although blasticidin selection ensured only cells where lentiviral had integrated were maintained, it didn't help determine the level of Cas9 expression and, consequently, its cutting efficiency. Consequently, Gene editing efficiency was validated using sgRNA targeting the *Beta-2-microoglobulin* (*B_2M*) gene (Section 2.7.1.2). High Cas9 activity was previously demonstrated in THP1Cas9 cells, which were a gift from Dr Jessica Forbester (The Wellcome Trust Sanger Institute, UK). ARPE-19 cells exhibited natural resistance to blasticidin, making it difficult to evaluate Cas9 activity (Figure 4.1 A), making ARPE-19-Cas9 cells an unattractive target for CRISPR screening using libraries containing this particular selection marker. In contrast, high Cas9 activity was demonstrated in TERTCas9 and TETCas9 cells as approximately 70% and 80% B2M knockout was observed

respectively (Figure 4.1 B-E). The knockout was stable even after 20 days post-transduction (data not shown).

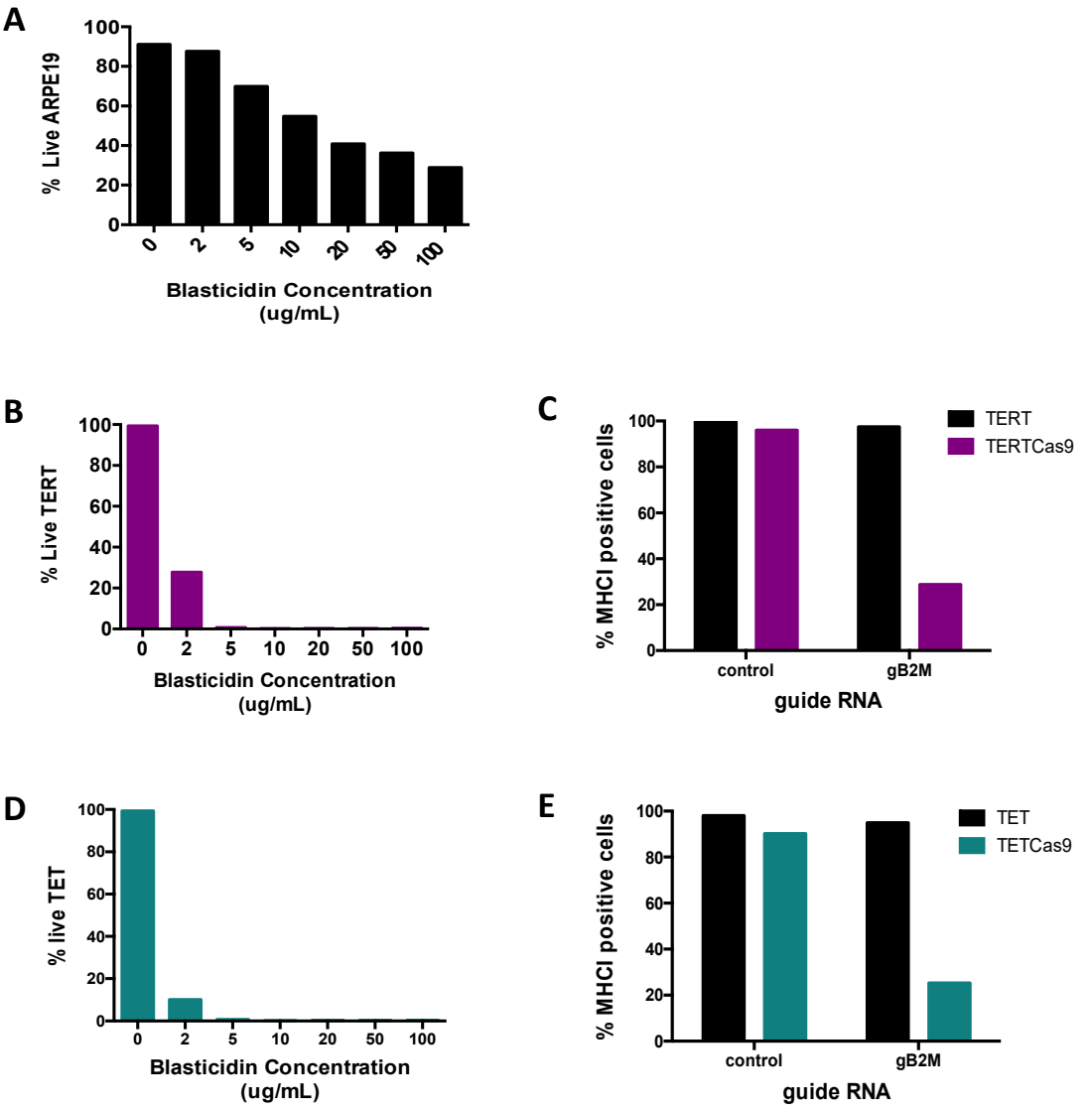

Figure 4.1: Validation of Cas9 activity in Cas9-expressing target cells.

(A) Sensitivity of ARPE-19 cells to various concentration of blasticidin as assessed by cell death post treatment. Results are expressed as percentage viability at 1-week post-treatment. **(B)** Sensitivity of HFFF-TERTs to different concentrations of blasticidin after one week. **(C)** Cas9 activity in TERTCas9 cells determined by the percentage of MHCI-positive cells after using guide RNA targeting β2-microglobulin gene (β2M), as measured by X. **(D)** Sensitivity of HFFF-TETs to various concentration of blasticidin. **(E)** Cas9 activity of TETCas9 cells determined by percentage of MHCI-positive cells following Cas9-mediated knockout of β2M. Non-Cas9 cells were used as control. Results represent two experiments.

4.2.2 Establishing efficient HCMV infection in Cas9-expressing target cells

4.2.2.1 Monitoring HCMV infection in vitro

Use of HCMV strain containing an enhanced GFP ORF linked to UL36 with a P2A peptide resulted in high-level GFP expression by 24 hpi of target cells and their Cas9-expressing derivatives[66], allowing infection state to be monitored using flow cytometry (Figure 4.2 A). Consequently, the experimental setup allowed me to distinguish between target cells that are sensitive (GFP+) from those that are resistant (GFP-) to HCMV infection (Figure 4.2 B). Additionally, it has previously been shown that the Merlin strain downregulates major histocompatibility complex class I (MHC-I) upon viral infection[74]. Thus, to ensure that infection in target cells (as assessed by GFP expression) was not underestimated, the degree of infection was also determined by measuring the percentage of major MHC-I downregulation upon viral infection (Figure 4.2 B).

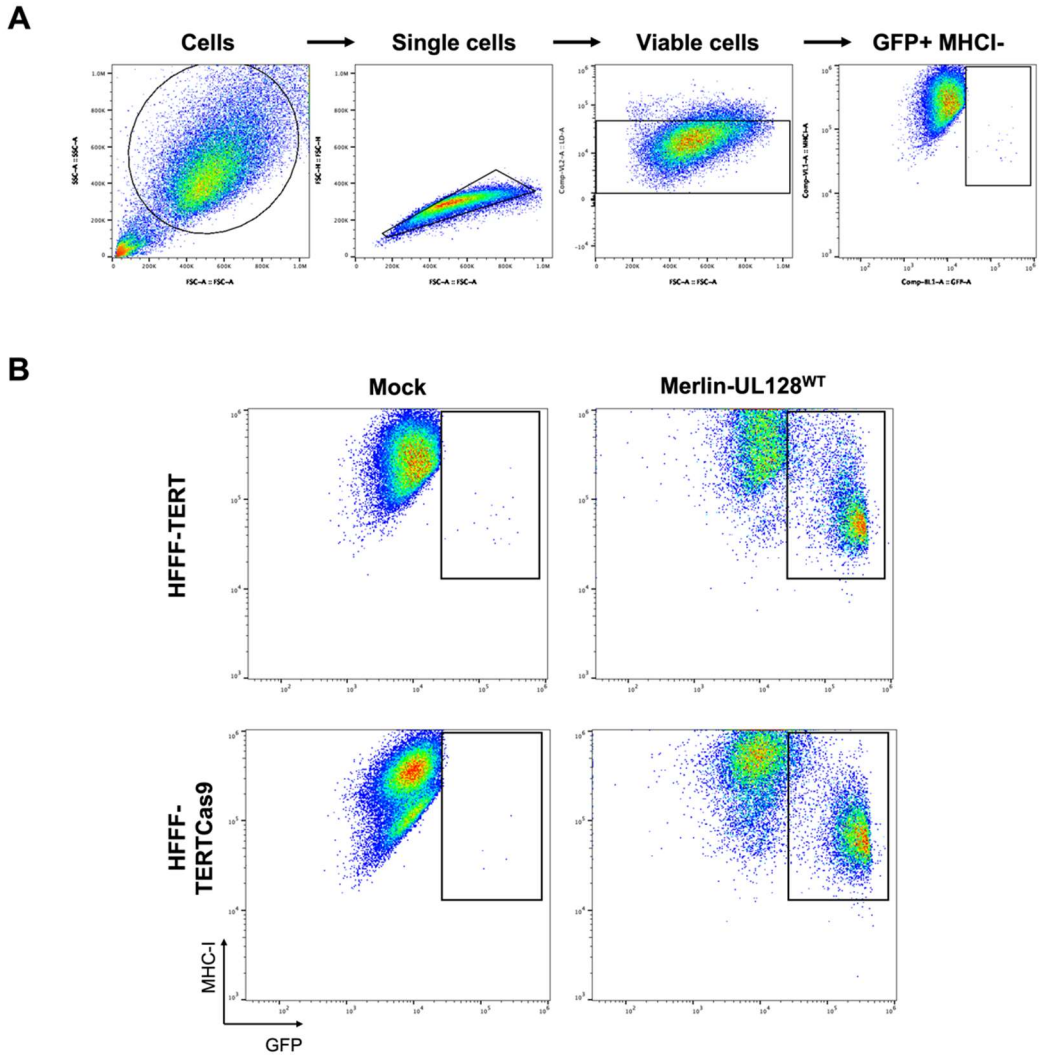

Figure 4.2: Productive HCMV infection leads to GFP expression and MHC-I downregulation.

(A) Representative gating strategy for flow cytometric analysis to assess GFP and MHC-I expression in HFFF-TERTs and HFFF-TERTCas9 cells 72 hpi with Merlin-UL128^{WT}GFP (MOI 2). Productive HCMV infection determined by percentage of GFP positive HFFF-TERTs 72hpi with Merlin-UL128^{WT}GFP (MOI: 2). **(B)** Productive HCMV infection determined by percentage of GFP-positive and downregulated MHC-I. Uninfected HFFF-TERT/TERTCas9 cells were used as mock control.

4.2.2.2 High frequencies of HCMV (Merlin-UL128^{WT}) infection could not be established in monocyte-derived macrophages

It was next necessary to establish conditions that permitted high levels of HCMV infection in Cas9-expressing cells. HCMV establishes latency in monocytes. Therefore, monocytic cell lines were first differentiated into macrophages as described in Section 2.2.5. Monocyte-like THP-1 and THP-1-Cas9 cells were first differentiated into macrophage-like cells with PMA, thus enabling productive infection[321]. Differentiated cells became adherent, lost the ability to proliferate, demonstrated increased cytoplasmic volume (Figure 4.3 A) and upregulated expression of macrophage-specific markers (CD11b) on their cell surface (Figure 4.3 B). Consequently, the expression of CD11b was used to determine the degree of differentiation prior to viral infection (Figure 4.3 B). The results showed that both PMA stimulated Cas9+ and Cas9- THP1 cells positively expressed CD11b (Figure 4.3 B).

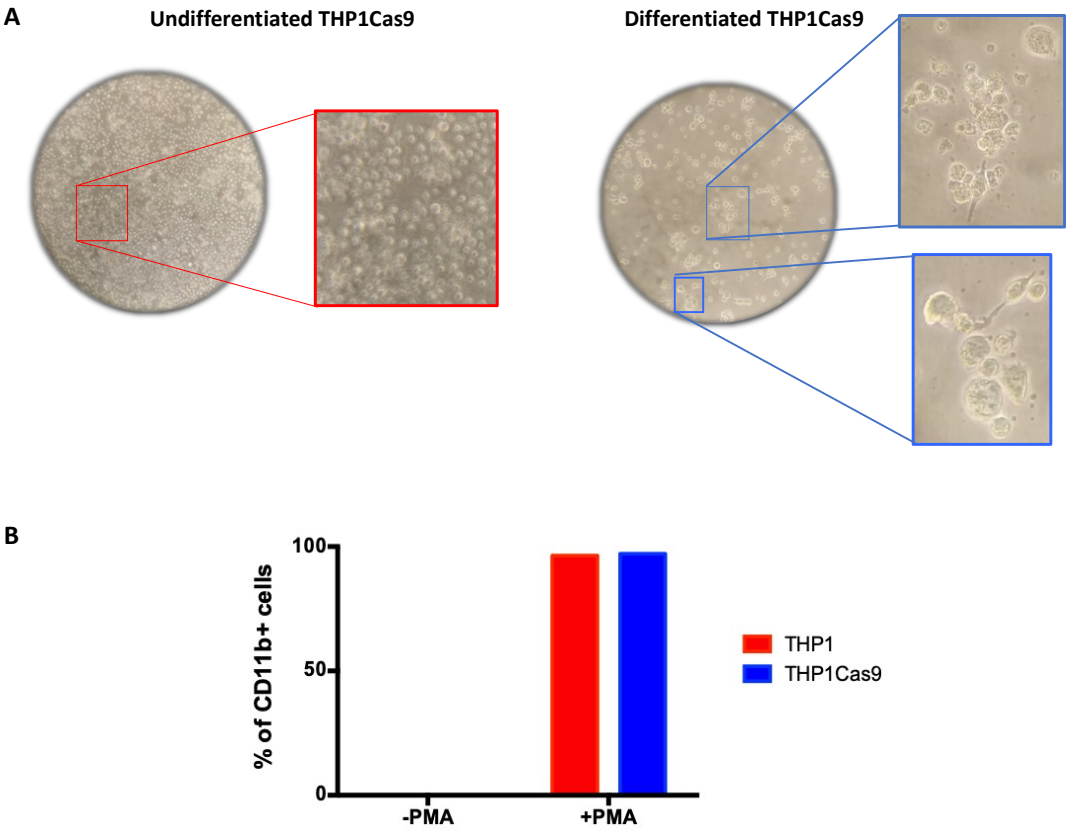

Figure 4.3: Differences between undifferentiated and differentiated THP1/THP1Cas9 cells.

(A) Comparing the morphology of undifferentiated (-PMA) and differentiated (+PMA) THP1Cas9 cells. Images were taken under X5 or X20 magnifications. **(B)** Expression of CD11b by PMA-stimulated THP1/THP1Cas9 cells was measured by flow cytometry. Data is expressed as mean values of duplicates and represent four experiments.

As described in Section 2.3.2, Merlin-UL128^{WT} is grown in fibroblasts containing tetR, preventing mutations in UL128 to occur when propagated *in vitro*[27,53]. Subsequent infection in fibroblasts lacking tetR (HFFF-TERT or HFFF) restores the pentameric complex in resulting virions after a complete infectious cycle[27,53]. Wildtype HCMV does not produce high titres of the cell-free virus but does spread efficiently by direct cell-cell contact. Infection of epithelial and terminally differentiated myeloid cell lines was therefore achieved by co-culture with HFFF-TERTs infected with Merlin-UL128^{WT} HCMV strain (iTERTs) [27,53,74].

Merlin did not efficiently infect PMA-differentiated THP1s even when co-cultured with three times more iTERTS; only 25% of dTHP1Cas9 cells were GFP-positive after 72 hpi(Figure 4.4 A). In fact, increasing the number of iTERTs did not lead to a higher HCMV infection in dTHP1Cas9, as the percentage of GFP-positive dTHP1Cas9 remained around 20% regardless of the amount of iTERTs present (Figure 4.4 A). Surprisingly, increasing duration post-co-culture did not increase HCMV infection either (Figure 4.4 B). The inability to achieve high infection in dTHP1Cas9 cells raised the question of whether Cas9 expression reduced infectivity. Consequently, the co-culture assay was performed in both PMA-stimulated THP1 and THP1Cas9 cells, using varying amounts of either uninfected or infected TERTs. No significant difference was observed between the infectivity of dTHP1 to that of dTHP1Cas9 cells (Figure 4.4 C). Furthermore, minimal MHC-I down-regulation was observed confirming that HCMV is unable to efficiently infect dTHP1Cas9 cells (data not shown). Consequently, I concluded that THP1 were not ideal for a positive selection genome-wide CRISPR screen. Additionally, since THP1 cells lose their proliferative potential following terminal differentiation, post CRISPR screen analysis will most likely require FACS sorting infected (GFP+) and uninfected (GFP-) cells within 24-72hpi. Ideally, a positive selection screen will involve multiple rounds of infection to reduce false positives (i.e., cells that remain uninfected despite not having a gene required for HCMV infection deleted). Thus, THP1 cells were not suitable for this approach. Moreover, other monocytic cells that can be grown indefinitely (Mono-Mac-6 and U937) did not support HCMV replication (data not shown).

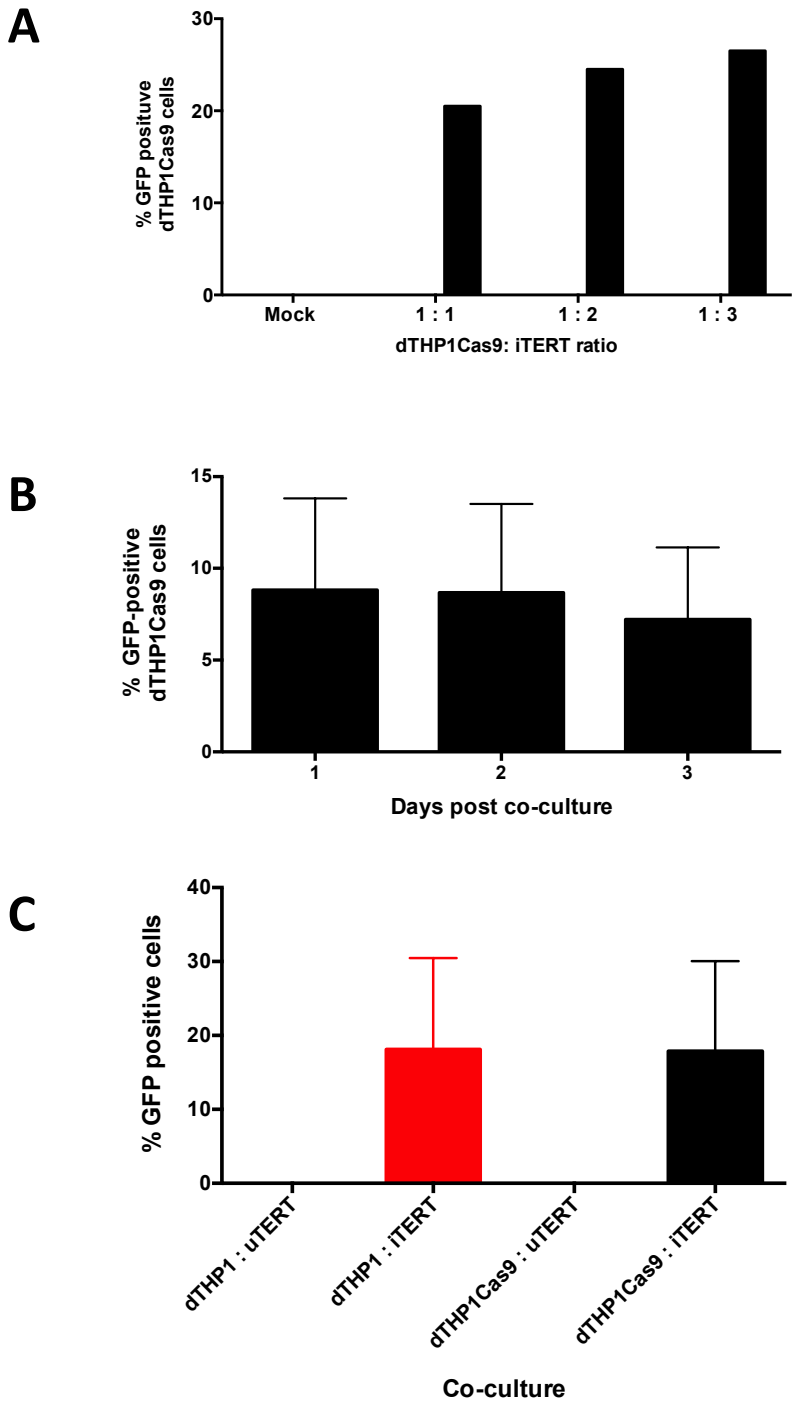

Figure 4.4: HCMV infection in monocyte-derived macrophages.

(A) dTHP1Cas9 cells expressing GFP three days post co-culture with increasing number of iTERTs (ratio of 1:1, 1:2 and 1:3). **(B)** dTHPCas9 cells positively expressing GFP 1-3 days post co-culture with three times more iTERTs. **(C)** HCMV infection in dTHP1 and dTHP1Cas9 cells when co-cultured with three times more iTERTs. Uninfected TERTs (uTERTs) were used as controls. Experiment was performed in duplicates and data represented as mean. Graphs represent results seen in three individual experiments.

Since Merlin strain was unable to efficiently infect dTHP1Cas9 cells, TB40/E-BAC4 HCMV strain tagged with GFP (TB40-GFP) was used to directly infect dTHP1Cas9s at different MOIs. As explained in Section 1.1.5, TB40-BAC4 can propagate efficiently in fibroblasts and non-fibroblast cells, even after extensive passaging in fibroblasts after isolation. This is because the virus has an intact trimeric (gH/gL/gO) and pentameric complex (gH/gL/UL128/UL130/UL13A), allowing cell-free infection of epithelial, endothelial, and myeloid cells[54].

The cell-free infection assay showed 8%, 25% and 58% of dTHP1Cas9 cells infected with TB40/E-GFP at MOI 1, 2 and 10, respectively (Figure 4.5). Although TB40/E-GFP can efficiently infect dTHP1Cas9 cells, it is not ideal to use this virus as it contains multiple mutations, including a frameshift mutation in UL141[72]. Furthermore, desired levels of HCMV infection in PMA-differentiated THP1 cells could only be achieved at high MOI (Figure 4.5). Consequently, a very high amount of TB40/E would be required for positive selection during CRISPR screening, which would be challenging to prepare.

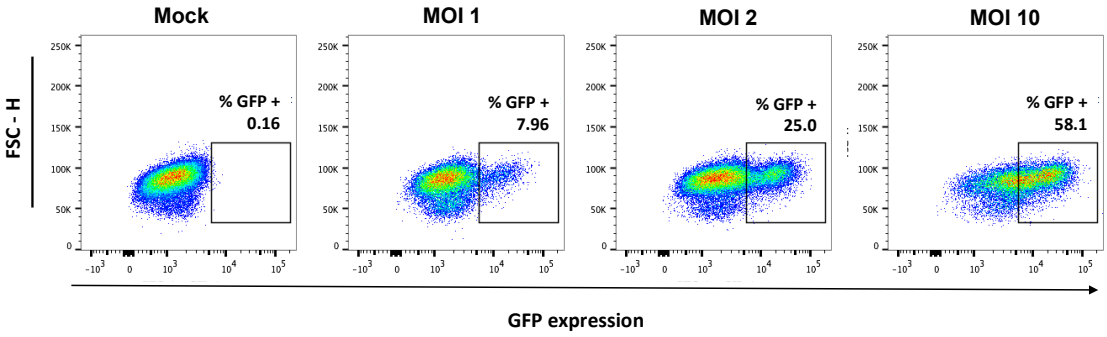

Figure 4.5: TB40/E-GFP can efficiently infect dTHP1Cas9 at high multiplicity.

Productive HCMV infection was determined by the percentage of GFP-positive cells 72 hpi. Uninfected cells were used as control.

4.2.2.3 ARPE-19s are not an ideal cell system to conduct a genome-wide assessment of pro-viral host genes.

Epithelial cells represent prime targets for HCMV replication *in vivo*. Similar to THP1 cells, co-culture is necessary to infect epithelial cell lines with wild-type virus. Efficient HCMV infection was established in ARPE-19 cells post-co-culture (Figure 4.6). Increasing the amount of iTERTs significantly increased the percentage of GFP-positive ARPE-19 cells (Figure 4.6B). Approximately 37%, 49% and 72% of ARPE-19 positively expressed GFP when co-cultured with iTERTs at ratios 1:1, 1:2 and 1:4, respectively (Figure 4.6B). Additionally, increasing the duration post-co-culture showed increasing numbers of infected cells as measured by the percentage of GFP-positive and MHC-I-negative cells (Figure 4.6C). Although relatively high levels of HCMV infection could be achieved in ARPE-19s cells as compared to THP1 cells, performing a screen in this cell line was potentially challenging. Firstly, it might be difficult to manage the amount of iTERTs required to successfully infect ARPE-19s through co-culture. Secondly, a large volume of Merlin-UL128^{WT} will be needed to ensure TERTs show 100% CPE prior to co-culture. Finally, although, 70% of ARPE-19s could be infected with HCMV when co-cultured with four times more iTERTs, the infection efficiency remains insufficient for fulfilling the purpose of the designed screen. Ideally, an infection level of 90% is preferred to ensure that majority of cells die post-viral challenge, increasing the likelihood of accurately identifying only essential genes for HCMV infection (Section 4.1.2). Furthermore, it was observed that regardless of the amount of iTERTs or duration post-co-culture, around 25-30% ARPE-19 cells remain uninfected, suggesting that it may not be possible to reach the required HCMV infection threshold without altering cell densities and ratios. Nevertheless, since it was possible to establish productive HCMV infection in ARPE-19s, Cas9-expressing ARPE-19s were generated. In the interest of time, cell-free infection of ARPE-19 and its Cas9-expressing derivative was carried out in order to investigate whether expression of Cas9 altered the infection state in this cell system. As seen in Figure 4.6 D, Cas9 expression seemed to reduce infectivity by 50%, making ARPE-19s a questionable choice for the screen.

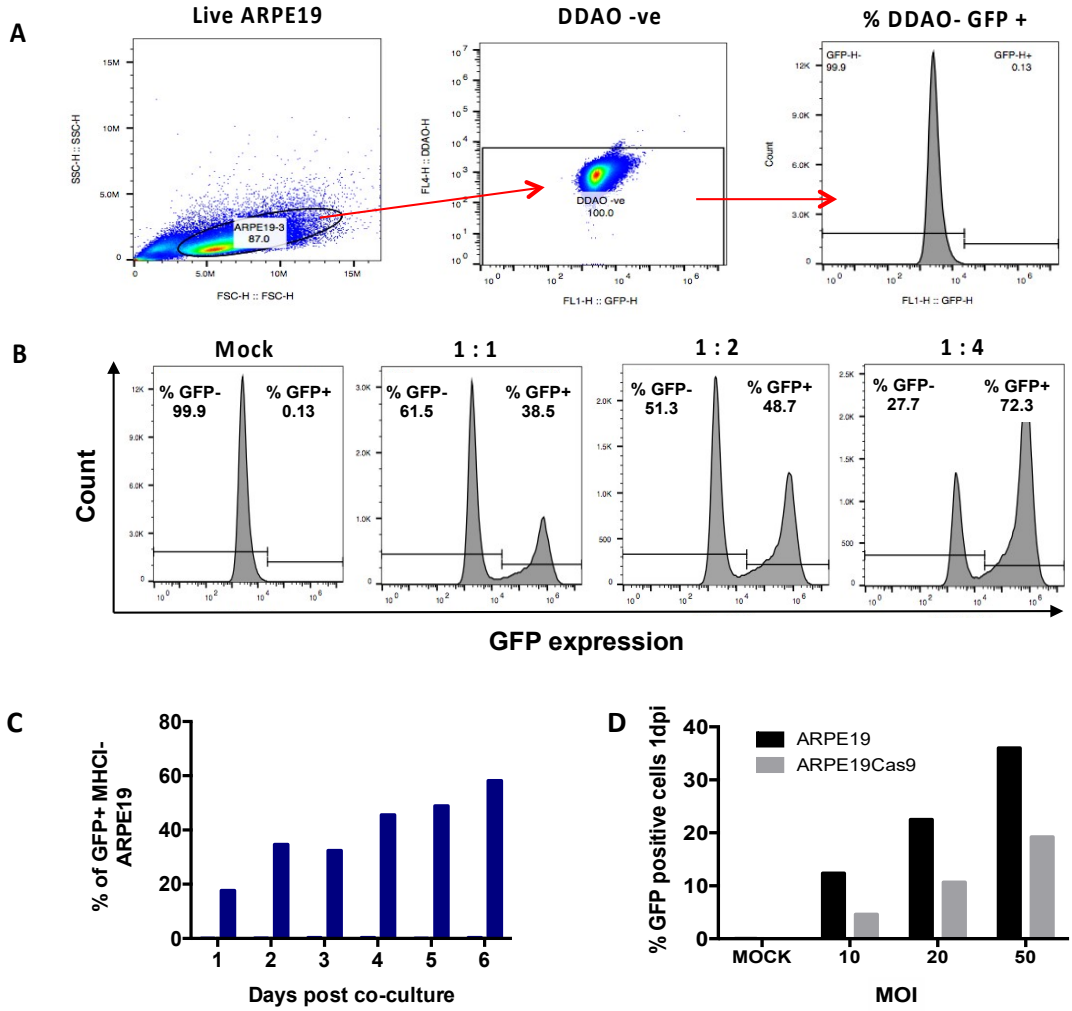

Figure 4.6: HCMV infection in a representative epithelial cell line.

(**A)** Representative gating strategy for flow cytometric analysis of ARPE-19 co-cultured with iTERTs. Infected HFFF-TERTs (DDAO+) cells were excluded and only DDAO negative cells were assessed for GFP expression. **(B)** Percentage of GFP+ ARPE-19 cells post co-culture with different concentrations of iTERTs 3dpi (ratios of 1:1, 1:2 and 1:4). (**C**) Percentage of GFP-positive and MHCI-negative ARPE-19 cells when co-culture with two times more iTERTs over a week. (**D**) HCMV infection in ARPE-19 compared to ARPE-19-Cas9 cells a day post infection (1dpi) with TB40/E-GFP HCMV strain at different MOIs (10, 20 or 50). Experiments were performed in duplicates.

4.2.2.4 High frequencies of HCMV infection can be established in immortalised fibroblasts

4.2.2.4.1 Infection with Merlin-UL128^{WT} in HFFF-TERTs

Fibroblasts are major targets of HCMV *in vivo* and, thus, are commonly used as a cell-culture model for *in vitro* studies. Due to reasons mentioned in Section 1.1.3, high titre replication of most HCMV strains in cell culture is restricted to human fibroblasts. Consequently, productive cell-free HCMV infection was established in HFFF-TERTs one day post-infection (1 dpi) with GFP-expressing Merlin-UL128^{WT} HCMV strain (Figure 4.7 A). Additionally, Cas9-expression in fibroblasts did not alter the infection state, making it suitable for genome-wide CRISPR screening (Figure 4.7 A). Furthermore, increasing the MOI subsequently increased the percentage of infected TERTs/TERTCas9s (Figure 4.7 A and B).

4.2.2.4.2 Spinoculation increases Merlin-UL128^{WT} infection efficiency in HFFF-TERTs.

Although efficient HCMV infection could be established in fibroblasts using UL128-repaired Merlin-GFP (Figure 4.7 A-B), infection conditions were further optimised to achieve high frequencies of HCMV infection with a minimal amount of virus inoculum. Spinoculation is a process that can be used to facilitate virus binding and entry into target cells through centrifugation (Section 2.4). The efficiency of HCMV infection was significantly enhanced in Cas9-expressing HFFF-TERTs following spinoculation (Figure 4.7C), especially for low MOI HCMV infection where the GFP-positive iTERTCas9 population increased from 30% (without spinoculation) to around 70% (following spinoculation). Although spinoculation increased HCMV infection in TERTCas9 cells to desirable levels for the CRISPR screen, this is an artificial infection system for studying HCMV infection *in vitro*. However, the largest problem is that spinoculation resulted in an uneven distribution of infected cells within the well (data not shown). There were clusters of uninfected cells in the middle of the well, with HCMV infection concentrated at the outer edges of the well. Consequently, it was decided that spinoculation would not be used to infect target cells during CRISPR screening as uneven distribution of HCMV will make it difficult

to achieve greater than 90% infection target cells. Furthermore, leaving the infection to spread within the monolayer following low MOI infection did not subsequently increase the number of infected cells. (Figure 4.7D). In fact, I observed a slight decrease in the percentage of GFP-positive cells at 72 hpi, indicating that uninfected cells might be outgrowing infected cells. (Figure 4.7D).

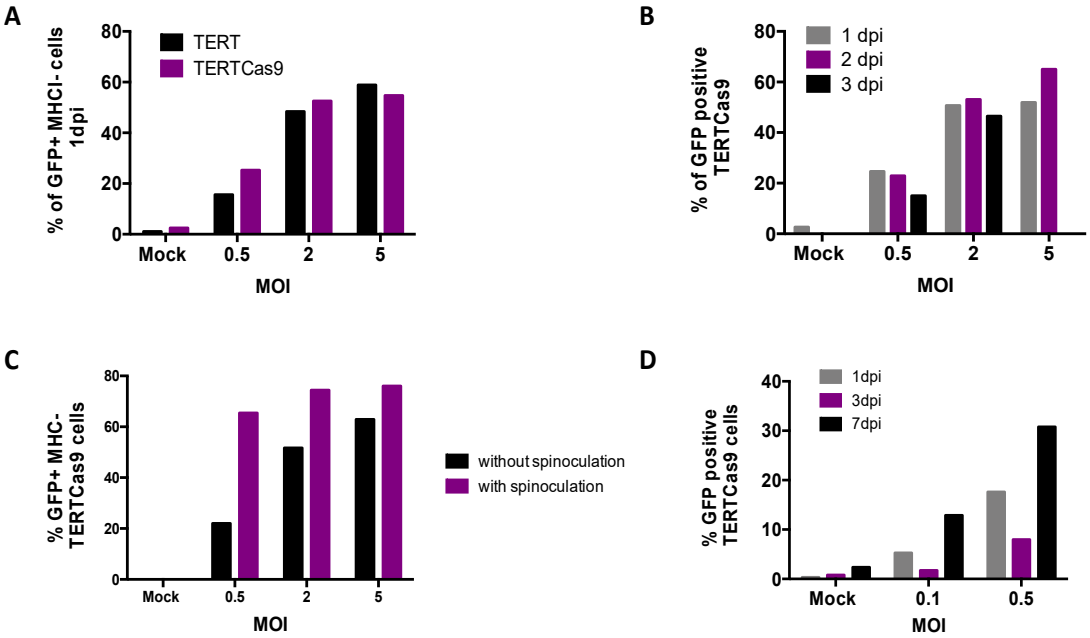

Figure 4.7: Merlin-UL128^{WT} establishes productive infection in HFFF-TERTs.

(A) Productive HCMV infection in TERTs compared to TERTCas9 cells determined by percentage of GFP-positive and MHCI-negative cells a day post infection at MOIs of 0.5, 2 or 5. **(B)** Percentage of HCMV infected TERTCas9 cells following infection with GFP-tagged HCMV (MOI 0.5, 2 and 5). HCMV infection was determined by measuring percentage of GFP-positive cells 1-3 days post infection (dpi). **(C)** HCMV infection in TERTCas9 cells following spinoculation (2800 rpm for 2h at 26°C) with HCMV at different MOIs (0.5, 2 or 5). **(D)** Low MOI (0.1 or 0.5) HCMV infection in TERTCas9 cells. Infection efficiency was determined by the percentage of GFP-positive cells 1, 3 and 7 dpi. All experiments were performed in duplicates. Results represent two individual experiments.

4.2.2.4.3 A high frequency of HCMV infection is achieved in immortalized fibroblasts expressing a tetracycline repressor (tetR).

In order to improve infection efficiency, HCMV infection was optimized in fibroblasts expressing tetR (HFFF-TET). Although both HFFF-TET and HFFF-TERTs are highly permissive to infection with Merlin-UL128^{WT}, the new virions released in HFFF-TET infect fibroblasts more efficiently. This is because tetR inhibits the expression of UL128 (which has been placed under the control of tetR), releasing high tires of cell-free HCMV after initial infection. Consequently, as expected, the percentage of infected HFFF-TETs (iTETs) was significantly increased when the cells were infected with Merlin-UL128^{WT}GFP at a low MOI (MOI of 0.1 or 0.5) and allowed to spread through the monolayer post-infection (Figure 4.8). Approximately 90% of HFFF-TETs were infected with HCMV (GFP+ MHC-) after a week, regardless of the MOI (Figure 4.8A). However, infecting HFFF-TET with HCMV at MOI 0.5 did slightly increase the number of iTETs at earlier timepoints compared to MOI 0.1 (Figure 4.8A). Additionally, HCMV infected a similar proportion of TETs and Cas9-expressing TET cells, indicating that Cas9 expression did not alter the cell line susceptibility to HCMV, making it suitable for the CRISPR screen design. Morphological changes observed following cell-free infection at MOI 0.5 were more striking and dynamic than those observed at MOI 0.1 (Figure 4.8 C). There were significantly fewer cells remaining after HCMV infection at MOI 0.5 (Figure 4.8C). Infected TET/TETCas9 cells had a more spherical shape following HCMV infection at MOI 0.5 compared to mock-infected HFFF-TETs (elongated and flat) and TET/TETCas9 cells infected at an MOI of 0.1 (hemispherical)(Figure 4.8 C). I concluded that such a dramatic phenotype post HCMV challenge would help select cells that harbour mutations that protect them against HCMV-induced CPE during large-scale CRISPR-based screening (section 4.1.2). Hence, I concluded that Merlin-UL128^{WT} infection of HFFF-TETCas9 cells could be a potential virus-cell combination for conducting a CRISPR-based screen to identify novel host factors essential for productive viral infection.

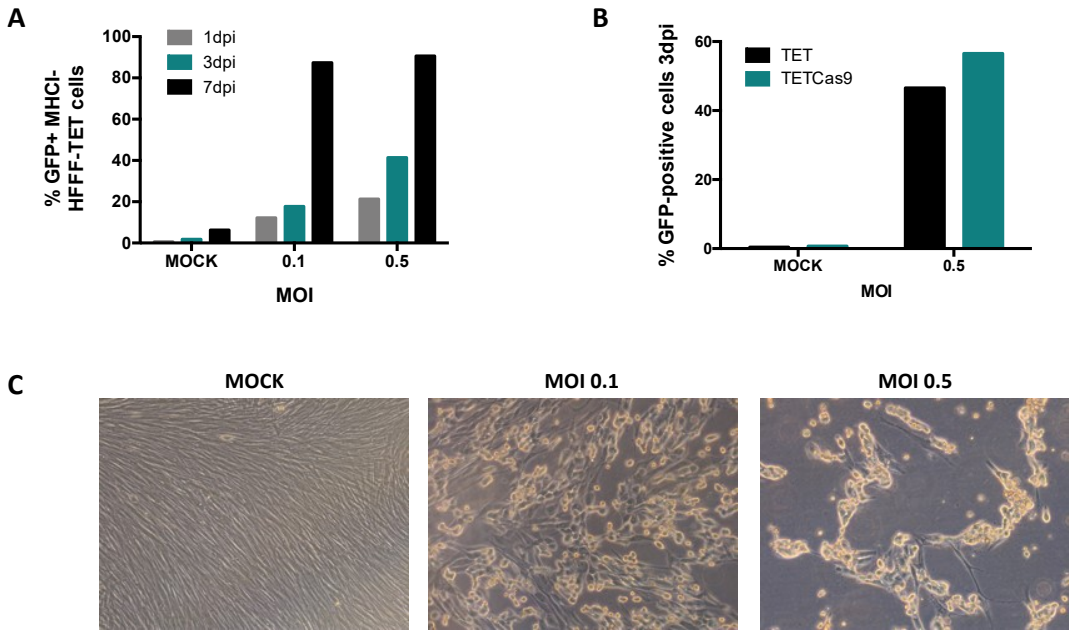

Figure 4.8: Merlin-UL128^{WT} is highly efficient at infecting HFFF-TET cells in vitro at low MOI.

(A) Productive HCMV infection determined by percentage of GFP-positive and MHCI-negative TET cells following infection Merlin-UL128^{WT}GFP (MOI: 0.1 or 0.5). Uninfected cells were used as control. Infection state was monitored 1, 3 and 7 dpi. **(B)** HCMV infection in TET and Cas9-expressing TETs (TETCas9) 3dpi with GFP-tagged HCMV at MOI 0.5. **(C)** Representative microscope images of TETCas9 cells 7dpi with HCMV at MOI 0.1 or 0.5. Uninfected cells (MOCK) were used as control. All images were taken under X20 magnification. Experiments were performed in duplicates and results are displayed as mean values. Results represent two experiments.

4.2.2.4.4 Infection with Merlin-UL128^{mut} dramatically improved infection efficiency in HFFF-TERTs

In an attempt to improve HCMV infection efficiency in fibroblasts lacking tetR, cells were infected with Merlin-UL128^{mut}. The only difference between wildtype and UL128-mutated Merlin is that after 72h, the mutated virus spreads through HFFF-TERTs more efficiently because of higher cell-free infectivity. This is because a mutation in the UL128 region allows the virus to spread through the monolayer faster, forming larger plaques and producing greater amounts of infectious cell-free virus. Consequently, HCMV-induced CPE was enhanced when infection was allowed to spread through the monolayer following low MOI infection with Merlin-UL128^{mut} compared to Merlin-UL128^{WT} (Figure 4.9). In fact, leaving the infection to spread through the monolayer produced 100% CPE within a week post-low MOI infection (MOI 0.1 or 0.5) with UL128-mutated Merlin strain, regardless of MOI (Figure 4.9). Thus, Merlin-UL128^{mut} and TERTCas9 represented another virus-cell combination applicable for a proviral CRISPR screen. Although UL128-mutated Merlin lacks a major entry complex (i.e. virions lack pentamer), the use of this virus is unlikely to affect the readout of a CRISPR screen designed to investigate HCMV entry and replication in fibroblasts as the pentameric complex is not required for productive HCMV infection in this cell type[(22)].

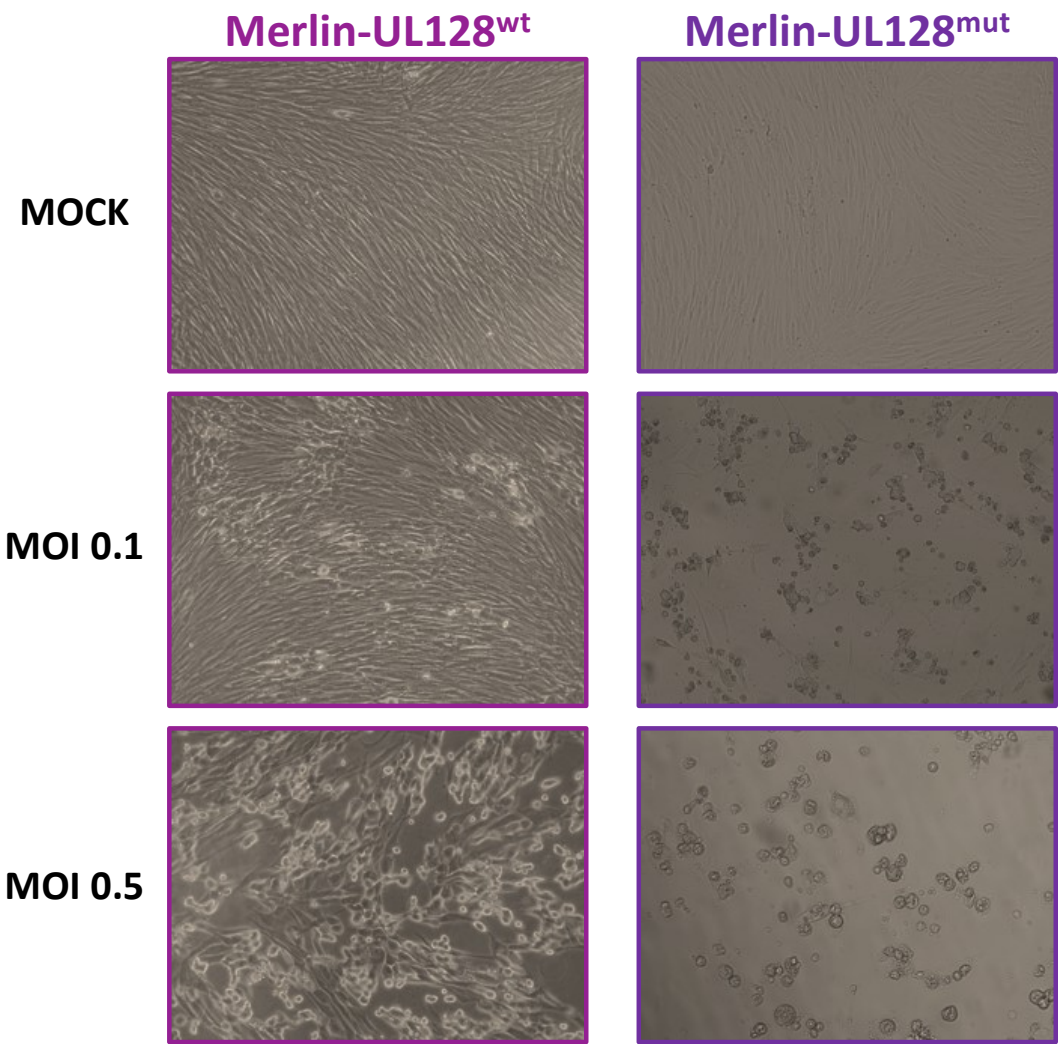

Figure 4.9: Merlin-UL128mut infects Cas9-expressing HFFF-TERTs with extremely high efficiency, resulting in a dramatic phenotype.

TERTCas9 cells were infected with Merlin-UL128^{wt} or Merlin-UL128^{mut} at low MOI (0.1 or 0.5). Uninfected cells were used as control. The impact of viral infection on cell morphology was assessed by light microscopy. All images were taken under X20 magnification.

4.2.3 Transduction of fibroblasts with pooled CRISPR knockout lentiviral library

4.2.3.1 Cas9-heterogeneity observed in heterogenous Cas9 target cell population

As discussed in section 4.1.2, Cas9 heterogeneity could negatively impact the success of the CRISPR-Cas9 screen as variable cutting efficiencies will skew gRNA representation following mutagenesis of target cells. Consequently, single-cell cloning using the heterogenous Cas9-expressing TERT cells was carried out in order to identify a clone that has the highest Cas9 cutting efficiency. A gRNA targeting β2M was used to measure Cas9-cutting efficiency in individual clones; where low expression of MHCI is indicative of high Cas9 cutting efficiency. As seen in Figure 4.10, Cas9-heterogeneity was observed across different TERTCas9 clones. Single-cell cloning helped identify a clone that is highly efficient (clone 13, Figure 4.10). Individual clones from a heterogenous Cas9-expressing TET cell population were also generated. However, none of the clones exhibited high Cas9 cutting efficiency (data not shown). Consequently, in the interest of time, it was decided not to use HFFF-TETCas9 for the screen.

Although there was no reason to suspect that TERTCas9_clone13 would not be permissive to HCMV, a cell-free infection assay was carried out to confirm this. There was no significant difference in the infectivity of TERTs compared to TERTCas9_clone13 7dpi (data not shown). Therefore, since TERTCas9_clone13 was highly permissive to HCMV and demonstrated a high Cas9-cutting efficiency, I concluded this was an ideal cell line for conducting a genome-wide CRISPR screen.

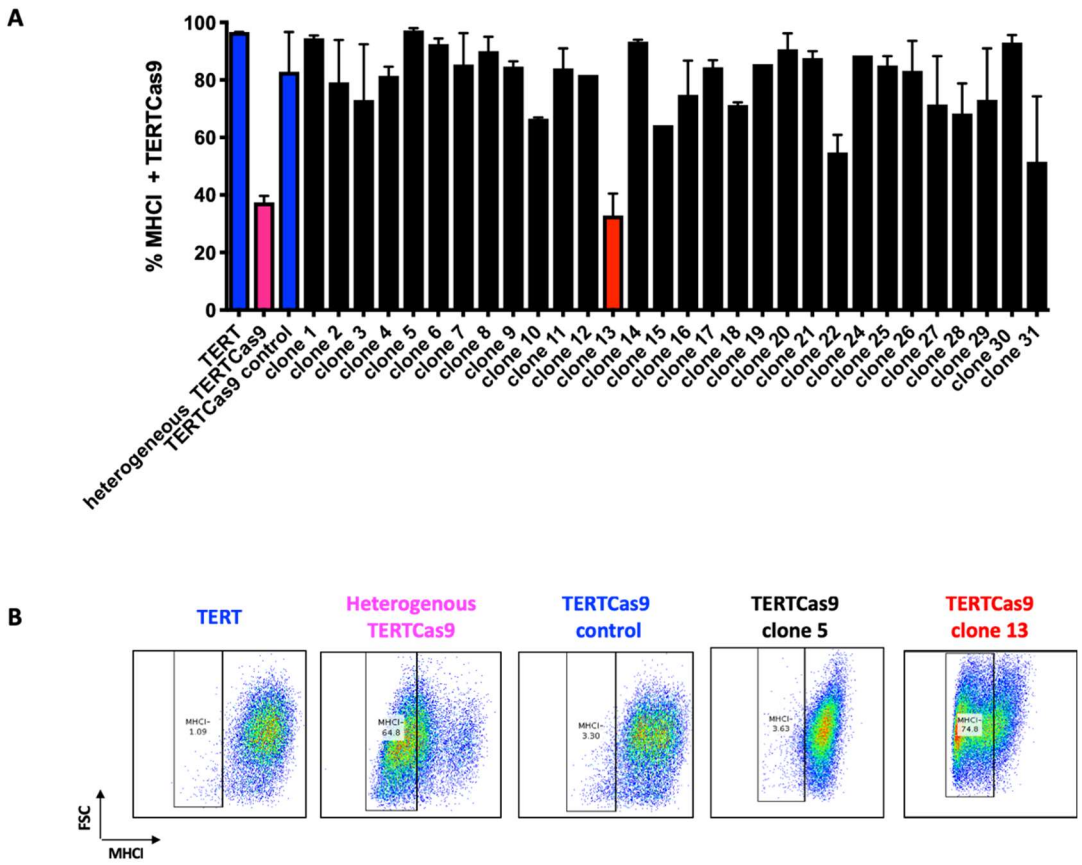

Figure 4.10: Cas9 heterogeneity assessed through single cell cloning and loss of MHCI expression in Cas9-expressing TERTs.

(A) Percentage of MHC-I positive cells in individual Cas9-expressing clones compared to controls (**blue bars**) and heterogenous TERTCas9 cells (**pink bar**) a week post-delivery of gRNA targeting β2M. Error bars represent standard error of mean (n = 2). **(B)** Representative FACS plots showing MHC-I expression in negative and positive controls, a clone with <5% Cas9 activity (**clone 5**) and a clone with high Cas9 cutting efficiency (**clone 13**). All clones were cultured in blasticidin containing media to select for Cas9-expression. Clone 23 did not survive blasticidin selection.

4.2.3.2 Optimising lentivirus delivery in Cas9-expressing target cells

The 'human Brunello genome-wide CRISPR knockout lentiviral pooled library' (Addgene Cat. No. 73178-LV) was used to carry out a genome-wide assessment of pro-HCMV host factors. Prior to executing the CRISPR screen, it was important to determine the ideal conditions for delivering lentivirus into the chosen Cas9-expressing target cell line. It was recommended to achieve lentivirus infection efficiency of 30-50% to ensure only one gRNA is delivered per cell. Additionally, once lentivirus delivery was optimised, the number of cells required for the screen can be calculated.

Using a GFP-lentivirus, I first determined optimal conditions for lentivirus delivery into Cas9-expressing TERTs. It was possible to achieve 30% infection efficiency when infecting TERTCas9_clone13 cells at MOI 1.0 for 72h (Figure 4.11). Puromycin selection (2μg/mL) ensured only cells expressing lentivirus (GFP+) cells survive. It was recommended to maintain a gRNA representation of ~400 cells per gRNA during the CRISPR-Cas9 screen[276]. Therefore, since the 'Brunello' library contained around 77,000 gRNAs, a total of approximately 3×10^7 cells were required to be infected with lentivirus to maintain the desired gRNA representation. Consequently, since the infection efficiency of TERTCas9_clone13 cells at desired MOI is 30%, a total of around 1×10^8 cells were needed for mutagenesis to ultimately achieve the desired number of cells harbouring mutations, prior to the HCMV challenge. The strategy used to identify HCMV host-dependency factors (HDFs) using a genome-wide CRISPR-Cas9 mediated knockout screen is outlined in Figure 4.12.

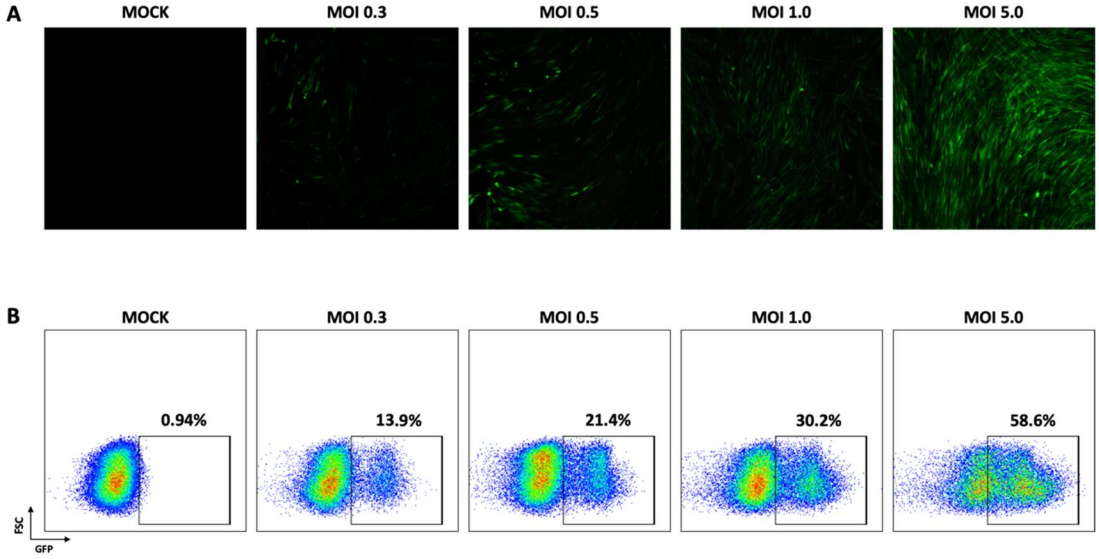

Figure 4.11: Lentivirus infection efficiencies in TERTCas9_clone13 corresponding to MOI 0.3-5.

(A) TERTCas9_clone13 cells were infected with GFP-LV at MOIs ranging from 0.3-5 and the percentage of GFP+ cells was assessed by fluorescence microscopy. All images were taken under X5 magnification. **(B)** Quantification of GFP-LV efficiency observed in (A) by flow cytometry. Uninfected cells were used as control.

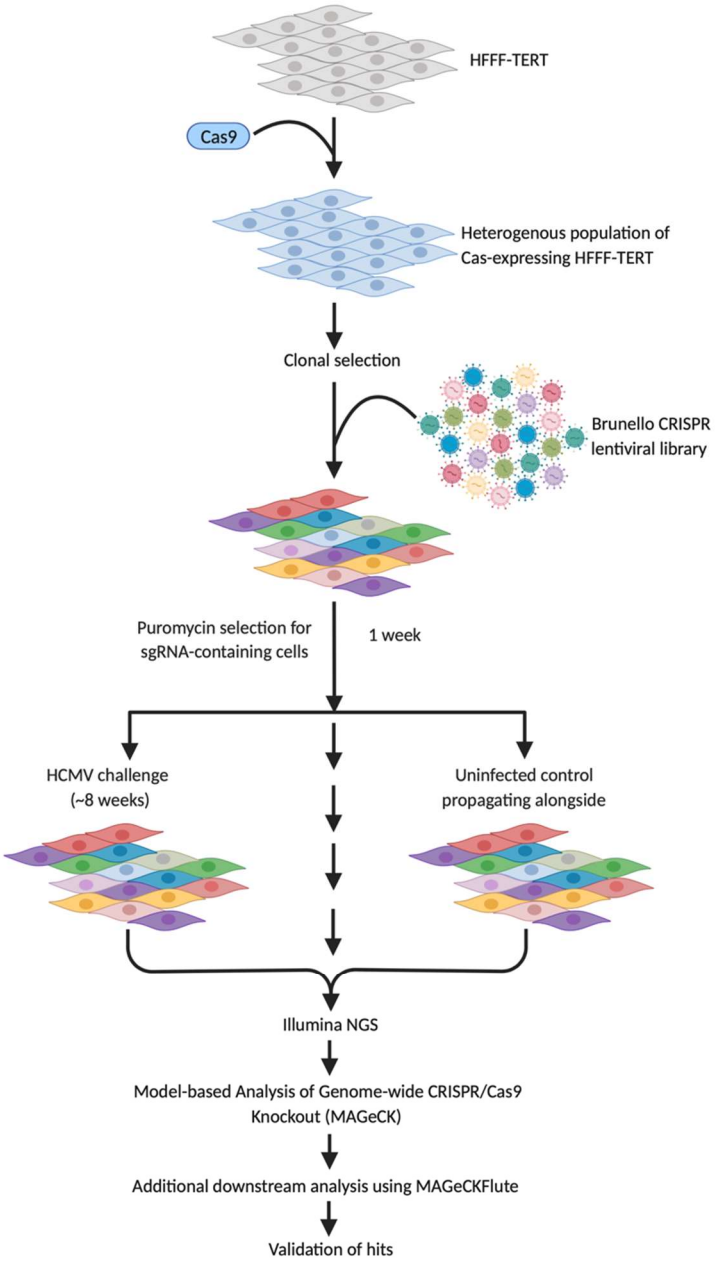

Figure 4.12: Outline of genome-wide pooled CRISPR-Cas9-based knockout screen for HCMV infection.

Approximately 130 million TERTCas9 (clone 13) cells were transduced with the Brunello lentiviral library (MOI 1). After 24h, non-transduced cells were removed with puromycin (1 µg/mL). One week later, genomic DNA (gDNA) was extracted from two-thirds of mutant cell population to use as uninfected baseline control. The remaining puromycin-resistant cells were propagated in culture. After about two weeks, 150 million puromycin-resistant cells were infected with HCMV Merlin-UL128^{mut} at an MOI of 0.5 (as described in Section 2.7.2.3). Four weeks later, cells were seeded into fresh flasks and re-infected with HCMV. After four additional weeks, gDNA was extracted from surviving cells. An uninfected 'mock' population was propagated alongside as an additional control. Samples were sequenced to a depth of 20 million reads per sample, as previously described (Section 2.8). The outline was created with BioRender.com.

4.2.4 Genome-wide pooled CRISPR-Cas9 screen identifies genes essential for HCMV infection

4.2.4.1 Quality control measurements for CRISPR-Cas9 based screen

I performed a genome-wide CRISPR-Cas9 mediated knockout screen using Brunello CRISPR library in Cas9-expressing HFFF-TERTs. This multistep process is described in Figure 4.12 and Section 2.7.2. Prior to hit identification, MAGeCK and MAGeCKFlute were used to assess the quality of each data set. These computational tools contain several functions required to analyse CRISPR-Cas9 screen data (2.9). MAGeCKFlute uses MAGeCK to map raw reads to a known CRISPR library (Brunello library) and normalise sgRNA read counts to enable different samples to be compared. The pipeline evaluated the quality of my datasets at both read count and sequencing levels. The results are output as a range of graphs that include the following:

- The number and percentage of mapped reads (Figure 4.13 A), where a high mapping ratio (> 65%) indicates successful sample preparation and sequencing[278,279,322].
- The number of missing sgRNAs, that is, the number of sgRNAs that didn't map to any reads (Figure 4.13 B). A low number of zero sgRNAs (< 1%) implies that the sample is of high quality [278,279,322].
- The evenness of sgRNA read counts using the Gini index (Figure 4.13 C), which is commonly used to measure income inequality[323]. A low Gini index (<0.2) indicates that sgRNA read counts are perfectly distributed in the sample, whereas a high Gini index (>0.5) suggests a highly inequal read count distribution [278,279,322].
- The distribution of median base (Figure 4.13 D) and mean sequence (Figure 4.13 E) qualities, where quality scores should be greater than 25[278,279,322].
- The distribution of GC content of sequencing reads (Figure 4.13 F), where central peak should be similar across all samples[278,279,322].

All four samples (pDNA, baseline control, mock and HCMV-infected) displayed a high percentage of mapped reads (>84%), indicating that the samples were of good quality and free of contamination (Figure 4.13 A). Additionally, all samples had a similar and sufficient number of sgRNA reads to allow downstream analysis, that is approximately 200 reads for each sgRNA (Figure 4.13 A). The number of missed sgRNA and Gini index was very high in the HCMV-infected dataset (Figure 4.13 B-C). This was expected due to strong selection pressure (HCMV challenge) after which the majority of the cells died. In contrast, the evenness of sgRNA read counts should be low (<0.2) across initial (pDNA and uninfected baseline) and unselected (Mock) samples. However, this was not the case as the Gini index for pDNA, baseline and Mock were 0.06, 0.28 and 0.92, respectively (Figure 4.13 C). A Gini index between 0.2 and 0.3 represents that the distribution of sgRNA read counts is relatively equal across target genes in the sample[278,279,322,323]. Whereas the Gini index greater than 0.5 suggests highly heterogeneous read count distribution, respectively[278,279,322]. At the sequencing level, all samples were of good quality as indicated by a median base and mean sequence quality above the threshold value of 25 (Figure 4.13 D-E). Although the distribution of GC content was similar across all datasets, that is a central peak between 40-60%, the GC-content of mock displayed a 'split-peak', which can occur due to poor manual injection of sample into the column, poor column installation, solvent mismatch, or temperature fluctuations during NGS run[324,325]. The split peak distribution of GC content for the mock dataset was likely due to erratic or jerky sample loading because changes to the other parameters would have affected all samples. Therefore, I concluded that the mock sample was unlikely to be reliable. Instead, the initial pool of puromycin-resistant cells was used as uninfected control for downstream analysis.

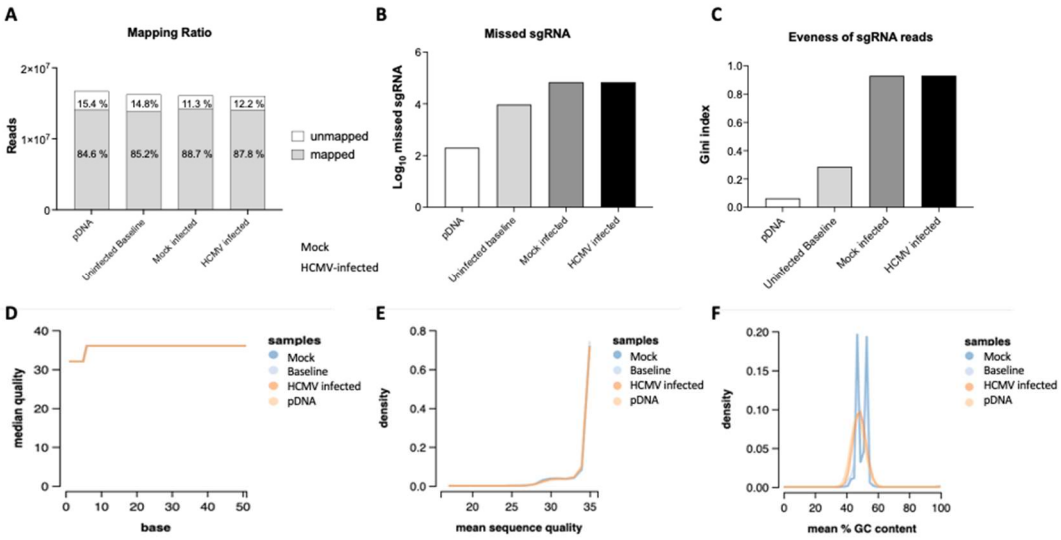

Figure 4.13: Quality control assessment of data from CRISPR-Cas9 screen for HCMV HDFs.

For each sample, quality control was assessed by **(A)** total number and percentage of mapped reads, **(B)** the number of zero sgRNAs, that is, the number of sgRNAs that didn't map to any reads, **(C)** the Gini index, **(D)** distribution of median base quality, **(E)** mean sequence quality and **(F)** GC content distribution of sequencing reads across all samples. MAGeCKFlute allowed visualisation of quality control assessment.

4.2.4.2 Genome-wide CRISPR screen identifies five novel HCMV host dependency factors (HDFs).

To identify HDFs critical for HCMV infection, I performed a pooled genome-wide CRISPR-Cas9 based screen using the Brunello CRISPR knockout lentiviral library. Cell viability post multiple rounds of HCMV infection was a phenotypic readout. This approach identified a restricted list of HCMV HDFs that included both novel and previously known factors. MAGeCK analysis identified 13 host genes (FDR < 0.05) that could be important during HCMV infection (Figure 4.14). In fact, the top 11 ranking genes scored strongly above the threshold with FDR < 0.01 (Supplementary Table 15). Their sgRNAs were significantly enriched in the cell population that survived the HCMV challenge compared to the uninfected baseline population. For each identified HCMV HDF, at least three and up to four sgRNAs were enriched (Figure 4.15).

MAGeCK analysis identified *NF2* as the most significant hit (Figure 4.14) for infection with pentamer-deficient HCMV. All sgRNAs targeting *NF2* were significantly enriched in fibroblasts surviving Merlin-UL128^{mut} infection (Figure 4.14). *NF2* encodes a protein that is a crucial regulator of the Hippo signalling pathway[326–328]. *NF2*-encoded protein phosphorylates large tumour suppressor kinase 2 (LATS2), which is a serine-threonine kinase that negatively regulates yes-associated protein (YAP) and its transcriptional coactivator with PDZ-binding motif (TAZ) [326–328]. YAP is a major downstream effector of Hippo pathway signalling[326–328]. *LATS2* was another significant HCMV HDF identified from the genome-wide CRISPR screen (Figure 4.14). All *LATS2*-targeting sgRNA were enriched in the population that survived the HCMV challenge (Figure 4.15). Both *NF2* and *LATS2* were unique hits from our screen not previously associated with HCMV infection. My CRISPR screen identified *KIRREL* as another novel HCMV HDF (Figure 4.14) with all its sgRNAs enriched in the HCMV-resistant population (Figure 4.15). *KIRREL* encodes a protein that also positively regulates the Hippo signalling pathway[329]. It senses cell-cell interaction and recruits Salvador family WW domain-containing protein 1 (SAV1) at sites of cell adhesion[326–328]. SAV1 is an adapter protein that enhances the

activation of kinases upstream of YAP [327,328,330]. *NF2*, *LATS2* and *KIRREL* are important for activation of the Hippo pathway for the subsequent inhibition of YAP activity (Table 14).

The second most significant HCMV HDF identified was *PDGFRA* (Figure 4.14), with all four *PDGFRA*-targeting sgRNA significantly enriched in the HCMV-resistant dataset (Figure 4.15). The role of PDGFR α during HCMV infection is well-documented literature. For example, another genome-wide CRISPR screen has previously identified PDGFRα as an essential host factor involved in HCMV entry, where PDGFRα-knockout completely protected cells from "trimer only" HCMV strains[22]. Furthermore, PDGFRα has been shown to facilitate the cell-to-cell spread of pentamer-deficient HCMV strains[22]. Interestingly, PDGFRα was not essential for the entry and spread of HCMV strains containing both trimeric and pentameric complexes[331]. Additional functions of PDGFRα are summarised in Table 14.

MAGeCK analysis identified several hits (*SLC39A9*, *PTAR1*, *HS6ST1*, *EXT1* and *GLCE*) that are known to be involved directly or indirectly in the biosynthesis of heparan sulphate proteoglycans (HSPGs) (Table 14). Although many of these genes have not been studied in the context of HCMV infection, the role of HSPGs in facilitating HCMV infection is well-documented in the literature. For example, many studies have shown that HSPGs play an important role in HCMV binding to the host cell[79].

PTEN was the final statistically significant hit identified in our HCMV HDF CRISPR-Cas9 screen (Figure 4.13 and Figure 4.14). *PTEN* encodes a phosphatase that is a key modulator of the AKT-mTOR signalling pathway[331]. Previous studies have shown that HCMV induces activation of the mTOR signalling pathway[331], which is essential for replication in myeloid cells, particularly in the late phase of the viral lytic cycle. In fact, studies have shown that the occurrence of HCMV disease was significantly reduced in kidney transplant recipients treated with inhibitors of mTOR [208]. Intriguingly, HCMV has also been shown to upregulate *PTEN* to inhibit Akt-

dependent eNOS activation[308]. Other functions of the protein encoded by PTEN are listed in Table 14.

The CRISPR-Cas9 screen also identified three other novel candidate HDF (*MED23*, *C16orf72* and *KIF5B*) that could be important for HCMV infection. Table 14 describes known functions of proteins encoded by these genes.

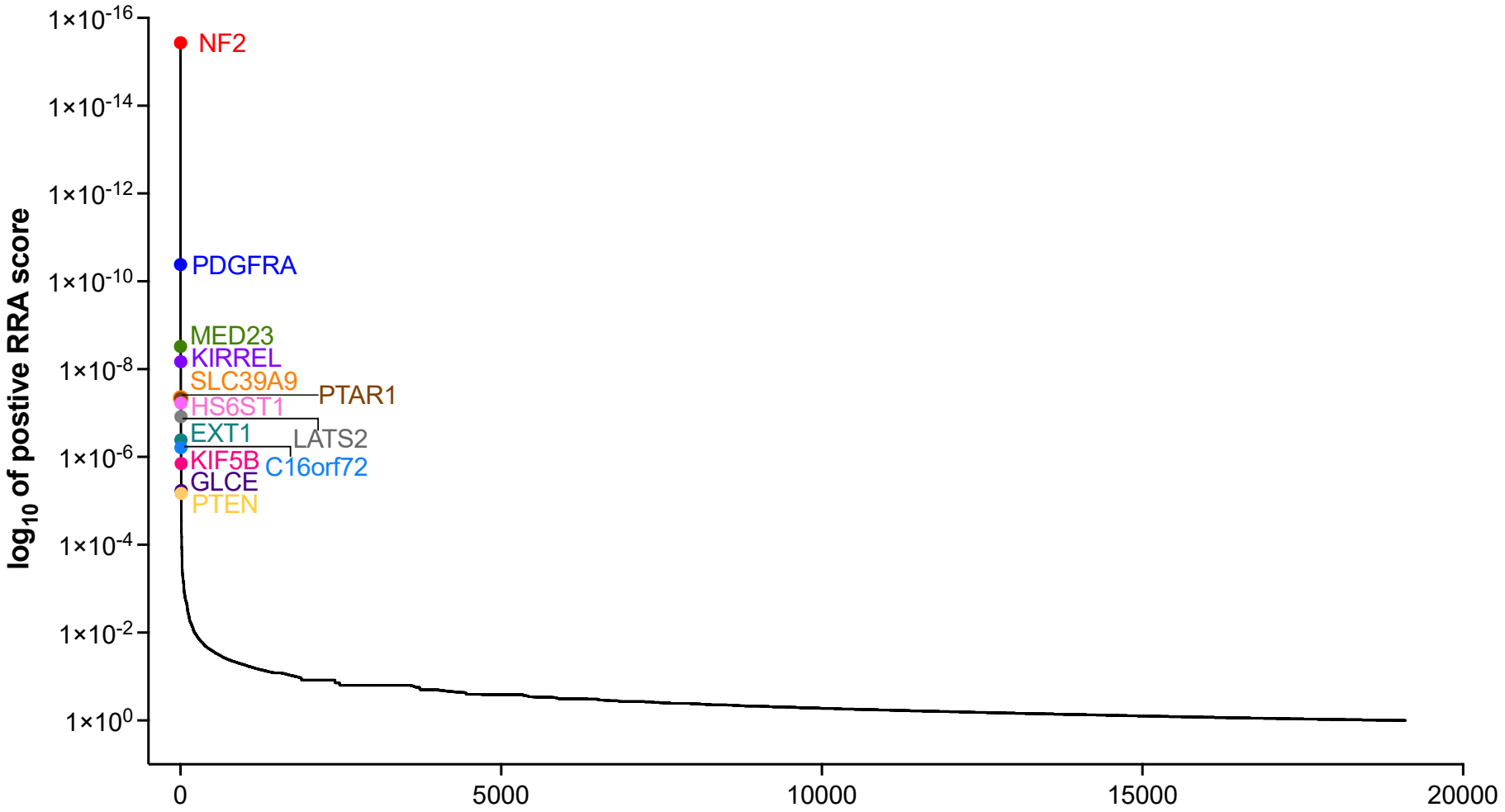

Figure 4.14: Top-ranking HCMV HDFs identified from genome-wide CRISPR screen using the MAGeCK algorithm.

The graph shows the distribution of positive MAGeCK RRA scores of all genes following comparison of uninfected (baseline) and HCMV-infected cell populations. Smallest score denotes highest gene essentiality and vice versa. MAGeCK analysis identified 13 positively selected gene candidates that were statistically significant with FDR < 0.05 (annotated in colour)

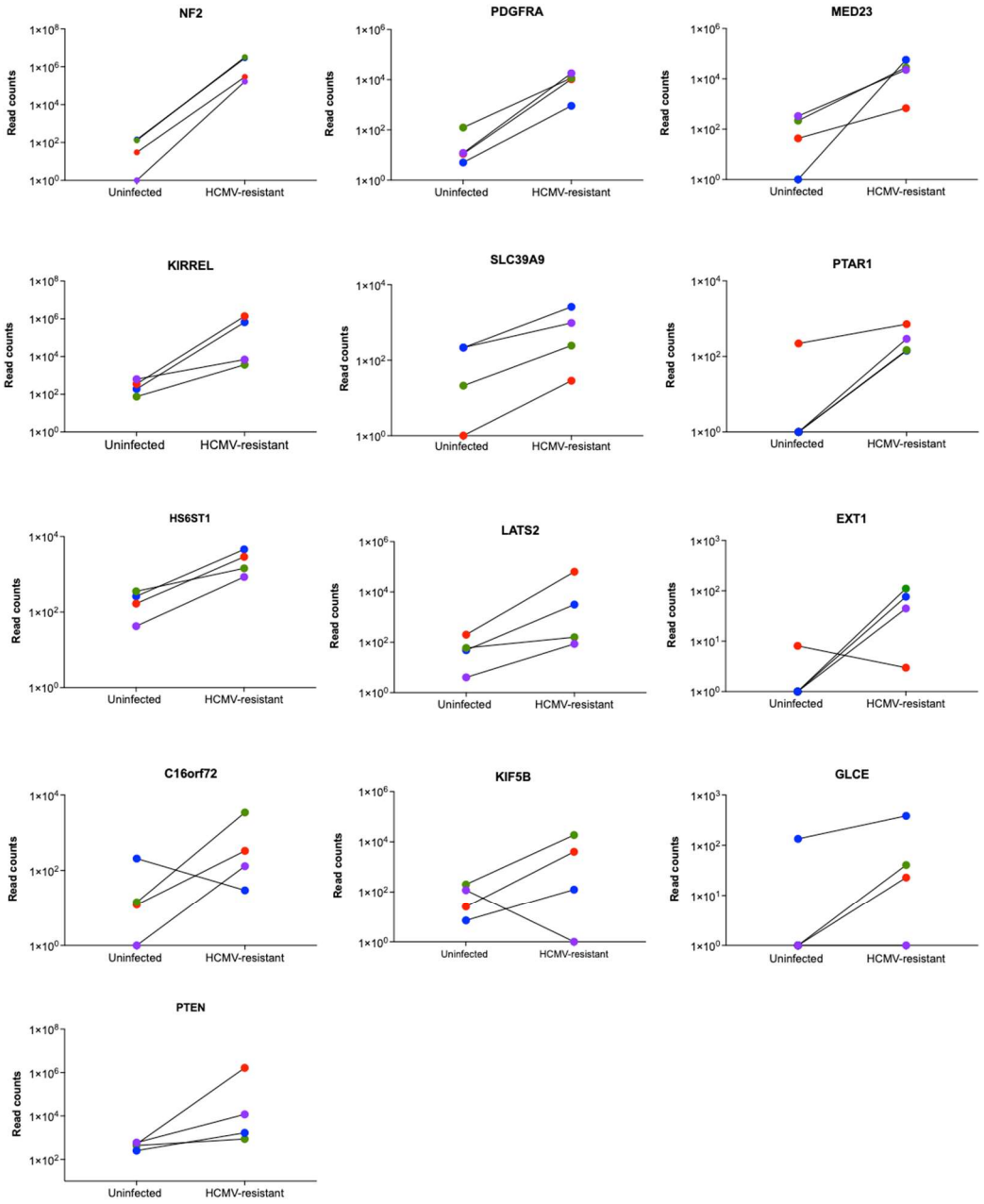

Figure 4.15: Distribution of normalised sgRNA read counts of essential genes present in the uninfected and HCMV-resistant (cells surviving HCMV challenge) datasets.

Essential genes were identified by MAGeCK. The CRISPR-Cas9 knockout library contained ~ 4 sgRNA per gene. Each coloured circle represents a different sgRNA.

Table 14: Molecular function and biological processes previously associated with the top-ranking genes (FDR < 0.05) identified from -wide CRISPR screen using the MAGeCK algorithm.

Gene	Protein	Function	OMIM ID
NF2	Merlin	• Positive regulator of the Hippo signalling pathway through phosphorylation of LATS kinases[328]. • A key regulator of contact-dependent inhibition of cell proliferation, controlling cell shape, survival, and cell-cell adhesion[332]. • May act as a tumour suppressor, preventing uncontrolled proliferation of cells[333].	607379
PDGFRA	PDGFRα	• A tyrosine-protein kinase that acts as a cell surface receptor and induces activation of signalling pathways upon stimulation[217,283]. • Phosphorylates PI3K, leading to activation of the AKT1 signalling pathway[217,283]. • An essential role in cell proliferation, survival, migration, and chemotaxis[334]. • Essential for entry and cell-cell spread of “trimer-only” HCMV[22].	173490
MED23	Mediator of RNA Polymerase II Transcription Subunit 23	• Regulates transcription by RNA polymerase II, which transcribes all protein-coding and most of the non-coding RNA genes in eukaryotes[335,336].	605042

KIRREL	Kirre-like Nephrin Family Adhesion Molecule	• A positive regulator of the Hippo signalling pathway. KIRREL-facilitated cell adhesion inhibits YAP activity[329].	607428
SLC39A9	Solute Carrier Family 39 (Zinc Transporter) Member 9	• A transmembrane protein predicted to be involved in transport of zinc ion[337]. • Required for biosynthesis of N- and O- glycans[337]. • Involved in multiple glycosylation pathways, including heparan sulfate glycosylation[338].	619116
PTAR1	Protein prenyltransferase alpha subunit repeat containing 1	• Involved in protein prenylation and regulate multiple glycosylation pathways, including heparan sulfate glycosylation[339]. • Increase expression of heperan sulfate on the cell surface[339].	134635
HS6ST1	Heparan-sulfate 6-O-sulfotransferase 1	• A heparan sulfate biosynthetic enzyme.	604846
LATS2	Large Tumor Suppressor Kinase 2	• A serine/threonine-protein kinase that is a negative regulator of YAP/TAZ in the Hippo signalling pathway, controlling genes involved in cell proliferation, growth, migration, and death[328,333]. • Inhibits transition from cell growth phase 1 (G1) to DNA synthesis phase (S) of the cell cycle through downregulation of cyclin E/CDK2 kinase[340,341].	604861
EXT1	Exostosin Gylcotransferase 1	• A glycosyltransferase involved in heparan sulphate biosynthesis[342,343]. • May also act as a tumour suppressor[344].	608177

C16orf72	-	• Unannotated at the time of MAGeCK analysis but recently identified by [345] as a regulator of p53, protecting cells from telomerase inhibition. The protein encoded by C16orf72 was termed by [345] "Telomere Attrition and p53 Response 1 (TAPR1)".	-
KIF5B	Kinesin Family Member 5B	• A microtubule-dependent motor protein that regulates distribution of organelles [346,347].	602809
GLCE	Glucuronic Acid Epimerase	• Involved in maturation of heparan sulfate and heparin[348,349].	612134
PTEN	Phosphatase and Tensin Homolog	• Encodes a tumour suppressor with dual-specificity phosphatase. Negatively regulates PI3K and MAPK signalling pathways through lipid and protein phosphatase activity, respectively[350,351]. • YAP inactivates lipid phosphatase of PTEN, promoting cell proliferation[331]. • May have a role in preparation for DNA synthesis phase of the cell cycle.[352]	601728

4.2.5 Validation of unique hits as HCMV HDFs

My CRISPR-Cas9 screen for HCMV HDFs identified six novel genes that could be important for productive HCMV infection (Figure 4.14). Five of these gene candidates (*NF2*, *MED23*, *KIRREL*, *LATS2* and *KIF5B*) were selected for further validation. C16orf72 was excluded as at the time the gene was unannotated, encoding a protein with unknown function. Since the role of PDGFRα in HCMV entry is well documented, *PDGFRA* was included as a positive control in further experiments. To understand how the loss of *NF2*, *MED23*, *KIRREL*, *LATS2* and *KIF5B* provided protection against HCMV infection, the CRISPR-Cas9 system was used to generate polyclonal knockout (KO) HFFF-TERTCas9 cell lines for each individual gene (Section 2.10). All polyclonal KO cell lines were viable (data not shown). Ideally, gene-specific staining or sequencing should be performed to confirm the KO phenotype(), but this was not possible within the timeline of my PhD and delays associated with the COVID-19 pandemic.

At 24hpi, GFP expression served as a marker for HCMV entry, as new virions are not generated until 72hpi. Overall, deletion of target genes conferred partial protection against entry of UL128-repaired Merlin-GFP (Figure 4.16). For example, *NF2* KO only led to a 40% reduction in viral entry (18.3% GFP+) as compared to infected HFFF-TERT (32.8% GFP+) at 24hpi (Figure 4.16). A similar decrease in HCMV entry was observed in cells without *MED23* and *KIRREL* (Figure 4.16). Whereas *KIF5B* KO led to a 60% reduction in viral entry (only 13.1% GFP+) compared to normal HFFF-TERT (32.8% GFP+) (Figure 4.16). In contrast, *PDGFRA* KO provided the least protection against entry of UL128-repaired Merlin (Figure 4.16). This was expected as PDGFRα is not required for entry of pentamer-containing HCMV [(22)]. In fact, HCMV virions with an intact trimer and pentamer have been shown to use an alternative mechanism to enter clonal *PDGFRA*-null fibroblasts[(22,86)]. Consequently, these preliminary results seem to imply that the novel HDFs identified from my CRISPR-Cas9 screen may not be important for the entry of pentamer-containing HCMV virions. However, the findings need to be confirmed in homozygous KO clones.

Additionally, a reduction in viral replication would be a more robust readout for the impact of gene-specific KO. Consequently, HCMV-induced CPE was observed at 72hpi following infection with Merlin-UL128^{mut} HCMV. As compared to infection with Merlin-UL128^{WT} (Figure 4.16), *NF2* polyclonal KO fibroblasts were completely resistant to Merlin-UL128^{mut} HCMV (Figure 4.17). No HCMV-induced CPE was visible in HCMV-infected *NF2*-null HFFF-TERTs (Figure 4.17). Apart from *MED23*-null fibroblasts, which remained susceptible to virus-induced CPE, deletion of *PDGFRA, KIRREL*, *LATS2* and *KIF5B* partially protected against Merlin-UL128^{mut} (Figure 4.17). Previous studies have shown that HCMV strains lacking the pentameric complex could not enter or replicate in clonal PDGFRα-KO cell lines[22]. Consequently, CPE observed following infection with pentamer-deficient HCMV, particularly in polyclonal *PDGFRA* KO cells, could be a consequence of inefficient sgRNAs that allow partial gene expression in Cas9-expressing target cells. This further emphasizes the importance of validating hits in several homozygous KO clones; preferably generated using multiple different sgRNAs. Nonetheless, strong protection against HCMV in *NF2*-null fibroblasts suggests a potential role of Hippo signalling in viral replication.

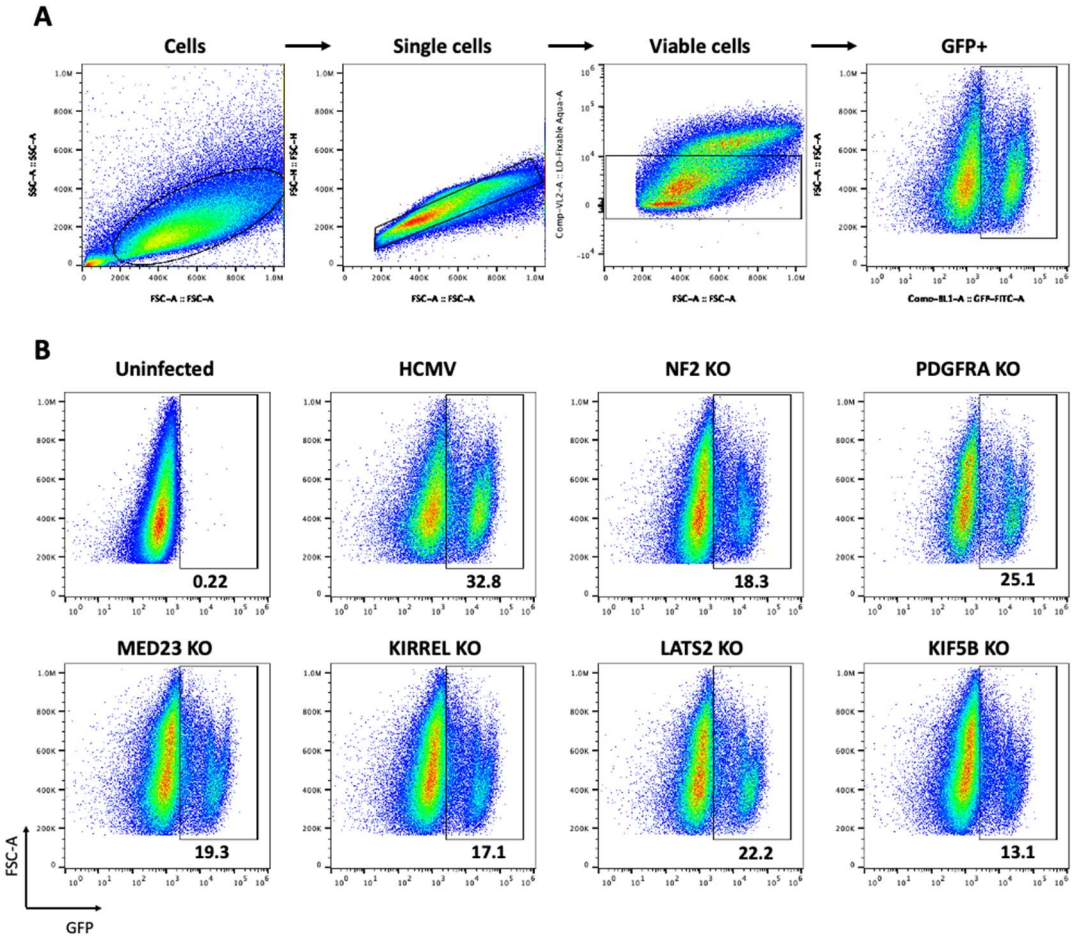

Figure 4.16: Gene-specific polyclonal knockouts in HFFF-TERTs partially inhibited infection with Merlin-UL128^{WT}.

(A) Representative gating strategy for flow cytometric analysis of gene-specific polyclonal knockout cell lines infected with Merlin-UL128^{WT}GFP (MOI 5). **(B)** Productive HCMV infection was determined by the percentage of GFP-positive cells 24 hpi. Uninfected and HCMV-infected TERTCas9 cells were used as control.

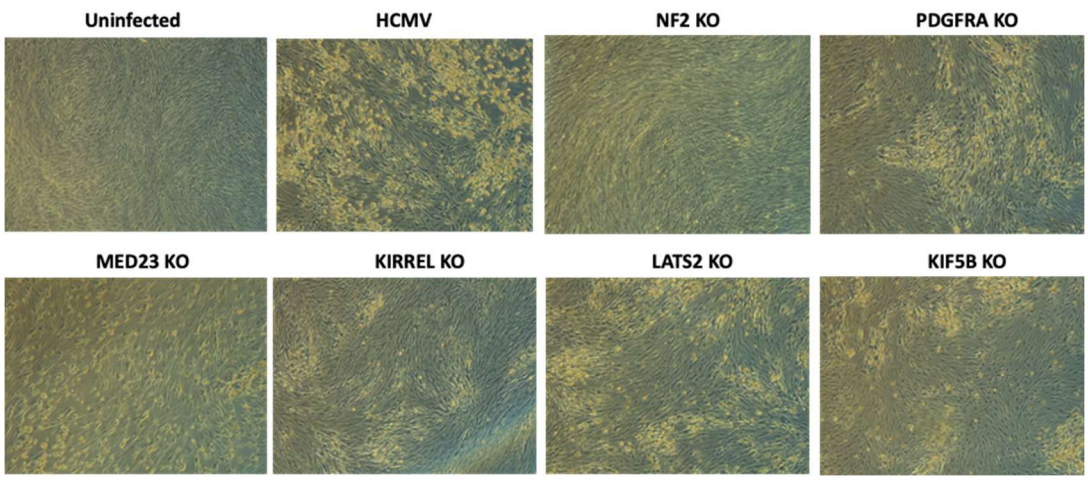

Figure 4.17: Polyclonal HFFF-TERTCas9 cells with gene-specific knockouts inhibited infection with UL128-mutated Merlin strain with varying degrees of success.

Polyclonal knockout cell lines were infected with Merlin-UL128^{mut} at MOI 5. After 72h, the impact of HCMV-induced CPE on cell morphology was assessed by light microscopy. Uninfected and HCMV-infected HFFF-TERTCas9 cells were used as control. All images were taken under X5 magnification.

4.2.6 Pharmacological inhibition of the Hippo signalling pathway reduces the production of new virions following cell-free HCMV infection

The CRISPR-Cas9 screen identified three hits (*NF2*, *KIRREL* and *LATS2)* that are directly involved in the Hippo signalling pathway (Figure 4.14 and Table 14). In fact, *NF2* was the most significant HCMV HDF identified by MAGeCK (Figure 4.14). Additionally, downstream functional analysis by MAGeCKFlute RRA function identified the Hippo signalling pathway as enriched with top-ranking positively selected genes (Figure 4.18), following comparison of uninfected and HCMV-infected datasets. Therefore, to confirm whether the Hippo signalling was important for viral entry and replication, HFFF-TERT were pre-treated with an inhibitor of Hippo signalling (XMU-MP) and infected with HCMV (Merlin-UL128^{WT}GFP at MOI 5). Treatment with XMU-MP did not prevent viral entry as all cells expressed GFP at 72 hpi (Figure 4.19). However, most of the infected XMU-MP treated cells were morphologically similar to uninfected fibroblasts (Figure 4.19), indicating inhibition of Hippo signalling may reduce HCMV-induced CPE through inhibition of viral replication.

To determine if Hippo signalling facilitated HCMV replication, virus production at 72hpi was measured by plaque assay, using supernatants from HCMV infected fibroblasts that were treated with or without XMU-MP. Inhibition of Hippo signalling seemed to reduce HCMV replication (Figure 4.20). As compared to cells treated with DMSO, inhibition of the Hippo pathway significantly inhibited HCMV replication in fibroblasts, leading to around a 2-fold decrease in viral load in the supernatant after 2 weeks (Figure 4.20). Additional functional assays are required to elucidate the molecular mechanism and physiological role of Hippo signalling in regulating HCMV replication. Nevertheless, my CRISPR-Cas9 screen has identified a novel pro-viral host pathway that facilitates HCMV replication and can potentially be targeted for the development of anti-HCMV therapies.

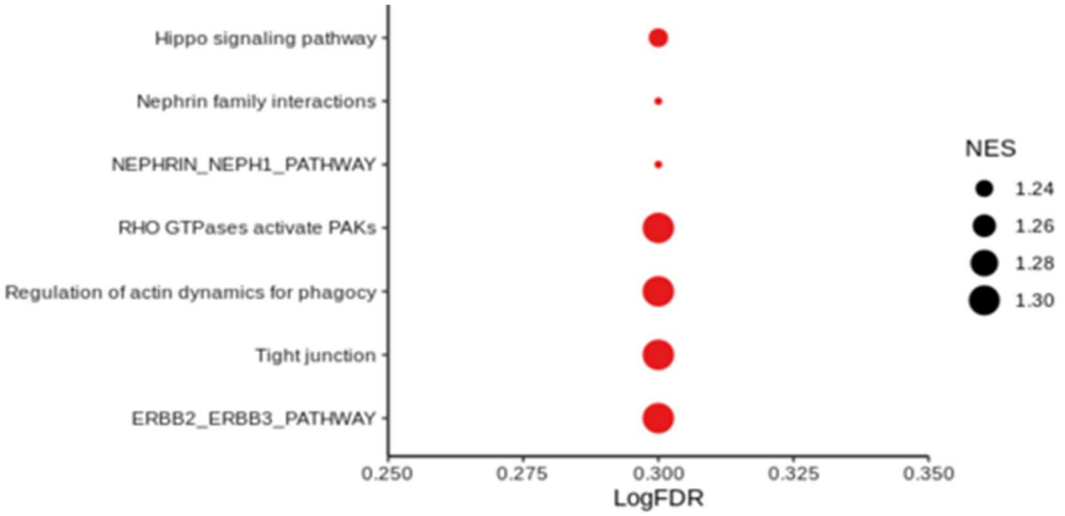

Figure 4.18: Significantly enriched gene ontology (GO) biological processes identified by MAGeCKFlute RRA function.

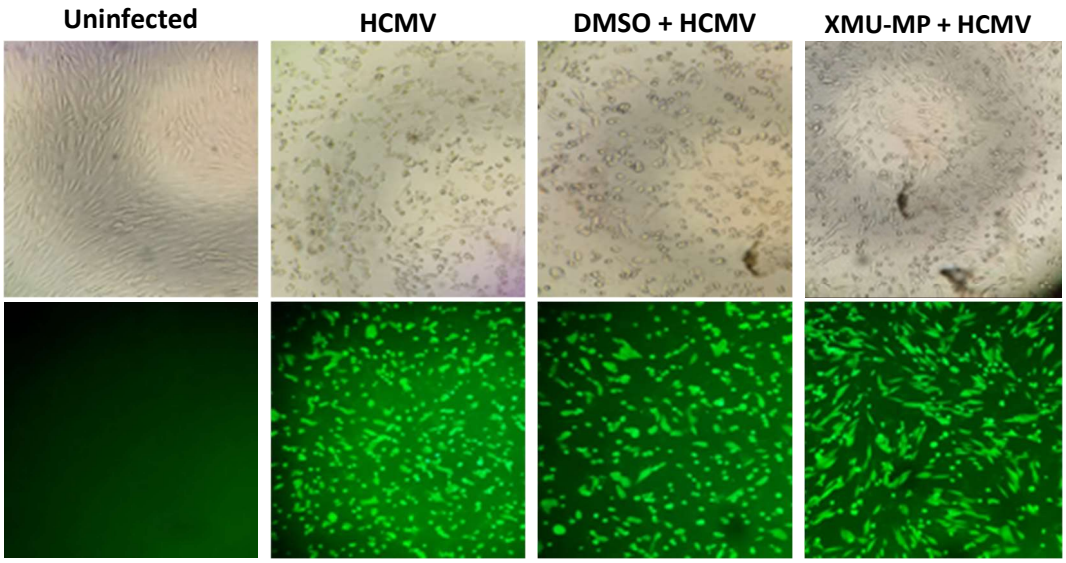

Figure 4.19: Inhibition of Hippo signalling pathway did not prevent HCMV entry. HFFF-TERTs were pre-treated with inhibitor of Hippo pathway (3µM XMU-MP) or vehicle control (DMSO) prior to infection with HCMV (Merlin-UL128^{WT}GFP at MOI 5). Uninfected and HCMV-infected HFFF-TERT that were not pre-treated with XMU-MP were used as controls. At 72hpi, the impact HCMV-induced CPE was assessed by light microscopy (top row) and the percentage of infected (GFP+) cells was assessed by fluorescence microscopy (bottom row). All images were taken under X5 magnification.

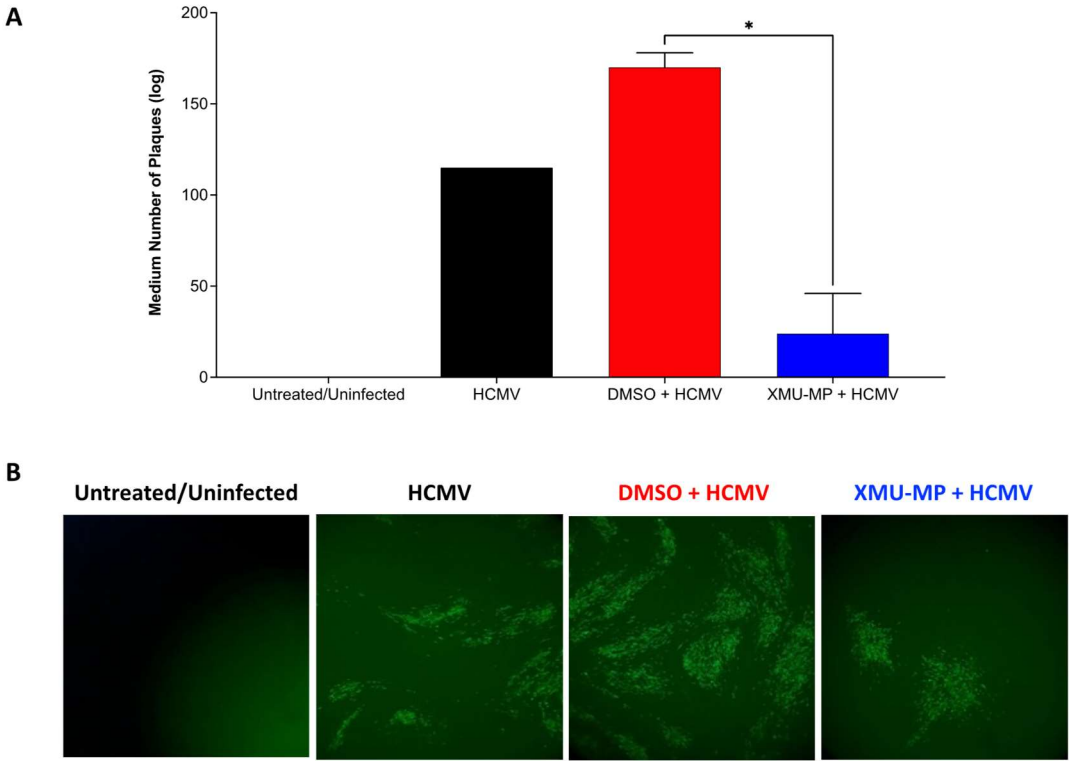

Figure 4.20: Inhibition of Hippo signalling pathway may affect HCMV replication and production of infectious virions.

(A)HFFF-TERTs were pre-treated with an inhibitor of Hippo pathway (3µM XMU-MP) or vehicle control (DMSO) prior to infection with HCMV (Merlin-UL128^{WT}GFP at MOI 5) (n = 4). Uninfected or HCMV-infected HFFF-TERT that were not pre-treated with XMU-MP were used as controls. After 72hpi, supernatants were collected and virus load was quantified by plaque assay. Data was plotted as median$\pm$ SEM. Statistical significance relative vehicle control (DMSO) was calculated using Mann-Whitney U test (*p<0.05) **(B)** Representative fluorescence images of plaques produced from supernatants of HCMV infected fibroblasts that have been treated with or without XMU-MP. All images were taken under X10 magnification.

4.3 Discussion

Pooled genome-wide CRISPR-Cas9 lentiviral libraries have successfully been used to introduce loss-of-function mutations across the entire genome to identify genes that are required to produce the phenotype of interest[268]. One of the aims of my PhD was to use this technology to rapidly screen for host genes that are essential for HCMV entry and replication. Prior to designing a genome-wide CRISPR-Cas9 based assay, it was important to address several key technical and practical considerations associated with large-scale phenotypic screening. For example, a successful genome-wide CRISPR screen requires the generation of Cas9-expressing cells with high Cas9-cutting efficiencies, optimal lentiviral transduction for efficient mutagenesis, and strong selection pressure. In this chapter, I provided an overview of the measures taken to identify a suitable cell line and virus combination for the identification of HCMV HDFs using a genome-wide CRISPR-Cas9 lentiviral library.

As discussed in Section 4.1.2, one of the most important decisions to make, before setting up a genome-wide CRISPR-based assay, is the choice of the cell line. For example, it is extremely important to ensure that the chosen cell line is highly sensitive to the selection agent(s) being applied during the screen. Consequently, to optimise HCMV infection in a physiologically relevant cell line that could be used for CRISPR-based screening, it was important to develop a system that allows HCMV infection to easily be monitored *in vitro*. Therefore, GFP-expressing HCMV strains were used for optimisation assays. This allowed target cells that are sensitive to HCMV (GFP+) to be easily distinguished from those that are less permissive to HCMV infection (GFP-).

From a panel of Cas9-expressing cell lines that were infected with GFP-expressing HCMV, the HFFF-TERTCas9 cell line was identified as the most suitable cell line for carrying out a genome-wide assessment of host genes that are essential for HCMV. It was also necessary to derive a single cell clone from a pool of Cas9-expressing HFFF-TERTs due to observed Cas9 heterogeneity (Figure 4.10). Clone 13 showed

the highest cutting efficiency (Figure 4.10) so it was used to perform the CRISPR screen for HCMV HDFs. Furthermore, it was possible to achieve the desired lentiviral infection efficiency of 30% in HFFF-TERTCas9 cells (Figure 4.11). Therefore, the Brunello CRISPR lentiviral library could be used to generate a mutant population with the recommended sgRNA representation (~400 cells per sgRNA) in this cell model. Additionally, it was possible to infect greater than 90% of these cells with Merlin-UL128^{mut} HCMV strain (Section 4.2.2.4.4). Since the pentameric complex is not required for productive HCMV infection in fibroblasts[22], it was decided that using a virus lacking the pentameric complex was unlikely to affect the readout of my CRISPR screen. Almost 100% CPE was observed in HFFF-TERTCas9 cells when the infection was allowed to spread through the monolayer for several days, following low MOI infection with Merlin-UL128^{mut} (Figure 4.9). This not only helped reduce the total amount of HCMV required for our CRISPR screen but also increased the likelihood of identifying only the most essential HCMV HDFs as most cells would die post HCMV challenge. Consequently, it was expected that puromycin-resistant cells that survive multiple rounds of HCMV infection harbour mutations in pro-viral genes, making them resistant to resistant to HCMV infection. The multistep process of my genome-wide CRISPR-Cas9 screen is outlined in Figure 4.12.

The genome-wide CRISPR-Cas9 screen identified 13 host genes (FDR < 0.05) of potential importance during HCMV infection (Figure 4.14). A majority of the hits overlapped with known HCMV HDFs (e.g. *PDGFRA*) or were associated with pathways that had previously been implicated in HCMV infection. For example, *SLC39A9*, *PTAR1*, *HS6ST1*, *EXT1* and *GLCE* are known to be involved in HSPG biosynthesis (Table 14). Many studies have previously shown that HSPGs promote HCMV entry and subsequent replication in target cells[79]. The fact that many hits overlapped with well-known HCMV HDFs from previous studies indicate that my CRISPR-Cas9 screen was reliable and successful.

Apart from previously known HCMV HDFs, my CRISPR-Cas9 screen also identified six novel gene candidates (*NF2*, *MED23*, *KIRREL*, *LATS2*, *C16orf72* and *KIF5B*) that could

be important for productive HCMV replication (Figure 4.14). Although gene-specific polyclonal KO cells mainly conferred partial protection against both wildtype and UL128-mutated Merlin viruses, further validation of these hits as HCMV HDFs is required.

Of the six novel genes identified, *NF2*, *KIRREL* and *LATS2* are directly involved in the Hippo signalling pathway (Table 14). The Hippo signalling pathway is evolutionarily conserved and plays an important role in organ size control through the regulation of cell proliferation, apoptosis, and self-renewal of stem cells[327,328,330]. Disruption of the Hippo pathway is associated with many disease pathologies, particularly the development of cancer[327,328,330]. A range of intrinsic and extrinsic signals can activate the Hippo pathway, including oxidative stress, cell-cell contact, cell polarity and extracellular matrix stiffness[327,328]. When the Hippo pathway is active, YAP/TAZ is phosphorylated, causing cytoplasmic retention[327,328,330]. In contrast, when the Hippo signalling pathway is inactive, YAP/TAZ are unphosphorylated and free to translocate to the nucleus[327,328,330]. YAP/TAZ bind to transcriptional enhanced associate domain (TEAD) transcription factors in the nucleus and activate transcription of genes involved in cell proliferation, migration, and survival[327,328,330]. The Hippo signalling pathway is also the only known inhibitor of YAP [317,341,34]. LATS kinases directly interact with YAP to prevent its localisation into the nucleus[327,328,330]. YAP is a negative regulator of the innate immune response[327,328,330]. In fact, HBV, ZIKV, and KSHV inhibit Hippo signalling to allow nuclear translocation of YAP, suggesting the Hippo pathway exerts antiviral functionality[326,353–356]. Intriguingly, my data suggest that the Hippo signalling pathway facilitates rather than inhibits HCMV replication. Preliminary experiments demonstrated that inhibition of Hippo signalling restricted HCMV replication, not at the point of HCMV entry (Figure 4.19) but rather reduced the production of infectious virions (Figure 4.20).

One mechanism through which the Hippo signalling pathway may promote HCMV replication is by controlling cell adhesion and thus enabling cell-to-cell

dissemination of HCMV[329,357]. High cell densities trigger activation of LATS1/2, which in turn phosphorylates YAP, leading to its cytoplasmic retention[329,357]. Interestingly, KIRREL mediates cell adhesion and could serve as a sensor for cell-cell interactions at high cell densities[329,357]. KIRREL recruits SAV1 to sites of cell-cell contact which, in turn, enhances activation of kinases upstream of YAP, inhibiting cell proliferation[329,357]. It is expected that depletion in KIRREL and LATS kinases would increase the expression of non-phosphorylated YAP in the nucleus[329,357]. Monitoring YAP expression in the nucleus of normal and gene-specific KO cell lines could help confirm the role of active Hippo signalling in HCMV infection. Furthermore, a co-culture infection model could be used to assess the cell-to-cell spread of HCMV using *KIRREL*- and *SAV1*-KO cell lines. It will also be interesting to compare the cell-to-cell spread of pentamer-deficient and pentamer-containing HCMV in the presence of Hippo pathway inhibitors.

Intriguingly, *in vitro* studies have shown that the inactivation of YAP is essential for cell contact inhibition[329,357]. In contact-inhibited cells, HCMV has been shown to inhibit G1/S transition at 24hpi, blocking host cell DNA synthesis to enhance conditions for viral gene replication[358]. At early time points after infection, HCMV induces expression of Cyclin E/CDK2[359]. Cyclins associated with different CDK complexes regulate progression through different cell-cycle checkpoints, by activating or inhibiting target substrates[358–360]. LATS kinases are also known to regulate G1/S transition through modulation of cyclin E/CDK2 kinase activity[340]. It would be interesting to measure the expression of cyclin E/CDK2 in HCMV infected cells incubated with inhibitors of the Hippo pathway to determine if HCMV inhibits cell cycle progression through Hippo-mediated G1 arrest. PTEN has also been shown to inhibit progression into the S phase of the cell cycle by downregulating cyclin D1 in the nucleus[220,352]. Intriguingly, HCMV inhibits the expression of cellular cyclin D1 during replication thus suggesting a potential link between HCMV-induced inhibition of cyclin D1 and PTEN[360].

Many of the other unique HCMV HDFs identified from my CRISPR screen are known to promote viral gene replication of different viruses. For example, MED23 encodes a crucial transcriptional activator, that has been shown to be activated by adenovirus E1A (viral IE gene) to promote replication[361]. Adenovirus E1A interacts with MED23 to drive transcriptional activation of other adenovirus early genes[361. MED23 forms a complex with other co-activators to mediate activation of RNA polymerase II[361]. As described in Section 1.1.6, HCMV relies on host RNA Polymerase II for the transcription of viral genes[76]. Other herpes viruses, such as HSV-1, also use RNA polymerase II to transcribe viral genes[76]. HCMV recruits cellular RNA Polymerase II to sites of viral IE RNA synthesis and processing[76]. Therefore, it is possible that HCMV IE1 and IE2 interact with MED23, like adenovirus E1A, to promote transcriptional activation of RNA Polymerase II for transcription of HCMV early genes. Monitoring the transcriptional activity of RNA polymerase II or expression of HCMV early genes in both *MED23*-depleted and *MED23*-KO cells could help confirm HCMV-MED23 interaction.

Similarly, KIF5B has been shown to facilitate the nuclear translocation of HIV[346,347]. Mutations in *KIF5B* prevented uncoating and subsequent delivery of the HIV genome into the nucleus[346,347]. Furthermore, KIF5B plays an important role in the transport of newly produced HSV virions towards axon tips in nerve cells[362]. Prior to onset of HCMV IE gene expression, HCMV capsids associate with microtubules to transport HCMV genome into the nucleus[363]. In absence of microtubules, HCMV capsids do not move towards the nucleus *in vitro*. Kinesins, such as KIF5B, are motor proteins that move along microtubule filaments carrying cargo to mediate intracellular transport [347,362,364]. It is possible that KIF5B interacts with HCMV capsid and moves it along the microtubule network, transporting it to the nucleus. Transmission electron microscopy could be used to compare proximity of HCMV capsids to the nucleus in normal and *KIF5B*-KO cells at different timepoints within the first 24 hpi. Additionally, previous studies report that capsid-microtubule association is vital to initiate expression of HCMV IE genes[363]. Therefore, measuring levels of HCMV IE1 and IE2 in the nucleus of *KIF5B*-KO could help validate

the role of KIF5B in facilitating movement of viral capsids from the cytoplasm to the nucleus.

It might be easier to determine how the loss of candidate genes confers protection against HCMV using homozygous KO clones. Additionally, if re-expression of the genes were to restore efficient HCMV replication in KO cell lines, it would provide confidence that the observed HCMV-resistant phenotype in gene-deficient cells was not a consequence of off-target effects. Furthermore, performing a smaller secondary screen that targets a reduced number of genes (e.g., top 500 positively ranked hits from the primary screen), with a different set of sgRNAs, could also help validate hits and eliminate any false negatives. Performing small-scale CRISPR-Cas9 screens in a range of HCMV-susceptible cell lines could also help identify cell-specific and/or universal HCMV-HDFs. Although validation of hits was beyond the scope of this project, the CRISPR screen identified novel pro-viral host pathways that may facilitate HCMV replication, which could potentially be targeted for the development of anti-HCMV therapies.

In conclusion, my data reveal a number of potential pro-viral host factors that support HCMV replication. However, further functional experiments are necessary to validate the role of these genes and identify the mechanisms through which they support HCMV entry and/or subsequent replication. Overall, in accordance with previous studies, data collected here highlight the potential of targeting host factors for the development of antivirals against HCMV infection.

5 General Discussion

There is no licensed vaccine currently available against HCMV, and existing anti-viral strategies target HCMV genes and proteins[56]. Although this approach is relatively effective, its therapeutic potential is limited due to drug-associated toxicity and the emergence of antiviral resistance among HCMV strains[194,195,365]. Consequently, there is an urgent need for developing safe and effective anti-HCMV treatments that can prevent primary infection and/or curb the reactivation of latent HCMV in clinical settings[183]. An encouraging therapeutic strategy is offered by targeting host factors that are indispensable for productive viral infection[275]. HCMV replication is entirely dependent on cellular factors within the host cell and yet surprisingly few HCMV-host interactions have been identified[363].

The overall aim of this thesis was to identify and characterise host genes and pathways that are essential for HCMV replication but dispensable for cellular physiology. Different strategies were employed to identify HCMV HDFs. Initially, I used a panel of ROS inhibitors and identified that peroxynitrite is essential for viral replication in both *in vitro* and *in vivo* of CMV. Furthermore, I conducted a genome-wide CRISPR-Cas9 based screen and identified six novel host factors required for HCMV replication. I also used the CRISPR-Cas9 system to generate individual gene-specific KO cell lines and validated the role of identified hits in HCMV replication. Finally, since three of the unique hits are known to be involved in Hippo signalling, I used inhibitors of the pathway to evaluate the contribution of Hippo signalling in HCMV replication.

5.1 The role of ROS in HCMV replication

ROS generation is a by-product of cellular metabolism during viral infections[128]. Effects of intracellular ROS can be beneficial or deleterious to the cell[216]. At both low and high concentrations, different types of ROS can serve as signalling

molecules, driving multiple pathways and metabolic functions[216]. Virus-induced oxidative stress can enhance viral replication (West Nile and rhinovirus), pathogenesis (rabies virus and SARS-CoV-2) or both (HSV-1, HCMV, IAV and HIV) [255]. Treatment with ROS inhibitors has been shown to reduce replication and virus-mediated pathogenesis in both *in vitro* and *in vivo* models of several viral infections[295]. I used a similar approach to elucidate whether intracellular redox state and redox-mediated signalling are important for HCMV infection.

In chapter 3, I revealed that HCMV exploits endogenous ROS to establish infection. Firstly, I showed that HCMV rapidly induced generation of peroxynitrite (within seconds) upon cell-free infection. Treatment with potent peroxynitrite scavengers dramatically reduced viral replication in both *in vitro* and *in vivo* models of CMV. The antiviral effect of peroxynitrite scavengers was most profound during the initial stages of CMV replication. In fact, inhibition of peroxynitrite prior to or at onset HCMV infection completely blocked viral replication. Furthermore, peroxynitrite seems to be essential for cell-free HCMV entry in fibroblasts. Although treatment with FeTPPS also seemed to reduce cell-to-cell HCMV spread, additional studies are required to elucidate how peroxynitrite facilitates cell-to-cell viral dissemination. Overall, the findings of chapter 3 indicate a potential role for intracellular peroxynitrite in promoting virus entry and facilitating the initiation of viral replication.

5.2 The scope of targeting peroxynitrite to reduce HCMV replication and associated pathology in clinical settings

Pre-emptive treatment with compounds that regulate tissue redox status could help reduce the development of CMV viremia and prevent oxidative stress-induced cellular damage during clinical procedures, including transplantation[183,184]. This is particularly significant if peroxynitrite inhibition prevents the reactivation of latent HCMV. *In vitro* models of HCMV latency should be used to determine the role of peroxynitrite in the CMV reactivation. There is also overwhelming experimental

evidence that suggests attenuation of ROS is beneficial in all stages of transplantation[366]. Furthermore, it is well-established that the success of transplantation correlates with oxidative stress levels[366].

The highly reactive and short-lived nature of peroxynitrite makes it challenging to effectively target *in vivo*[216]. Antioxidant therapy that uses different combinations of drugs to both reduce peroxynitrite production and increase the activity of cellular antioxidant systems could help inhibit peroxynitrite-mediated HCMV replication. Furthermore, blocking enzymes that produce superoxide and/or nitric oxide is likely to be more effective at controlling peroxynitrite levels *in vivo*. However, existing inhibitors of ROS-producing enzymes are not very strong, ROS-type specific, or isoform-selective[255,281]. Moreover, synthetic inhibitors can be highly toxic and associated with drug-induced cellular damage at high doses[281]. For example, many commercially available NOS inhibitors, including L-NMMA, have been associated with septic shock and asthma *in vivo*[367]. Consequently, natural peroxynitrite antagonists, such as serotonin, may provide a safer alternative to synthetic compounds in decreasing HCMV-induced peroxynitrite generation[299]. In chapter 3 I showed that endogenous levels of serotonin did not affect viral load in affected mice. Additionally, although the antiviral effect of exogenous serotonin was not as potent as FeTPPS, it did reduce viral replication in different cell types *in vitro*. Accordingly, studying the pharmacokinetics and pharmacodynamics of natural redox modulators may assist in identifying dosage and understanding drug-protein interactions in different tissues[368].

Another challenge in developing antiviral therapies targeting intracellular ROS is selectively interfering with signalling pathways that promote viral replication without compromising cellular antiviral defence mechanisms that facilitate virus clearance. Consequently, in order to inhibit virus-induced peroxynitrite formation, it will be important to locate ROS-producing enzymes that induce the generation of superoxide and nitric oxide. This will allow the development of pharmacological drugs that selectively target subcellular compartments that trigger simultaneous

production of superoxide and nitric oxide in close proximity[216]. In contrast, targeting cellular proteins and signalling pathways sensitive to HCMV-induced peroxynitrite could be more efficient at selectively blocking peroxynitrite-mediated viral replication and inflammation.

The mechanism by which peroxynitrite mediates HCMV infection may involve peroxynitrite-induced modifications in host factors involved in viral entry, replication, assembly, and egress. For example, previous *in vitro* studies have shown that peroxynitrite-induced phosphorylation of tyrosine residues activates PDGFRα and other cell-surface receptors[217]. Furthermore, it is well-documented that peroxynitrite can modulate the activation of pro-viral transcription factors, including NF-κB and MAPK[217]. A combination of functional studies is required to elucidate the underlying mechanisms by which peroxynitrite mediates HCMV infection. Redox-sensitive pathways activated upon HCMV infection can provide novel targets for anti-HCMV therapies.

5.3 Identification and characterisation of host genes essential for HCMV infection

Pooled genome-wide CRISPR-Cas9 knockout screening provides a platform to rapidly scan the entire genome to identify genes of interest[266,268]. In Chapter 4, I used this unbiased approach to identify host genes that are essential for HCMV infection. Using the Brunello CRISPR lentiviral library, I performed targeted mutagenesis in Cas9-expressing HFFF-TERT (TERTCas9) cells. Following mutagenesis, the mutant target cell population were infected with HCMV (Merlin-UL128^{mut}). High-throughput sequencing was then used to determine sgRNA representation in uninfected controls and HCMV-resistant cell populations. It was expected that surviving cells most likely lack genes required for HCMV entry and replication. Post-CRISPR screen, MAGeCK analysis revealed essential 'hits' by identifying sgRNAs enriched in cells that survived multiple rounds of HCMV compared to uninfected controls. The genome-wide CRISPR-Cas9 screen identified

six novel factors of potential importance during HCMV infection. In fact, three hits (*NF2*, *KIRREL* and *LATS2)* are directly involved in the activation of the Hippo signalling pathway. The Hippo signalling pathway is the only known inhibitor of YAP, a negative regulator of innate antiviral responses within the host[327,330]. In fact, many viruses, including EBV and KSHV herpesviruses, inhibit the Hippo signalling to allow nuclear translocation of YAP, suggesting that the Hippo pathway modulates host antiviral defence mechanisms[327,330]. In contrast, I have shown in Chapter 4 that the Hippo pathway enables, rather than prevent, HCMV replication. Preliminary experiments demonstrated that inhibition of Hippo signalling restricted HCMV replication, not at the point of viral entry but at the level of viral DNA synthesis and release of infectious viral progeny. Further experiments are required to elucidate how the Hippo pathway mediates HCMV replication. For example, *in vivo* targeting of identified signalling and metabolic pathways could help determine if it is possible to safely inhibit the pro-viral host mechanism to prevent infection. MCMV is the most well-characterised and commonly used *in vivo* model for CMV. It provides a robust tool for studying the effects of antiviral therapies within a host during active CMV infection. Therefore, Cas9-expressing mice could be used to KO or modify genes/proteins of interest to study CMV phenotype and test new antiviral treatments.

5.4 Conclusion

I have shown that HCMV induces the production of peroxynitrite early upon infection and is required for productive viral replication in a range of different cell types. Furthermore, inhibition of peroxynitrite prior to and at the onset of cell-free HCMV infection completely blocked HCMV replication. In fact, in mice peroxynitrite inhibition significantly reduced MCMV viral load in different organs. Although further experiments are required to elucidate how peroxynitrite facilitates HCMV replication, data collected in Chapter 3 demonstrate a novel role of endogenous peroxynitrite in CMV replication and implies that peroxynitrite could be a potential antiviral target. Additionally, I conducted a genome-wide assessment of host factors and identified six novel genes as essential for HCMV infection. Out of the six genes, three encode proteins that are vital for Hippo signalling. Preliminary experiments in Chapter 4 demonstrate that inhibition of the Hippo pathway restricted the release of infectious viral progeny. Overall, my thesis identifies a number of potential pro-viral host factors that mediate HCMV replication. Further functional experiments are necessary to validate the role of these cellular factors and identify the mechanisms through which they support HCMV infection. Nonetheless, the data collected here highlight the potential of targeting host factors for the development of antivirals against HCMV infection.

References

1. Weir, J. P. Genomic organization and evolution of the human herpesviruses. *Virus Genes* **16**, 85–93 (1998).
2. Davison, A. J. *et al.* The order Herpesvirales. *Arch. Virol.* **154**, 171–177 (2009).
3. Lan, K. & Luo, M. H. Herpesviruses: epidemiology, pathogenesis, and interventions. *Virol. Sin.* **32**, 347–348 (2017).
4. Grinde, B. Herpesviruses: latency and reactivation - viral strategies and host response. *J. Oral Microbiol.* **1**, 1–9 (2013).
5. Liu, F. & Zhou, Z. H. Comparative virion structures of human herpesviruses. *Hum. Herpesviruses Biol. Ther. Immunoprophyl.* 27–43 (2007). doi:10.1017/CBO9780511545313.004
6. Gruffat, H. *et al.* Herpesvirus Late Gene Expression : A Viral-Specific Pre-initiation Complex Is Key. **7**, 1–15 (2016).
7. Poole, E. & Sinclair, J. Sleepless latency of human cytomegalovirus. *Med. Microbiol. Immunol.* **204**, 421–429 (2015).
8. McGeoch, D. J., Rixon, F. J. & Davison, A. J. Topics in herpesvirus genomics and evolution. *Virus Res.* **117**, 90–104 (2006).
9. Luczkowiak, J., Álvarez, M., Sebastián-Martín, A. & Menéndez-Arias, L. *DNA-dependent DNA polymerases as drug targets in herpesviruses and poxviruses*. *Viral Polymerases: Structures, Functions and Roles as Antiviral Drug Targets* (2018). doi:10.1016/B978-0-12-815422-9.00004-8
10. Martí-Carreras, J. & Maes, P. Human cytomegalovirus genomics and transcriptomics through the lens of next-generation sequencing: revision and future challenges. *Virus Genes* **55**, 138–164 (2019).
11. Sijmons, S., Van Ranst, M. & Maes, P. Genomic and functional characteristics of human cytomegalovirus revealed by next-generation sequencing. *Viruses* **6**, 1049–1072 (2014).
12. Patro, A. R. K. Subversion of immune response by human cytomegalovirus. *Front. Immunol.* **10**, 1–7 (2019).
13. Dolan, A. *et al.* Genetic content of wild-type human cytomegalovirus. *J. Gen.*

Virol. **85**, 1301–1312 (2004).

14. Van Damme, E. & Van Loock, M. Functional annotation of human cytomegalovirus gene products: An update. *Front. Microbiol.* **5**, 1–12 (2014).
15. Davison, A. J. *et al.* The human cytomegalovirus genome revisited: Comparison with the chimpanzee cytomegalovirus genome. *J. Gen. Virol.* **84**, 17–28 (2003).
16. Davison, A. J. & Bhella, D. Comparative genome and virion structure. in (eds. Arvin, A. et al.) (2007).
17. Crough, T. & Khanna, R. Immimobiology of human cytomegalovirus: From bench to bedside. *Clin. Microbiol. Rev.* **22**, 76–98 (2009).
18. Kalejta, R. F. Tegument Proteins of Human Cytomegalovirus. *Microbiol. Mol. Biol. Rev.* **72**, 249–265 (2008).
19. Varnum, S. M. *et al.* Identification of Proteins in Human Cytomegalovirus (HCMV) Particles: the HCMV Proteome †. *J. Virol.* **78**, 10960–10966 (2004).
20. Li, G. & Kamil, J. P. Viral Regulation of Cell Tropism in Human Cytomegalovirus. *J. Virol.* **90**, 626–629 (2016).
21. Nguyen, C. C. & Kamil, J. P. Pathogen at the Gates: Human Cytomegalovirus Entry and Cell Tropism. (2018). doi:10.3390/v10120704
22. Wu, K., Oberstein, A., Wang, W. & Shenk, T. Role of PDGF receptor-α during human cytomegalovirus entry into fibroblasts. *Proc. Natl. Acad. Sci. U. S. A.* **115**, E9889–E9898 (2018).
23. Wille, P. T., Knoche, A. J., Nelson, J. A., Jarvis, M. A. & Johnson, D. C. A Human Cytomegalovirus gO-Null Mutant Fails To Incorporate gH/gL into the Virion Envelope and Is Unable To Enter Fibroblasts and Epithelial and Endothelial Cells. *J. Virol.* **84**, 2585–2596 (2010).
24. Wang, D. & Shenk, T. Human Cytomegalovirus UL131 Open Reading Frame Is Required for Epithelial Cell Tropism. *J. Virol.* **79**, 10330–10338 (2005).
25. Adler, B. *et al.* Role of human cytomegalovirus UL131A in cell type-specific virus entry and release. *J. Gen. Virol.* **87**, 2451–2460 (2006).
26. Hahn, G. *et al.* Human Cytomegalovirus UL131-128 Genes Are Indispensable for Virus Growth in Endothelial Cells and Virus Transfer to Leukocytes. *J. Virol.*

78, 10023–10033 (2004).

27. Murrell, I. *et al.* The pentameric complex drives immunologically covert cell-cell transmission of wild-type human cytomegalovirus. *Proc. Natl. Acad. Sci. U. S. A.* **114**, 6104–6109 (2017).
28. Gerna, G., Kabanova, A. & Lilleri, D. Human cytomegalovirus cell tropism and host cell receptors. *Vaccines* **7**, 1–18 (2019).
29. Scrivano, L., Sinzger, C., Nitschko, H., Koszinowski, U. H. & Adler, B. HCMV spread and cell tropism are determined by distinct virus populations. *PLoS Pathog.* **7**, (2011).
30. Sinzger, C. *et al.* Fibroblasts, epithelial cells, endothelial cells and smooth muscle cells are major targets of human cytomegalovirus infection in lung and gastrointestinal tissues. *J. Gen. Virol.* **76**, 741–750 (1995).
31. Sinzger, C., Digel, M. & Jahn, G. Cytomegalovirus Cell Tropism. in *Human Cytomegalovirus* (eds. Shenk, T. E. & Stinski, M. F.) 63–83 (Springer Berlin Heidelberg, 2008). doi:10.1007/978-3-540-77349-8_4
32. Jackson, J. W. & Sparer, T. There is always another way! cytomegalovirus' multifaceted dissemination schemes. *Viruses* **10**, 1–14 (2018).
33. Taylor-Wiedeman, J., Sissons, J. G. P., Borysiewicz, L. K. & Sinclair, J. H. Monocytes are a major site of persistence of human cytomegalovirus in peripheral blood mononuclear cells. *J. Gen. Virol.* **72**, 2059–2064 (1991).
34. Smith, M. S., Bentz, G. L., Alexander, J. S. & Yurochko, A. D. Human Cytomegalovirus Induces Monocyte Differentiation and Migration as a Strategy for Dissemination and Persistence. *J. Virol.* **78**, 4444–4453 (2004).
35. Sinclair, J. & Reeves, M. The intimate relationship between human cytomegalovirus and the dendritic cell lineage. *Front. Microbiol.* **5**, 1–14 (2014).
36. Forte, E., Zhang, Z., Thorp, E. B. & Hummel, M. Cytomegalovirus Latency and Reactivation: An Intricate Interplay With the Host Immune Response. *Frontiers in Cellular and Infection Microbiology* **10**, 130 (2020).
37. Sacher, T. *et al.* The role of cell types in cytomegalovirus infection in vivo. *Eur. J. Cell Biol.* **91**, 70–77 (2012).

38. Bodaghi, B. *et al.* Entry of human cytomegalovirus into retinal pigment epithelial and endothelial cells by endocytosis. *Investig. Ophthalmol. Vis. Sci.* **40**, 2598–2607 (1999).

39. Compton, T. An immortalized human fibroblast cell line is permissive for human cytomegalovirus infection. *J. Virol.* **67**, 3644–3648 (1993).

40. Arcangeletti, M. C. *et al.* Human cytomegalovirus reactivation from latency: Validation of a 'switch' model in vitro Herpes viruses. *Virol. J.* **13**, 1–15 (2016).

41. Sinzger, C. *et al.* Hepatocytes are permissive for human cytomegalovirus infection in human liver cell culture and in vivo. *J. Infect. Dis.* **180**, 976–986 (1999).

42. Hargett, D. & Shenk, T. E. Experimental human cytomegalovirus latency in CD14+ monocytes. *Proc. Natl. Acad. Sci. U. S. A.* **107**, 20039–20044 (2010).

43. Lee, J.-H., Pasquarella, J. R. & Kalejta, R. F. Cell Line Models for Human Cytomegalovirus Latency Faithfully Mimic Viral Entry by Macropinocytosis and Endocytosis. *J. Virol.* **93**, 1–21 (2019).

44. Crawford, L. B., Diggins, N. L., Caposio, P. & Hancock, M. H. Advances in Model Systems for Human Cytomegalovirus Latency and Reactivation. *MBio* **13**, (2022).

45. Poole, E. *et al.* An iPSC-Derived Myeloid Lineage Model of Herpes Virus Latency and Reactivation. *Front. Microbiol.* **10**, 1–11 (2019).

46. Monkley, S. *et al.* Optimised generation of iPSC-derived macrophages and dendritic cells that are functionally and transcriptionally similar to their primary counterparts. *PLoS One* **15**, 1–17 (2020).

47. Kerkar, S. P. *et al.* Timing and intensity of exposure to interferon-γ critically determines the function of monocyte-derived dendritic cells. *Immunology* **143**, 96–108 (2014).

48. Miller, M. S. & Hertel, L. Onset of Human Cytomegalovirus Replication in Fibroblasts Requires the Presence of an Intact Vimentin Cytoskeleton. *J. Virol.* **83**, 7015–7028 (2009).

49. Lieber, D. *et al.* A permanently growing human endothelial cell line supports productive infection with human cytomegalovirus under conditional cell

growth arrest. *Biotechniques* **59**, 127–136 (2015).

50. Sinzger, C. *et al.* Modification of human cytomegalovirus tropism through propagation in vitro is associated with changes in the viral genome. *J. Gen. Virol.* **80**, 2867–2877 (1999).
51. Weiler, N. *et al.* Role of envelope glycoprotein complexes in cell-associated spread of human cytomegalovirus. *Viruses* **13**, 1–20 (2021).
52. Stanton, R. J. *et al.* Reconstruction of the complete human cytomegalovirus genome in a BAC reveals RL13 to be a potent inhibitor of replication. *J. Clin. Invest.* **120**, 3191–3208 (2010).
53. Murrell, I. Developing a human cytomegalovirus strain for better in vitro research. *PQDT - UK Irel.* (2014).
54. Murrell, I. *et al.* Impact of Sequence Variation in the UL128 Locus on Production of Human Cytomegalovirus in Fibroblast and Epithelial Cells. *J. Virol.* **87**, 10489–10500 (2013).
55. Frascaroli, G. & Sinzger, C. Distinct Properties of Human Cytomegalovirus Strains and the Appropriate Choice of Strains for Particular Studies. in *Human Cytomegaloviruses: Methods and Protocols* (eds. Yurochko, A. D. & Miller, W. E.) 29–46 (Humana Press, 2014). doi:10.1007/978-1-62703-788-4_3
56. Griffiths, P., Baraniak, I. & Reeves, M. The pathogenesis of human cytomegalovirus. *J. Pathol.* **235**, 288–297 (2015).
57. Griffiths, P. & Reeves, M. Pathogenesis of human cytomegalovirus in the immunocompromised host. *Nat. Rev. Microbiol.* **19**, 759–773 (2021).
58. Cannon, M. J., Hyde, T. B. & Schmid, D. S. Review of cytomegalovirus shedding in bodily fluids and relevance to congenital cytomegalovirus infection. *Rev. Med. Virol.* **21**, 240–255 (2011).
59. Pass, R. F. & Anderson, B. Mother-to-child transmission of cytomegalovirus and prevention of congenital infection. *J. Pediatric Infect. Dis. Soc.* **3**, 2–6 (2014).
60. Swanson, E. C. & Schleiss, M. R. Congenital Cytomegalovirus Infection. New Prospects for Prevention and Therapy. *Pediatr. Clin. North Am.* **60**, 335–349 (2013).

61. Naing, Z. W. *et al.* Congenital cytomegalovirus infection in pregnancy: A review of prevalence, clinical features, diagnosis and prevention. *Aust. New Zeal. J. Obstet. Gynaecol.* **56**, 9–18 (2016).

62. Springer, K. L. & Weinberg, A. Cytomegalovirus infection in the era of HAART: Fewer reactivations and more immunity. *J. Antimicrob. Chemother.* **54**, 582–586 (2004).

63. Shafer, R. W. & Vuitton, D. A. Highly active antiretroviral therapy (Haart) for the treatment of infection with human immunodeficiency virus type 1. *Biomed. Pharmacother.* **53**, 73–86 (1999).

64. Stern, L. *et al.* Human Cytomegalovirus Latency and Reactivation in Allogeneic Hematopoietic Stem Cell Transplant Recipients. *Front. Microbiol.* **10**, (2019).

65. Boeckh, M. & Nichols, W. G. The impact of cytomegalovirus serostatus of donor and recipient before hematopoietic stem cell transplantation in the era of antiviral prophylaxis and preemptive therapy. *Blood* **103**, 2003–2008 (2004).

66. Houldcroft, C. J. *et al.* Assessing Anti-HCMV Cell Mediated Immune Responses in Transplant Recipients and Healthy Controls Using a Novel Functional Assay. *Front. Cell. Infect. Microbiol.* **10**, 1–21 (2020).

67. Azevedo, L. S. *et al.* Cytomegalovirus infection in transplant recipients. *Clinics* **70**, 515–523 (2015).

68. Sijmons, S. *et al.* High-Throughput Analysis of Human Cytomegalovirus Genome Diversity Highlights the Widespread Occurrence of Gene-Disrupting Mutations and Pervasive Recombination. *J. Virol.* **89**, 7673–7695 (2015).

69. Prichard, M. N., Penfold, M. E. T., Duke, G. M., Spaete, R. R. & Kemble, G. W. A review of genetic differences between limited and extensively passaged human cytomegalovirus strains. *Rev. Med. Virol.* **11**, 191–200 (2001).

70. Bradley, A. J. *et al.* High-throughput sequence analysis of variants of human cytomegalovirus strains Towne and AD169. *J. Gen. Virol.* **90**, 2375–2380 (2009).

71. Gerna, G., Percivalle, E., Sarasini, A., Baldanti, F. & Revello, M. G. The attenuated Towne strain of human cytomegalovirus may revert to both

endothelial cell tropism and leuko- (neutrophil- and monocyte-) tropism in vitro. *J. Gen. Virol.* **83**, 1993–2000 (2002).

72. Al Qaffas, A. *et al.* Genome sequences of human cytomegalovirus strain TB40/E variants propagated in fibroblasts and epithelial cells. *Virol. J.* **18**, 1–5 (2021).
73. Murrell, I. *et al.* Genetic Stability of Bacterial Artificial Chromosome-Derived Human Cytomegalovirus during Culture *In Vitro*. *J. Virol.* **90**, 3929–3943 (2016).
74. Wilkinson, G. W. G. *et al.* Human cytomegalovirus: taking the strain. *Med. Microbiol. Immunol.* **204**, 273–284 (2015).
75. Wang, Y. Q. & Zhao, X. Y. Human Cytomegalovirus Primary Infection and Reactivation: Insights From Virion-Carried Molecules. *Frontiers in Microbiology* **11**, (2020).
76. Ye, L. *et al.* Functional Profile of Human Cytomegalovirus Genes and Their Associated Diseases: A Review. *Front. Microbiol.* **11**, 1–13 (2020).
77. Weekes, M. P. *et al.* Quantitative temporal viromics: An approach to investigate host-pathogen interaction. *Cell* **157**, 1460–1472 (2014).
78. J Heath, J. & D Grant, M. The Immune Response Against Human Cytomegalovirus Links Cellular to Systemic Senescence. *Cells* **9**, (2020).
79. Song, B. H., Lee, G. C., Moon, M. S., Cho, Y. H. & Lee, C. H. Human cytomegalovirus binding to heparan sulfate proteoglycans on the cell surface and/or entry stimulates the expression of human leukocyte antigen class I. *J. Gen. Virol.* **82**, 2405–2413 (2001).
80. Baldwin, J. *et al.* A Role for 3- O -Sulfated Heparan Sulfate in Promoting Human Cytomegalovirus Infection in Human Iris Cells . *J. Virol.* **89**, 5185–5192 (2015).
81. Tang, J., Frascaroli, G., Lebbink, R. J., Ostermann, E. & Brune, W. Human cytomegalovirus glycoprotein B variants affect viral entry, cell fusion, and genome stability. *Proc. Natl. Acad. Sci. U. S. A.* **116**, 18021–18030 (2019).
82. Fulkerson, H. L. *et al.* HCMV-induced signaling through gB-EGFR engagement is required for viral trafficking and nuclear translocation in primary human

monocytes. *Proc. Natl. Acad. Sci. U. S. A.* **117**, 19507–19516 (2020).

83. Wang, X., Huong, S. M., Chiu, M. L., Raab-Traub, N. & Huang, E. S. Epidermal growth factor receptor is a cellular receptor for human cytomegalovirus. *Nature* **424**, 456–461 (2003).
84. Stegmann, C., Rothemund, F., Laib Sampaio, K., Adler, B. & Sinzger, C. The N Terminus of Human Cytomegalovirus Glycoprotein O Is Important for Binding to the Cellular Receptor PDGFRα. *J. Virol.* **93**, 1–16 (2019).
85. Paradowska, E. *et al.* Distribution of the CMV glycoprotein gH/gL/gO and gH/gL/pUL128/pUL130/pUL131A complex variants and associated clinical manifestations in infants infected congenitally or postnatally. *Sci. Rep.* **9**, 1–15 (2019).
86. Liu, J., Jardetzky, T. S., Chin, A. L., Johnson, D. C. & Vanarsdall, A. L. The Human Cytomegalovirus Trimer and Pentamer Promote Sequential Steps in Entry into Epithelial and Endothelial Cells at Cell Surfaces and Endosomes. *J. Virol.* **92**, 1–15 (2018).
87. Soroceanu, L., Akhavan, A. & Cobbs, C. S. Platelet-derived growth factor-α receptor activation is required for human cytomegalovirus infection. *Nature* **455**, 391–395 (2008).
88. Kabanova, A. *et al.* Platelet-derived growth factor-α receptor is the cellular receptor for human cytomegalovirus gHgLgO trimer. *Nat. Microbiol.* **1**, 1–8 (2016).
89. Martinez-Martin, N. *et al.* An Unbiased Screen for Human Cytomegalovirus Identifies Neuropilin-2 as a Central Viral Receptor. *Cell* **174**, 1158-1171.e19 (2018).
90. Vanarsdall, A. L. *et al.* CD147 Promotes Entry of Pentamer-Expressing Human Cytomegalovirus into Epithelial and Endothelial Cells. *MBio* **9**, (2018).
91. Stein, K. R. *et al.* CD46 facilitates entry and dissemination of human cytomegalovirus. *Nat. Commun.* **10**, 2699 (2019).
92. Xiaofei, E. *et al.* OR14I1 is a receptor for the human cytomegalovirus pentameric complex and defines viral epithelial cell tropism. *Proc. Natl. Acad. Sci. U. S. A.* **116**, 7043–7052 (2019).

93. Paul, J. & Iii, T. Human cytomegalovirus tegument proteins Human cytomegalovirus tegument proteins. *Virol. J.* **9**, 22 (2012).

94. Mohammad, A.-A. Human Cytomegalovirus: From Novel Strain, miRNAs to Interplay with Breast Cancer. (2017).

95. Meier, J. L. & Pruessner, J. A. The human cytomegalovirus major immediate-early distal enhancer region is required for efficient viral replication and immediate-early gene expression. *J. Virol.* **74**, 1602–1613 (2000).

96. Technology, D. N. A. L. crossm Real-Time Visualization and Quantification of Human Cytomegalovirus Replication in Living Cells Using the ANCHOR.

97. Ruiz-Masó, J. A. *et al.* Plasmid Rolling-Circle Replication. *Microbiol. Spectr.* **3**, 3.1.16 (2015).

98. Xu, Y., Cei, S. A., Rodriguez Huete, A., Colletti, K. S. & Pari, G. S. Human Cytomegalovirus DNA Replication Requires Transcriptional Activation via an IE2- and UL84-Responsive Bidirectional Promoter Element within ori Lyt . *J. Virol.* **78**, 11664–11677 (2004).

99. Borst, E.-M. & Messerle, M. Analysis of Human Cytomegalovirus ori Lyt Sequence Requirements in the Context of the Viral Genome . *J. Virol.* **79**, 3615–3626 (2005).

100. Smith, J. A. & Pari, G. S. Human cytomegalovirus UL102 gene. *J. Virol.* **69**, 1734–1740 (1995).

101. Smith, J. A., Jairath, S., Crute, J. J. & Pari, G. S. Characterization of the human cytomegalovirus UL105 gene and identification of the putative helicase protein. *Virology* **220**, 251–255 (1996).

102. Ertl, P. F., Thomas, M. S. & Powell, K. L. High level expression of DNA polymerases from herpesviruses. *J. Gen. Virol.* **72**, 1729–1734 (1991).

103. Ertl, P. F. & Powell, K. L. Physical and functional interaction of human cytomegalovirus DNA polymerase and its accessory protein (ICP36) expressed in insect cells. *J. Virol.* **66**, 4126–4133 (1992).

104. Isomura, H. *et al.* The Human Cytomegalovirus Gene Products Essential for Late Viral Gene Expression Assemble into Prereplication Complexes before Viral DNA Replication. *J. Virol.* **85**, 6629–6644 (2011).

105. Reynolds, A. E. *et al.* U L 31 and U L 34 Proteins of Herpes Simplex Virus Type 1 Form a Complex That Accumulates at the Nuclear Rim and Is Required for Envelopment of Nucleocapsids . *J. Virol.* **75**, 8803–8817 (2001).

106. Fuchs, W., Klupp, B. G., Granzow, H., Osterrieder, N. & Mettenleiter, T. C. The interacting UL31 and UL34 gene products of pseudorabies virus are involved in egress from the host-cell nucleus and represent components of primary enveloped but not mature virions. *J. Virol.* **76**, 364–378 (2002).

107. Scholl, B. C. *et al.* Prokaryotic expression of immunogenic polypeptides of the large phosphoprotein (pp150) of human cytomegalovirus. *J. Gen. Virol.* **69**, 1195–1204 (1988).

108. Sanchez, V., Greis, K. D., Sztul, E. & Britt, W. J. Accumulation of Virion Tegument and Envelope Proteins in a Stable Cytoplasmic Compartment during Human Cytomegalovirus Replication: Characterization of a Potential Site of Virus Assembly. *J. Virol.* **74**, 975–986 (2000).

109. Sanchez, V., Mahr, J. A., Orazio, N. I. & Spector, D. H. Nuclear Export of the Human Cytomegalovirus Tegument Protein pp65 Requires Cyclin-Dependent Kinase Activity and the Crm1 Exporter. *J. Virol.* **81**, 11730–11736 (2007).

110. Das, S., Ortiz, D. A., Gurczynski, S. J., Khan, F. & Pellett, P. E. Identification of Human Cytomegalovirus Genes Important for Biogenesis of the Cytoplasmic Virion Assembly Complex. *J. Virol.* **88**, 9086–9099 (2014).

111. Azzeh, M., Honigman, A., Taraboulos, A., Rouvinski, A. & Wolf, D. G. Structural changes in human cytomegalovirus cytoplasmic assembly sites in the absence of UL97 kinase activity. *Virology* **354**, 69–79 (2006).

112. Lee, C. H. & Grey, F. Systems Virology and Human Cytomegalovirus: Using High Throughput Approaches to Identify Novel Host-Virus Interactions During Lytic Infection. *Front. Cell. Infect. Microbiol.* **10**, 1–15 (2020).

113. Nightingale, K. *et al.* High-Definition Analysis of Host Protein Stability during Human Cytomegalovirus Infection Reveals Antiviral Factors and Viral Evasion Mechanisms. *Cell Host Microbe* **24**, 447-460.e11 (2018).

114. Beltran, P. M. J. & Cristea, I. M. The lifecycle and pathogenesis of human cytomegalovirus infection: lessons from proteomics. *Expert Rev Proteomics*

11, 697–711 (2015).

115. Elder, E. & Sinclair, J. HCMV latency: what regulates the regulators? *Med. Microbiol. Immunol.* **208**, 431–438 (2019).
116. Reeves, M. & Sinclair, J. Regulation of human cytomegalovirus transcription in latency: Beyond the major immediate-early promoter. *Viruses* **5**, 1395–1413 (2013).
117. Human, L. E. *et al.* crossm Cytomegalovirus US28 Attenuates Cell Infection. **8**, 1–21 (2017).
118. Murphy, J. C., Fischle, W., Verdin, E. & Sinclair, J. H. Control of cytomegalovirus lytic gene expression by histone acetylation. *EMBO J.* **21**, 1112–1120 (2002).
119. Poole, E. *et al.* Latency-Associated Viral Interleukin-10 (IL-10) Encoded by Human Cytomegalovirus Modulates Cellular IL-10 and CCL8 Secretion during Latent Infection through Changes in the Cellular MicroRNA hsa-miR-92a. *J. Virol.* **88**, 13947–13955 (2014).
120. Poole, E., Neves, T. C., Oliveira, M. T., Sinclair, J. & da Silva, M. C. C. Human Cytomegalovirus Interleukin 10 Homologs: Facing the Immune System. *Front. Cell. Infect. Microbiol.* **10**, 1–14 (2020).
121. O'Connor, C. M., Nukui, M., Gurova, K. V. & Murphy, E. A. Inhibition of the Facilitates Chromatin Transcription (FACT) complex reduces transcription from the HCMV MIEP in models of lytic and latent replication. *J. Virol.* **90**, JVI.02501-15 (2016).
122. Nevels, M., Paulus, C. & Shenk, T. Human cytomegalovirus immediate-early 1 protein facilitates viral replication by antagonizing histone deacetylation. *Proc. Natl. Acad. Sci. U. S. A.* **101**, 17234–17239 (2004).
123. Kim, S. J. *et al.* Renal ischemia/reperfusion injury activates the enhancer domain of the human cytomegalovirus major immediate early promoter. *Am. J. Transplant.* **5**, 1606–1613 (2005).
124. Rosa, C. La & Diamond, D. J. The immune response to human CMV. *Futur. Virol* **7**, 279–293 (2012).
125. Rossini, G. *et al.* Interplay between Human Cytomegalovirus and

Intrinsic/Innate Host Responses: A Complex Bidirectional Relationship. *Mediators Inflamm.* **2012**, 1–16 (2012).

126. SPEIR, E. Cytomegalovirus gene regulation by reactive oxygen species. Agents in atherosclerosis. *Ann. N. Y. Acad. Sci.* **899**, 363–374 (2000).
127. Weis, M. *et al.* Cytomegalovirus Infection Impairs the Nitric Oxide Synthase Pathway: Role of Asymmetric Dimethylarginine in Transplant Arteriosclerosis. *Circulation* **109**, 500–505 (2004).
128. Schwarz, K. B. Oxidative stress during viral infection: A review. *Free Radic. Biol. Med.* **21**, 641–649 (1996).
129. Medzhitov, R. Recognition of microorganisms and activation of the immune response. *Nature* **449**, 819–826 (2007).
130. Kim, J. E., Kim, Y. E., Stinski, M. F., Ahn, J. H. & Song, Y. J. Human cytomegalovirus IE2 86 kDa protein induces STING degradation and inhibits cGAMP-mediated IFN-β induction. *Front. Microbiol.* **8**, 1–14 (2017).
131. Zhong, B. *et al.* The adaptor protein MITA links virus-sensing receptors to IRF3 transcription factor activation. *Immunity* **29**, 538–550 (2008).
132. Forrest, C., Gomes, A., Reeves, M. & Male, V. NK cell memory to cytomegalovirus: Implications for vaccine development. *Vaccines* **8**, 1–19 (2020).
133. Picarda, G. & Benedict, C. A. Cytomegalovirus: Shape-Shifting the Immune System. *J. Immunol.* **200**, 3881–3889 (2018).
134. Gabor, F., Jahn, G., Sedmak, D. D. & Sinzger, C. In vivo Downregulation of MHC Class I Molecules by HCMV Occurs During All Phases of Viral Replication but Is Not Always Complete. *Front. Cell. Infect. Microbiol.* **10**, 1–13 (2020).
135. Wang, E. C. Y. *et al.* Suppression of costimulation by human cytomegalovirus promotes evasion of cellular immune defenses. *Proc. Natl. Acad. Sci. U. S. A.* **115**, 4998–5003 (2018).
136. Vlahava, V. M. *et al.* Monoclonal antibodies targeting nonstructural viral antigens can activate ADCC against human cytomegalovirus. *J. Clin. Invest.* **131**, 1–15 (2021).
137. Bieniasz, P. D. Intrinsic immunity: A front-line defense against viral attack.

Nat. Immunol. **5**, 1109–1115 (2004).

138. Dell'Oste, V. *et al.* Tuning the Orchestra: HCMV vs. Innate Immunity. *Front. Microbiol.* **11**, 1–20 (2020).
139. Baasch, S., Ruzsics, Z. & Henneke, P. Cytomegaloviruses and Macrophages—Friends and Foes From Early on? *Front. Immunol.* **11**, (2020).
140. Thomas, D. C. The phagocyte respiratory burst: Historical perspectives and recent advances. *Immunol. Lett.* **192**, 88–96 (2017).
141. Iles, K. E. & Forman, H. J. Macrophage signaling and respiratory burst. *Immunol. Res.* **26**, 95–105 (2002).
142. Frascaroli, G. *et al.* Human macrophages escape inhibition of major histocompatibility complex-dependent antigen presentation by cytomegalovirus and drive proliferation and activation of memory CD4+ and CD8+ T cells. *Front. Immunol.* **9**, (2018).
143. Gredmark-Russ, S. & Söderberg-Nauclér, C. Dendritic cell biology in human cytomegalovirus infection and the clinical consequences for host immunity and pathology. *Virulence* **3**, 621–634 (2012).
144. Schraml, B. U. & Reis e Sousa, C. Defining dendritic cells. *Curr. Opin. Immunol.* **32**, 13–20 (2015).
145. Geijtenbeek, T. B. H. *et al.* Identification of DC-SIGN, a novel dendritic cell-specific ICAM-3 receptor that supports primary immune responses. *Cell* **100**, 575–585 (2000).
146. Avdic, S. *et al.* Human IL-10 in Monocytes. **90**, 3819–3827 (2016).
147. Pourgheysari, B. *et al.* The Cytomegalovirus-Specific CD4 + T-Cell Response Expands with Age and Markedly Alters the CD4 + T-Cell Repertoire . *J. Virol.* **81**, 7759–7765 (2007).
148. Sylwester, A. W. *et al.* Broadly targeted human cytomegalovirus-specific CD4+ and CD8+ T cells dominate the memory compartments of exposed subjects. *J. Exp. Med.* **202**, 673–685 (2005).
149. Lim, E. Y., Jackson, S. E. & Wills, M. R. The CD4+ T Cell Response to Human Cytomegalovirus in Healthy and Immunocompromised People. *Front. Cell. Infect. Microbiol.* **10**, (2020).

150. Terrazzini, N. & Kern, F. Cell-mediated immunity to human CMV infection: a brief overview. *F1000Prime Rep.* **6**, 28 (2014).

151. Klenerman, P. The (gradual) rise of memory inflation. *Immunol. Rev.* **283**, 99–112 (2018).

152. Kim, J., Kim, A.-R. & Shin, E.-C. Cytomegalovirus Infection and Memory T Cell Inflation. *Immune Netw.* **15**, 186–90 (2015).

153. Dna, E. T., Ampure, E. & Coulter, B. Broad GPP.

154. Weber, B., Braun, W., Cinatl, J. & Doerr, H. W. Humoral immune response to human cytomegalovirus infection: diagnostic potential of immunoglobulin class and IgG subclass antibody response to human cytomegalovirus early and late antigens. *Clin. Investig.* **71**, 270–276 (1993).

155. Revello, M. G., Fornara, C., Arossa, A., Zelini, P. & Lilleri, D. Role of human cytomegalovirus (HCMV)-specific antibody in HCMV-infected pregnant women. *Early Hum. Dev.* **90**, S32–S34 (2014).

156. Sandonís, V., García-Ríos, E., McConnell, M. J. & Pérez-Romero, P. Role of Neutralizing Antibodies in CMV Infection: Implications for New Therapeutic Approaches. *Trends Microbiol.* **28**, 900–912 (2020).

157. Shibamura, M. *et al.* Association of human cytomegalovirus (HCMV) neutralizing antibodies with antibodies to the HCMV glycoprotein complexes. *Virol. J.* **17**, 1–10 (2020).

158. Nelson, C. S. *et al.* Preexisting antibodies can protect against congenital cytomegalovirus infection in monkeys. *JCI insight* **2**, (2017).

159. Klimpel, G. R. Immune Defenses. in *Medical Microbiology 4th. 4th Edition.* (1996).

160. Kabanova, A. *et al.* Antibody-driven design of a human cytomegalovirus gHgLpUL128L subunit vaccine that selectively elicits potent neutralizing antibodies. *Proc. Natl. Acad. Sci. U. S. A.* **111**, 17965–17970 (2014).

161. Jenks, J. A., Goodwin, M. L. & Permar, S. R. The roles of host and viral antibody fc receptors in herpes simplex virus (HSV) and human cytomegalovirus (HCMV) infections and immunity. *Front. Immunol.* **10**, (2019).

162. Manandhar, T., Hò, G. G. T., Pump, W. C., Blasczyk, R. & Bade-Doeding, C.

Battle between host immune cellular responses and hcmv immune evasion. *Int. J. Mol. Sci.* **20**, (2019).

163. Goodwin, C. M., Ciesla, J. H. & Munger, J. Who's driving? Human cytomegalovirus, interferon, and NFκB signaling. *Viruses* **10**, (2018).
164. Park, A. *et al.* HCMV-encoded US7 and US8 act as antagonists of innate immunity by distinctively targeting TLR-signaling pathways. *Nat. Commun.* **10**, 1–15 (2019).
165. Eaglesham, J. B. & Kranzusch, P. J. Conserved strategies for pathogen evasion of cGAS–STING immunity. (2020).
166. Lee, J., Koh, K., Kim, Y. E., Ahn, J. H. & Kim, S. Upregulation of Nrf2 expression by human cytomegalovirus infection protects host cells from oxidative stress. *J. Gen. Virol.* **94**, 1658–1668 (2013).
167. Tilton, C., Clippinger, A. J., Maguire, T. & Alwine, J. C. Human cytomegalovirus induces multiple means to combat reactive oxygen species. *J. Virol.* **85**, 12585–93 (2011).
168. Sandhu, P. K. & Buchkovich, N. J. Human Cytomegalovirus Decreases Major Histocompatibility Complex Class II by Regulating Class II Transactivator Transcript Levels in a Myeloid Cell Line. *J. Virol.* **94**, 1–19 (2020).
169. Furman, M. H., Dey, N., Tortorella, D. & Ploegh, H. L. The Human Cytomegalovirus US10 Gene Product Delays Trafficking of Major Histocompatibility Complex Class I Molecules. *J. Virol.* **76**, 11753–11756 (2002).
170. Patel, M. *et al.* HCMV-encoded NK modulators: Lessons from in vitro and in vivo genetic variation. *Front. Immunol.* **9**, 1–8 (2018).
171. Wilkinson, G. W. G. *et al.* Modulation of natural killer cells by human cytomegalovirus. **41**, 206–212 (2010).
172. Fielding, C. A. *et al.* Two Novel Human Cytomegalovirus NK Cell Evasion Functions Target MICA for Lysosomal Degradation. *PLoS Pathog.* **10**, (2014).
173. Rölle, A. *et al.* Effects of Human Cytomegalovirus Infection on Ligands for the Activating NKG2D Receptor of NK Cells: Up-Regulation of UL16-Binding Protein (ULBP)1 and ULBP2 Is Counteracted by the Viral UL16 Protein. *J.*

Immunol. **171**, 902–908 (2003).

174. Fernández-Messina, L., Reyburn, H. T. & Valés-Gómez, M. Human NKG2D-ligands: Cell biology strategies to ensure immune recognition. *Front. Immunol.* **3**, 1–9 (2012).
175. Fielding, C. A. *et al.* Control of immune ligands by members of a cytomegalovirus gene expansion suppresses natural killer cell activation. *Elife* **6**, 1–27 (2017).
176. Tomasec, P. *et al.* Downregulation of natural killer cell-activating ligang CD155 by human cytomegalovirus UL141. *Nat. Immunol.* **6**, 181–188 (2005).
177. Prod'homme, V. *et al.* Human Cytomegalovirus UL40 Signal Peptide Regulates Cell Surface Expression of the NK Cell Ligands HLA-E and gpUL18. *J. Immunol.* **188**, 2794–2804 (2012).
178. Ameres, S., Besold, K., Plachter, B. & Moosmann, A. CD8 T Cell–Evasive Functions of Human Cytomegalovirus Display Pervasive MHC Allele Specificity, Complementarity, and Cooperativity. *J. Immunol.* **192**, 5894–5905 (2014).
179. Kim, S. *et al.* Human cytomegalovirus microRNA miR-US4-1 inhibits CD8(+) T cell responses by targeting the aminopeptidase ERAP1. *Nat. Immunol.* **12**, 984–991 (2011).
180. Scarpini, S. *et al.* Development of a vaccine against human cytomegalovirus: Advances, barriers, and implications for the clinical practice. *Vaccines* **9**, 1–26 (2021).
181. Boeckh, M., Murphy, W. J. & Peggs, K. S. Recent Advances in Cytomegalovirus: An Update on Pharmacologic and Cellular Therapies. *Biol. Blood Marrow Transplant.* **21**, 24–29 (2015).
182. Krishna, B. A., Wills, M. R. & Sinclair, J. H. Advances in the treatment of cytomegalovirus. *Br. Med. Bull.* **131**, 5–17 (2019).
183. Griffiths, P. New vaccines and antiviral drugs for cytomegalovirus. *J. Clin. Virol.* **116**, 58–61 (2019).
184. Tan, B. H. Cytomegalovirus Treatment. *Curr. Treat. options Infect. Dis.* **6**, 256–270 (2014).

185. Kapoor, A. *et al.* Validation and Characterization of Five Distinct Novel Inhibitors of Human Cytomegalovirus. *J. Med. Chem.* **63**, 3896–3907 (2020).

186. Gerna, G., Lilleri, D. & Baldanti, F. An overview of letermovir: a cytomegalovirus prophylactic option. *Expert Opin. Pharmacother.* **20**, 1429–1438 (2019).

187. Kachaeva, M. V. *et al.* In vitro activity of novel derivatives of 1,3-oxazole-4-carboxylate and 1,3-oxazole-4-carbonitrile against human cytomegalovirus. *Med. Chem. Res.* **28**, 1205–1211 (2019).

188. Gugliesi, F. *et al.* Where do we stand after decades of studying human cytomegalovirus? *Microorganisms* **8**, 1–30 (2020).

189. Piret, J. & Boivin, G. Clinical development of letermovir and maribavir: Overview of human cytomegalovirus drug resistance. *Antiviral Res.* **163**, 91–105 (2019).

190. Maertens, J. *et al.* Maribavir for Preemptive Treatment of Cytomegalovirus Reactivation. *N. Engl. J. Med.* **381**, 1136–1147 (2019).

191. Meyers, J. D. Prevention and treatment of cytomegalovirus infection. [Review]. *Annu. Rev. Med.* **42**, 179–187 (1991).

192. Prichard, M. N. & Kern, E. R. The search for new therapies for human cytomegalovirus infections. *Virus Res.* **157**, 212–221 (2011).

193. Hussein, I. T. M., Brooks, J. & Bowlin, T. L. The discovery and development of filociclovir for the prevention and treatment of human cytomegalovirus-related disease. *Antiviral Res.* **176**, 104710 (2020).

194. Venton, G. *et al.* Risk factors of Ganciclovir-related neutropenia after allogeneic stem cell transplantation: a retrospective monocentre study on 547 patients. *Clin. Microbiol. Infect. Off. Publ. Eur. Soc. Clin. Microbiol. Infect. Dis.* **20**, 160–166 (2014).

195. Goldfarb, D. S. & Coe, F. L. Foscarnet crystal deposition and renal failure. *American journal of kidney diseases : the official journal of the National Kidney Foundation* **32**, 519–520 (1998).

196. Chen, S. J., Wang, S. C. & Chen, Y. C. Antiviral agents as therapeutic strategies against cytomegalovirus infections. *Viruses* **12**, 1–11 (2019).

197. Lin, A. *et al.* Letermovir for primary and secondary cytomegalovirus prevention in allogeneic hematopoietic cell transplant recipients: Real-world experience. *Transpl. Infect. Dis.* **21**, 1–6 (2019).

198. Komatsu, T. E., Pikis, A., Naeger, L. K. & Harrington, P. R. Resistance of human cytomegalovirus to ganciclovir/valganciclovir: A comprehensive review of putative resistance pathways. *Antiviral Res.* **101**, 12–25 (2014).

199. Lurain, N. S. & Chou, S. Antiviral drug resistance of human cytomegalovirus. *Clinical Microbiology Reviews* (2010). doi:10.1128/CMR.00009-10

200. Hanley, P. J. & Bollard, C. M. Controlling cytomegalovirus: Helping the immune system take the lead. *Viruses* **6**, 2242–2258 (2014).

201. Acquaye-seedah, E., Frye, Z. P. & Maynard, J. a. Immunotherapeutic Approaches To Prevent Cytomegalovirus- Mediated Disease. *Microbiol. Spectr.* **1957**, 1–14 (2013).

202. Kaeuferle, T., Krauss, R., Blaeschke, F., Willier, S. & Feuchtinger, T. Strategies of adoptive T -cell transfer to treat refractory viral infections post allogeneic stem cell transplantation. *J. Hematol. Oncol.* **12**, 1–10 (2019).

203. Maleki, A., Russo, G., Parasiliti Palumbo, G. A. & Pappalardo, F. In silico design of recombinant multi-epitope vaccine against influenza A virus. *BMC Bioinformatics* **22**, 1–18 (2021).

204. Barbier, A. J., Jiang, A. Y., Zhang, P., Wooster, R. & Anderson, D. G. The clinical progress of mRNA vaccines and immunotherapies. *Nat. Biotechnol.* (2022). doi:10.1038/S41587-022-01294-2

205. Turner, J. S. *et al.* SARS-CoV-2 mRNA vaccines induce persistent human germinal centre responses. *Nature* **596**, 109–113 (2021).

206. Corbett, K. S. *et al.* SARS-CoV-2 mRNA vaccine design enabled by prototype pathogen preparedness. *Nature* **586**, 567–571 (2020).

207. Poglitsch, M. *et al.* CMV late phase-induced mTOR activation is essential for efficient virus replication in polarized human macrophages. *Am. J. Transplant.* **12**, 1458–1468 (2012).

208. Moorman, N. J. & Shenk, T. Rapamycin-Resistant mTORC1 Kinase Activity Is Required for Herpesvirus Replication. *J. Virol.* **84**, 5260–5269 (2010).

209. Radi, R. Oxygen radicals, nitric oxide, and peroxynitrite: Redox pathways in molecular medicine. *Proc. Natl. Acad. Sci. U. S. A.* **115**, 5839–5848 (2018).

210. Gutierrez, J., Ballinger, S. W., Darley-Usmar, V. M. & Landar, A. Free radicals, mitochondria, and oxidized lipids: The emerging role in signal transduction in vascular cells. *Circ. Res.* **99**, 924–932 (2006).

211. Nathan, C. & Cunningham-Bussel, A. Beyond oxidative stress: an immunologist's guide to reactive oxygen species. *Nat. Rev. | Immunol.* **13**, 349 (2013).

212. Li, Y. R. & Trush, M. Defining ROS in Biology and Medicine. *React. Oxyg. Species* **1**, 9–21 (2016).

213. Sies, H. & Jones, D. P. Reactive oxygen species (ROS) as pleiotropic physiological signalling agents. *Nat. Rev. Mol. Cell Biol.* **21**, 363–383 (2020).

214. Di Meo, S., Reed, T. T., Venditti, P. & Victor, V. M. Role of ROS and RNS Sources in Physiological and Pathological Conditions. *Oxid. Med. Cell. Longev.* **2016**, 1–44 (2016).

215. Ray, P. D., Huang, B.-W. & Tsuji, Y. Reactive oxygen species (ROS) homeostasis and redox regulation in cellular signaling. *Cell. Signal.* **24**, 981–990 (2012).

216. Nathan, C. & Cunningham-Bussel, A. Beyond oxidative stress: An immunologist's guide to reactive oxygen species. *Nat. Rev. Immunol.* **13**, 349–361 (2013).

217. Pacher, P., Beckman, J. S. & Liaudet, L. Nitric oxide and peroxynitrite in health and disease. *Physiol. Rev.* **87**, 315–424 (2007).

218. Laher, I. *Systems biology of free radicals and antioxidants*. *Systems Biology of Free Radicals and Antioxidants* **9783642300**, (2014).

219. Sies, H. & Jones, D. P. Reactive oxygen species (ROS) as pleiotropic physiological signalling agents. *Nat. Rev. Mol. Cell Biol.* **21**, 363–383 (2020).

220. Moldogazieva, N. T., Mokhosoev, I. M., Feldman, N. B. & Lutsenko, S. V. ROS and RNS signalling: adaptive redox switches through oxidative/nitrosative protein modifications. *Free Radic. Res.* **52**, 507–543 (2018).

221. Müllebner, A., Dorighello, G. G., Kozlov, A. V. & Duvigneau, J. C. Interaction between mitochondrial reactive oxygen species, heme oxygenase, and nitric

oxide synthase stimulates phagocytosis in macrophages. *Front. Med.* **4**, 1–10 (2017).

222. Daiber, A. *et al.* Regulation of vascular function and inflammation via cross talk of reactive oxygen and nitrogen species from mitochondria or nadph oxidase—implications for diabetes progression. *Int. J. Mol. Sci.* **21**, 1–30 (2020).
223. Dikalov, S. Cross talk between mitochondria and NADPH oxidases. *Free Radic. Biol. Med.* **51**, 1289–1301 (2011).
224. Zhao, R. Z., Jiang, S., Zhang, L. & Yu, Z. Bin. Mitochondrial electron transport chain, ROS generation and uncoupling (Review). *Int. J. Mol. Med.* **44**, 3–15 (2019).
225. Nolfi-Donegan, D., Braganza, A. & Shiva, S. Mitochondrial electron transport chain: Oxidative phosphorylation, oxidant production, and methods of measurement. *Redox Biol.* **37**, 101674 (2020).
226. Bedard, K. & Krause, K.-H. The NOX family of ROS-generating NADPH oxidases: physiology and pathophysiology. *Physiol. Rev.* **87**, 245–313 (2007).
227. Panday, A., Sahoo, M. K., Osorio, D. & Batra, S. NADPH oxidases: An overview from structure to innate immunity-associated pathologies. *Cell. Mol. Immunol.* **12**, 5–23 (2015).
228. Sumimoto, H. Structure, regulation and evolution of Nox-family NADPH oxidases that produce reactive oxygen species. *FEBS J.* **275**, 3249–3277 (2008).
229. Parascandolo, A. & Laukkanen, M. O. Carcinogenesis and Reactive Oxygen Species Signaling: Interaction of the NADPH Oxidase NOX1-5 and Superoxide Dismutase 1-3 Signal Transduction Pathways. *Antioxid. Redox Signal.* **30**, 443–486 (2019).
230. Thomas, D. C. *et al.* Eros is a novel transmembrane protein that controls the phagocyte respiratory burst and is essential for innate immunity. *J. Exp. Med.* **214**, 1111–1128 (2017).
231. O'Neill, S., Brault, J., Stasia, M.-J. & Knaus, U. G. Genetic disorders coupled to ROS deficiency. *Redox Biol.* **6**, 135–156 (2015).

232. Thomas, D. C. *et al.* EROS/CYBC1 mutations: Decreased NADPH oxidase function and chronic granulomatous disease. *The Journal of allergy and clinical immunology* **143**, 782-785.e1 (2019).

233. Arnadottir, G. A. *et al.* A homozygous loss-of-function mutation leading to CYBC1 deficiency causes chronic granulomatous disease. *Nat. Commun.* **9**, 4447 (2018).

234. Snelgrove, R. J., Edwards, L., Rae, A. J. & Hussell, T. An absence of reactive oxygen species improves the resolution of lung influenza infection. 1364–1373 (2006). doi:10.1002/eji.200635977

235. Förstermann, U. & Sessa, W. C. Nitric oxide synthases: Regulation and function. *Eur. Heart J.* **33**, 829–837 (2012).

236. Alderton, W. K., Cooper, C. E. & Knowles, R. G. Nitric oxide synthases: Structure, function and inhibition. *Biochem. J.* **357**, 593–615 (2001).

237. Alkaitis, M. S. & Crabtree, M. J. Recoupling the cardiac nitric oxide synthases: Tetrahydrobiopterin synthesis and recycling. *Curr. Heart Fail. Rep.* **9**, 200–210 (2012).

238. Birben, E., Sahiner, U. M., Sackesen, C., Erzurum, S. & Kalayci, O. Oxidative stress and antioxidant defense. *World Allergy Organ. J.* **5**, 9–19 (2012).

239. Auten, R. L. & Davis, J. M. Oxygen toxicity and reactive oxygen species: The devil is in the details. *Pediatr. Res.* **66**, 121–127 (2009).

240. Pizzino, G. *et al.* Oxidative Stress: Harms and Benefits for Human Health. *Oxid. Med. Cell. Longev.* **2017**, (2017).

241. Biron, C. A. Chapter 4 - Innate Immunity: Recognizing and Responding to Foreign Invaders—No Training Needed. in (eds. Katze, M. G., Korth, M. J., Law, G. L. & Nathanson, N. B. T.-V. P. (Third E.) 41–55 (Academic Press, 2016). doi:https://doi.org/10.1016/B978-0-12-800964-2.00004-5

242. Kohchi, C., Inagawa, H., Nishizawa, T. & Soma, G. I. ROS and innate immunity. *Anticancer Res.* **29**, 817–822 (2009).

243. Sun, Y. *et al.* ROS systems are a new integrated network for sensing homeostasis and alarming stresses in organelle metabolic processes. *Redox Biol.* **37**, 101696 (2020).

244. Chakrabarti, S. & Visweswariah, S. S. Intramacrophage ROS Primes the Innate Immune System via JAK/STAT and Toll Activation. *Cell Rep.* **33**, 108368 (2020).

245. Hyodo, K., Hashimoto, K., Kuchitsu, K., Suzuki, N. & Okuno, T. Harnessing host ROS-generating machinery for the robust genome replication of a plant RNA virus. *Proc. Natl. Acad. Sci. U. S. A.* **114**, E1282–E1290 (2017).

246. Paiva, C. N. & Bozza, M. T. Are Reactive Oxygen Species Always Detrimental to Pathogens? *Antioxid. Redox Signal.* **20**, 1000–1037 (2014).

247. Thomas, D. C. How the phagocyte NADPH oxidase regulates innate immunity. *Free Radic. Biol. Med.* **125**, 44–52 (2018).

248. Yun, H. R. *et al.* Roles of Autophagy in Oxidative Stress. *Int. J. Mol. Sci.* **21**, (2020).

249. Chang, K.-C. *et al.* The interplay of autophagy and oxidative stress in the pathogenesis and therapy of retinal degenerative diseases. *Cell Biosci.* **12**, 1 (2022).

250. Dupré-Crochet, S., Erard, M. & Nüβe, O. ROS production in phagocytes: why, when, and where? *J. Leukoc. Biol.* **94**, 657–670 (2013).

251. Dryden, M. Reactive oxygen species: a novel antimicrobial. *Int. J. Antimicrob. Agents* **51**, 299–303 (2018).

252. Herb, M. & Schramm, M. Functions of ros in macrophages and antimicrobial immunity. *Antioxidants* **10**, 1–39 (2021).

253. Lei, H. & Kazlauskas, A. A Reactive Oxygen Species-Mediated, Self-Perpetuating Loop Persistently Activates Platelet-Derived Growth Factor Receptor α. *Mol. Cell. Biol.* **34**, 110–122 (2014).

254. Ascenzi, P., Di Masi, A., Sciorati, C. & Clementi, E. Peroxynitrite-An ugly biofactor? *BioFactors* **36**, 264–273 (2010).

255. Sander, W. J. *et al.* Reactive oxygen species as potential antiviral targets. *Rev. Med. Virol.* **32**, (2022).

256. Barrangou, R. & Marraffini, L. A. CRISPR-Cas systems: Prokaryotes upgrade to adaptive immunity. *Mol. Cell* **54**, 234–244 (2014).

257. Rath, D., Amlinger, L., Rath, A. & Lundgren, M. The CRISPR-Cas immune

system: Biology, mechanisms and applications. *Biochimie* **117**, 119–128 (2015).

258. Westermann, L., Neubauer, B. & Köttgen, M. Nobel Prize 2020 in Chemistry honors CRISPR: a tool for rewriting the code of life. *Pflugers Arch.* **473**, 1–2 (2021).
259. Hryhorowicz, M., Lipiński, D., Zeyland, J. & Słomski, R. CRISPR/Cas9 Immune System as a Tool for Genome Engineering. *Arch. Immunol. Ther. Exp. (Warsz).* **65**, 233–240 (2017).
260. Ran, F. A. *et al.* Genome engineering using the CRISPR-Cas9 system. *Nat. Protoc.* **8**, 2281–2308 (2013).
261. Zhang, H. X., Zhang, Y. & Yin, H. Genome Editing with mRNA Encoding ZFN, TALEN, and Cas9. *Mol. Ther.* **27**, 735–746 (2019).
262. Gaj, T., Gersbach, C. A. & Barbas, C. F. ZFN, TALEN, and CRISPR/Cas-based methods for genome engineering. *Trends Biotechnol.* **31**, 397–405 (2013).
263. Barrangou, R. & Doudna, J. A. Applications of CRISPR technologies in research and beyond. *Nat. Biotechnol.* **34**, 933–941 (2016).
264. Min, Y.-L., Bassel-Duby, R. & Olson, E. N. CRISPR Correction of Duchenne Muscular Dystrophy. *Annu. Rev. Med.* **70**, 239–255 (2019).
265. Dara, M. *et al.* Dystrophin gene editing by CRISPR/Cas9 system in human skeletal muscle cell line (HSkMC). *Iran. J. Basic Med. Sci.* **24**, 1153–1158 (2021).
266. Sanjana, N. E., Shalem, O. & Zhang, F. Improved vectors and genome-wide libraries for CRISPR screening. *Nat. Methods* **11**, 783–784 (2014).
267. Chen, C. H. *et al.* Improved design and analysis of CRISPR knockout screens. *Bioinformatics* **34**, 4095–4101 (2018).
268. Miles, L. A., Garippa, R. J. & Poirier, J. T. Design, execution, and analysis of pooled in vitro CRISPR/Cas9 screens. *FEBS J.* **283**, 3170–3180 (2016).
269. Miles, L. A. DISCOVERY AND CHARACTERIZATION OF ESSENTIAL VIRAL AND HOST PROTEINS FOR THE ONCOLYTIC SENECA VALLEY VIRUS (SVV) By. (2016).
270. Sanjana, N. E. Genome-scale CRISPR pooled screens. *Anal. Biochem.* **532**, 95–

99 (2017).

271. Ma, H. *et al.* A CRISPR-based screen identifies genes essential for west-nile-virus-induced cell death. *Cell Rep.* **12**, 673–683 (2015).
272. Han, J. *et al.* Essential for Influenza Virus Replication. **23**, 596–607 (2018).
273. Park, R. J. *et al.* A genome-wide CRISPR screen identifies a restricted set of HIV host dependency factors. *Nat. Genet.* **49**, 193–203 (2017).
274. Zhang, R. *et al.* A CRISPR screen defines a signal peptide processing pathway required by flaviviruses. *Nature* **535**, (2016).
275. McCormick, D., Lin, Y. T. & Grey, F. Identification of host factors involved in human cytomegalovirus replication, assembly, and egress using a two-step small interfering RNA screen. *MBio* **9**, e00716-18 (2018).
276. Doench, J. G. & Root, D. . Optimized sgRNA design to maximize activity and minimize off-target effects of CRISPR-Cas9 Synthesis of an arrayed sgRNA library targeting the human genome. *Nat. Biotechnol.* **34**, 184–191 (2016).
277. Koike-Yusa, H., Li, Y., Tan, E.-P., Velasco-Herrera, M. D. C. & Yusa, K. Genome-wide recessive genetic screening in mammalian cells with a lentiviral CRISPR-guide RNA library. *Nat. Biotechnol.* **32**, 267–73 (2014).
278. Li, W. *et al.* MAGeCK enables robust identification of essential genes from genome-scale CRISPR/Cas9 knockout screens. *Genome Biol.* **15**, 554 (2014).
279. Wang, B. *et al.* MAGeCK Flute. **14**, (2019).
280. Arunachalam, G., Samuel, S. M., Ding, H. & Triggle, C. R. Peroxynitrite Biology. in *Systems Biology of Free Radicals and Antioxidants* 207–242 (Springer Berlin Heidelberg, 2014). doi:10.1007/978-3-642-30018-9_5
281. Szabó, C., Ischiropoulos, H. & Radi, R. Peroxynitrite: Biochemistry, pathophysiology and development of therapeutics. *Nat. Rev. Drug Discov.* **6**, 662–680 (2007).
282. Korkmaz, A., Oter, S., Seyrek, M. & Topal, T. Molecular, genetic and epigenetic pathways of peroxynitrite-induced cellular toxicity. *Interdiscip. Toxicol.* **2**, 219–228 (2009).
283. Liaudet, L., Vassalli, G. & Pacher, P. Role of peroxynitrite in the redox regulation of cell signal transduction pathways. *Front. Biosci.* **14**, 4809–4814

(2009).

284. Speckmann, B., Steinbrenner, H., Grune, T. & Klotz, L. O. Peroxynitrite: From interception to signaling. *Arch. Biochem. Biophys.* **595**, 153–160 (2016).

285. Matata, B. M. & Galiñanes, M. Peroxynitrite is an essential component of cytokines production mechanism in human monocytes through modulation of nuclear factor-κB DNA binding activity. *J. Biol. Chem.* **277**, 2330–2335 (2002).

286. Ríos, N., Prolo, C., Álvarez, M. N., Piacenza, L. & Radi, R. *Peroxynitrite Formation and Detection in Living Cells*. *Nitric Oxide: Biology and Pathobiology: Third Edition* (Elsevier Inc., 2017). doi:10.1016/B978-0-12-804273-1.00021-1

287. Möller, M. N. *et al.* Detection and quantification of nitric oxide-derived oxidants in biological systems. *J. Biol. Chem.* **294**, 14776–14802 (2019).

288. Chen, X., Chen, H., Deng, R. & Shen, J. Pros and cons of current approaches for detecting peroxynitrite and their applications. *Biomed. J.* **37**, 120–126 (2014).

289. Chen, K. K. *et al.* Redox control in the pathophysiology of influenza virus infection. *BMC Microbiol.* **20**, 1–22 (2020).

290. Li, X., Feng, J. & Sun, R. Oxidative Stress Induces Reactivation of Kaposi's Sarcoma-Associated Herpesvirus and Death of Primary Effusion Lymphoma Cells. *J. Virol.* **85**, 715–724 (2011).

291. Glingston, R. S., Deb, R., Kumar, S. & Nagotu, S. Organelle dynamics and viral infections: at cross roads. *Microbes Infect.* **21**, 20–32 (2019).

292. Dhawan, V. Studies on Respiratory Disorders. (2014). doi:10.1007/978-1-4939-0497-6

293. Kim, J. H. *et al.* Reactive oxygen species-induced parthanatos of immunocytes by human cytomegalovirus-associated substance. *Microbiology and Immunology* **62**, 229–242 (2018).

294. Xiao, J. *et al.* Hydrogen Peroxide Induce Human Cytomegalovirus Replication through the Activation of p38-MAPK Signaling Pathway. *Viruses* **7**, 2816–33 (2015).

295. Aquaro, S. *et al.* The contribution of peroxynitrite generation in HIV replication in human primary macrophages. *Retrovirology* **4**, 1–10 (2007).

296. Padalko, E. *et al.* Peroxynitrite inhibition of coxsackievirus infection by prevention of viral RNA entry. *Proc. Natl. Acad. Sci. U. S. A.* **101**, 11731–11736 (2004).

297. Liu, T. *et al.* L-NAME releases nitric oxide and potentiates subsequent nitroglycerin-mediated vasodilation. *Redox Biol.* **26**, 101238 (2019).

298. Garvey, E. P. *et al.* 1400W is a slow, tight binding, and highly selective inhibitor of inducible nitric-oxide synthase in vitro and in vivo. *J. Biol. Chem.* **272**, 4959–4963 (1997).

299. Soung, D. Y., Chung, H. Y. & Yokozawa, T. A novel action of 5-hydroxytryptamine as a peroxynitrite scavenger. *Pharm. Pharmacol. Commun.* **4**, 583–586 (1998).

300. Kuhn, D. M. & Hasegawa, H. Chapter 12 - Tryptophan hydroxylase and serotonin synthesis regulation. in *Handbook of the Behavioral Neurobiology of Serotonin* (eds. Müller, C. P. & Cunningham, K. A. B. T.-H. of B. N.) **31**, 239–256 (Elsevier, 2020).

301. Bai, Y. *et al.* 4-Chloro-DL-phenylalanine protects against monocrotaline-induced pulmonary vascular remodeling and lung inflammation. *Int. J. Mol. Med.* **33**, 373–382 (2014).

302. Kramer, J. A. *et al.* Early Toxicology Signal Generation in the Mouse. *Toxicol. Pathol.* **38**, 452–471 (2010).

303. Fraternale, A. *et al.* Intracellular redox-modulated pathways as targets for effective approaches in the treatment of viral infection. *Int. J. Mol. Sci.* **22**, (2021).

304. DeMeritt, I. B., Milford, L. E. & Yurochko, A. D. Activation of the NF-kappaB pathway in human cytomegalovirus-infected cells is necessary for efficient transactivation of the major immediate-early promoter. *J. Virol.* **78**, 4498–4507 (2004).

305. Gustems, M. *et al.* Regulation of the Transcription and Replication Cycle of Human Cytomegalovirus Is Insensitive to Genetic Elimination of the Cognate

NF-κB Binding Sites in the Enhancer. *J. Virol.* **80**, 9899–9904 (2006).

306. Xiao, J. *et al.* Hydrogen peroxide induce human cytomegalovirus replication through the activation of p38-MAPK signaling pathway. *Viruses* **7**, 2816–2833 (2015).
307. Bottero, V., Chakraborty, S. & Chandran, B. Reactive Oxygen Species Are Induced by Kaposi's Sarcoma-Associated Herpesvirus Early during Primary Infection of Endothelial Cells To Promote Virus Entry. *J. Virol.* **87**, 1733–1749 (2013).
308. Shen, Y. H. *et al.* Human cytomegalovirus inhibits Akt-mediated eNOS activation through upregulating PTEN (phosphatase and tensin homolog deleted on chromosome 10). *Cardiovasc. Res.* **69**, 502–511 (2006).
309. Bradford, R. D. *et al.* Murine CMV-Induced Hearing Loss Is Associated with Inner Ear Inflammation and Loss of Spiral Ganglia Neurons. *PLoS Pathog.* **11**, 1–21 (2015).
310. Pecha, P. P. *et al.* Role of Free Radical Formation in Murine Cytomegalovirus-Induced Hearing Loss. *Otolaryngol. Head. Neck Surg.* **162**, 709–717 (2020).
311. Croen, K. D. Evidence for antiviral effect of nitric oxide. Inhibition of herpes simplex virus type 1 replication. *J. Clin. Invest.* **91**, 2446–2452 (1993).
312. Kawanishi, M. Nitric oxide inhibits Epstein-Barr virus DNA replication and activation of latent EBV. *Intervirology* **38**, 206–213 (1995).
313. Mokry, R. L., Schumacher, M. L., Hogg, N. & Terhune, S. S. Nitric oxide circumvents virus-mediated metabolic regulation during human cytomegalovirus infection. *MBio* **11**, 1–25 (2020).
314. Mokry, R. L., Schumacher, M. L., Hogg, N. & Terhune, S. S. Nitric Oxide Circumvents Virus-Mediated Metabolic Regulation during Human Cytomegalovirus Infection. *MBio* **11**, e02630-20 (2020).
315. Drutman, S. B. *et al.* Fatal Cytomegalovirus Infection in an Adult with Inherited NOS2 Deficiency. *N. Engl. J. Med.* **382**, 437–445 (2020).
316. Casarotto, P. C. *et al.* Inducible nitric oxide synthase (NOS2) knockout mice as a model of trichotillomania. *PeerJ* **6**, e4635–e4635 (2018).
317. Tanaka, K. *et al.* Nitric oxide mediates murine cytomegalovirus-associated

pneumonitis in lungs that are free of the virus. *J. Clin. Invest.* **100**, 1822–1830 (1997).

318. Schneider, W. M. *et al.* Genome-Scale Identification of SARS-CoV-2 and Pan-coronavirus Host Factor Networks. *Cell* **184**, 120-132.e14 (2021).
319. Ong, S. H., Li, Y., Koike-Yusa, H. & Yusa, K. Optimised metrics for CRISPR-KO screens with second-generation gRNA libraries. *Sci. Rep.* **7**, 1–10 (2017).
320. Koujah, L., Shukla, D. & Naqvi, A. R. CRISPR-Cas based targeting of host and viral genes as an antiviral strategy. *Semin. Cell Dev. Biol.* **96**, 53–64 (2019).
321. Park, E. K. *et al.* Optimized THP-1 differentiation is required for the detection of responses to weak stimuli. *Inflamm. Res.* **56**, 45–50 (2007).
322. Li, W. *et al.* Quality control, modeling, and visualization of CRISPR screens with MAGeCK-VISPR. *Genome Biol.* **16**, 281 (2015).
323. Sitthiyot, T. & Holasut, K. A simple method for measuring inequality. *Palgrave Commun.* **6**, 1–9 (2020).
324. Illumina, I. NextSeq ® 500 System WGS Solution. *Pub. No. 770-2013-049* 1–6 (2015).
325. Illumina Inc. Introduction to the NextSeq System. *Manual* (2015).
326. O'Brien, S. Hippo pathway control of KSHV latency. (2017).
327. Wang, S. *et al.* The Crosstalk Between Hippo-YAP Pathway and Innate Immunity. *Front. Immunol.* **11**, 1–14 (2020).
328. Misra, J. R. & Irvine, K. D. The hippo signaling network and its biological functions. *Annu. Rev. Genet.* **52**, 65–87 (2018).
329. Paul, A. *et al.* Cell adhesion molecule KIRREL1 is a feedback regulator of Hippo signaling recruiting SAV1 to cell-cell contact sites. *Nat. Commun.* **13**, 1–14 (2022).
330. Ma, S., Meng, Z., Chen, R. & Guan, K.-L. The Hippo Pathway: Biology and Pathophysiology. *Annu. Rev. Biochem.* **88**, 577–604 (2019).
331. Xu, W. *et al.* YAP manipulates proliferation via PTEN/AKT/mTOR-mediated autophagy in lung adenocarcinomas. *Cancer Cell Int.* **21**, 30 (2021).
332. Curto, M. & McClatchey, A. I. Nf2/Merlin: A coordinator of receptor signalling and intercellular contact. *Br. J. Cancer* **98**, 256–262 (2008).

333. Murakami, H. *et al.* LATS2 is a tumor suppressor gene of malignant mesothelioma. *Cancer Res.* **71**, 873–883 (2011).

334. Kundra, V. *et al.* Regulation of chemotaxis by the platelet-derived growth factor receptor-beta. *Nature* **367**, 474–476 (1994).

335. Conaway, R. C. & Conaway, J. W. Origins and activity of the Mediator complex. *Semin. Cell Dev. Biol.* **22**, 729–734 (2011).

336. Griffiths, S. J. *et al.* A Systematic Analysis of Host Factors Reveals a Med23-Interferon-λ Regulatory Axis against Herpes Simplex Virus Type 1 Replication. *PLoS Pathog.* **9**, (2013).

337. Yamaji, T. *et al.* A CRISPR Screen Using Subtilase Cytotoxin Identifies SLC39A9 as a Glycan-Regulating Factor. *iScience* **15**, 407–420 (2019).

338. Tanaka, A. *et al.* Genome-Wide Screening Uncovers the Significance of N-Sulfation of Heparan Sulfate as a Host Cell Factor for Chikungunya Virus Infection. *J. Virol.* **91**, 1–22 (2017).

339. Riblett, A. M. *et al.* A Haploid Genetic Screen Identifies Heparan Sulfate Proteoglycans Supporting Rift Valley Fever Virus Infection. *J. Virol.* **90**, 1414–1423 (2016).

340. Li, Y. *et al.* Lats2, a putative tumor suppressor, inhibits G1/S transition. *Oncogene* **22**, 4398–4405 (2003).

341. Furth, N. & Aylon, Y. The LATS1 and LATS2 tumor suppressors: beyond the Hippo pathway. *Cell Death Differ.* **24**, 1488–1501 (2017).

342. Busse, M. *et al.* Contribution of EXT1, EXT2, and EXTL3 to Heparan Sulfate Chain Elongation*. *J. Biol. Chem.* **282**, 32802–32810 (2007).

343. Presto, J. *et al.* Heparan sulfate biosynthesis enzymes EXT1 and EXT2 affect NDST1 expression and heparan sulfate sulfation. *Proc. Natl. Acad. Sci. U. S. A.* **105**, 4751–4756 (2008).

344. Craig, M., Gillian, D., Tina, G. K. & Frank, T. The putative tumor suppressors EXT1 and EXT2 form a stable complex that accumulates in the Golgi apparatus and catalyzes the synthesis of heparan sulfate. *Proc. Natl. Acad. Sci.* **97**, 668–673 (2000).

345. Benslimane, Y. *et al.* A novel p53 regulator, C16ORF72/TAPR1, buffers against

telomerase inhibition. *Aging Cell* **20**, 1–11 (2021).

346. Dharan, A. *et al.* KIF5B and Nup358 Cooperatively Mediate the Nuclear Import of HIV-1 during Infection. *PLoS Pathog.* **12**, 1–24 (2016).
347. Scherer, J., Yi, J. & Vallee, R. B. Role of cytoplasmic dynein and kinesins in adenovirus transport. *FEBS Lett.* **594**, 1838–1847 (2020).
348. Qin, Y. *et al.* Structural and functional study of D-glucuronyl C5-epimerase. *J. Biol. Chem.* **290**, 4620–4630 (2015).
349. Dierker, T. *et al.* Altered heparan sulfate structure in Glce(-/-) mice leads to increased Hedgehog signaling in endochondral bones. *Matrix Biol.* **49**, 82–92 (2016).
350. Delgado-Esteban, M., Martin-Zanca, D., Andres-Martin, L., Almeida, A. & Bolaños, J. P. Inhibition of PTEN by peroxynitrite activates the phosphoinositide-3- kinase/Akt neuroprotective signaling pathway. *J. Neurochem.* **102**, 194–205 (2007).
351. Li, S. *et al.* The tumor suppressor PTEN has a critical role in antiviral innate immunity. *Nat. Immunol.* **17**, 241–249 (2016).
352. Brandmaier, A., Hou, S.-Q. & Shen, W. H. Cell Cycle Control by PTEN. *J. Mol. Biol.* **429**, 2265–2277 (2017).
353. Wang, S. *et al.* YAP antagonizes innate antiviral immunity and is targeted for lysosomal degradation through IKKI-mediated phosphorylation. *Nat. Immunol.* **18**, 733–743 (2017).
354. Wang, Z. *et al.* The Hippo Pathway and Viral Infections. *Front. Microbiol.* **10**, 1–11 (2020).
355. Garcia, G. *et al.* Hippo Signaling Pathway Has a Critical Role in Zika Virus Replication and in the Pathogenesis of Neuroinflammation. *Am. J. Pathol.* **190**, 844–861 (2020).
356. Xue, Y. *et al.* Hepatitis C Virus Mimics Effects of Glypican-3 on CD81 and Promotes Development of Hepatocellular Carcinomas via Activation of Hippo Pathway in Hepatocytes. *Am. J. Pathol.* **188**, 1469–1477 (2018).
357. Cooper, J. & Giancotti, F. G. Molecular insights into NF2/Merlin tumor suppressor function. *FEBS Lett.* **588**, 2743–2752 (2014).

358. Dittmer, D. & Mocarski, E. S. Human cytomegalovirus infection inhibits G1/S transition. *J. Virol.* **71**, 1629–1634 (1997).

359. Bresnahan, W. A., Boldogh, I., Thompson, E. A. & Albrecht, T. Human cytomegalovirus inhibits cellular DNA synthesis and arrests productively infected cells in late G1. *Virology* **224**, 150–160 (1996).

360. Spector, D. H. Human cytomegalovirus riding the cell cycle. *Med. Microbiol. Immunol.* **204**, 409–419 (2015).

361. Vijayalingam, S. & Chinnadurai, G. Adenovirus L-E1A activates transcription through mediator complex-dependent recruitment of the super elongation complex. *J. Virol.* **87**, 3425–3434 (2013).

362. DuRaine, G., Wisner, T. W., Howard, P. & Johnson, D. C. Kinesin-1 Proteins KIF5A, -5B, and -5C Promote Anterograde Transport of Herpes Simplex Virus Enveloped Virions in Axons. *J. Virol.* **92**, (2018).

363. Ogawa-Goto, K. *et al.* Microtubule network facilitates nuclear targeting of human cytomegalovirus capsid. *J. Virol.* **77**, 8541–8547 (2003).

364. Ravindran, M. S., Engelke, M. F., Verhey, K. J. & Tsai, B. Exploiting the kinesin-1 molecular motor to generate a virus membrane penetration site. *Nat. Commun.* **8**, 1–14 (2017).

365. Strasfeld, L. & Chou, S. Antiviral drug resistance: Mechanisms and clinical implications. *Infect. Dis. Clin. North Am.* **24**, 809–833 (2010).

366. Van Erp, A. C. *et al.* The Crosstalk between ROS and Autophagy in the Field of Transplantation Medicine. *Oxid. Med. Cell. Longev.* **2017**, 7120962 (2017).

367. Hamad, A. M. *et al.* The effect of the nitric oxide synthase inhibitor, L-NMMA, on sodium metabisulphite-induced bronchoconstriction and refractoriness in asthma. *Eur. Respir. J.* **14**, 702–705 (1999).

368. Dao, V. T. V. *et al.* Pharmacology and Clinical Drug Candidates in Redox Medicine. *Antioxidants Redox Signal.* **23**, 1113–1129 (2015).

Appendices

Table 15: Top 20 genes that were identified by MAGeCK as enriched in the HCMV -resistant group compared to uninfected control.

FDR	id	num	pos|score	pos|p-value	pos|fdr	pos|rank	pos|goodsgrna	pos|lfc
<0.01	NF2	4	3.67E-16	2.59E-07	0.000619	1	4	14.424
	PDGFRA	4	4.18E-11	2.59E-07	0.000619	2	4	8.4958
	MED23	4	3.04E-09	2.59E-07	0.000619	3	4	6.5575
	KIRREL	4	6.82E-09	2.59E-07	0.000619	4	4	8.6752
	SLC39A9	4	4.57E-08	2.59E-07	0.000619	5	4	3.5318
	PTAR1	4	4.65E-08	2.59E-07	0.000619	6	4	6.1805
	HS6ST1	4	5.95E-08	2.59E-07	0.000619	7	4	4.1147
	LATS2	4	1.21E-07	2.59E-07	0.000619	8	4	5.0575
	EXT1	4	4.08E-07	1.30E-06	0.002475	9	3	4.8857
	C16orf72	4	6.12E-07	1.30E-06	0.002475	10	3	5.3466
	KIF5B	4	1.41E-06	2.33E-06	0.00405	11	3	5.2571
<0.05	GLCE	3	5.84E-06	2.00E-05	0.029322	12	3	3.5665
	PTEN	4	6.73E-06	1.27E-05	0.020215	13	3	3.5174
<0.25	AMBRA1	4	2.76E-05	6.66E-05	0.090877	14	2	2.1131
	IL1RAPL1	4	4.51E-05	0.00010809	0.137624	15	2	-0.89771
	EXT2	4	5.18E-05	0.00011794	0.14078	16	2	3.1402
	KRTAP13-4	3	6.56E-05	0.00014541	0.163366	17	1	-2.7852
	ASNA1	4	0.00010989	0.00024132	0.248267	18	2	2.3041
	KCTD5	3	0.00011435	0.00025117	0.248267	19	2	4.3476
	C6orf163	4	0.00011823	0.00025998	0.248267	20	2	-0.64476